The University of Adelaide

Elder Conservatorium of Music

Faculty of Arts

A Musicological Study of the Japanese *Koto* using Heuristic Finite Element Models

Submitted in fulfilment of the requirements for the degree of

Doctor of Philosophy

Iran Sanadzadeh

November 2019

Volume I

Declaration

I certify that this work contains no material which has been accepted for the award of any other degree or diploma in my name, in any university or other tertiary institution and, to the best of my knowledge and belief, contains no material previously published or written by another person, except where due reference has been made in the text. In addition, I certify that no part of this work will, in the future, be used in a submission in my name, for any other degree or diploma in any university or other tertiary institution without the prior approval of the University of Adelaide. I give permission for the digital version of my thesis to be made available on the web, via the University's digital research repository, the Library Search and also through web search engines. I acknowledge the support I have received for my research through the provision of an Adelaide Graduate Research Scholarship.

Signature:……..

Date: :……

Acknowledgments

I would like to acknowledge the guidance and mentorship from my principal supervisor, Associate Professor A. Kimi Coaldrake and the help of my co-supervisor, Professor Aaron Corn. I would also like to thank my fellow Ph.D. candidates and friends Dylan Crismani and Sebastian Phlox, for years of friendship and camaraderie and especially David Blackwell, for his practice of presentations with me and for proof-reading my writing in its final stages. I am indebted to Eric. H. Dunlop for technical guidance and the inspiring example he sets in perseverance. Thanks to my colleagues at the Writing Centre at the University of Adelaide; I cherish our friendship and work together and my stay at the University is much richer for their presence. I would like to acknowledge the continued support from the academic and professional staff at the Elder Conservatorium of Music throughout my studies. Lastly, I would like to thank Mohammad and Khaled Sanadzadeh and Adi Rai, for their continued love and support especially in the difficult parts of this Ph.D. journey.

Table of Contents

Volume I

Part Two: Using Heuristic Models for the Study of the Japanese *Koto*

Volume II: Datasets

List of Figures

Chapter Seven: Heuristic finite element models of the *koto*

Chapter Eight: Conclusion – No figures

List of Tables

Chapter One: Introduction

Chapter Two: Literature review

Chapter Three: Methods

Chapter Four: Validation and verification of the models and the methods of this study

Chapter Five: Broader considerations of modelling the physical properties of *paulownia*

Chapter Six: Finite element model of a *koto*-sized plank

Chapter Seven: Heuristic finite element models of the *koto*

Chapter Eight: Conclusion

Abstract

This musicological study investigates the sound of the Japanese *koto*, a 13-string zither, using heuristic finite element models. It aims firstly to test a new integrated analytical approach with finite element methods; these methods have become more accessible to scholars across many disciplines including systematic musicology in recent decades. This thesis demonstrates how these methods can provide powerful analytical tools for technical studies of musical instruments as part of organological research. Secondly, it applies this method in a heuristic study of the *koto* to characterise its sound envelope by using a series of models; these models range from a simple box to a more complex and geometrically accurate lofted model developed as part of this study. These models permitted the continual development of the integrated analytical approach during the period of investigation. COMSOL Multiphysics®, the finite element method software used to develop the models, also enabled specialist analysis of sound from the instrument including its qualitative visual representation. Results of these models in turn were validated by comparison with the limited existing literature on the *koto*'s acoustics and additional physical experiments. During this process initial tests on a plank of *paulownia* wood were undertaken in order to understand the *paulownia* wood from which the *koto* is made. These results then informed more complex, subsequent models.

Findings from the study reveal that the anisotropic nature of *paulownia* significantly influenced predicted resonances when compared to a simple isotropic model. Key characteristics of the *koto* body that help to explain the relationship between sound production and geometry of the instrument were also identified, for example, the significant influence of the curvature of the top plate and the arching down the length of the instrument on the sound envelope produced. These findings contribute to the understanding of the acoustical behaviour of the *koto* in particular and East Asian zithers in general. The methods identified and validated in this study also serve more broadly as a template for future organological and acoustical investigations of geometrically complex wooden musical instruments.

Chapter 1

Introduction

Over the past century, the acoustical understanding of musical instruments has greatly expanded. Scholars can now investigate how the construction and assembly, geometry, physical properties of the material, and the performer's actions affect the production of sound of a musical instrument (Bissinger 2008; Gough 2015; Leman 2008). Similarly, discoveries in room acoustics show the effects of the performance space on the radiation and perception of the sound (Bader 2009). Finite element methods have increasingly been used in such studies. They have been applied to the study of stringed instruments such as the violin family (Gough 2018) and the studies (Coaldrake 2018) of the Japanese *koto*, a 13 stringed zither made of *paulownia* wood. However, acoustical studies of Asian stringed instruments in general remain limited.

Instrumental studies in the past have often fallen within the broad framework of musicology and organology. More recently, they have become part of the sub-branch of systematic musicology. This is clearly seen for example, in *Current Research in Systematic Musicology* (2017) which has a range of acoustic studies including the *q'in*, a Chinese seven string zither (Waltham, Coaldrake, Koster and Lan 2017). This thesis contributes to this emerging branch of instrumental acoustics. It presents the development of a method for the study of stringed wooden instruments of using COMSOL Multiphysics® (hereafter COMSOL) and its application to the technical study of the characteristics of the sound of the *koto.* [1] The aims and research questions which focus on this two-fold approach are presented in Table 1.1.

[1] COMSOL is now recognised as the best tool available to researchers for this type of acoustical and technical study. It is a powerful, but user-friendly software that can incorporate both simple and complex geometry. Although this software does not need knowledge of coding or detailed undertaking of signal processing, it does nevertheless require a considerable initial learning curve to use.

Table 1.1 Aims and research questions of the study

	Methods developed in this study	The study of the *koto* using the methods
Aims	To develop heuristic finite element models. To evaluate the heuristic finite elements models by applying them to the study of the *koto*. To create a template for the analysis of the sound of Asian zithers using heuristic finite element models.	To characterise the sound envelope of the *koto* using these finite element models. To understand the role of the components of the *koto* body on its sound.
Research questions	How can heuristic finite element models be used to study the characteristics of the sound of the *koto*? Do heuristic finite element models have potential applications for the study of Asian zithers or other under-studied instruments?	What is the sound envelope of the *koto*? What are the resonant frequencies of the body? How does the wood interact with air? How does the sound the *koto* body emits change over time?

The analytical framework in the thesis is used to investigate the overarching question of "What is the sound envelope of the *koto*?" and seek answers to the more specific research questions in Table 1.1. The study starts with knowledge gained from the simpler heuristic finite elements models to inform subsequent more complex models. In the context of this study, a heuristic model is one that allows discoveries to be made about the physical instrument. It is not intended to duplicate the exact sound of the instrument. It also does not assess the relationship between the performer's actions are the response of the instrument or the effect of the room. The study is framed by musicology and grounded in the author's background in sonic arts and music technology.

Four sets of studies are used to investigate the research questions leading up to the overarching question of "What is the sound envelope of the *koto*?". These studies are represented by individual ovals (shown with green lines) within Figure 1.1. The first two sets of studies shown as the smallest ovals, focus on the resonances of the individual plates and the resonant modes of the full body of the *koto*, modelled using heuristic models; these two sets are conducted in the modal domain. The third oval represents the frequency scans using the models in a sphere of air; this set is used to examine the interaction of the *koto* models with the air. The final oval represents the study of the response of the model over a period of time.

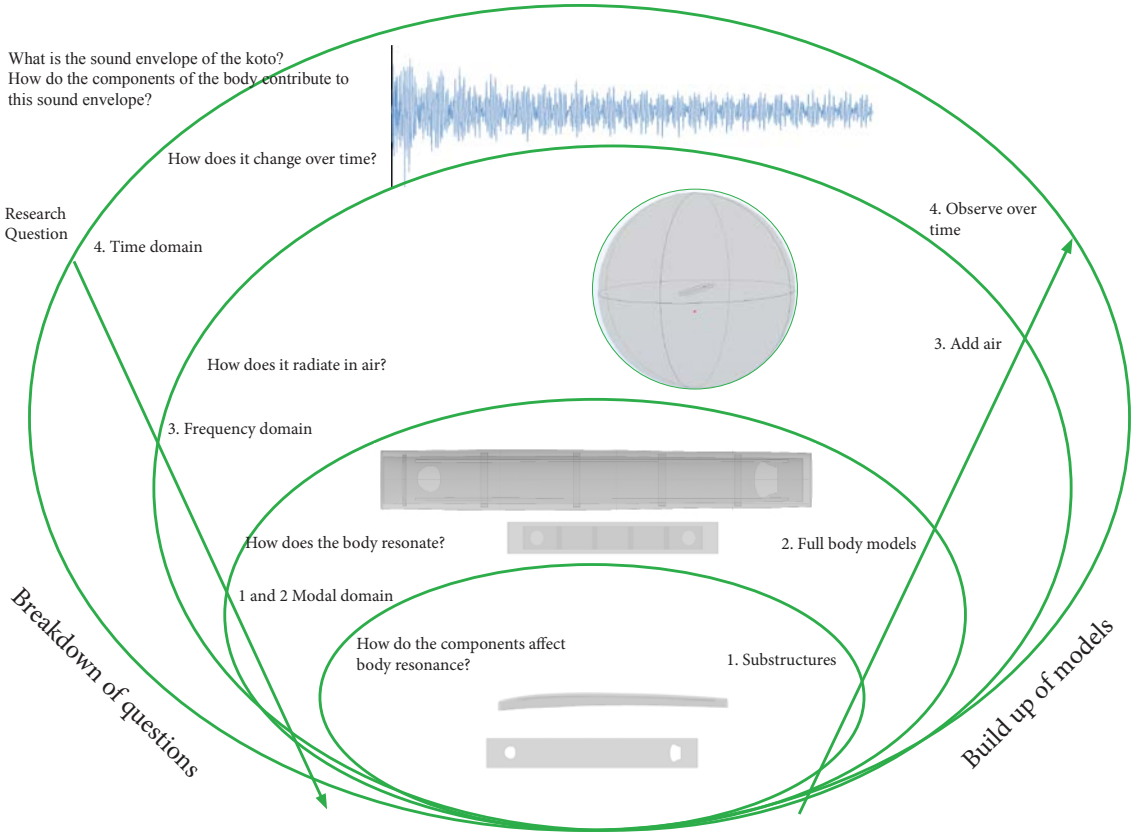

Figure 1.1 The analytical framework of COMSOL models

The same overarching question of "What is the sound envelope of the *koto*?" can also be answered, instead of heuristic analytical models, with a complex model based on a framework of synthesising the most detailed information available. Coaldrake's (2018) high-resolution CT scan model provides an example of the compound approach to the *koto* study.

Such a model can replicate the process of sound radiation from the instrument better than the simple analytical models which are being proposed in this thesis. However, it does not allow for the analysis of individual parts of the instrument or for exploring variations in the *koto'*s basic components. It requires significant computational power. The complexity of Coaldrake's high-resolution model can also obscure the effect of small changes in the model.

An analytical framework is therefore used in this study rather than the synthesis approach to allow the detailed evaluation of components that contribute to the overall sound envelope and other characteristics of the sound of the *koto.* It is an essential part of the evaluation of the method to answer the critical question: how simple can the model be to remain heuristic and permit discoveries? It is helpful at times to compare the heuristic models with Coaldrake's high resolution studies in order to answer this question.

Organisation of the thesis

This thesis is divided into two volumes. Volume I now presents the literature review in Chapter Two. It discusses the musicological, organological and acoustical literature relevant to this study. The study is then divided into two parts. Part One focuses on the methods and the validation of both the methods and the models developed. Chapter Three describes the methods associated with the development of the heuristic models. Chapter Four discusses the verification and validation of the models. This includes the comparison of model results against known literature and physical experiments conducted as part of the study. Chapter Five brings together results from Chapter Three and Chapter Four to present broader considerations of modelling the physical properties of *paulownia*. It discusses the use of isotropic and orthotropic material properties for this study and attempts at refining the data available. Part Two focuses on using the heuristic models for the discovery of the basic acoustical response of the *koto;* Chapter Six discusses modelling of a *koto*-sized plank of *paulownia* to provide a baseline for the analysis of the real instrument. Chapter Seven presents the results of studies using the heuristic *koto* models in the modal, frequency and time domains. The final chapter discusses the findings of the study, the implications for applying the method to other traditional stringed wooden instruments and future work in the acoustical study of the *koto.* Volume II (Datasets) presents detailed materials from the

studies that were used as the basis of the analyses as well as the discussion of the heuristic models and the sound of the *koto.*

It is helpful here to represent visually how the two parts and chapters of the thesis serve to address the aims and the research questions of the study. Figure 1.2 presents the organisational framework and its relationship to the aims. It shows Chapters Two to Four in Part One in yellow on the horizontal plane relating to the development of the models and their validation and Chapter Five, also in yellow, as part of the broader considerations of the development of the models. Part Two is shown in green, on the vertical perspective, with reference to Chapter Six and Seven. It represents how the heuristic finite elements models are used for the study of the *koto.* The work completed as part of this research and the chapter is then summarised in the boxes that form the main body of Figure 1.2. The interpretation of the results connects the simpler studies to the more complex analysis and converges to the final understanding of the *koto* body.

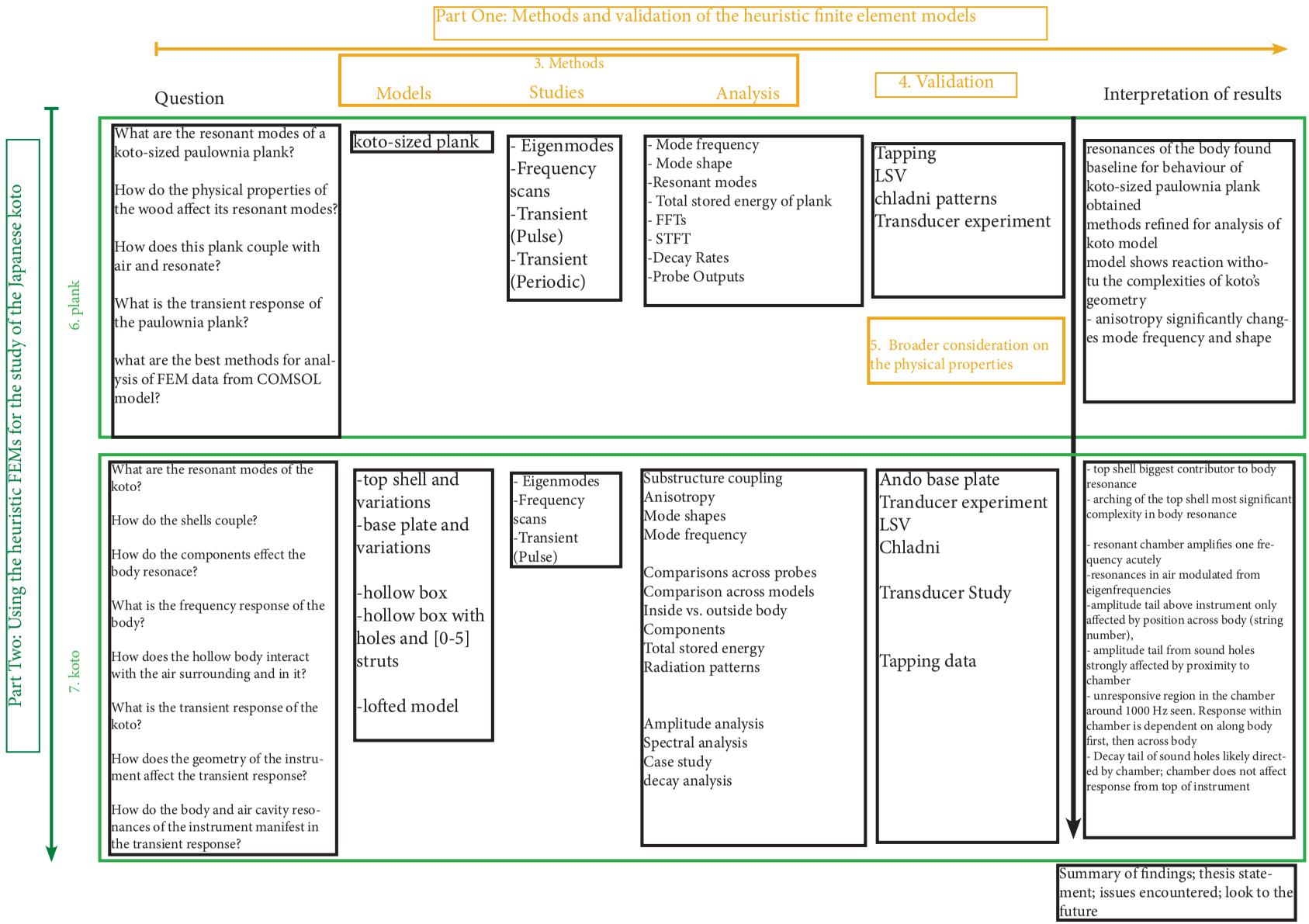

Figure 1.2 Thesis organisation and its relationship to the aims of this study

Finally, a simplified work flow chart for the study is shown in Figure 1.3. This work flow chart is included at the start of each part of the thesis and the chapters to assist the reader.

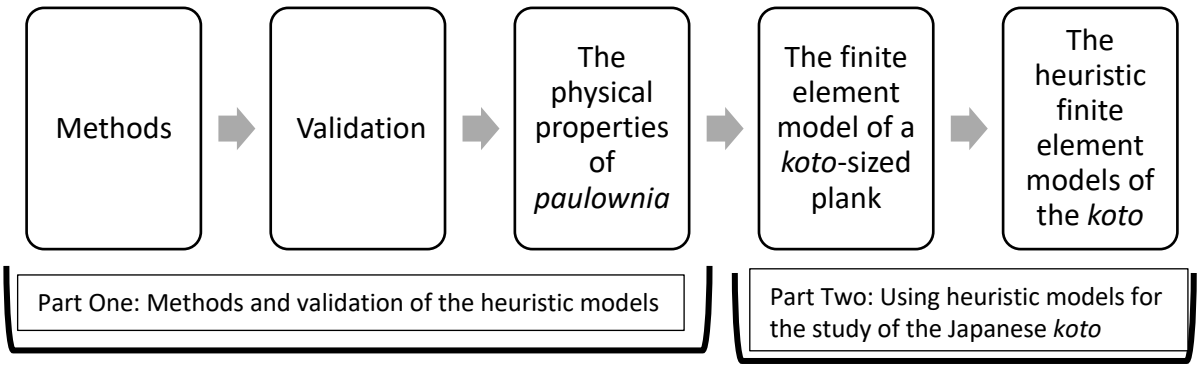

Figure 1.3 The work flow of this study

Chapter 2

Literature Review

The study of musical instruments and their sound has become a multidisciplinary field. Recent new technologies have led to unprecedented insights into the acoustical mechanisms of musical instruments within systematic musicology and related fields such as cognitive psychology, acoustics, and computer science. Importantly, these technologies are now available to musicologists including those working in systematic musicology and its subbranches. These areas have advanced greatly in recent decades (Schneider 2018). This is evident in recent publications such as *The Springer Handbook of Systematic Musicology* (Bader ed. 2018), which presents a range of the current research including studies of embodiment, interaction, psychology, acoustics, signal processing, ethnographic studies, and material studies. Organology, as a study of instruments, fits within this purview.

The organological study of instruments historically focused attention on the classification of musical instruments. The pioneering *Hornbostel and Sachs Classification System* (1914), which is still widely used, examines the body of the instrument, how it makes sound and how it is played. Kartomi's work (1990) expands on this framework to incorporate the discussion of cultural concepts surrounding the instruments themselves. By contrast, Lysloff and Matson in 1985 developed another useful classification system, based on the similarity of instruments across a large number of factors including the interaction between the player and the instrument, that expanded the cross-cultural comparison of instruments (Lysloff and Matson 1985). These classification systems remain an integral part of musicological study and bring a wide perspective to meticulous measurements and cultural factors used to study musical instruments and their sound.

The scientific study of musical sound, now formalised as musical acoustics, can relate cultural studies of music to the scientific understanding of the mechanisms of sound production. It is in this context that this study of the *koto* fits. There are many methods of studying the mechanisms of musical instruments. Some studies compare instruments based on their material or construction. For example, Yoshikawa and Waltham (2014) provide an overview of woods used to make musical instruments and compares a number of woodwinds made using bamboo (*shakuhachi* and *xiao*) with others made of African blackwood (clarinet and oboe). Their study considers the unique behaviour of wood depending on the construction of the instrument and the way it is played. Other studies have used a combination of different

techniques to obtain information about the resonances of the instruments chosen. In such studies, techniques of acoustic holography, interferography, and the comparison of measured and predicted eigenmodes can be used in the discussion of the "most important" resonances of the instrument (Molin and Lingden 1988, 286-287).

Instrumental modelling is another technique that can be used for the study of instruments, and depending on the research aims, different studies have shown how this tool can be employed in different ways. If replicating the sound of the instrument or the process of sound creation in the instrument is the focus, numerical models and transfer functions can be used (Smyth 2011; Smyth and Rouhipour 2013). If the geometry of the instrument and its construction are the focus of an analysis, two or three dimensional geometric models are commonly used (Giordano 2016). Increased computational power has helped researchers to tackle modelling more complex objects such as musical instruments, a range of materials, geometries, and construction methods. Ravina for example has introduced a new framework for conceptualising musical instruments in the modelling process (2006). Horner and Beauchamp's studies have similarly introduced a newer comprehensive method for sound analysis (Horner and Beauchamp 2007).

This study of the *koto* employs more recent tools of computational modelling. Computational modelling of musical instruments involves creating an abstracted version of an instrument, its behaviour, or its components. Depending on available *a priori* information about the instrument or its acoustical behaviour, the user can also create a model which can be used to predict the behaviour of the instrument (Candy 2006, 3). The study of structural modifications of the guitar by French (2007) is one example. Deciding which modelling method to employ depends on the information desired about the system at the end of the process. For example, according to Gough (2017), a 'generic' or idealised model allows the researcher to begin with a model which is as simple as possible but reproduces salient physical properties.

Models can be made to be analytical or synthetical. Synthetical models create a model that combines the total effect of the system to replicate its function.[1] While these models can best

[1] A model may show the output of a system or to replicate the way that system works. Musical instruments are complex objects; in the process of understanding their behaviour, many modelling studies have taken approaches

represent the instrument, they offer less ability to analyse its individual parts than analytical models do. Analytical models are considered those which break down the complex starting object to its simpler components. These studies use the abstraction of the parts to build up an understanding of the mechanisms of each part of the instrument. However, they can lack the intricacies of the actual system of study because each part is simplified. The output of simpler models can assist in the understanding of the basics of the instrument body, components, and physical properties (Giordano 2018).[2]

Studies of acoustics of instruments are not restricted to computational modelling. Acoustical studies of musical instruments are wide-ranging and include the analysis of individual body components in an instrument (Gough 2015), the response of the full instrument body (Giordano 2018; Gough 2016 and 2017; Waltham 2008) and analysis of how the excitation of the instrument affects the sound output (Lau et al. 2010).

The study of an instrument, its development over time and the comparison between the sound and acoustical behaviour similar instruments in different cultures are also part of contemporary approaches to musical acoustics (Yoshikawa and Waltham 2014; Rossing 2014). These studies use a variety of tools and analytical techniques which often include either direct or indirect reference to existing physical experiments and data gathered from the instruments. Among wooden musical instruments, the violin family has received the most comprehensive attention (Bissinger 2008; Hutchins and Benade 1997; Gough 2015 and 2018; Weinreich 1993). In contrast, Asian string instruments have only recently begun to be studied in more detailed acoustical studies (Coaldrake 2012, 2018, 2019; Waltham, Yang and Koster 2016; Yoshikawa 2007 and 2010; Yoshikawa and Waltham 2014). In modelling the geometry of the instrument, finite element and finite difference methods give highly detailed information. To model

that aim to uncover the underlying principles and basic features of the instruments (Gough 2016, 22-24). James Candy illustrates a hierarchy of models, detailing the features of the simplest black box to fully parametric models (Candy 2006, 3). A black box study replicates the output of the system and from the connection between the input and output, infers the behaviour of the system. In musical acoustics, black box studies were pioneered by J. Woodhouse et al. in acoustics of the violin family (Woodhouse 1978). Parameterised models, which examine individual features of the response instead of the final output, were later made following Woodhouse's work (Bader, 2005; Cremer 1984; Gough, 2016; Waltham, 2008). The studies aid the understanding of how the instrument behaves or what the most critical aspects of its sound are. They do not focus on resynthesising the sound of the instrument with audible accuracy.

[2] Ritchey (1991) expands on this discussion in terms of the fundamental approaches to acoustics, as seen in Helmholtz' analytical studies and Bernhard Riemann's synthesis method

instruments with these methods, information about the geometry of the instrument and its material properties are critical to their study. Built in equations for the physical interactions are also required.

Finite element method (FEM) is a tool for understanding complex structures and their properties. Models made using this tool are called finite element models. This approach to modelling has been used with musical instruments since 1975, (University of California, Berkeley 2016).[3] FEM can show how instruments react to various inputs of energy and can provide detailed insight into the internal process within the instrument that converts the input energy (plucking, bowing, tapping, etc.) to the complex resultant tone. FEM has been used to provide a previously unavailable level of detail about musical instruments, their sound quality, physical characteristics and properties, as well as insight into choices by expert craftspersons (Gough 2016; Hutchins 1981, 177). Examples of studies of instrument behaviour using FEMs include the Elejabarrieta et al.'s 2002 studies on the guitar, Fletcher et al.'s 1982 work on flute head joints, Rose and Holloway's 2012 study of brass instruments and Mansour et al.'s modelling of the *setar* in 2009. New instruments can now be prototyped with FEMs, and variations on existing instruments can be tested in a reliable and timely fashion. While many of these studies were possible before FEM, the use of this technology can vastly expand the possible research avenues as well as offer a new perspective.

The finite element method is useful as a tool for the study of an under-studied instruments, as it can provide detail about the minutiae of the acoustical response of the body. FEM has been considered as a quasi-experimental tool (Gough 2015, 2018). As such, it is also a useful tool because it allows for a non-invasive examination of the material. With knowledge of the internal geometry of the instrument, the detail of the sound events that happen inside can be captured and examined. This detail is impossible to obtain with most physical experiments. Finite element models are therefore useful for both analytical and synthetical approaches to acoustical studies.

[3] Finite element modelling and finite element methods are used interchangeably in this study. Both are abbreviated as FEM.

Zithers and the *Koto*

The study of Asian instruments and their performance practice has been a focus of musicology and ethnomusicology for many decades. Ethnomusicological studies of Japanese music were pioneered by scholars such as William Malm (1959; 1977; 1986). Discussions around musical instruments in these documents focused on the role of instruments in the broader performance practice within ethnographic studies. With regards to the *koto*, Adriaanz (1973), Wade (1976), and Johnson (1996a, 1996b, 1996c, 1999, 2004) further elaborate on the discussion of *koto* construction, music, tuning, and the material and sound culture of the instrument. Malm's pioneering work on Japanese music included limited discussion on the acoustics of the instruments until his later publications, which includes some discussion of acoustics of Japanese drums (Malm 1986, 22-35).

Box shaped zithers are a wide family of instruments that have a documented connection from East Asia to North Africa (Hirota 1994). Additionally, it is thought that these instruments connect to both Eastern and Western European zithers as well as those found in the Americas (Reck 1977, 143). From the Japanese *koto* and Chinese *qin* to the Finnish *kantele,* this wide family of zithers globally make up an important group of instruments. While these instruments are all connected, they show particular regional features. For instance, the Middle Eastern and Eastern European instruments including the *santur, qanun,* and *gusli* are trapezoidal, whereas the Chinese and Japanese *qin* and *koto* are both long hollow boxes (Reck 1997,143).

The *koto* is closely related to many other instruments along the Silk Road, some invented as late as the 20th century. The acoustics of these instruments, much like the Japanese 13-string *koto*, are largely unknown. Table 2.1 shows a list of some known instruments in this zither family to which the Japanese *koto* belongs.

Table 2.1 The koto family (adapted from Hirota 1994)

Instrument	Location	Instrument	Location
Tonkori *Wagon* 1-string *koto* 2-string *koto*[4]	Japan	*Ajien* *Komungo* *Kayagum*	Korean peninsula
Taishogoto	Japan, India, Iran	*Zheng* *Qin*	China
Kuripi	Philippines	*Yanchin*	Mongolia, Korean peninsula, Japan
Mijon	Myanmar	*Sasando* *Churrenpun*	Indonesia
Veena	India	*Qanun*	West Asia, North Africa
Santur	Iran, India		

The list of instruments in the above figure is not exhaustive. The Asian zither family is a large family of instruments and it is beyond the scope of this discussion to include all of the instruments known in this family. Additionally, this thesis does not allow for a bigger discussion of the acoustics of the zither family as it aims to provide basic information about the acoustics of the *koto.*

The Japanese *koto*'s direct lineage is thought to be the Chinese *zheng*, and in its current form, the *koto* was established during the eighth century Nara period and its exterior has remained the same since (Johnson 2004, 169). However, stylistic and historical traditions have led to differences in the exact measurements and positioning used for each part of the instrument. Qualities of the materials, differing styles for preparing the wood, and even choices in the position of the tree from which the wood is cut all have an effect on the final instrument. Johnson (2004) gives a detailed discussion of these aspects and new studies are investigating the effect of these parameters on the acoustics of the instrument (Obataya, Zeniya and Endo-Ujie 2020).

[4] See Johnson (2004, 32) for reference to different variations of the 13-string instrument.

Gagaku, orchestral music of Japan from T'ang period (618-907 C.E.), can be traced as the original environment of *koto* performance.[5] Although the study refers to the *koto*, there are many variations of the instrument, each with its own size and measurements (Johnson 2004, 57). The instrument has been classified under a number of different groups within Japanese music based on its structure, sound, and performance tradition.[6] Two principal categories of *zōkuso* (common *koto*) are *Yamadagoto* and *Ikutagoto*. *Yamadagoto* (*Yamada koto*) are the most prominent today (Johnson 2004, 32). The *koto* model used in this study uses the measurements of a *Yamadagoto*. The sound holes are rounder than the key-hole shape of the *Ikutagoto*, and the tail of the instrument is more arched. It is also generally less ornamented than the *Ikutagoto*, shows more of the wood grain. It is historically played using pointed or rounded plectra, rather than the rounder plectra used in the *Ikuta* style of performance (Johnson 2004, 40-41). The *koto* has movable bridges, and so tuning of the pitches can vary. In *Hirajōshi* tuning (one of the most common), the pitches, starting from C, are as follows: E A B C E F A B C E F (Johnson 2004, 132).

The *Ikuta* and *Yamada* traditions remain the two prominent schools of *koto* performance today. The design of their instruments, performance styles, and repertoire are different (Wade 1976, 2-13). Since these two schools, the differences in design have been small adjustments that owe to performers, regional standards, performance schools of thought, and craft choices (Johnson 2004, 20-21). The Meiji Restoration of 1868 gave way for new

[5] The Heian period, the start of the "distinctive Japanese culture, secure in its adaptations of Chinese elements and confident of standing on its own" (Wade 1976, 4), started at the end of the eighth century. During this period, the arts flourished and so did the *koto* and its music. In the following centuries, analogous to and affected by societal changes, the performance settings of the *koto*, the music composed for the *koto*, and the performers of the instrument continued to change. The solo performance tradition on the instrument flourished in the tenth century. From this time forward *koto* music was varied across Japan. Buddhist and Confucian priests in Kyushu adapted *gagaku* performance of the *koto* from the popular to private spheres, facilitating the *kumiuta* repertoire of *koto* music. Historic figures from this point in the instrument's history include Yatsuhashi Kengyō, who brought *koto* music back to the public attention and Ikuta Kengyō, who repopularised the instrument and its performance by performing with the shamisen and used the shamisen as inspiration for *koto* music in his school of performance, *Ikuta ryū; Kengyō* was the highest title awarded to the blind male musician (Wade 1976, 10). Yamada Kengyō, was born nearly fifty years after Ikuta Kengyō's death and started the school of *Yamada ryū*, changing the common instrument accompanying the *koto* from the shamisen to the *biwa* and focusing more on narrative and song.

[6] Johnson (1996b, 22-23) provides a detailed explanation of the names of different types of *koto*, the reasoning and origin of the names and their use. In the 1996 paper, Johnson provides a comprehensive summary of the classifications of the *koto*, stating the instrument to be one of Japan's "most important national and traditional instruments" (Johnson 1996/1997, 43). Johnson uses this study to demonstrate concepts around lineage, cultural and national identity, especially in the historical context.

cross-cultural interaction and a wave of innovation in *koto* design followed, for example, the 17 string, 20 string, and the bass *koto*.

The *koto* body is made of *paulownia*, a light and flame-retardant wood (Johnson 2004, 58; Li and Oda 2007, 8544). Depending on the quality of the instrument, the wood is cut radially or tangentially to the direction of the growth of the tree. *Paulownia* itself is a highly anisotropic wood and electron microscope images of it show a porous structure with varying cell sizes and arrangements.[7] There exist 5 to 7 accepted species of *paulownia*, with up to around 30 variations documented in total (The Wood Database 2015). The single elastic modulus of three of the accepted varieties, *tomentosa*, *elongata*, and *fortune,* are 4.3, 2.6-3.8, and 4.9GPa respectively (The Wood Database 2015; Kayamakci et al. 2013, 918). Understanding the effect of the woods used can be helpful in classifying instruments, since they draw some common characteristics from the wood. Yoshikawa draws on Ando's 1986 and 1996 studies of the *koto* and relates the difference between the woods to the construction practices of instruments; he compares between East Asian and Western instruments in terms of sound radiation (2010, 170 and 190).

During the construction of the *koto*, the top plate is carved out with an adze and the plates are cut to the correct dimensions after which, the plates are dried. Internal carvings around the sound holes are often made. The plates are then joined, with internal struts positioned along the body. The plates are scorched and waxed repeatedly. The surface of the instrument is lightly scorched and waxed, unlike the *qin* or other similar instruments. Which are varnished or laquered. Strings are stretched and wound on top of the instrument. In the construction of the *koto*, knots in the wood are repaired using fillers or by plugging holes into the plates (Johnson 2004, 64). Since knots cause wood to have lower stiffness and strength (Gibson and Ashby 1997, 301), this repair during the construction contributes to the strength of the instrument body.

The first and one of the few acoustical studies of the *koto* is Yoshinori Ando's 1986 paper, *Acoustics of Sohs "koto"s,* is only two pages in length. The paper outlines the major modes of

[7] More details in the Chapter Five.

vibration of the plates of the instrument, the frequency spectra of the tones the instrument is played at, and how they decay over time (Ando 1986). Ando published a second paper on the resonances of the *koto* in 1996, but this paper is only available in Japanese. Subsequent publications such as those by Yoshikawa (2010), Fletcher and Rossing (1991) all refer back to Ando's 1986 and 1996 papers. Yoshikawa briefly discusses the *koto* in his overview of Asian plucked string instruments (Yoshikawa 2010). Fletcher and Rossing (1991, 289) briefly discuss the *koto*'s response, comment on Ando, and focus on the strength of the response near 400 Hz. Waltham and Yoshikawa report on the construction and the use of *paulownia* for East Asian string instrument soundboards (Waltham and Yoshikawa 2018). By comparison, Yoshikawa (2014) examines the *koto*'s behaviour in comparison to other East Asian zithers, using wood properties as a guide. Coaldrake's study of the *koto*'s acoustical properties is the most comprehensive study of the instrument's sound to date (Coaldrake 2012, 2018, 2019a and 2019b).

Coaldrake has designed a finite element model of the sounding box of her *koto,* which is of known provenance (from this point referred to as the Coaldrake Model and the CT scan model), and has also used CT (computered tomography) scans of the instrument to measure its internal dimensions, locate internal points, and refine the measurements on the model. She has also used SEM (scanning electron microscope) results to measure the grain of the *paulownia* wood and its density, to more accurately model the physical properties of the wood, which reveals its uneven grain structure (Coaldrake 2019, 7553). The Coaldrake model consists of a box with the dimensions, attributes, and the grain density of the *paulownia* wood. The model is represented as a physical body in a three-dimensional space in COMSOL Multiphysics, where it can be excited by energy input at any point on the body investigated closely[8]. This analysis can include the resonant motion of the box, the change in the

[8] Sonification of these waveforms can be misleading, as there are issues of DAC (digital to audio converter) algorithm and playback that cause the output of these models to sound similar to an early digital synthesiser. Future studies with a larger scope can focus on sonification of these waveforms. Replicating an instrument's behaviour in sonification of models often loses much allure, but sonification is a separate study that is outside the scope of this discussion. However, it is necessary to state, that although the sound heard from the model resembles simple synthesisers, that aspect can be refined and explored by addressing the signal chain that sonifies the result, and the sound as is *heard*, does not represent the accuracy of the model's output in terms of acoustical behaviour

surrounding air pressure in the form of an audio output, and the spatial diffusion of energy from the instrument.

This model, though the most rigorously accurate model of the instrument body yet, is extremely computationally-intensive to run, and therefore it cannot readily be used for studies of individual components. Unlike the violin studies, and other European wooden string instruments, no simple model of the *koto* has been available; a simple finite element model of the *koto* is needed to provide more information about the acoustical function of the components of the body and to study the basic features of the sound of the *koto*. A simpler model can be modified to investigate the changes in its design and predict the behaviour of the *koto* were it to be subject to such changes. The study, using simple models, with a case study of heuristic models of the *koto,* documented in this thesis, provides the groundwork for future analytical models of East Asian zithers.

Chapter 3

Methods

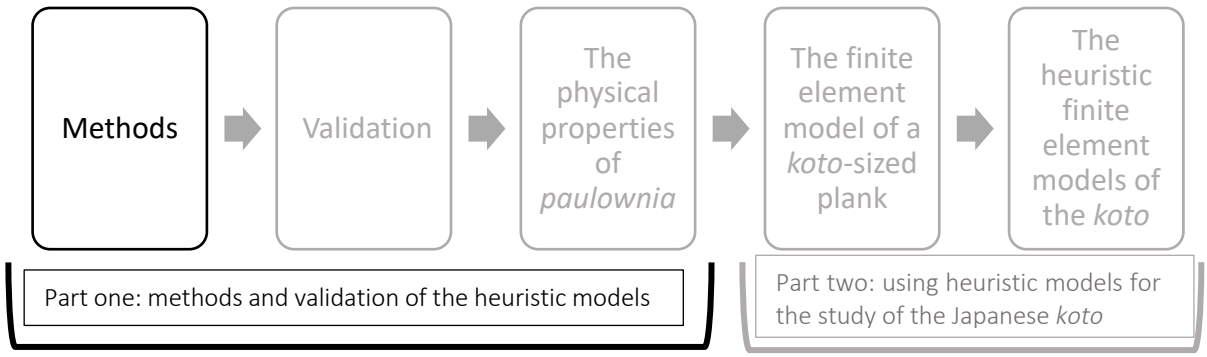

This chapter describes the finite element methods and the heuristic models used in this study. First, it presents an overview of the method before providing explanations of key terminology relating to the modelling discussion. The information presented in this chapter is directed at describing the methods used in this study of the *koto.* It is also intended to serve as a template of the studies undertaken with each model and the method of analysing results is presented. Results from the studies and this discussion are presented in Part Two. Figure 3.1 gives a summary of the methods used in this work.

Overview of the methods

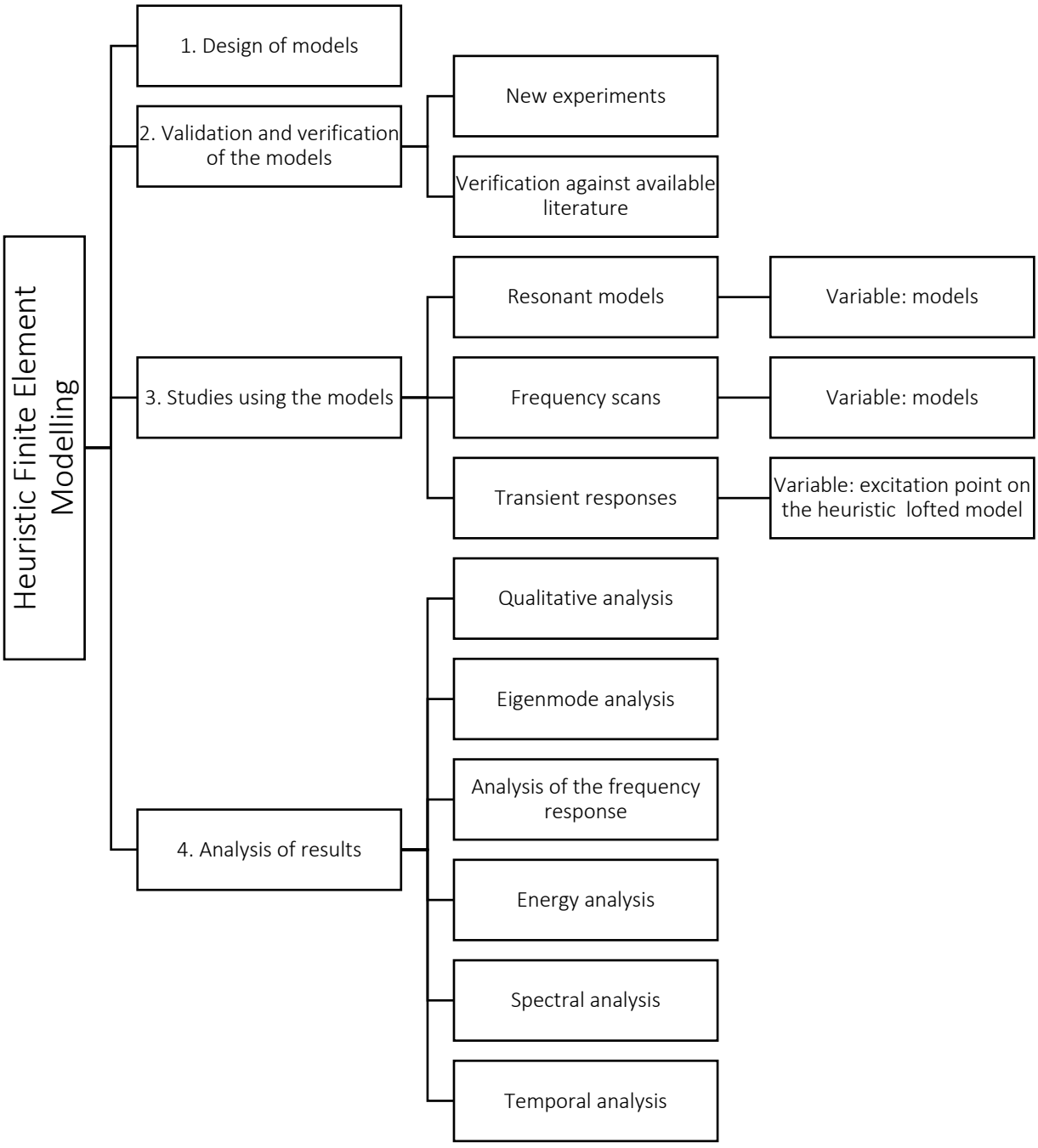

Figure 3.1 Overview of the methods used in the study

There are four main categories of methods used in this study: model design, validation, studies and analysis. Figure 3.1 presents an overview of these categories; these steps are taken for the investigation of the *koto* presented in Part Two.

In summary, models were designed in COMSOL, then validated using new experiments and verified against the limited existing literature to ensure that the analysis was as accurate as possible. When necessary, further work was undertaken to improve accuracy to within a determined margin of error.[1] The studies were conducted next; these studies follow the logic of COMSOL, where the models are designed, the study parameters are set, and the data collection is decided. these studies identified the resonances of the body (modal domain), analysed the radiation of different frequencies from the *koto* body into the air (frequency response) and studied the decay of sound from the instrument model (transient studies). Qualitative observations of the data obtained provided the initial steps towards the understanding of the instrument's basic acoustical response. Quantitative analysis of the heuristic models was then undertaken. The quantitative analysis aimed to uncover the basic features of the sound of the *koto* with heuristic models of the *koto* and a *koto*-sized *paulownia* plank. These models were used to obtain the resonances of the wooden body, its interaction with the surrounding air, followed by the assessment of the transient response. The steps detailed in Figure 3.1 are used first for the study of the model of a *koto*-sized plank (Chapter Six) and then for the study of the *koto* (Chapter Seven) using the heuristic models. The remainder of this chapter will discuss the application of each step in the study of the *koto.* The results from the studies and the findings of the analyses are presented in Part Two of this thesis.

Specific terminology used in this heuristic modelling of the *koto*

Models are considered heuristic in this study if they provide reliable information about one aspect of the acoustical response of the *koto*. These heuristic models do not individually provide comprehensive information about the instrument, but the information they do predict is considered accurate within the defined margins of the study. By contrast, a high-resolution model predicts the response of the instrument in a highly accurate way but does not allow for testing simple variations.

[1] Further details of the validation and verification process are documented in Chapter Four. Methods used for improving the available data on the physical properties of *paulownia* are documented in Chapter Five.

This study uses terminology from organology and musicology to refer to the instrument body, coordinates, and components. In Table 3.1, lists terminology used throughout the document to refer to components of the *koto*, tools, and techniques and provides an explanation for each. Generic disciplinary terms for acoustical analysis are presented in the Glossary at the end of Volume I.

Table 3.1 Terminology used in finite element modelling of the koto

Term	Definition	Details
Dragon's head	Player's end of the instrument, where the small chamber is located, as well as the maximum arching of the body.	The *koto* is symbolically shaped like a dragon, with its head at the player's end, and an ornamental dragon's tongue is sometimes seen at the end plate near the player's end. (Johnson 2004, 54). Other terms used include the end of the instrument with the small chamber; player's end.
Dragon's tail	End of the instrument away from the player, featuring a keyhole shaped sound hole. This end is the position at which the strings are wrapped together.	Symbolically, this position refers to the dragon's tail (Johnson 2004, 55).
Top shell	The curved shell found on the top of the *koto. T*he strings are stretched on this plate. This shell is in one piece and its side walls that are carved from the wood with the top part of the shell. The side walls from this shell attach to the base plate.	Also called top plate in this thesis. This shell is also called the soundboard (Johnson 2004, 58).
Base plate	The bottom plate found of the *koto*, where the sound holes are placed.	This plate is also called the backboard, a dragon's back or a dragon's belly; it can be connected to the top shell wither perpendicularly or at an angle; this plate is reportedly close to 1cm in thickness. (Johnson 2004, 55, 64).
Small chamber	A small chamber that can be found inside the *koto*'s body, at the dragon's head end of the instrument.	Also titled the resonant chamber; the small internal chamber. This chamber is separated with a dividing wall inside the body.
Main air cavity	The hollow inside of the *koto* body.	Main air chamber.
First sound hole	Sound hole close to smaller internal chamber at player's end of the instrument (dragon's head).	Round sound hole and distinguished from the keyhole-shaped sound hole.
Second sound hole	Sound hole at minimum arching, away from the player's end of the instrument (dragon's tail).	Keyhole-shaped sound hole.
Arching along body	The curvature along the top of the *koto* body observed from the side when it is placed horizontally in playing position on the floor.	Also described as "along a dragon's spine" (Johnson 2004, 54).
Curvature across top	The curvature across top plate where the 13 strings are placed. It is observed best from either end of the instrument or by using a cross-section in the model.	
Ears	Small indentation inside the body that run along the inside wall at the joining part of the side walls and the top of the top shell.	

Player's side	The player sits closest to string 13 on the resonant chamber end of the instrument. The opposite side is called the 'audience's side'	String 1 side; side 1.
Cross-section 1 location	1.58 meters away from player's end of instrument	Minimum arching.
Cross-section 2 location	0.42 meters away from player's end of the instrument	Maximum arching.
x, y and z-axes	These axes represent Cartesian axes. In this case, the x-axis points along the long axis of the instrument; the y-axis is perpendicular to the x-axis; the z-axis is the vertical axis, measured on a hypothetical (xy) plane on which the instrument sits.	
Heuristic models	Models that approximate the subject of the study with the aim of understanding the behaviour of the system. These models are different from models that try to replicate or synthesise the subject of the study.	
Lofted model	A heuristic model of the *koto* body made using measurements from 10 cross-sections along the body. The outer geometry is then 'stretched' on the outer perimeter of the cross-sections. This model thus incorporates the changing width, elevation and arching of the *koto.*	

The terminology used in Table 3.1 is visually represented on the model in Figure 3.2, where the features of the lofted model are shown.

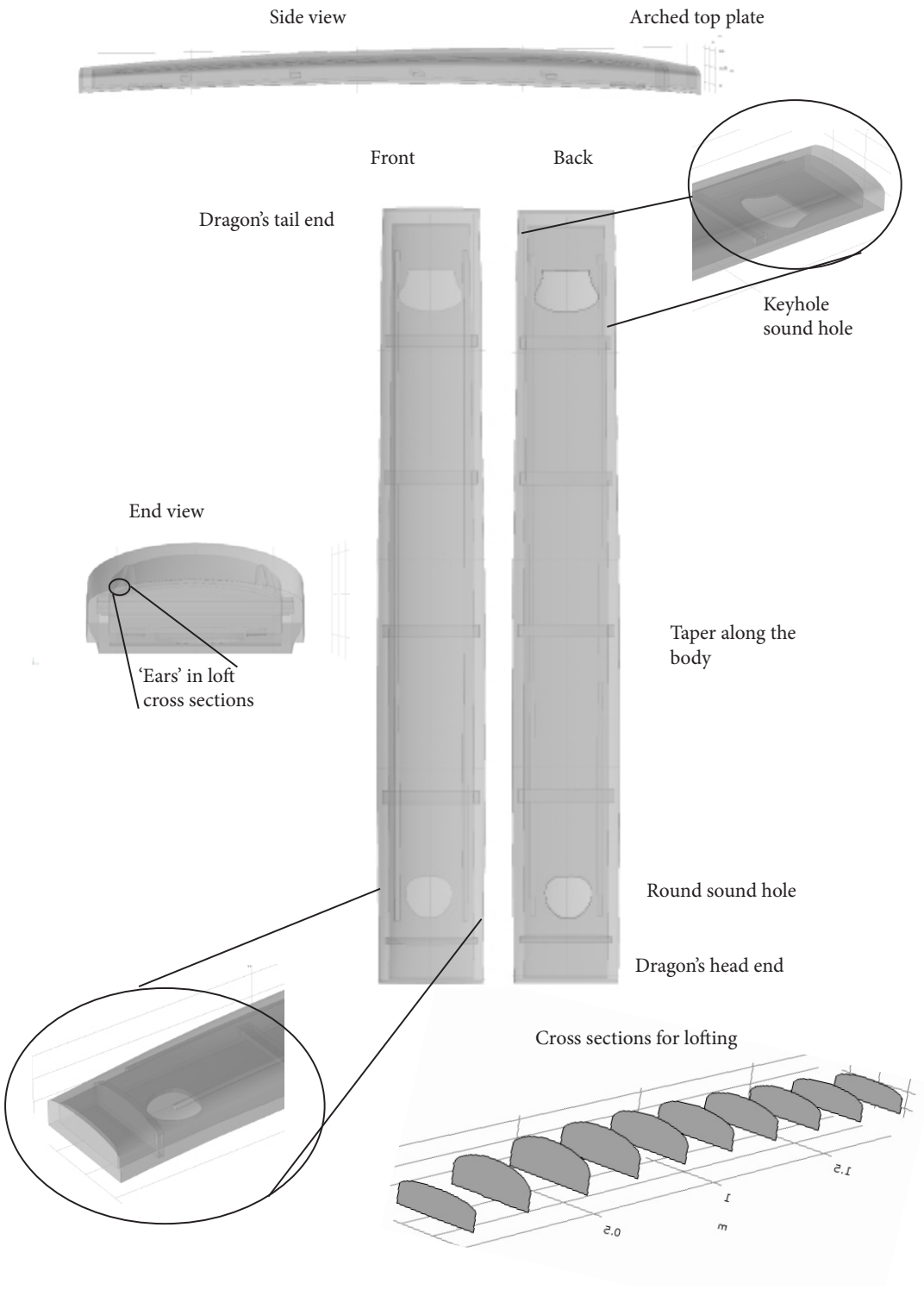

Figure 3.2 Lofted model of the koto and its features

Overview of the Heuristic Models

This study initially employed three sets of heuristic models: the model of a *koto*-sized plank, box models of the *koto*, and the lofted model. The designs of models increase in complexity from the plank to the lofted model. The plank model is the simplest model and is used to examine the response of the *paulownia* wood without the complexity of the *koto* geometry.[2] The box models provided an intermediary step in adding complexity to the models and were useful for testing purposes. The lofted model was then developed to follow the simpler models and provided useful material about the transient response of the *koto* in this investigation.

It was later found necessary to develop a fourth set of models comprising variations of the top shell and the base plate of the *koto* (hereafter substructure models). The box models and the models of the substructures were used to study the role of individual components of the body.[3] The results of the sets of models were compared with the findings from a CT scan-based, high resolution and fully validated finite element model of the *koto*, developed by Coaldrake (hereafter the Coaldrake Model or the Coaldrake CT scan model). Results from physical experiments using Coaldrake's own *koto* (a *Yamadagoto*) were also used for the validation and evaluation of the more complex lofted model.

From the plank model to the heuristic lofted model

The four sets of models contribute independently to the development of the methods of the study or investigation of the acoustics of the *koto*. Table 3.2 summarises the types of models

---

[2] Given the lack of information on the instrument and *paulownia*, required for COMSOL modelling, this step was necessary to anchor the study and provide a baseline for the analysis of *koto* models.

[3] For existing studies, it has been seen that the modes of uncoupled plates are not easily seen in the coupled full system of the instrument, and that sometimes the full instrument body can be considered as a separate object with its own characteristics (Bader 2005, 2-3). As shown for the violin, the full instrument has its own characteristic resonances that differ from individual plates. The final output of the full instrument is made up from the individual parts as well as their coupling. Untangling the individual parts from the whole instruments is not easily achieved due to the complex resonances of the full instrument. Even so, full body and substructure models are a reasonable way to approach the task of separating the role of individual parts from the response of the entire body.[3]

used, specific details of the models in each type, and their purpose. The first two sets of the models are more useful for refining the methods of the analysis whereas types 3 and 4 are employed for the discovery of the acoustical response of the *koto.*

Table 3.2 The four sets of models used in the study of the koto

Model type	Purpose	Models	Studies
1. Plank	1. Validation of the physical properties used for modelling. 2. Establishing a baseline for the use of the heuristic models of the *koto.*	Simple plank	All studies
2. Full-body box models	Exploratory models used to assess the merits of using box models as heuristic models in the study of the *koto*	1. Hollow box with no struts and no sound holes 2. Hollow box with two sound holes 3. Hollow box models with (0-5) struts; 4. The box model with four struts; the idealised box model.	Eigenmodes Frequency scans
3. Substructures of the *koto*	1. Examination of varying the geometry of the top shell and the base plate and observation of the role of individual components of the body (see Table 3.3) 2. Replicating Ando's (1986) method for the study of the modes of the *koto* as a means to clarify his results.	1. Top shell and variations 2. Base plate and variations	Eigenmodes
4. The lofted model	Discovery of the transient response of the *koto* and establishing a heuristic model for the detailed analysis of the results.	The lofted model (see Figure 3.2)	All studies

There are many other more possible variations that could be used to test specific features. The variations tested in this study are those that were considered the most crucial to understanding the basic response of the *koto*. The top shell of the *koto* and the curves along and across it are important to the geometry of the instrument. Many variations of the top shell were tested and to clarify the differences between them, Table 3.3 further visually elaborates on the detail of the variations in the top shell models from three perspectives.

Table 3.3 Geometric variations in the top shell substructures from 3 perspectives

Model	Top view (xy)	Side view (zx)	End view (yz)
Flat			
Steady arching			
Full arching			
Taper no arching			
Taper steady arching			
Taper full arching			
Taper full arching with ears			

In Table 3.3, three perspectives (views) are presented for each top shell. The effect of 'steady' arching is best observed in the end view; steady arching refers to uniform curvature along the body. The difference between the instrument arching and the 'steady' arching is made clear using the side view. Tapering is less visible, but clearest from the top view. For comparison, variations in the base plate models are charted in Table 3.4. With the base plate variations, the number and shape of sound holes was examined. The size of the base plate itself remains the same in all base plates.

Table 3.4 Variations in the base plate

Model	Top view (xy)
No holes	
Sound hole	
Sound hole 2	
one circular hole	
two circular holes	
two sound holes	

Struts, also called supports, or cross-pieces, are added to the hollowed out top plate before joining it with the bottom plate in an effort to stop the warping of the instrument; *koto* usually have four or five struts (Johnson 2004, 62). *Yamadagoto* usually have four struts and this study uses four struts in the idealised box and lofted models. To observe the sensitivity of the model's response to the number of struts, struts were added one by one to the model. Table 3.5 shows the main box models in this study from the top.

Table 3.5 The box models in this study

Model	Top view (xy)
Hollow box no struts	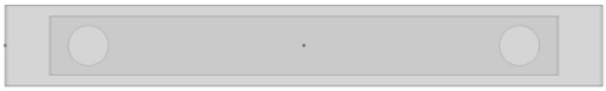
Hollow box 1 strut	
Hollow box 2 struts	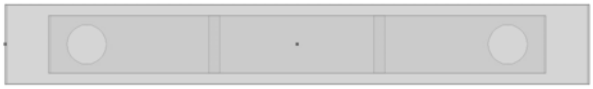
Hollow box 3 struts	
Box 4 struts (idealised box model)	

Table 3.5 shows the placement of the struts as they are individually added to the models; the struts are positioned symmetrically within the hollow part of the box models. As these are heuristic models, moving the struts would have caused additional complexity in the study before there was a baseline for the analysis and could have misled the analysis.

The lofted model

The lofted model includes new geometric details. This model combines the geometric detail in the top shell with the base plate and adds the small internal chamber, which is separated by a joining wall inside the body.[4] A lofted model uses cross-sections of the outer dimensions, with the geometry 'stretched' over the top. I

[4] Ideally, these aspects would be individually incorporated. However, this many model variations were not feasible within the resources available to the study. Coaldrake's earlier studies of the *koto* (Coaldrake 2012) have tested more of these variations in the lofted model.

The lofted model was made by using 10 cross-sections of the body (from measurement of a *Yamadagoto*). The lofted model's cross-sections (Figure 3.2) were constructed of a rectangle with an ellipse on top and the arching of the shell was achieved by lofting between the cross-sections.[5] Figure 3.3 shows the four steps of creating each cross-section.

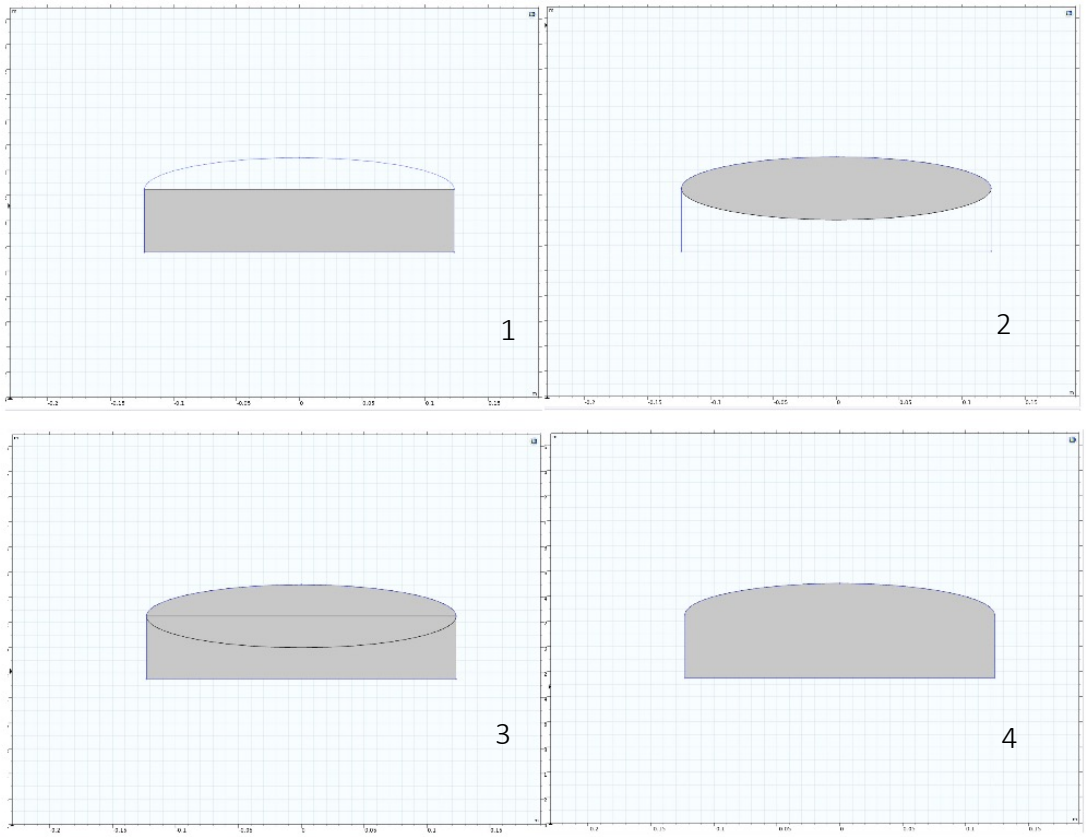

Figure 3.3 Building each cross-section used for lofting with a rectangle and an ellipse

Figure 3.3 shows the combination of the ellipse and rectangle to form each cross-section. The major axis in the ellipse (horizontal) is coincident with the length of the rectangle; this value determines the width of the body at each cross-section and is changed to build tapering into the model. The height of the minor semi-axis (vertical) in the ellipse determines the amount of arching at that cross-section and is changed to add the arching along the top shell. This heuristic study does not model the complex features in the inner wall; thus, it needs a systematic method for building the inner shell. The dimensions in each of the three axes were

[5]Measurements of ellipse and rectangle were made available to the author by A. K. Coaldrake.

scaled down from the outer loft to build the inner loft. The scaling is as follows: x=98%; y=80%; z=80%. This scaling gives an approximation of the thickness of the top shell. Also, with this scaling, the resultant side walls are 11mm thick, which matches the CT scan results of Coaldrake's *Yamadagoto.* The wooden wall that separates the main air cavity from the small internal chamber is estimated to be 1.2mm thick from the analysis of the cross-section images of a CT-scan of the instrument, provided to this author. The shape and size of the sound holes were traced from Coakdrake's own *Yamadagoto* and drawn in the model using Bézier curves.

Overview of the finite element set up

The finite element models are built and studied in the COMSOL Multiphysics environment. This section provides an overview of the main steps taken in COMSOL to do this work. The key factors are the models of the *koto* and its substructures, the physical properties used for *paulownia*, the meshing process, and (where necessary), the excitation of the model. Figure 3.4 shows the COMSOL study set up with the lofted model in a sphere of air.

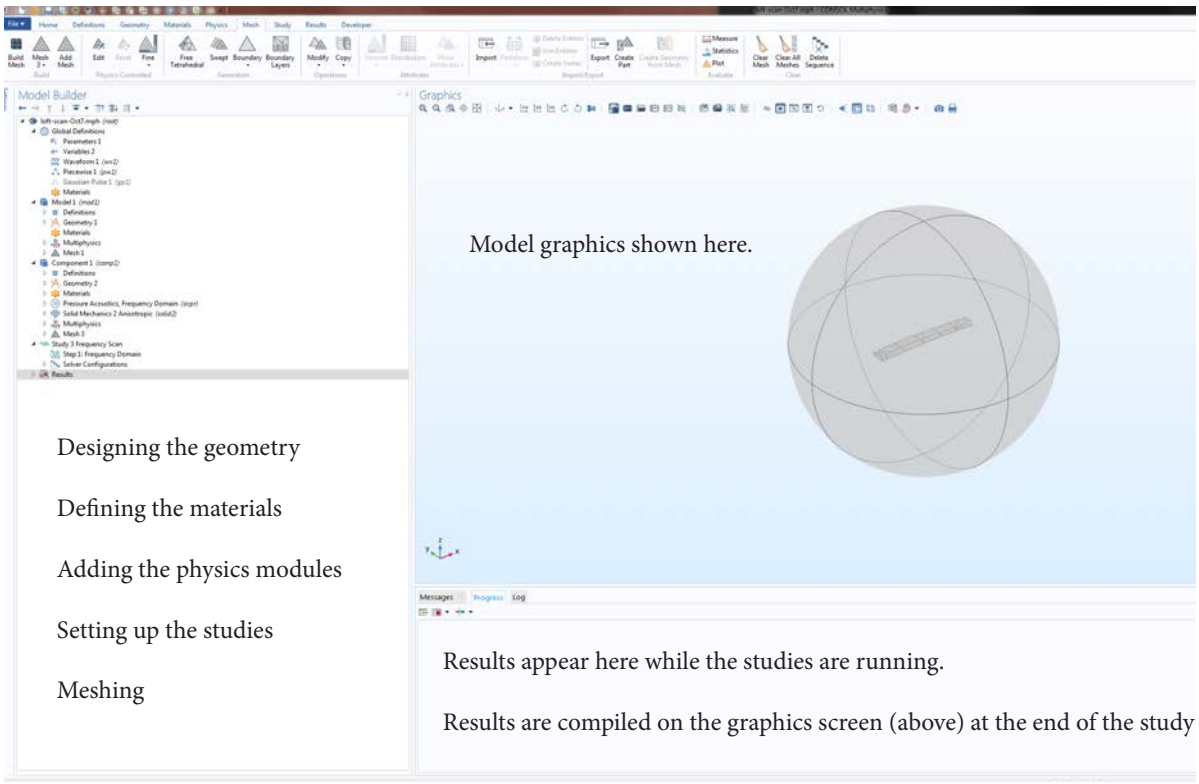

Figure 3.4 COMSOL study set up

All settings and steps needed are defined on the left-hand side bar in COMSOL (Figure 3.4); parameters for the geometry, the materials and physics modules necessary for the study, and

the study settings are all navigated in this side bar. The central window which shows the graphics is used for navigating the geometry and ensures that the researcher has a visual representation of the model. The bottom bar shows the results as they appear. Depending on the study, additional probes, detailed later, are used to gather results from the model.

This is a heuristic study and does not use high-performance computing. However, the transient studies are RAM-intensive and standard computer power available in most laptops and desktops is not enough for running these studies in COMSOL. The specifications of the computer used in this project are presented in Table 3.6.

Table 3.6 Computer specifications

Hardware	Specification
Computer	Lenovo Workstation T5 P700
Operating system	Windows 7 Professional
Processor	2 x Intel Xeon E5 3.4GHz
Memory	3 x 3TB HDDs
RAM	96GB
Software used throughout project	COMSOL Multiphysics (versions 5.2-5.4); OriginLab 9.2 and OriginPro 2018; Adobe Suite for visualisation and datasets.

In addition to the computer power needed for running the COMSOL models shown in Table 3.6, the results require a large hard drive storage. An additional 12TB of data was stored externally to the computer. This resource-intensive aspect of the simulations in the time domain studies is a reason transient studies are not often conducted with finite element modelling is. The heuristic studies undertaken required considerable RAM to operate and still took up to two weeks to return one second of results in a transient study (48,000 points). For this reason, the models and the studies were carefully selected to ensure that only the most critical studies were conducted in the time domain.

Paulownia wood

Within the COMSOL environment, approximations of the physical properties of the wood are attributed to the geometry of the models to simulate the materials. The physical properties

used for the *paulownia* body of the *koto* in this study are orthotropic in symmetry and were the best available information at the time of the analysis.[6] Woods are considered to be (generally) anisotropic; they have different amounts of stiffness and elasticity in each direction, which leads from the general observation that they are stronger along than across their grain. This anisotropy is often simplified to orthotropic symmetry in their stiffness and elasticity, which means the material has 3 axes of symmetry.[7] Some woods have been extensively investigated and reliable information exists on their elastic constants, density, and the speed of sound in each of the tangential, radial and longitudinal directions. In contrast, there is far less literature available on the anisotropic properties of *paulownia*. In this work, the values shown in Table 3.7 have been used for elasticity.[8] This table contains the best values available to the author at the time of the analysis. Chapters Four and Five discuss the process of validating and attempts at optimising the values. As further discussed in these chapters, these values are kept and used for the studies of the models. Throughout this study, the properties are referred to as CW.2 properties, as the properties were obtained by Chris Waltham of the University of British Columbia and made available to the author and A. K. Coaldrake for the *koto* research.

Table 3.7 CW.2 Properties used in this study to model the elasticity of paulownia, based on Waltham's results (2015).

Parameter	Definition	Value used (GPa)
EL	Longitudinal Young's modulus	5.6
ER	Radial Young's modulus	0.63
ET	Tangential Young's modulus	0.26
GLR	Shear modulus (longitudinal/radial)	0.52
GLT	Shear modulus (longitudinal/tangential)	0.37

[6] Coaldrake's recent work (2019) shows that the assumption of orthotropic symmetry is an issue in high-resolution modelling of the wood. This aspect is discussed further in Chapter Five.

[7] Materials can be generally divided to isotropic and anisotropic materials. Isotropic materials are approximated or considered to have the same elasticity in all three Cartesian directions, and so they have one Young's modulus of elasticity, one Poisson's ratio, and shear modulus. Broadly, all other materials are anisotropic, though full anisotropy in materials is not often included.

[8] Voigt matrix is a method for representing a symmetrical matrix, here used for the physical properties of the *paulownia* wood.

To input these parameters (Table 3.7) into the COMSOL environment, they are converted to a Voigt matrix, which is a system of matrix notation. Poisson's ratio of 0.4 is used in this model. According to Gibson and Ashby, the in-plane Poisson's ratios of the wood are 0.65 and 0.35, and in the axial direction is about 0.4 (Gibson and Ashby, 308). The wood density is 260kg/m^3 and the speed of sound in wood is 3200m/s. No material damping is considered in this work. There are no adjustable parameters for the physical properties of *paulownia*.

Air

Air is added to the models of the wooden body to analyse transmission and dissipation of sound from the body to the air. The air is in the form of a sphere of 2.2 meters in radius in the frequency scans. The transient studies are much more computationally intensive than frequency scans and the surrounding air was reduced to a cylinder of 1.3m radius and 3.6 meters height. The Young's modulus of the air is 10kPa, and the Poisson's ratio is 0.5. The speed of sound 343m/s in air. The temperature in the COMSOL model is 20 degrees Celsius.

Perfectly Matched Layers

Frequency domain studies absorb reflections from the edges of the sphere of air using six perfectly matched layers (PMLs). PMLs are artificial layers added to the outer edges of the sphere that simulate a continuing boundary. These added layers help to absorb the simulated sound waves, so that they do not reflect off of the internal boundaries of the air, which would cause standing waves and affect the radiation patterns for each frequency as well as the frequency response peaks. The space between two PML layers is 4cm. Adding any PMLs increased computation time of time domain studies too much and therefore PMLs were not included in the transient studies. Once the wooden body and the surrounding air are defined in the COMSOL model, probes are placed in the air model. These probes are placed at points which are of interest to the analysis.

Probes

Probes are placed within the air surrounding the instrument as well as inside the models. They measure the time-averaged total air pressure at each frequency in the frequency scans and the air pressure at each point in time for transient studies. Figure 3.5a includes every probe used in the frequency scans and in the transient studies.

After initial observations, only the probes in Figure 3.5b were used for detailed analysis. The analysis of the transient responses first used the waveforms. General observations about the sound can be made using qualitative assessment of the waveform output. This meant plotting all probes of each transient response; the observations from this analysis show which probes show a stronger response i.e. where the air pressure changes are highest and consequently, the sound is loudest. They also show the directionality of the sound, from observing any differences between the probes. The probes placed inside two air chambers of the *koto* model are marked in green; the probes placed in the surrounding air are in red. Although the transient studies do not use a sphere of air, the probes shown in Figure 3.5 are used in the same positions relative to the heuristic lofted models.

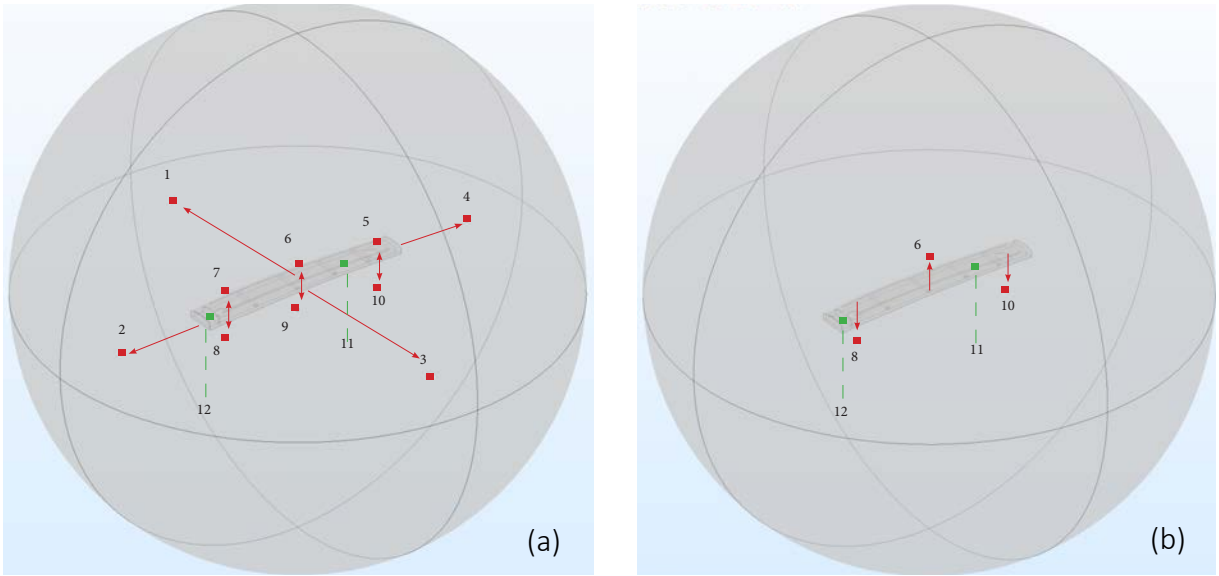

Probes 1 and 3: parallel to lofted model, either side; probes 2 and 4: parallel to lofted model, either end; probes 6 and 9: above and below midpoint; probes 5, 7, 8, 10: above and below sound holes; probes 11: inside main air cavity; probe 12: inside small chamber.[9]

[9] In the software modelling environment of this study (COMSOL), the virtual object that measures this pressure is called a probe. The thesis uses the term probe to retain consistency across the modelling platform, the data presented in the study, and the thesis. In a laboratory, the object used to measure pressure is a barometer; in

Figure 3.5 Probes used in the COMSOL studies

Selecting fewer probes for detailed analysis (Figure 3.5b) is a part of the heuristic modelling and also helps to manage the amount of data analysed, thereby allowing for more analysis of a smaller, more critical, dataset.

After defining the shapes and dimensions in the models, the geometries of the wood and air in the models need to be meshed. The meshing step is a critical part of finite element modelling, as the geometry is turned into the mesh 'elements' for simulation.

Meshing

In the meshing process, the geometry is broken down into small tetrahedra, or elements, and is rebuilt from these elements. The exact response of a complex object such as the *koto* is almost impossible to simulate in one event. The idea behind finite element modelling is to divide a complex system (such as the *koto*) to small elements; the response of each element to a force can be determined; the final response of the complex object is then predicted from the response of individual elements. Given this design, the more elements there are in a system, or the smaller the mesh size, the more computationally intensive the study is. With more elements, there are more degrees of freedom (DOF) and computation time increases because the software predicts the response in each element.

To create the model's mesh in COMSOL, the wooden body can be meshed separately from the air. Six elements per wavelength of the sound is generally considered necessary; for instance, if the model is aimed to have an accurate result in frequencies as low as 100Hz in air, the model mesh size would have to be a maximum of 0.57 meters.[10] Coaldrake (2019) has found that as many as 20 elements per wavelength are needed for the air and 12 elements

---

this modelling environment, it is a probe in a simulation of a sphere of air. Given that the study measures acoustical pressure, in a physical experiment a microphone may be used.

[10] As the frequency of analysis increases, the wavelength becomes smaller and the maximum element size decreases. To model 1000Hz in air, the maximum element size is 0.057 meters. Both material and geometry are important in meshing. Complex parts of the *koto* models' geometry require smaller meshes to build the curves accurately.

per wavelength is needed for the wood. Here, it was not feasible to use 12 mesh elements per wavelength, and instead, mesh analysis was done to find three levels of mesh sizes which gave a consistent response from the model, thereby ensuring that the model was mesh-independent. The validation of the model (detailed in Chapter Five) also suggests that the meshes used are reliable. The model used for the analyses, after varying mesh sizes, has 135,723 elements and a total of 1,655,310 DOF and an average mesh quality of 0.7. However, it was beyond the resources available to this study to conduct a formal analysis of meshes. Mesh size was tested for the lofted model using eigenmodes and refined until three consecutive mesh sizes showed the same response. A transient study of the plank was used to test the meshing of the air because the plank is less resource intensive to test.

Mesh analysis of the koto model

Mesh analysis of the lofted model showed consistent results with mesh element sizes equal to and smaller than 0.14m. The COMSOL 'normal' mesh size has a maximum element size of 0.183m; in the lofted model, this mesh size gives 10685 domain elements, 7132 boundary elements and 1248 edge elements. The 'fine' mesh setting has a maximum mesh size of 0.146m; this size gives 24629 domain elements, 15264 boundary elements and 1731 edge elements. The 'finer' mesh setting has a maximum element size of 0.1m; this setting gives 88028 domain elements, 44834 boundary elements, and 2861 edge elements. The 'extra fine' setting has a maximum element size of 0.0639m; this setting gives 343938 domain elements, 96698 boundary elements and 5179 edge elements.

Figure 3.6 details the comparison of the three acceptable mesh sizes and the unacceptable (too large) 'normal' mesh size of 0.18m.

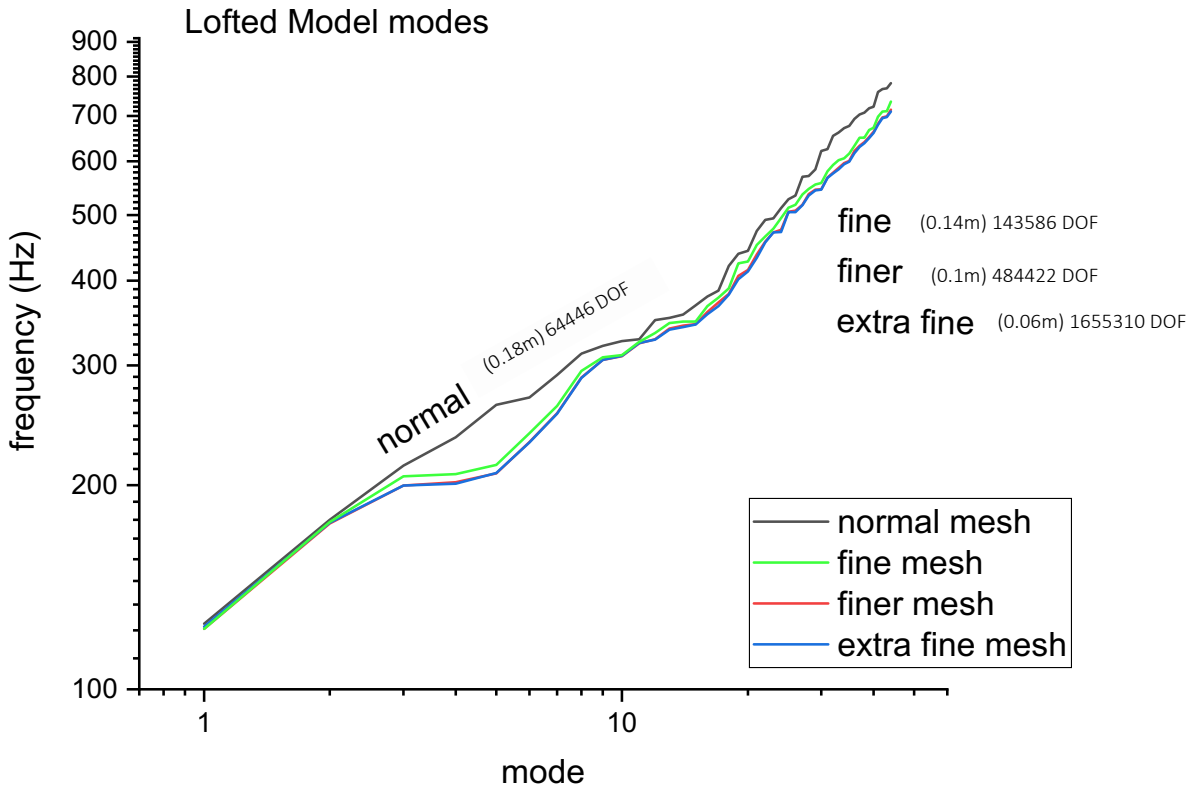

Figure 3.6 Mesh variation in lofted model

Figure 3.6 shows that the normal mesh size of 0.18m is too large and it can be considered a bad mesh because the results from this mesh are not seen in other mesh sizes. The next three levels of mesh size provide consistent values for frequency and approach a better mesh. Table 3.8 shows the slopes of the four mesh sizes tested obtained.

Table 3.8 Slopes of resonant modes of the heuristic lofted model for each mesh size

PLOT	NORMAL MESH	FINE MESH	FINER MESH	EXTRA FINE MESH
INTERCEPT	169.68	166.26	162.47	161.33
SLOPE	14.32	13.08	12.77	12.71
R-SQUARE (COD)	0.99	0.99	0.99	0.99
ADJ. R-SQUARE	0.99	0.99	0.99	0.99

The slopes of the models are closer in the final mesh sizes and within the bounds of the study, the extra fine mesh size (0.06m) can be considered reliable. Smaller meshes could not be

tested as they would cause a crash in the computer. The average mesh quality of the wood is 0.85 at this mesh size and the results were as stable as possible at the three smaller levels. The mesh analysis for the wood was done in isolation, using its resonant modes. By contrast, the mesh analysis of the air needed to be done with frequency scans or transient studies because the study of the eigenmodes are done *in vacuo*.

Because the sound pressure is measured in the air inside and outside the *koto* models, the air mesh is critical. Since the speed of sound is lower in air, the wavelength in air is shorter and therefore element sizes are smaller in air.

Mesh analysis of the air model

Figure 3.7 shows the transient response of the plank in a cylinder of air, tested with three mesh sizes. The maximum element size in the mesh sizes is shown in brackets. The average mesh quality for the air was 0.7 in all three mesh sizes.

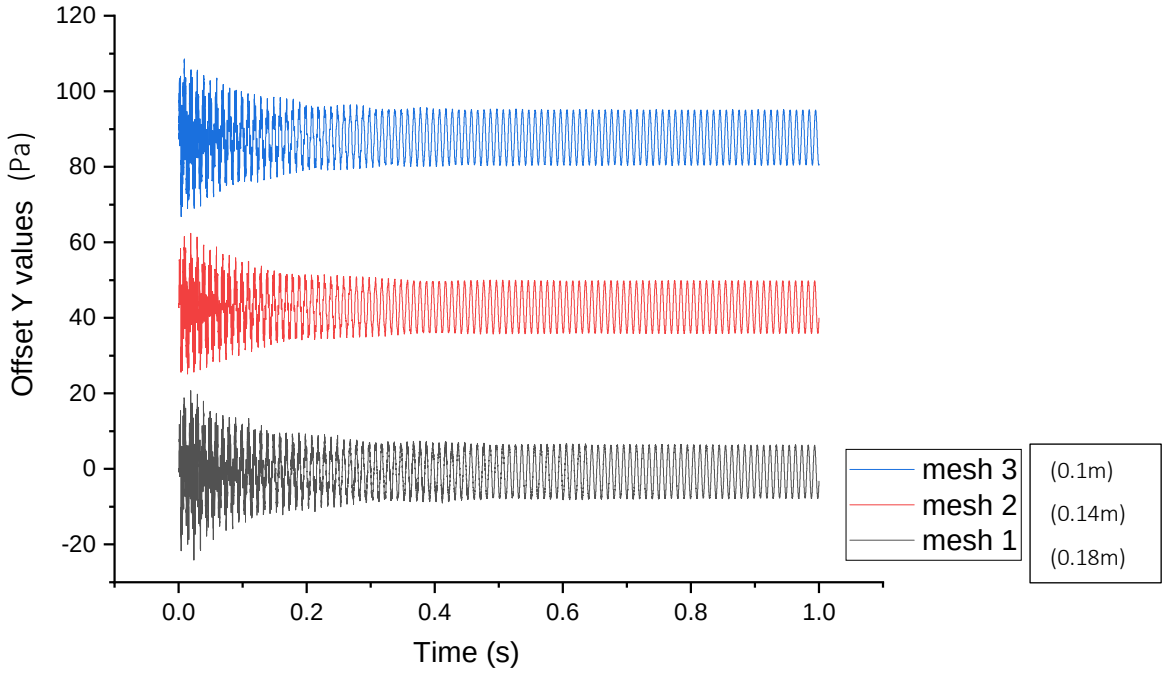

Figure 3.7 Mesh analysis in transient response with plank

Figure 3.7 shows that the model is independent of mesh size because the responses are similar, which means that the response can be relied on. In this case, no 'bad' mesh was used because of the time-intensive feature of the transient studies.[11] [12]

The meshed models were 'excited' in the frequency scans and the transient studies; energy was input to them to observe the response of the heuristic models.

Excitation

In the frequency scans and transient studies, a force is input to the models and the response is measured. In the frequency scans the force is a 0.1 Newton point load into the centre of the top of each model. In the transient studies, an impulsive force of duration 4.5ms is applied. The force is input to the lofted model to excite it and capture the transient response. Table 3.9 shows the definition of the pulse. This force is input perpendicularly to the plate.

Table 3.9 Piecewise pulse used to excite the lofted model in the transient studies [13] [14]

Time period	Amplitude (N)
0 to (0.8/f)	1250*f*t
(0.8/f) to (1/f)	5000-(5000*f*t)
Amplitude = 1000 N ; f = 220 frequency (Hz) ; t= time(s)	

The excitation shown in Table 3.9 is based on a Helmholtz forced excitation (Helmholtz 1898, 84-85). In this study, the excitation is only a trigger to obtain the response of the model. The position of this excitation is important in the heuristic lofted model and is a variable in this study.

[11] Fast Fourier transforms of probes in all three mesh sizes also showed very similar responses in frequency, suggesting that the results are mesh-independent.
[12] Figure 3.7 also shows the seemingly periodic tail of the response, seen from 0.3s onwards; because this artefact appears at all three mesh sizes, it is not caused by the mesh size. This tail is explored further in Chapter Seven.
[13] To obtain a value for the first point in time (t=0), a frequency domain study is done of one frequency, applied at the excitation position.
[14] Most transient studies in this work do not use a steady-state or periodic excitation. In the only case where a continuous excitation is used, the piecewise pulse (Table 3.9) is extrapolated periodically at 220Hz (more details in Chapter Six).

Excitation points

In frequency domain studies, the focus is on obtaining a 'general' frequency response, so the models are excited at the midpoint of the top plate. By contrast, the transient studies focus on obtaining the natural response to excitation at different points on the top shell.[15] In these studies, the changing excitation point is itself the variable of the studies. The lofted model is excited in three sets: at 13 points corresponding to the position of the strings at two cross-sections at either end of the body and 13 points corresponding to the midpoint of the bridge position; the bridge positions are based on the standard *hirajōshi* tuning (starting from E4).[16] The bridge positions are used help to maximise the coverage of excitation points along the top shell.

In each of the two cross-sections used for excitation points, the string number refers to the point at which a string would be crossing that particular cross-section of the body. The two chosen cross-sections correspond to the most-raised point in the height of the *koto* (the dragon's head cross-section) and the lowest end of the *koto* (the dragon's tail cross-section). Figure 3.8 shows the positions of excitation. On the side view, the position of maximum arching is identified in the black rectangle, the minimum arching cross-section is in blue, and the bridge position for string 1 is shown in red. The figure shows the lofted model from the top view, above its top shell; the transparency shows the position of the sound holes and the struts below the top shell; the position of the excitations on the top shell is numbered.

15 With a real string, the initial pluck causes a continuous energy transfer to the body of the instrument via the moveable and fixed bridges. After the initial pluck, the string energy would exponentially or otherwise rapidly decay, but it would continue to vibrate at the frequency of the string, therefore there would be a continuous input of energy with decaying amplitude. The examinations of strings and the effect of exciting them is beyond the scope of this work. Bridge positions allow the author to compare three excitation points along one line that stretches above the instrument, with two extremes of arching and one usual bridge position analogous to the instrument

16 Measurements from the position of the bridges were provided to this author by Coaldrake.

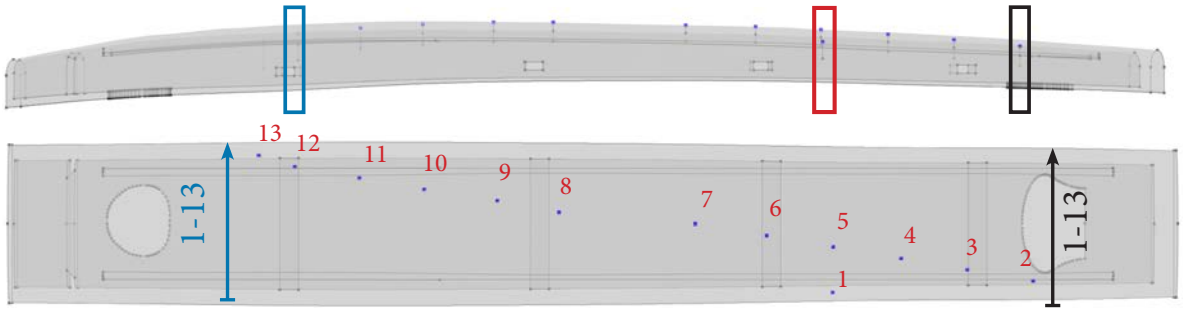

Figure 3.8 Excitation points in transient studies of the lofted model

The three sets in Figure 3.8 share the same y-coordinate -co-ordinate along the y-axis- in the Cartesian axes at each string position (e.g. string 1). It is only the x and z-coordinates that are changed when excitation position changes. Changing excitation points in this study is used to examine the relationship between the transient response and the position of excitation along and across the body.[17] The excitation of the model and the transient studies in this work do not replicate the strings of the instrument or the force input from strings into the body.[18] Defining the excitation was the last step in setting up the finite element models, after which the models could be used in the three sets of studies (Figure 3.1).

Overview of the Studies and Analysis of Results

The models in this study became increasingly complex from the plank to the lofted model. The studies similarly progressed in order of complexity and were conducted in three domains - the modal domain, the frequency domain and the time domain. Each domain of study used the insights gathered from the previous investigations.

First, resonant modes (eigenmodes) present in each model were examined in the modal domain. Between the models, the resonant modes were compared and showed which

[17] The effect of moving excitation along the body is found by comparing the same string points (e.g. string 6) at the three points: maximum arching, minimum arching, and the bridge position. The effect of moving the excitation across the body is found by comparing different string points in the same cross-sections (e.g. maximum arching, strings 1-13).

[18] In performance, strings 1 and 5 (Figure 3.8) are not aligned in the y-axis and are adjusted by the performers to suit the needs of the performance. This heuristic study uses the basic position and strings 1 and 5 as aligned in the y-axis.

eigenmodes carry forward from individual shells and simpler models to the heuristic lofted model of the *koto.* This analysis was followed by frequency scans. Air is added in the frequency scans; these scans document how much each frequency is radiated out of the instrument to the surrounding air. Finally, the transient response of the lofted model is investigated. The effect of each component in the body components can be studied by changing the excitation points (detailed earlier).

Eigenmodes

In the modal domain, the eigenmodes of the models, or their resonant modes, are predicted. Resonant modes are frequencies at which a system or object vibrates at the eigenmodes of an instrument are critical resonances of the object and are affected by the material, geometry and construction of the instruments. Comparing the eigenmodes allows the researcher to observe the differences caused by changing the geometry of a model. The first 44 resonant modes of each heuristic model were derived using COMSOL. The modes were identified as much as is possible and charted against variations in the models. This study has its own 'mode chart' or 'periodic table of modes'; this chart was made using the plank model as the baseline and uses images of each mode alongside the mode name and number. The mode chart in this study is similar to others seen in Waller's collection (1961, 43) and Fletcher and Rossing's work (1998, 82).[19] This mode chart minimises misalignment of eigenmodes and also helps in the latter stage of comparing plate modes and the modes of the assembled body. With this method, mode shapes can be traced from one plate to the full instrument body model to see if they carry through.[20]

[19] Though such a table and generalised equations exist for rectangular plates, it was beneficial to this study to have a periodic table with the modes of a plate with the aspect ratios of the *koto*. A table featuring modes of a rectangular plate of the *koto* of the same aspect ratio as the top surface of the *koto* has not been found in the literature by the author.

[20] Modes are compared in terms of shape and are defined as transverse bending modes, in-plane bending modes, torsional modes, (m,2), and (m,3) modes. Once mode shapes have been identified, mode frequencies are plotted. The slopes of progression for each mode type is compared between models. As the components are added to the models, modes shapes deform. Sometimes there are more than one mode that seem to fit a certain mode number e.g. (4,1), the fourth torsional mode. These uncertain modes were revisited and compared ((4,1) in this example). The two modes were separately plotted against other torsional modes. A significantly better-fitting mode to a linear progression of this mode was not often seen. The mode which exhibited a lower frequency was usually the clearer mode.

Total energy

It is difficult to understand the effect of geometric changes in the model on its resonance with the mode shapes and frequencies alone. Therefore, resonances were analysed in terms of the total stored energy of the system. In the modal domain, a decrease in the total stored energy of the system results in a more stable body; therefore, the objective of this analysis was to find how the stability of the models differ by way of comparing their stored energy. The total energy was derived for the whole system at each eigenvalue. The sum of the stored energy for all modes was able to give a clearer description of the relationship between eigenmodes and the geometry. The substructures have different masses, and the total energy depends on the mass of the vibrating body.[21] The mass of the individual subsystems is shown in Table 3.10:

Table 3.10 Mass of substructures

Substructure	Mass (kg)
Top Plate	
Flat	1.91
Steady arched top	2.20
Changing arched top	2.54
Tapered no arch	1.98
Tapered steady arch	2.20
Arched and tapered	2.55
Arched and tapered with 'ears'[22]	2.51
Base plate	
Flat no holes	1.35
One hole (SH 1 shape)	1.25
One hole (SH 2 shape) - keyhole	1.24
One hole (circular)	1.31
2 holes (SH shapes)	1.22
2 holes circular	1.28
Full-body models	
No struts	4.01
1 strut	4.03

[21] There is more or less material available for energy to be stored in, and the system energy is higher where the mass is higher and more material is present in the model.

[22] The indents seen along the inside of the top shell, near the joint of the side panels, are called 'ears'. It has been suggested to the author that the ears may be acting as a hinge between the side wall and the top part of the shell (Chris Waltham personal correspondence 2018). The ears did not make a clear change in the modes of the plates when combined with other variations on the plate (tapering, arcing); their effect on mode frequency remains under 10Hz. They were not studied individually.

2 struts	4.05
3 struts	4.07
4 struts	4.09
Lofted model	3.53

The total sum of the stored energy of each model is divided by the mass of the model (Table 3.10) to give the total energy per unit mass, which is compared between all models. The modal domain analyses were finalised with the study of the stored energy. After this stage, the frequency response of the models in a sphere of air was examined.

Frequency scans

Frequency scans give a time-averaged response of the system to a set of frequencies and allow the researcher to see the response of the air and the wooden model as a unified system. In these scans, the frequency response, the stored energy of the body, and the pattern of the radiation of sound were obtained using COMSOL.[23] The outputs of this study are in the form of a frequency response plot from each probe, where the peaks indicate frequencies at which the model radiates loudly into the air. Figure 3.9 shows an example of the results page in COMSOL. The frequency response plots at each probe are shown in a different colour.

[23] Frequency scans of the plank were done to 2500Hz (where the modes are present), and up to 1000Hz for the full-body *koto* models.

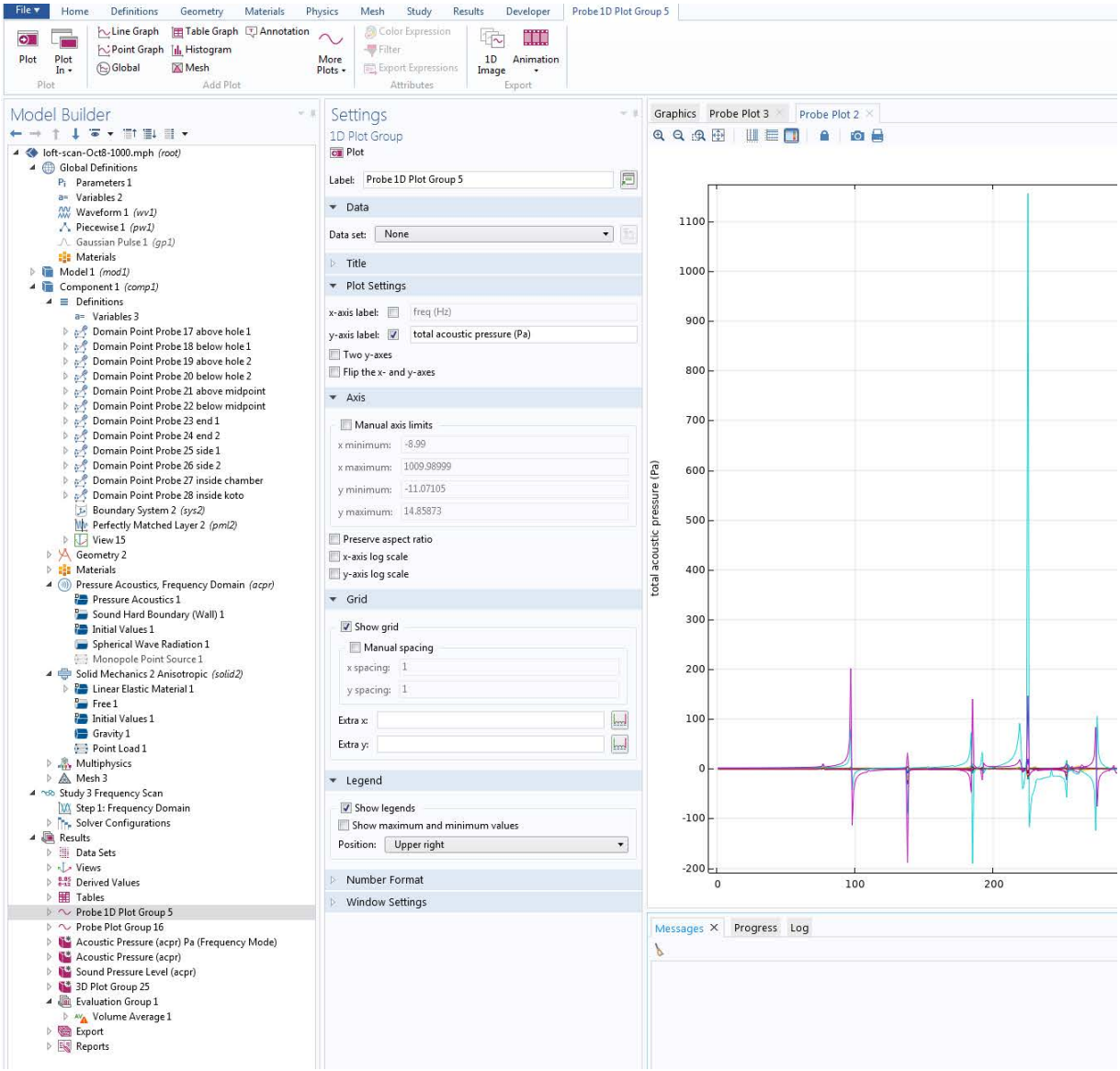

Figure 3.9 An example of frequency scan results in COMSOL

In Figure 3.9, the frequency response inside the lofted model shows a peak at 255Hz (light blue); by comparison, the probe above the heuristic model shows smaller, evenly spaced, peaks (purple). This example shows the difference in frequency responses inside and outside the body and is useful for examining the small air chambers inside the instrument. Without modelling, a frequency response can be obtained from the real instrument using a microphone, but access to the small internal chambers is impossible in heuristic studies

without damaging an instrument.[24] In these cases, frequency scans allow the researcher to predict the response of inaccessible components. The patterns of radiation for each frequency and the stored energy at each frequency can also be exported from COMSOL in these studies.

First, the frequency response of the lofted model inside each of the two internal chambers was compared with the response observed in the surrounding air. This comparison was used to gain insight into how each internal air cavity responds to different frequencies and was a part of understanding the role of each internal air cavity. Secondly, the patterns of sound radiation at frequency peaks and at eigenmodes were compared to observe any changes in the radiation of the sound based on whether an eigenmode was present or not.

The main analysis of the frequency scans was the comparison of the frequency response with the stored energy at each frequency and the eigenmodes of the heuristic models; this comparison illustrates the relationship between eigenmodes and peak frequencies. This relationship is important to understanding the sound of the instrument because only some of the eigenmodes of the body radiate out into the air effectively and the coupling between the air and the body creates new resonances. Staging the analysis from eigenmodes to frequency scans helps to distinguish the cause of each resonance observed.

Energy peaks in this analysis are used to discern which eigenmodes are stronger; weak eigenmodes do not result in a peak in the total stored energy of the body.[25] For example, the strongest resonances align with an eigenmode, show a peak in the frequency response and also cause a spike of the energy. By contrast, peaks without an eigenmode are not resonances from the body but appear as a part of air-wood coupling. The weakest resonances are those

[24] High-resolution studies can make use of acoustical cameras and other high-performance technologies for physical experiments (Coaldrake 2018).

[25] In the modal domain, total stored energy of the body refers to the energy of the body at frequencies it has a tendency to vibrate in; this energy is minimised in stable bodies. In the frequency domain, total stored energy of the body at a particular frequency refers to how much the body is responding to excitation at a particular frequency; here, increase in the energy equates to increase in the response of the body. In the frequency and time domains, energy is input as a point load into the body; when the body has less kinetic and potential energy, more energy exists as sound within the space, because from the total energy of the system, less is stored at the body. The existence of less total stored energy in body entails more energy leaving the body; this additional energy within the surrounding air results in either a louder sound or a longer decay of sound.

that appear in only one type of observation and do not align with any other observation. These weak resonances appear either only as a peak in the probe or as an energy peaks of the body. The compilation of the frequency scans and the eigenmodes give a set of resonances which are used in analysing the transient response.

Transient studies

The transient response is used to measure the sound emitted by the model into the air over a period of time. Unlike the frequency scan, this study does not give the response of the system to each frequency but instead outputs the value of air pressure at the probes for each point in time. The main objective of these studies was to arrive at a basic understating of the sound of the *koto*. The transient studies presented in this work examined the effect of moving the excitation point on the model on the resultant decaying sound. The analysis aimed to show how each component of the heuristic lofted model contributes to the decaying tail of the sound. The transient response up to one second was recorded with a sampling rate of 48000Hz; at each probe, 48000 values were exported for a duration of one second; this sampling rate is equivalent to DVD-rate audio quality and was considered appropriate for this study.

The thirteen string points at the two cross-sections resulted in 39 simulations and 143 waveforms to compare. Due to the extremely large volume of data generated, it was not possible to analyse the material without either automated analysis or visualisation. Following an initial qualitative analysis of the results, the quantitative analysis then focused on a smaller set of the observations selected to obtain more detailed analyses.

The analysis of the results from the transient studies can be divided to the two categories of spectral analysis and temporal analysis; spectral analysis uses tools such as fast Fourier transforms (FFTs) to find the frequencies in the response. The peak frequencies in the range

of 1-1000Hz were derived using FFTs and compared with the frequency scan data and the eigenmodes of the *koto*.[26]

Temporal analysis examines the changes in amplitude of the sound over a period of time. Decay analysis is a form of temporal analysis. The amplitude of the sound in the one second window of observation is presented as a time-series graph. This representation is commonly referred to as the waveform. The waveforms were observed inside and outside the lofted model. The rate of the decay of the critical waveforms was found using exponential decays.[27] The decay of the sound was measured both inside the body's air chambers and outside the body. Finally, parameters of the geometry for each excitation point were compared with the results of decay analyses and spectral analysis. This final comparison connects the geometry of the heuristic model to the transient response. For example, moving the excitation point is compared with the length of the decays in all simulations to observe whether exciting the instrument model closer to the dragon's head causes any changes in the length of the decaying sound. This analysis relies on the insights from the eigenmodes and frequency scans but is itself the key component in understanding the acoustical response of the *koto* using heuristic models.

The results from the eigenmodes, the frequency scans, and the transient studies were compiled to obtain an understanding of the basic acoustical response of the *koto* using the heuristic models. The three-domain analysis allows for characterising the response by separating resonances that appear in the transient response between body (eigenmodes) and air (frequency scan) resonances.

Explanatory notes for the datasets in Volume II

[26] For each of the three sets of excitations, the response observed above the midpoint of the body of the excitation at the string 7 position was chosen as the representative. The Fourier transforms are then compiled to find a set of peaks.

[27] The natural logarithm of the absolute value from the probe was plotted against time to observe the exponential decay of the waveform. The exponential decay was then compared across all excitation points and all models.

This technical study of the *koto* uses a large set of data and relies on qualitative and visual analysis tools. Datasets are included in the second volume and are organised by order of reference to the discussion in Volume I. These datasets summarise the original waveforms in the study and spectral analysis in the transient studies, compilations of radiation patterns in the frequency domain, and the resonant modes of all models. The purpose of the datasets is to provide readers and scholars in musical acoustics and musicology access to observations made and the original data.

Chapter 4

Validation and Verification of the Models and Methods in this Study

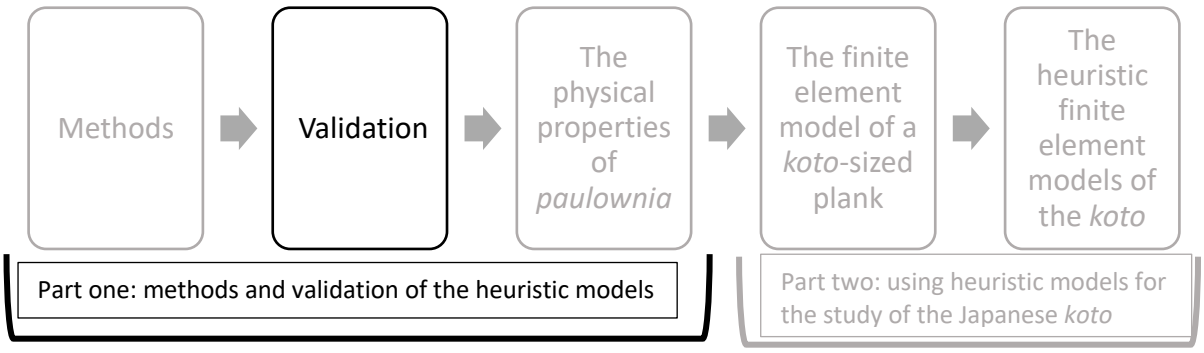

Introduction

Validation of models is necessary to ensure that each part of the modelling process is reliable. The aim of the validation is to have confidence to use the heuristic models for studying the *koto.* In this process, the methods were verified against existing literature by independently replicating Ando's 1986 and 1996 studies of the base plate of the *koto* and Rossing and Russell's 1990 experiment on an aluminium bar. The base plate was verified due to its relatively simple geometry in comparison with the top shell (details later in this chapter). Following, the values used for modelling the physical properties of *paulownia* were validated using new physical experiments using transducers, a laser scanning vibrometer, and a Chladni pattern test. Next, the heuristic models were verified against Coaldrake's CT scan model results and physical data from the *koto.* Finally, the margin of error for the study was established. A summary of the validation studies is shown in Table 4.1.

Table 4.1 Validation studies

Subject of validation	Actions
Method	Replicating Rossing and Russell (1990)
	Ando base plate (1986 and 1996)
Physical properties	Transducer studies
	Laser scanning vibrometer (LSV)
	Chladni test
Models	Comparison with *koto* tapping data from Coaldrake
	Comparison with CT scan data.

Although in Table 4.1 each test is shown in one category, no test only serves one purpose; this is especially so with analysis such as the comparison with Ando's work. This set of validation aimed to obtain evidence from independent sources about the resonances of the *koto* and *paulownia*. First, the verification of the methods is discussed.

Verification of the methods in this study

The objective of this section was to provide an independent assessment of the main tool of this study, the finite element modelling software, against available data in the literature.

Rossing and Russell 1990

First, Rossing and Russell's 1990 study of aluminium bar modes was repeated in COMSOL to capture the first 39 modes of an aluminium bar with dimensions of 35.6 by 3.8 by 0.95cm. This example was chosen because the aluminium bar is a small rectangular plate, which is straightforward for modelling, but it is not a wooden object; therefore, the method can be verified without relying on the physical properties of woods and the complexity for modelling woods. The aluminium material properties chosen were the in-built data in the COMSOL material library as of August 2017. The experiment yielded highly similar results, shown in Figure 4.1. The full icons obtained from COMSOL are overlayed with the purple shapes from Rossing and Russell's study.

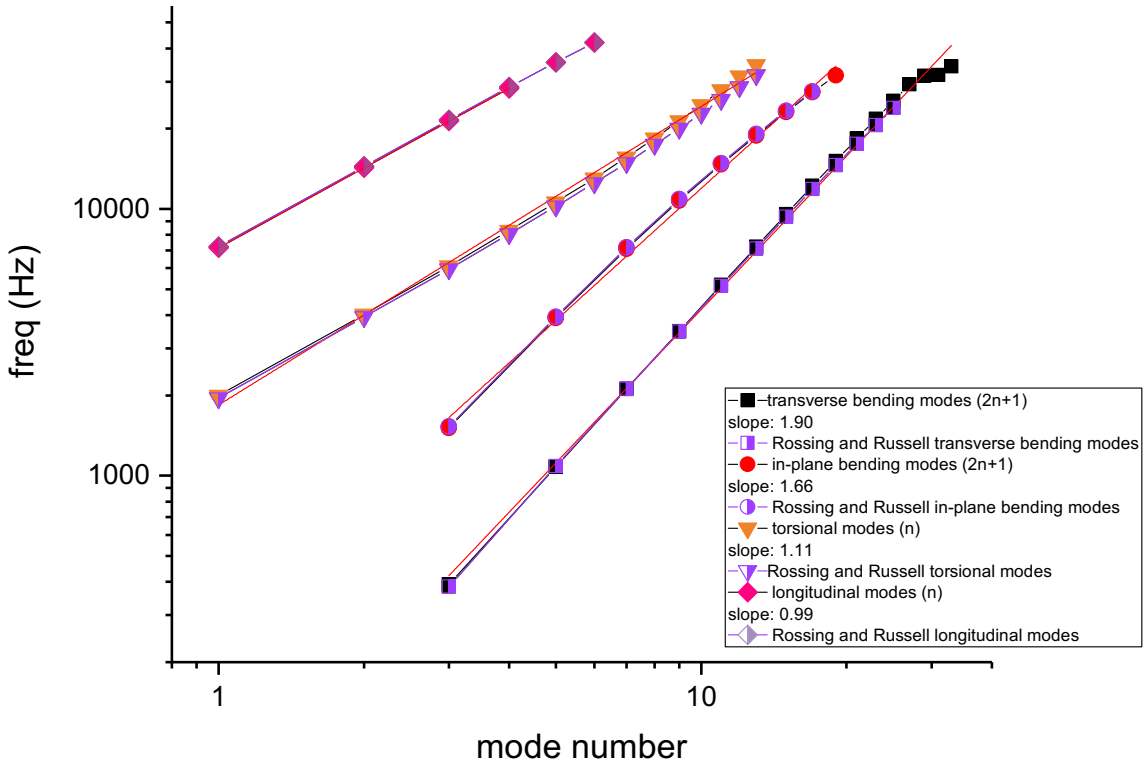

Figure 4.1 Replicating Rossing and Russell (1990)

Figure 4.1 shows that the modes predicted in COMSOL match those measured in Rossing and Russell's 1990 experiment closely. These results support the use of COMSOL for modelling in this work.

Ando base plate (1986 and 1996)

Other than Coaldrake's analyses using FEM (2015, 2018, 2019), the only detailed publication on the *koto*'s acoustics are from Yoshinori Ando. He published his findings on the resonances of the top and base plates of the *koto* in a short paper in 1986, followed by a paper in 1996 (Ando 1986 and 1996); the second paper was published in Japanese only. The findings about the same resonances are different between the two publications; no clear reason has been shown yet for these differences. This work attempted to independently verify a model of the *koto*'s base plate against Ando's findings. The base plate is used because the top shell has many features that can change, specifically the three curves along the top of the dragon's spine, across the 13 strings on the top curvature, and the tapering of the plate from the sides. Details of Ando's top shell results are not sufficient for the author to replicate them with a heuristic model. By comparison, the base plate is a simpler geometry to model and with a simpler model to verify, differences can be traced more clearly. In Figure 4.2, the findings of the comparison between COMSOL predictions and Ando's two publications are shown.

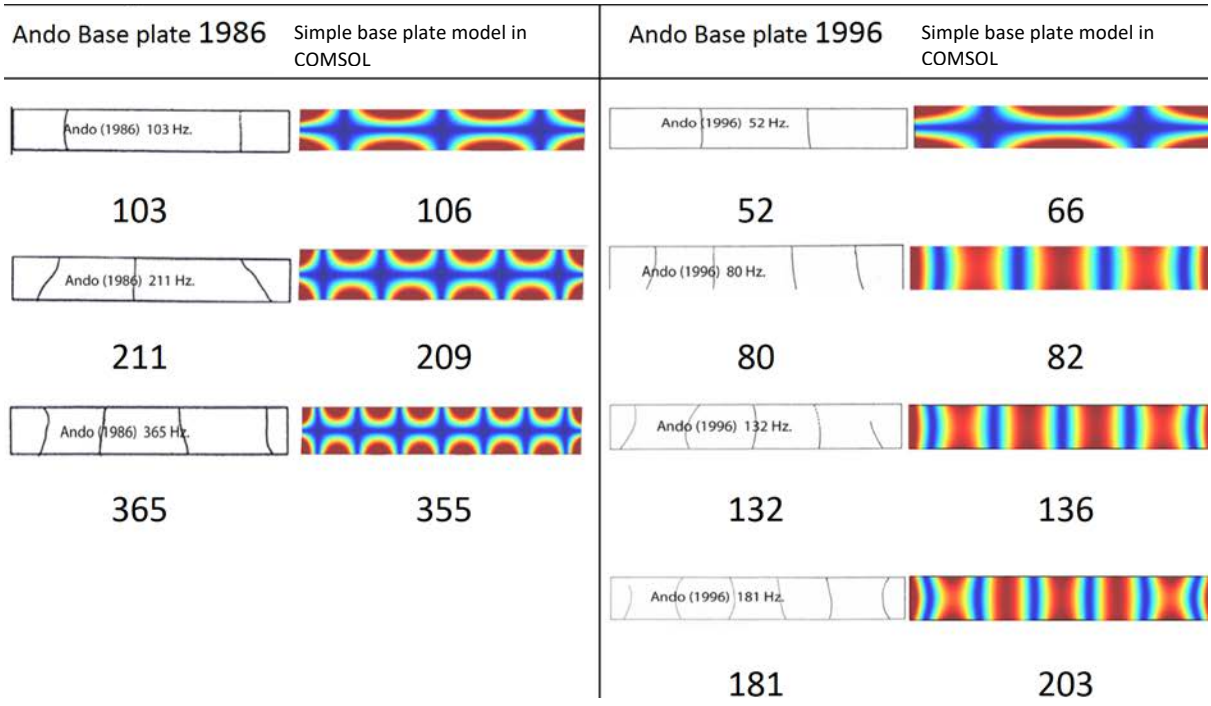

ß∑

Figure 4.2 Ando's 1986 and 1996 findings of the base plate compared with COMSOL results

Figure 4.2 shows that the model of the base plate aligns well with Ando's findings across both publications. The alignment of modes indicates that Ando likely found different modes across the two publications but did not correlate them all as one set of results. Physical experiments used to obtain the shape of resonant modes can be very energy consuming, especially for a large wooden plate. It is possible that Ando's experiments missed some of the nodal lines due to this issue. This issue is not as prominent for smaller plates, as seen in the guitar or the violin family, which helps to explain the comparatively large body of studies using Chladni patterns in these instruments (Hutchins and Benade 1997).

It will be shown in Chapter 7 that the torsional modes of the body are highly reliant on the constraints of the full body and are less affected by the individual plates. Ando's findings from 1986 are unclear in the torsional modes (Figure 4.2). Ando's separated the two plates, which may have caused issues with observing torsional modes of the full body in the individual plates. However, this separation but would not have affected transverse bending modes of the body as much; these bending modes have been found to translate more clearly from the top shell to the full body than torsional modes (discussed further in Chapter Seven). The findings in this section were able to clarify Ando's results and were a part of validating the simple model against existing literature.[1]

Validation of physical properties

The available physical properties of the *paulownia* wood, detailed in the Methods chapter, were tested in a series of physical experiments using a plank. The results from the experiments were then compared with a COMSOL model of the plank that used the available *paulownia* properties.[2] Three types of experiments were conducted: a) transducer experiments, which excited the plank using a surface transducer; b) a laser scanning vibrometer (LSV) test, which

[1] Unlike Ando, this study has no access to individual plates of the *koto* to physically test and it is out of the scope of this work to obtain any new sample plates of the *koto* or its components. Therefore, the only physical experiments possible are of the simplest (plank) model discussed earlier and the most complex (full body). The full body are compared with recordings and scans done on a *koto*, the results of which have been made available to the author by Coaldrake.

[2] The scan used a 0.1 Newton load at the midpoint of the surface of the plank model suspended in a sphere of air; the frequency scan range was 1-2000Hz.

gave a visual output of the excited modes; c) a Chladni pattern test. The studies are detailed in this section.

Transducer experiments

Two sets of transducer experiments were conducted. The aim of these tests was to obtain a reliable set of resonances for the *paulownia* plank. The first experiment was conducted in a private home and was able to capture one set of resonances up to 1000Hz; this experiment was halted due to health risks. The second transducer experiment was able to capture the necessary frequency peaks to compile a reliable set of resonances for the plank in triplicate, thus enabling the study to validate the physical properties of the model.[3]

During both transducer experiments, the plank was excited in a frequency sweep using a surface transducer. The transducer was placed 25.5cm from the edge of the plank, equidistant from either side. Vibration data was captured from an accelerometer placed on the centre of the plank. The frequencies at each point of the sweep were estimated from the length of the recording and the start and end frequencies. The resonant frequencies were derived from these estimates.[4] Table 4.2 details the equipment used in these studies.

Table 4.2 Equipment used in the transducer studies

Role	Equipment	Setup
Transducer	*8Zed Good Vibrations* 26 Watt surface transducer	Placed on top of plate, supported by bungee and tape
Bungee cord	*Theraband* tape	Supported plank[5]
Accelerometer	Accelerometer on an iPhone 6	Placed on the centre of the top of the plank, taped down.
Spectrum analyser	*Faber Acoustical SignalScope*	Used for monitoring, placed on Tripod 80cm from plank

[3] The first experiment was conducted in a private home. The second experiment used a vocal recording booth or "dead room". The recording booth is not anechoic but does provide ample insulation from outside noise. In this recording booth, the frequency sweep was started in the recording booth, but the author could monitor it from an adjacent room. The room setup makes it safer to observe the sweep because the researcher is not exposed to the loud sweep for the 10-minute length of the sweep, thus minimising health risks and interference with the data production and collection.

[4] The fourth derivative of the spectrum was derived to show additional smaller peaks.

[5] The plank was suspended in free-free boundary conditions via bungee tape. The constraints of movement in boundary conditions mean that different factors such as velocity are part of the equation (Blevins 2001). The free-free boundary conditions were set up in the COMSOL model to replicate the physical plank.

Frequency generator	*NCH Tone Generator* on OSX	Generated tone sent to transducer via audio cable
Support for equipment	*Nexcare Micropore Tape*	Used to stop rattling

Figure 4.3 show the setup used in both experiments; the images are from the second transducer experiment. The plank of *paulownia* used is helpful to validate the model in terms of the physical properties used for modelling the *koto;* it is not intended to validate the *koto* model itself. As such, it is a study of the material of the instrument and not its dimensions. plank was close to one year old at the time of the experiment, and had a small amount of warping on it, visible in Figure 4.3.

Figure 4.3 Set up and data capture in the second transducer experiment

The second transducer experiment was repeated three times for the frequency range of 10-1000Hz, followed by three iterations of the 1000-2000Hz range.[6] [7] Each sweep duration was 10 minutes, which equates to 0.6s for each step of 1Hz. The sampling rate was 30 samples per

[6] When the experiment was started at 1Hz (minimum the software allows) the first few seconds had 'pops', which rattled and distorted from the transducer, so the starting minimum was changed to 10Hz. These low frequencies from 1-10Hz are too large for the transducer to reproduce and they result in the popping sounds.
[7] The data necessary for this study was in the 0-1000Hz range, but the 1000-2000Hz sweeps were also conducted because of their possible use later in other parts of the study.

second, meaning that for every 1Hz step in the sweep, there are 18 samples.[8] Moving averages were used to minimise the effect of issues in individual sample points and to account for the 18 samples for each 1Hz step; at the thirty-point average, each averaged frequency has a less than 2Hz margin of error (given 18 points per 1Hz). For peak analysis, the data from the z-direction was chosen because this direction was clearer than the other two in all sweeps. However, this axis does not show in-plane bending modes, as there is no movement in the z direction in these modes. The raw data from the x-direction in the second sweep assisted in capturing these modes. The peaks were overlayed to compare all sweeps, and a set of peaks seen in all sweeps was derived. In these experiments, low equipment resolution obstructed attempts to isolate the amount of excitement in each direction and consequently the mode types were difficult to derive from the peaks. Therefore, a laser scanning vibrometer test was used to observe mode shapes more clearly. It was outside the scope of the heuristic model to account for the variation in the grain angle across the width of the plank.

Laser Scanning Vibrometer

A Polytec Scanning Vibrometer, with the PSV 400 Scanning Head and PSV A-420 Geometry Scan Unit were used to obtain the LSV results at the department of Mechanical Engineering at the University of Adelaide. The plank of *paulownia* was suspended at either end, allowing it to move freely in three directions. A speaker was used behind the plank, with a targeted chirp for the excitation signal. Due to laboratory restrictions, the movement of the total body of the plank was not possible to capture and the test was one-dimensional. This issue resulted in observing partial mode shapes, which made identification of modes more difficult. Also, due to the time-intensive nature of the test, only data up to 500Hz was processed and made available to the author. Mode shapes from the LSV results were compared with the COMSOL results of the plank. In Figure 4.4 the LSV images that align with COMSOL results are shown.

[8] The author manually triggered both playback and recording. The playback ends at the outer limit of frequency set. The frequency for each sample point is estimated from mapping the outer limits. The data was derived and compiled in OriginPro.

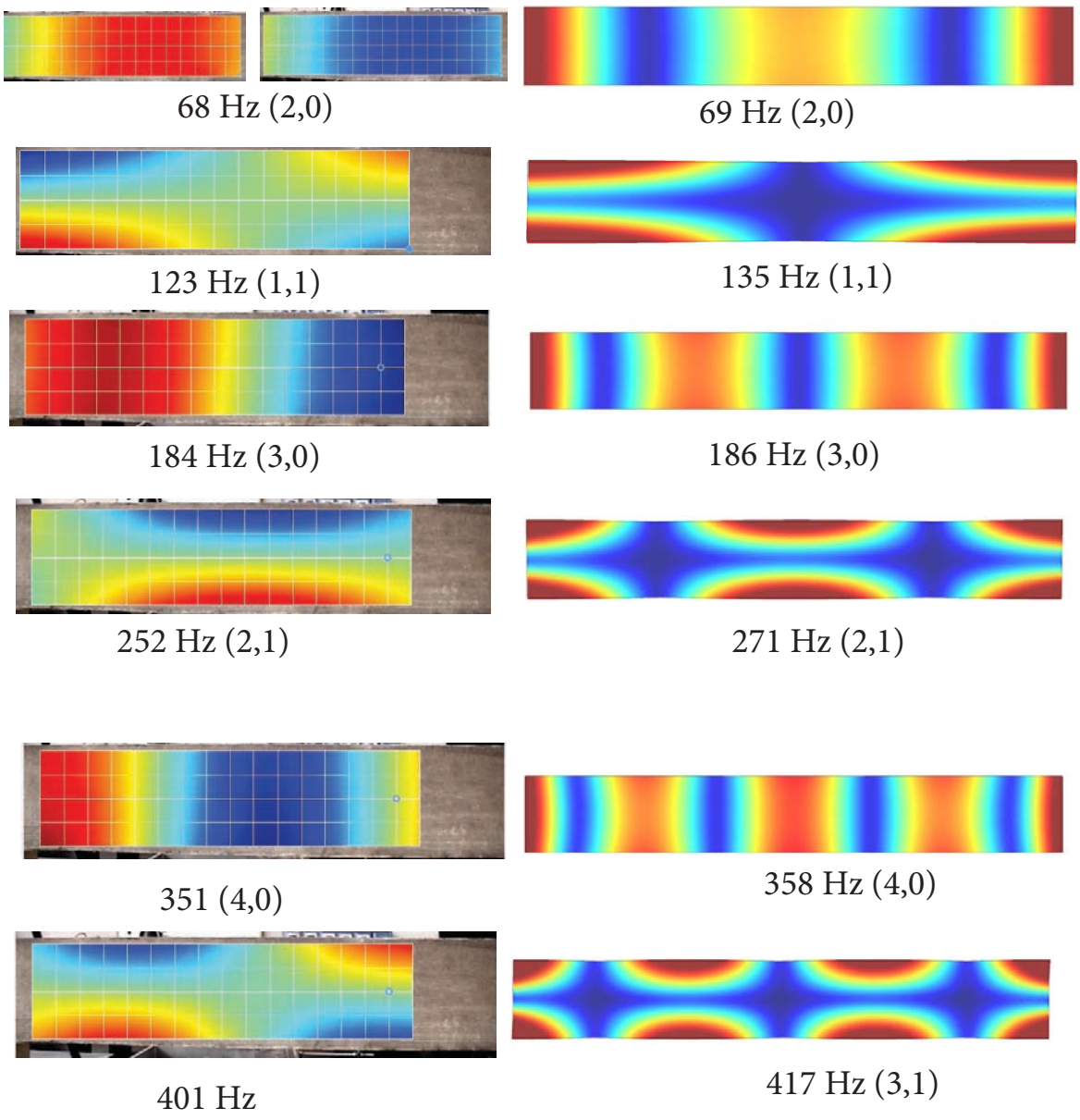

Figure 4.4 LSV Results compared with COMSOL Models

Figure 4.4 shows the bending and torsional modes identified and aligned between the LSV and the COMSOL results. The aligned modes were the strongest and clearest peaks observed from the LSV and are considered to be eigenmodes. Other smaller peaks from the LSV test include those at 35, 50, 200, 225, 431, 452, 489Hz (Figure 4.5). These smaller peaks were not identifiable in the LSV and did not resemble any mode shapes predicted by the COMSOL model. It is possible that these unidentified are weaker modes. Next, the frequency of the peaks in the transducer experiment spectrum were compared to the mode frequencies in both sets of

FEMs. The data of the first 500Hz is aligned across the experiments. The two transducer experiments and the LSV response are shown in Figure 4.5.

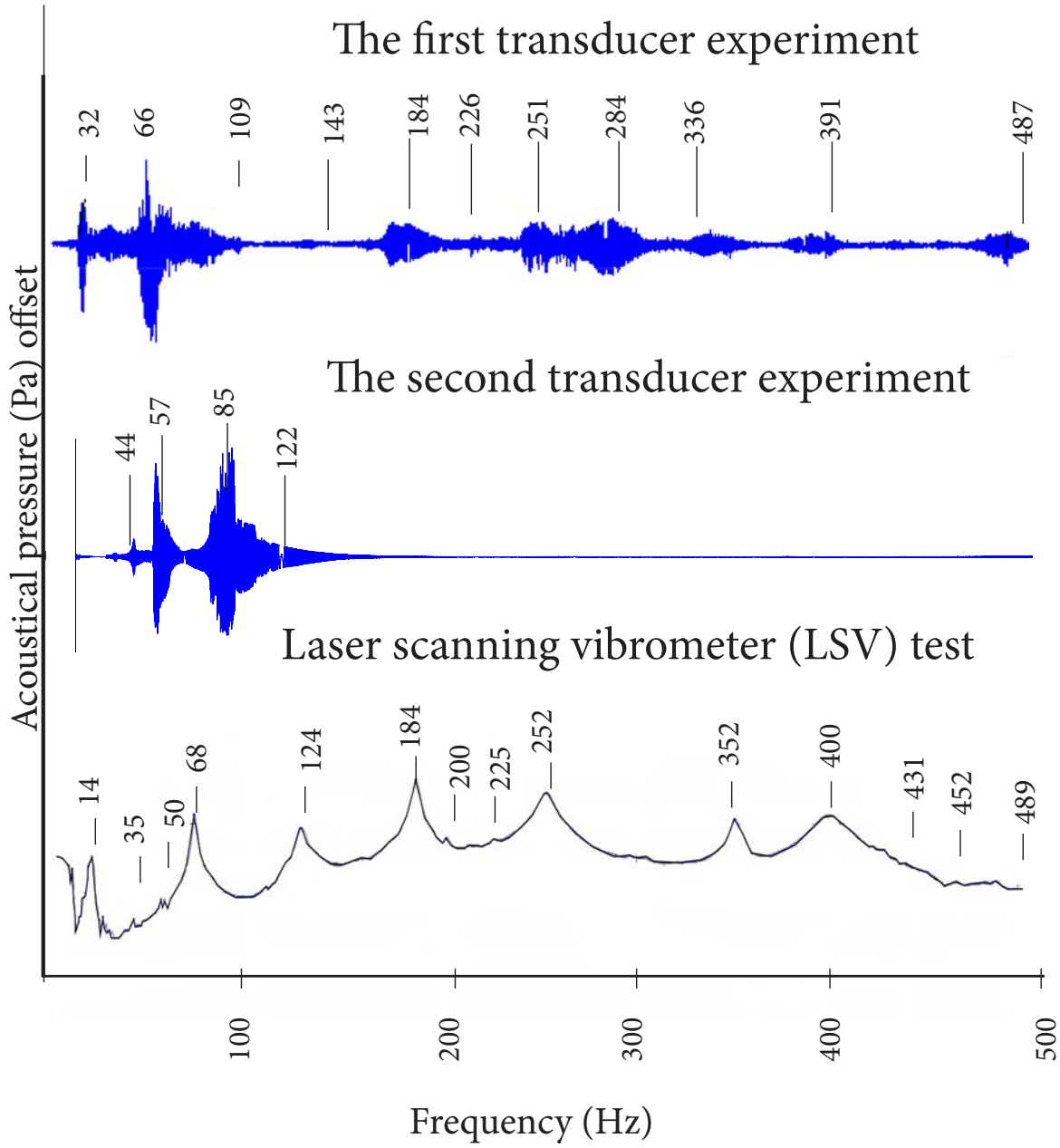

Figure 4.5 The compilation of the frequency responses obtained using transducer experiments and the LSV

Figure 4.5 shows that the resonances of the first transducer aligned well with the LSV, especially at 184, 252 and 400Hz. The second transducer shows a stronger alignment with the other two at 57, 85 and 122Hz; this experiment seems to drop in response above 200Hz. Following, the fourth derivative of the data was obtained to help show hidden peaks or smaller peaks that were obscured by individual data points or larger peaks. The fourth derivative of the thirty-point average clarified some of the smaller peaks that exist above 200Hz, especially those in

the 300-1000Hz range. These consolidated results of the physical experiments are compared to the model in Table 4.3. In the table, the green cells show peaks that aligned between physical experiments and simulations.

Table 4.3 Comparison of the physical experiments and FEM of plank in modal and frequency domains

Transducer experiment 1	Transducer experiment 2	LSV	Eigenmodes of plank model	Frequency scan peaks of plank model
1-500Hz				
--	--	13		
32	31	35		
50	52	50		
65	66	68	62	
97	93	--	--	
--	125	123	129	110
144	146		--	
187	185	184	170	188
--	207	200	--	
--	--	211	--	
--	--	215	--	
222	--	225	--	
255	--	252	259	
--	261	--	--	266
293	282	295	287	
--	305	--	--	
340	--	351	326	328
--	--		--	342
--	374	366	--	375
395	403	401	396	
--	423	--	--	419
--	451	441	--	459

Transducer experiment 1	Transducer experiment 2	LSV	Eigenmodes of plank model	Frequency scan peaks of plank model
500-2000Hz				
496	506	No data above 500Hz	--	488
--	530		524	535
--	--		549	
				570
582	583		--	
--	611		636	
				648
675				
				695
	724		731	718
--	--		738	
--	--		759	752
778	771		760	
--	817		826	831
869	--		--	
--	919		925	
--	949		940	
971	983		--	969
	990		1012	
No data above 1000Hz	1015		1019	
	1065		1059	
				1139
			1172	
				1190
				1360
	1530			
	1594			
	1631			1625
	1924			

Table 4.3 shows that most of the peak frequencies observed in each of the individual tests correlate to at least one of the other sources (marked as green cells); examples include resonances at 110, 188 and 328Hz. The physical peaks observed align well with the two modal and frequency domain studies of the plank. In the first 1000Hz the response of the plank is stronger than the 1000-2000Hz range. However, the LSV test did not sufficiently clarify the mode shapes and further tests were necessary to ascertain the shape of each eigenmode.

Chladni test

To ascertain the mode shapes for each frequency, a Chladni pattern experiment was conducted. The plank was suspended similarly to the transducer experiments. A thin layer of table salt was put on the plank. The plank was sanded down before the experiment, so that the surface would be sufficiently smooth for the grains of sand to move freely and the vibration patterns could be observed easily. At 64-66Hz, the salt repeatedly gathered at two bands, dispersed from the centre of the box. The salt did not respond to any frequencies above this range. At 69Hz, COMSOL predicts the first transverse bending mode. The salt pattern in the physical experiment showed a strong resemblance to this mode shape. Figure 4.6 shows the comparison of the pattern observed in the Chladni experiment and the COMSOL mode.[9]

[9] Due to the small size of the experiment room, low lighting and the large amount of equipment, it was not possible to obtain a representative photo of the experiment.

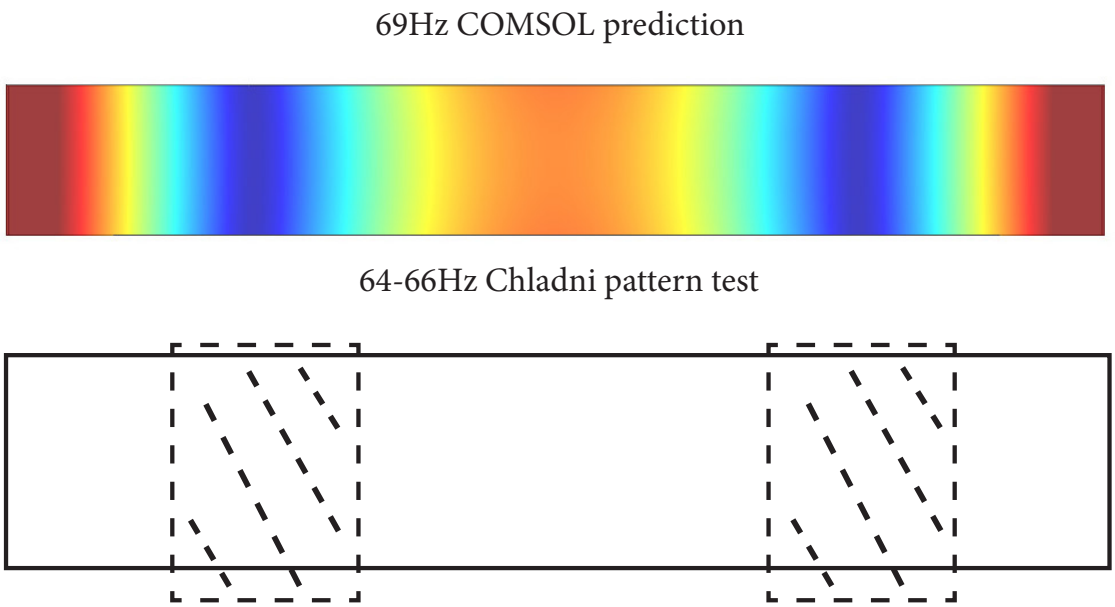

Figure 4.6 Comparison between the COMSOL prediction and the Chladni pattern obtained

The schematic shown in Table 4.6 shows that the nodal lines are gathered as a wide band similarly to where they are predicted in the COMSOL model. Additionally, the predicted frequency closely aligns with the frequencies in the Chladni observations. These observations indicate that the Chladni test was successful in capturing the first transverse bending mode, and the model reliably predicted this mode.

In higher frequencies, the lack of motion in the salt is likely to be due to the lack of sufficient power from the transducer. The higher frequencies need more power to excite the entire plank, and the surface transducer available in this project did not have enough power for the higher frequencies. More Chladni patterns were observed in the *koto* studies conducted by Coaldrake (2018). The difference is most likely the result of the shells of the actual instrument being much thinner than the solid plank used in this Chladni experiment.

In *Formulas for Natural Frequency and Mode Shape* (2001), Blevins sets a set of formulae for predicting the eigenmodes of isotropic materials in simple forms such as bars. In addition to the tests, undertaken, a number of isotropic models of the plank were made and the COMSOL results were compared with predictions based on Blevins' work. The modes predicted with Blevins' formulae were inconsistent and the results from the comparison were not clear. It was not possible to discern whether the mismatch was due to the assumption of isotropy or the

estimates available. Thus, in Chapter Five, the broader issue of using isotropic and orthotropic models for *paulownia* is explored further.

So far, the resonant frequencies of the plank have been observed clearly and a compiled set of them has been created. The shape of these resonant modes has proved elusive. Within the scope of this study, the physical properties are considered valid and useful. With validated methods and physical properties, the *koto* models used in this study are verified and discussed in the next section.

Validation of models

The finite element models developed as a part of this study were validated by comparison of the results from the box and the lofted model with Coaldrake's CT scan model and raw data from physical experiments on the instrument. The physical data, provided by Coaldrake, includes peaks from recordings of the instrument being tapped and a laser scanning vibrometer study. The aim of this comparison is to see whether the idealised box and the lofted model are valid as analytical models to study the *koto*'s acoustics with. The comparison of results is shown in Table 4.4.

Table 4.4 Comparison of physical data from the koto with heuristic models and Coaldrake's CT scan model

Box model	Lofted model	Coaldrake ct scan model	LSV (*koto*)	*Koto* physical recording
1-500Hz				
91	122	112		
135			132	
			148	
164	175		169	167
	199			
	201			
213	207			
			220	
251	230	233	236	231
252				
254	254	258		
264				
268				
280				
283				283
288	287			
299		296	293	
	305	302		
314	309	311	310	
323	322			
328	327			328
	339	345	339	
	342			
	344			
361	359	355		
365		357		
	371		372	
386	382			382
			396	
408	406		398	
410	414	410		409
416				
421				
426				
430	436			441
	456	456		
				463
473	471	468	477	
487	475	480		

Box model	Lofted model	Coaldrake ct scan model	LSV (*koto*)	*Koto* physical recording
500-1000Hz				
494	504			495
509	507			
	517		513	519
	536	525		530
541	544			
	545			557
	567			
	576	570		
585	586		581	
	595			
617	600			611
623	620	624		627
	632			
	639	640		
	651		654	659
666	662	676		
684	681	688		684
686				
690	695			
699	698			
711				
712		713		
	714	714	717	
724				727
739			747	
750		762		751
				773
		782		783
		792		
		809		
		821	829	829
		830		
		845		
		881	881	875
		899		
				910
		941		937
		949		
		969		
		985	990	988

There is no physical data of the *koto* above 1000Hz and so the comparison in Table 4.4 is truncated at 1000Hz. A strong alignment of peaks is found in Table 4.4 between the heuristic models (box and loft), the high-resolution CT scan model, and the recording of the instrument. This suggests that both the box and the lofted heuristic models are useful and reliable in terms of predicting the frequency of modes. Knowing the limitations, the heuristic models were considered to be reliable for further investigations of the *koto,* which will be presented in Part II.

Determining the range of experimental results and establishing the margin of error

Both the physical data and simulations provided a range of values for each resonance found. However, a margin of error needs to be established cross these different experiments so that the accuracy of the results from the models and those of the physical experiments can be ascertained.

The physical experiments used in establishing the margin of error included the first transducer experiment, the three sweeps from the second transducer experiment, and the LSV results. Peaks from all five sets of data were compared to arrive at a standard deviation for each matched peak. Table 4.5 details this compilation of all peak frequencies observed and the mean and standard deviation.

Table 4.5 Peaks across all physical experiments with means and standard deviations for each peak (all numbers in Hz)

LSV	Transducer experiment no. 1	Transducer experiment 2: sweep 1	Transducer experiment 2: sweep 2	Transducer experiment 2: sweep 3	standard deviation	mean
35	32	30	30	30	2.19	31
		39	41	39	1.15	40
		44		44	0	44
50	50	51	52	51	0.84	51
68	65				2.12	67
		84		84	0	84
		88	88	88	0	88
	97		101		2.83	99
		106		106	0	106
123		133	133	133	5	131
	144	143	142	143	0.82	143
				161		161
184	187	189	189	189	2.19	188
200		194	192	194	3.46	195
211		207		207	2.31	208
225	222	226	230	226	2.86	226
252	255	255	243	255	5.20	252
			269			269
295	293	286	280	287	5.97	288
	340	339	336	339	1.73	339
351						351
366						366
401	395	398	390	398	4.16	396
		415		415	0	415
		439	438	439	0.58	439
441		441	439	441	1	441
	496	497	492	497	2.38	496
		535	535	535	0	535
			568			568
	582	590	586	590	3.83	587
			657			657
	675	676	671		2.65	674
		687		687	0	687
		756	756	756	0	756
	778	776	776	776	1.00	777
		802	807	802	2.89	804
		821	816	821	2.89	819
		829		829	0	842
			934		N/A	934
	971	986	986	986	7.50	982
			Mean of standard deviations		2.75	

This mean of the standard deviation, presented in Table 4.5, indicates that for each peak, the deviation observed across the samples is 2.75Hz. Here it is assumed that the aligned peaks show the same resonance from the body. This means that for each resonance found, there is a 68% chance that the 'actual' resonance is within 5.5Hz of the approximated value a 95% chance

that it is within 11Hz of it. The error margin for the simulations and physical experiments in this study is considered to be 11Hz for two standard deviations in each direction.

The methods and models of the study were calibrated and validated through a number of physical experiments and comparisons with literature. This study has found resonant frequencies, but the shapes of eigenmodes has remained difficult to obtain.

Verification of the transient response of the lofted model against the real instrument

The lofted model is used in this work to examine the transient response of the instrument. This part of the discovery includes the most complex data used and is a focal point in the analysis. Therefore, a sample of the transient response from the lofted model was compared with physical data of tapping the instrument (provided by Coaldrake) to ensure that the response of the model in the time-dependent studies was reliable.[10] Table 4.6 shows the comparison between the simulated transient response and the physical observation.

[10] This comparison used the mean of resonant peaks from the FFTs of 7 excitations on the top curvature of the actual instrument with a representative waveform from the simulated transient response.

Table 4.6 Comparison of the transient response of the lofted model and a tapping experiment using the koto

1-500Hz		500-1000Hz		1000-1500Hz		1500-2000Hz	
Peaks from Transient response Lofted model	Peaks of tapping *koto*	Peaks from Transient response Lofted model	Peaks of tapping *koto*	Peaks from Transient response Lofted model	Peaks of tapping *koto*	Peaks from Transient response Lofted model	Peaks of tapping *koto*
Hz	Hz	Hz	Hz	Hz	Hz	Hz	Hz
	79	504	497		1013		1501
	81		507		1036	1541	
	87		513		1048		1571
95	96		515	1056	1056		1579
	104		520		1069	1591	
	120	533	522		1083		1616
126	123	550	543		1096		1622
	139				1121	1628	1628
	160		570		1126		1640
180	184		611	1137	1137		1643
	190	631	631		1155		1651
	196		651	1171	1166		1658
	208	659	654	1179	1180		1661
	219		677		1190		1671
220	227		684		1207	1682	1681
	236	692	692	1223	1213		1687
	254		696				1689
262	260		700		1233		1701
	266		719		1258		1709
	275		723		1268		1717
	289		735	1287			1719
	292	744	741		1298	1733	1736
	299		748	1311	1311	1745	1749
316	326		760		1324		1759
	330		771		1338		1770
	338	776	779		1353		1772
	351		793		1364		1780
372	378	811	808		1371	1795	1793
			827		1386		1814
	392		830		1389		1822
402	409		834		1396	1832	1830
428			851	1402	1408	1858	1849
	437		859		1422		1852
466	462	879	869		1425		1867
	476		884		1429		1881
	487		908	1442	1441		1883
		927	925	1460	1450		1891
		939	945	1476			1894
			954	1495	1491		1899
			962			1904	1902
		979	984			1919	1920
			995				1943
			1007				1948
						1961	1959

Table 4.6 shows that though not all the peaks observed through the physical recording are picked up in the model, the majority of the peaks seen in the model align with a resonant peak observed in the physical recording. The few peaks that do not align are the in the 1000-2000Hz range; the alignment of all the low-frequency resonances in the model leads to the conclusion

that the model is valid enough for the studies within this project. Given that the majority of the analysis done in this document Is within the 1-1000Hz and the maximum range considered is 1-2000Hz, the lofted model is considered valid as a heuristic model of the instrument.

At the completion of the validation process of the finite element method, the physical properties and the models, and with the margins of error established, it was concluded that the next phase of work could be undertaken. The idealised box and the lofted model were both found to be valid for use in investigating the basic acoustical response of the *koto.*

Chapter 5

Broader Considerations of Modelling the Physical Properties of *Paulownia*

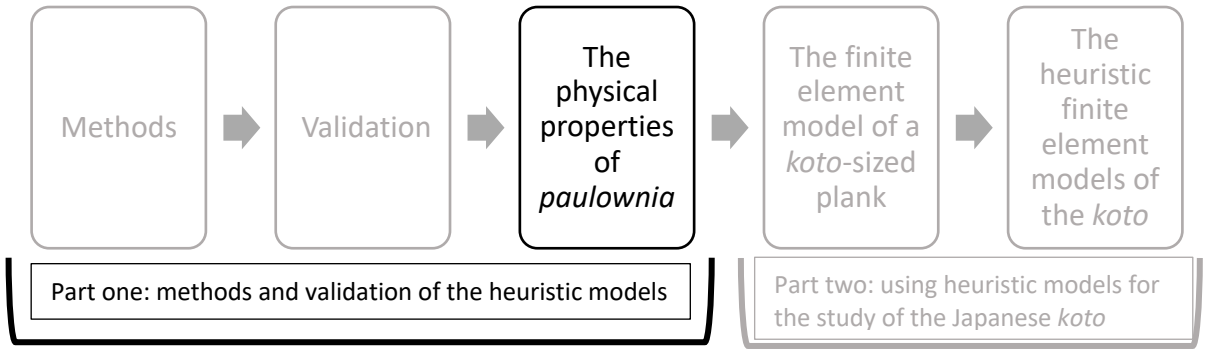

The previous chapter detailed the validation of the best available physical properties for this project. It was concluded that the anisotropic properties in this study are not an optimal match with experimental data and have room for improvement. This chapter documents exploration of options for improving the data available by optimisation, creating hybrid physical properties towards a 'generic' set of moduli, and testing of isotropic models. It was found that hybrid properties did not improve the response of the model towards a realistic set. An attempt to optimise the physical properties used for modelling *paulownia* was unsuccessful due to the assumption of linearity within each of the three directions. Nevertheless, this attempt was useful to find the limitations of using orthotropic values for modelling *paulownia* in analytical finite element modelling.

Isotropic moduli were explored because of their extensive use in musical acoustical studies of wooden instruments. The assumption of isotropy, whilst easier to manipulate, may be troubling as isotropic models do not capture fundamental features of the resonant modes of the body. Anisotropic moduli predict different sets of modes than the isotropic moduli in the first 2000Hz, the critical range in this study. By contrast to literature on other woods, (Bader 2006; Gough 2018; Rodgers 1988; Yoshikawa 2007), anisotropy does not result in a consistent and linear frequency drop in the modes in *paulownia.* It was observed that, though not optimal, the anisotropic properties reflect the resonance of the *koto* much more accurately than the isotropic models do. Throughout this study, the properties referred to as CW.2 are also referred to as anisotropic. This naming is done in the strictest sense, as they are not isotropic. These moduli are orthotropic and not triclinic in symmetry; the properties used in this study have 9 constants instead of 21 and these constants use the standard naming convention.

Isotropy vs. anisotropy

To investigate the issue of anisotropy more closely in its application on the heuristic modelling of the *koto,* this section tests the use of isotropic elastic moduli for studying the *paulownia* plank. It compares isotropic and anisotropic *koto*-sized planks[1], and tests isotropic box models

[1] Here *koto*-sized refers to the outer dimensions of the *yamadagoto* used for this study (1.85m x 0.264m x 0.074m). For norms of dimensions used by *koto* makers refer to Johnson (2004, 41)

against anisotropic box models to see the effect of isotropy versus anisotropy in modelling a highly asymmetrical wood such as *paulownia*.

Some materials, such as aluminium, have even structures at the fibre scale, but have close enough elasticity in each dimension that their acoustical response can be considered identical in all directions; they are effectively isotropic materials. Due to the nature of their growth, as cellular structures, all woods are anisotropic (Bucur 2006, 106); they have different elasticity in each of the length, width and radial dimensions. They are stronger along the grain than across it**,** and their cells grow differently in the three dimensions because of the direction and orientation of vessels, fibres and their cells (Bucur 2006, 106). Choosing to include fewer symmetries may produce more accurate results. A material can have up to 21 different elasticity constants. In anisotropic materials such as woods, it is desirable to simplify the elasticity using any symmetries (or approximations of them) available. Bucur states that for wood, we can find orthotropic symmetry and transverse symmetry to be useful; these symmetries result in 9 and 5 constants respectively. Bucur continues to state that using monoclinic symmetry and no symmetry (triclinic), which produce 13 and 21 constants respectively, are largely used for academic purposes (Bucur 2006, 106). Obtaining anisotropic moduli for materials is time and resource intensive. For some materials, anisotropic moduli are available (Bucur 2006, 46). For lesser-studied woods such as *paulownia*, such information is not available; recent discussions of the use of *paulownia* for musical instruments use 9 constants, which is the common level of anisotropy used in musical acoustics (Waltham and Yoshikawa 2018, 71).

Many studies on instrumental acoustics rely on isotropic models. Gough (2018) states that below 1kHz, the violin plate modes are not highly reliant on anisotropy, and that using a geometric mean of the Young's moduli along and across the grain is a practically viable solution. Gough is able to approximate the frequencies of the plates of the violin with isotropic Young's modulus. In earlier studies, he mentions that anisotropy reduces the plate mode frequency by 15 % but has little effect on shape (2015, 1211). Before discussing the investigations of the physical properties of *paulownia*, a brief overview of woods' material properties and particularities is presented.

Elasticity and Isotropy

The elastic constants (Young's moduli, shear moduli, Poisson's ratios) of a material, combined with its density determine its response stress and strain and affect the resonance of an object. Ashby charts the Young's modulus of a variety of materials against their density (2000, 37). In Figure 5.1, It is visible that woods have very different elastic moduli parallel and perpendicular to the grain, with the Young's modulus approximately 3 times higher parallel to the grain than perpendicular to it.[2]

[2] Shape and structure of the cells are directly related to the properties of cellular materials (Gibson and Ashby 1997, 11). Cell shape and size affect the mechanical properties of wood; cell shape does this much more significantly. Some of the anisotropy is also caused by the complicated arrangement of the cellulose fibres in the cell walls. The relative thickness of the cell walls is responsible for the density in one direction relative to the total density of the material, which in turn determines the material properties of the wood (Gibson and Ashby, 280, 313).

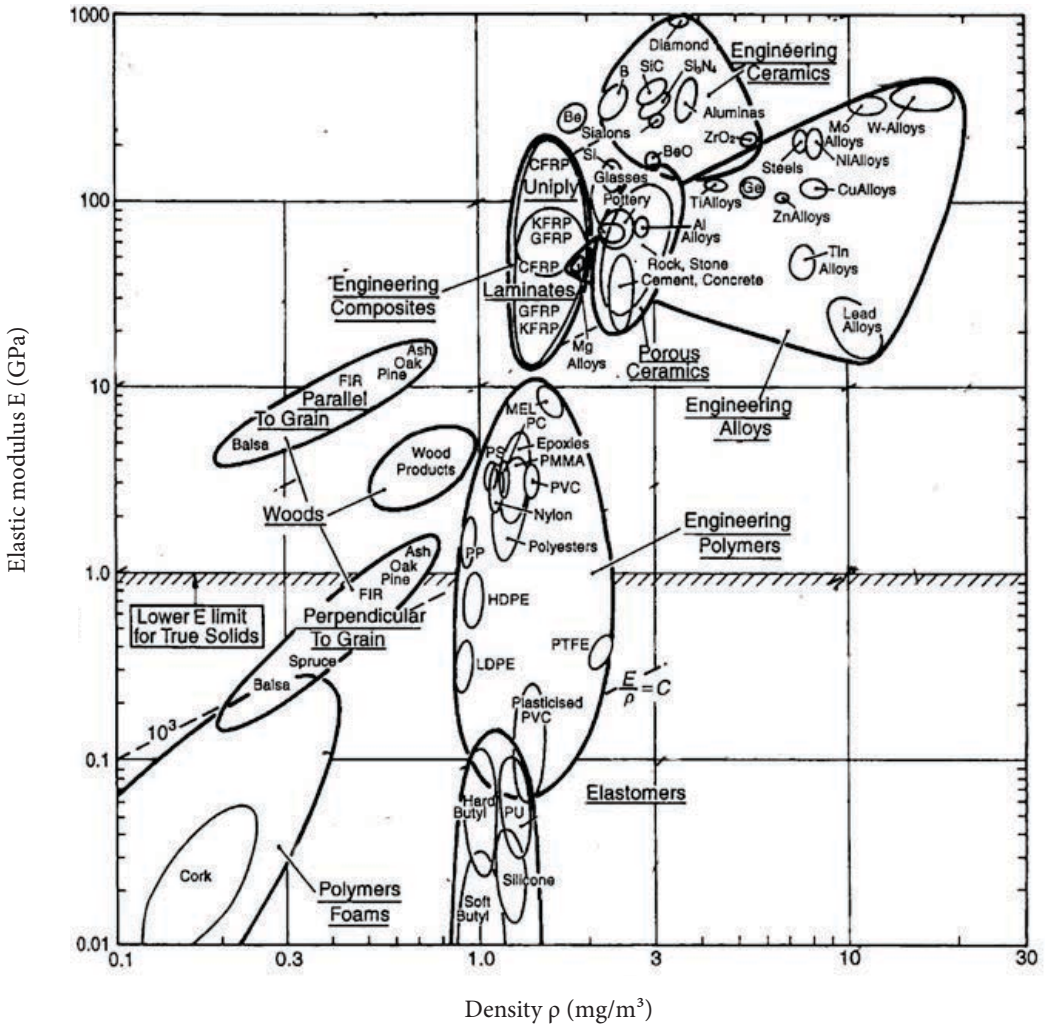

Figure 5.1 Elastic modulus of different materials as a function of density, adapted from Ashby (2000, 37).

In *Physics of Musical Instruments* (1991), Fletcher and Rossing provide a range of elastic parameters for woods, with the common value for Sitka spruce. In this list, longitudinal Young's modulus is said to range between 5-16GPa; radial Young's modulus between 0.7 – 2.2GPa; tangential Young's modulus between 0.4-1.1GPa (Fletcher and Rossing 1998, 721).

As Bucur states (2006, 106), anisotropy is relative and needs to be considered in the scale of examination. However, isotropy can be a problematic assumption in cellular solids such as wood because "when cells are equiaxed the properties are isotropic, but when the cells are even slightly elongated or flattened the properties depend on direction, often strongly so" (Gibson and Ashby, 11). This is an important issue for the *koto,* because the tension from the

13 strings may be an important cause of flattening of the cells. Even with the inclusion of the protective plate (Johnson 2004, 67), this effect would not be entirely alleviated. Bucur compares the percentage of anisotropy of various woods (2006, 64), with Sitka spruce at %100 anisotropy. SEM images of *paulownia* show it to be similar in anisotropy to spruce.

Paulownia

While the *koto* is made of *paulownia* grown in Japan, *paulownia* is also found in China, North America and Australia. There are six main varieties of the wood, with *paulownia tomentosa* being the dominant, and most likely the variety of *paulownia* of this author's sample. *Paulownia* is a very light and porous wood, and unlike some other woods, shows less radial symmetry (Coaldrake 2018). Recently, Waltham and Yoshikawa have discussed *paulownia*'s physical properties in the context of its use for musical instruments (2018, 71). The plank used in physical experiments of this study is a sample of *paulownia* grown in Australia. In this type of wood, the age affects the response significantly. The age of *paulownia* may be related to the high viscoelasticity of the wood. The anisotropic properties of *paulownia* used in this project were obtained from a study of North American samples. Therefore, there are three varieties involved in this study: the *yamadagoto* (Japanese), sample in this study (Australian), and the properties matrix available (Oregon, U.S.). It has not been possible in this study to ensure that the sample of *paulownia* used for physical experiments is the same as the wood used by *koto* manufacturers in Japan. Validation attempts expect variation between information of the three sources of data in this study and detail the results found. Figure 5.2 shows the SEM of a *paulownia* sample from a practice *koto* belonging to Coaldrake; the anisotropic cell structure can be seen clearly; a high level of anisotropy is visible in this sample.

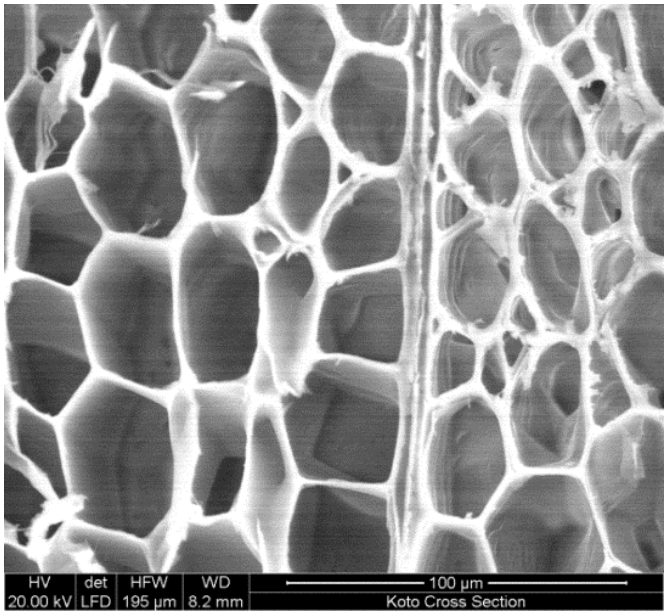

Figure 5.2 SEM of paulownia. Image courtesy of A. K. Coaldrake micrometer scale

Isotropic and Anisotropic studies of wooden musical instruments

Table 5.1 and Table 5.2 show a selection of studies that model the behaviour of wooden musical instruments, using isotropic and anisotropic grains in the models, the justification for use of the elastic constant(s). Table 5.1 shows studies that use isotropic approximations and Table 5.2 shows studies with different types of anisotropy.

Table 5.1 Previous studies with isotropic moduli

Study		
	Wood	Justification
Yoshikawa 2007	Spruce, *paulownia*, maple, etc.	Uses isotropic moduli only in the discussion of each wood and classifies based on characteristics. States "though the anisotropy is essential to the wood,4–6,9–12 only the longitudinal wave that propagates along the wood grain is analysed because it has the primary acoustical importance." (569)
Gough 2015	Spruce and maple	Finds reasonably close approximation to previous studies that employ or measure anisotropic data
Rodgers 1988	Spruce and maple	Found along-the-grain and across-the-grain stiffness and the corresponding shear stiffness as the most important properties for determining plate frequencies
Bader 2006	Not mentioned	12 cross-layers assumed to produce an isotropic result.

Table 5.2 Previous studies with anisotropic moduli

Study		
	Wood	Justification
Bécache, Chaigne, Derveaux and Joly 2004	Not mentioned	Orthotropic simulation of guitar (3 axes of symmetry, 9 elastic moduli)
Shepherd, Hambric, Wess 2014	Sitka spruce	Orthotropic simulation of guitar (3 axes of symmetry, 9 elastic moduli)
Elkabarietta, Ezcurra, Santamaría 2002	Canadian cedar, Indian rosewood and spruce	4 elastic moduli for each wood used (two Young's modulus, one shear modulus, one Poisson's ratio)
Bretos, Santamaría and Moral 1999	Maple and spruce	Constants along and across the grain
Giordano 1997	Spruce	uses isotropic and anisotropic models (orthotropic)
Chabassier, Chaigne and Joly 2013	Spruce and beech	Bidimensional orthotorpic
Bielski and Kujawa 2017	Mahogany, spruce, cedar, rosewood*	All except for Indian rosewood modelled orthotropic. Cites lack of physical information for isotropic values for rosewood
Trévisan, Ege, Laulagnet 2017	Spruce	Orthotropic ribbed plate for piano soundboard

Table 5.2 shows that most anisotropic models are assumed to be orthotropic in symmetry. This is a valid assumption as long as "a sample of wood is cut at a sufficient distance from the centre of the tree that the curvature of the growth rings can be neglected" (Gibson and Ashby 1997, 278). *Paulownia* is a very light hardwood with weak growth rings; a plank of *paulownia* weighs

one tenth of that of a same-sized aluminium plank. The lack of obvious growth rings in hardwoods is due to the even spacing of sap channels in these woods (Gibson and Ashby 1997, 279 and 303). It cannot be assumed that in this study the plank has been cut from sufficient distance from the centre and this may complicate the issues around isotropy and anisotropy. Figure 4.2 in the Validation chapter shows the growth rings, which appear to be close to the centre of the tree.

Testing isotropic moduli

Gough (2015a, 2015b, and 2018) uses the geometric mean of available values in the literature to obtain a Young's modulus. Waltham's 2015 report of isotropic properties for *paulownia*, which includes the anisotropic matrix used in this study, states the Young's moduli for the *tomentose* variety of *paulownia* tested to be 5.6, 0.63 and 0.26GPa. Taking Gough's approach of using the geometric mean will give an isotropic Young's modulus (E) for each direction of 1.2GPa. A simple isotropic plank at 1 to 1.5GPa in increments of 0.025GPa was tested to find a potential generic isotropic modulus to use. It was also used to see the sensitivity of the model's response in the modal domain to isotropic moduli and their predictive power in this study. For eigenfrequencies in isotropic planks with E = 1 to 1.5GPa, as the Young's modulus increased, so did the frequency of each mode. There were no observed changes in mode shape. The plank was also modelled with the isotropic Young's modulus of 5GPa (an estimate along the grain).

Figure 5.3 shows a comparison eigenmodes of a model of a *koto*-sized plank (1.825m x 0.245m x 0.074m) with different physical properties. A model with the elastic modulus along the grain is seen in black, and the range of models around the geometric mean are seen in the colour band. In contrast, the change in slope is seen with the anisotropic model (CW.2 properties) in red. This comparison is to evaluate whether an isotropic modulus can be used to predict values close to the anisotropic matrix used in this study.

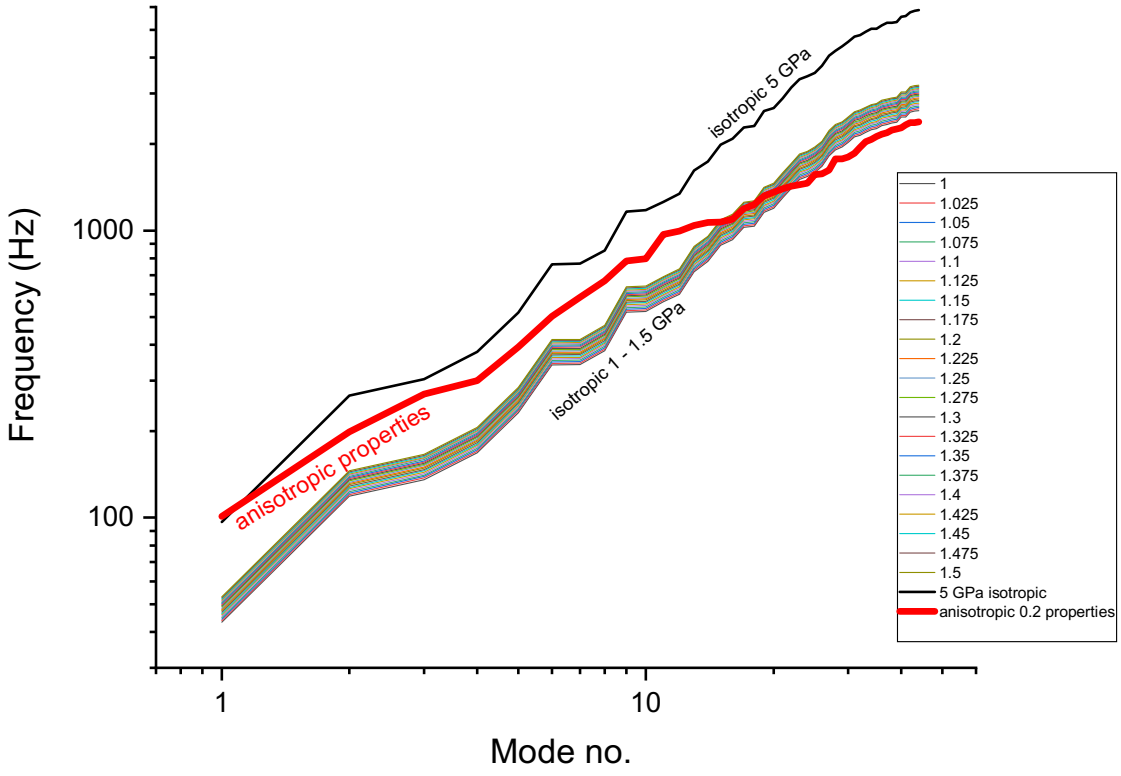

Figure 5.3 Eigenmodes of isotropic and anisotropic models of a koto-sized plank

With anisotropy, (m,2) and (m,3) modes appeared in the first 1000Hz; isotropic models did not show these modes in the first 5000Hz range. Some curved nodal lines were also observed in anisotropic models. The curved nodal lines may be caused by anticlastic bending, which is affected by elastic moduli and Poisson's ratio (Shepherd and Hambric 2016). The results indicate that isotropic models do not predict realistic mode shapes for the plank and the effect of anisotropy is not merely a frequency drop**.** This was seen in models with dimensions of the Australian plank.

In Figure 5.3, at lower frequencies, the anisotropic properties predict modes similar to those of the model with the Young's modulus of 5GPa. The lower slope of the anisotropic box means that by the 30th mode, anisotropic modes are lower in frequency than the lowest isotropic Young's modulus of 1GPa. Additionally, the responses of the isotropic range seem close to parallel. The results in Figure 5.3 indicate that Young's modulus and frequency are directly correlated, but that isotropic and anisotropic boxes have little response in common in *paulownia*. In Figure 5.4 and Figure 5.5, individual mode types are separated in isotropic and anisotropic planks.

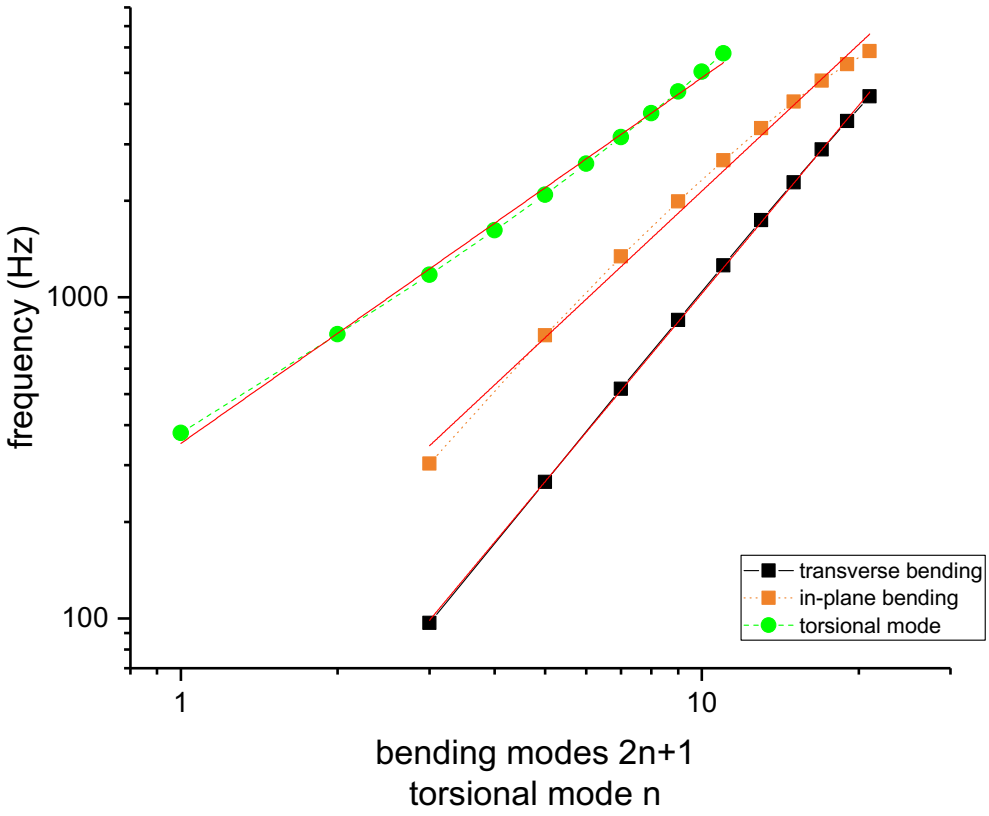

Figure 5.4 Identified mode shapes in isotropic models of a koto-sized plank model

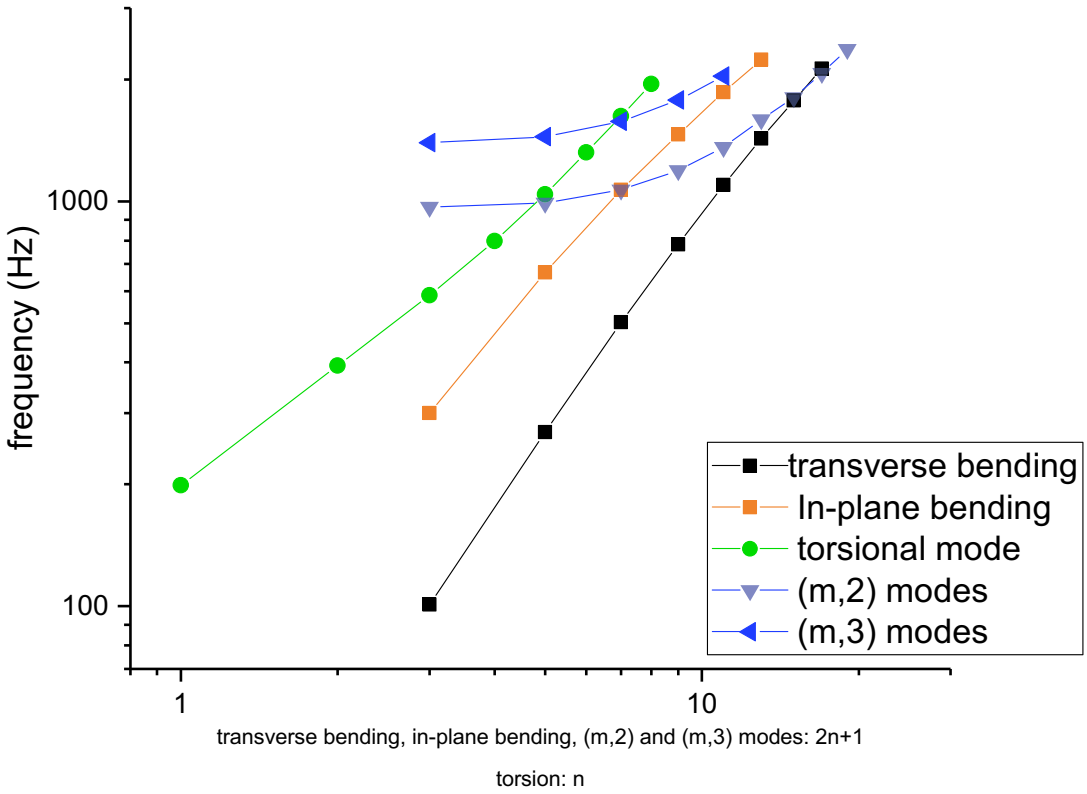

Figure 5.5 Identified mode shapes in an anisotropic koto-sized plank model

In Figure 5.4 and Figure 5.5, no significant change is seen in the frequency of modes for each of the transverse bending, torsion, or in-plane bending modes. However, when comparing all the modes of isotropic and anisotropic planks without separation of mode types, a clear difference exists in terms of slope. This difference owes to the extra (m,2) and (m,3) modes that are present in the anisotropic plank. These modes do not feature in the first 5000Hz in the isotropic plank. Therefore, consideration of the change in frequency for one mode or mode type is not sufficient in deducing the use of isotropic planks. In Table 5.3, the slopes of the modes of planks are compared.

Table 5.3 Isotropic and anisotropic models slopes and intercepts

	Isotropic slope	Isotropic intercept	Anisotropic slope	Anisotropic intercept
Transverse bending	1.94	1.06	1.75	1.19
Torsion	1.13	2.54	1.09	2.27
In-plane bending	1.51	1.81	1.36	1.84

In both the isotropic and the anisotropic planks, the slopes are highest for the torsional modes, followed by the in-plane bending and then transverse bending modes. The ratio of the isotropic to anisotropic slopes and intercepts for each mode type is shown in Table 5.4.

Table 5.4 Ratio of isotropic vs. anisotropic slopes and intercepts for each mode type

	Isotropic/anisotropic slope	Isotropic/anisotropic intercept
Transverse bending	1.1	0.89
Torsion	1.03	1.11
In-plane bending	1.11	0.98

Table 5.4 shows that all the slopes are higher in isotropic models than in anisotropic models. Comparing the slopes of each mode type between the boxes shows that in all three main mode types found, the slopes decrease in the anisotropic plank but the intercepts slightly increases with anisotropy, which shows that modes start to appear at slightly higher frequencies in anisotropic models, but they appear closer together.

Isotropic vs. anisotropic box models

In this section, isotropic box models were compared with anisotropic box models. These models are all full-body models and do not include model of individual plates. This comparison attempted to separate the effects of anisotropy from the effect of geometric complexity on eigenmodes and to check if isotropic box models approximated mode shapes well. The modes of isotropic and anisotropic boxes with the dimensions of the *koto* are shown. Each identified

mode is compared between isotropic and anisotropic box models in Table 5.5, Table 5.6 and Table 5.7.[3]

Table 5.5 Transverse bending modes seen in isotropic and anisotropic models

Transverse bending modes		MODE FREQUENCY VS. GEOMETRY			
TOP VIEW	END VIEW	SIMPLE PLANK	HOLLOW BOX	HOLLOW BOX WITH 2 SOUND HOLES	IDEALISED BOX
Anisotropic models					
Isotropic (E= 5 GPa) models					
	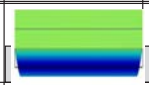	101	93	92	91
		96	92	92	91
		269			213
		265	267	262	259
		503			
		518	521	498	500
		782			
		851			776
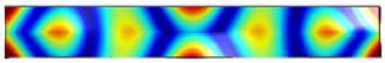		1097			
		1259			
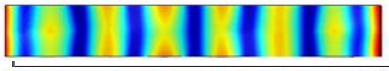		1428			
		1739			
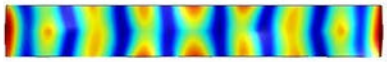		1774			
		2283			
		2128			
		2887			

Table 5.6 Torsional modes seen in isotropic and anisotropic models

[3] The (m,2) and (m,3) modes are only observed in the simple anisotropic plank, and so are not useful in this comparison with isotropic models, except that they do not appear in the isotropic model; the *koto* shows the (0,2) mode at 635Hz. These modes are discussed in the Plank and *koto* chapters further as necessary.

torsional modes

MODE FREQUENCY VS. GEOMETRY

TOP VIEW	END VIEW	SIMPLE PLANK	HOLLOW BOX	HOLLOW BOX WITH 2 SOUND HOLES	IDEALISED BOX
Anisotropic models					
Isotropic (E= 5 GPa) models					
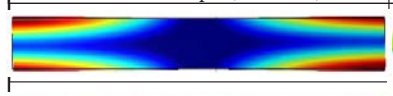	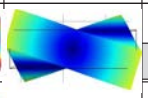	199	140	134	135
		378	259	249	255
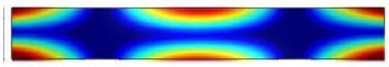		393	152	144	164
		768	366	339	386
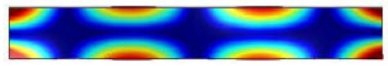		586	297	299	299
		1177	536	507	541
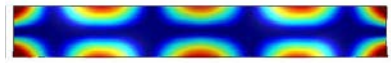		797	396	373	386
		1616	730	699	744
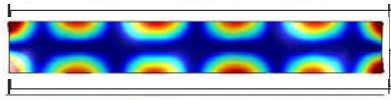			498		617
		2089	1072	1044	1070
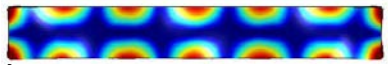		1041			
		2605	1462	1418	1247
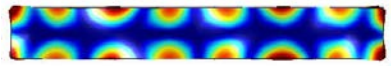		1319			
		3749	1887		
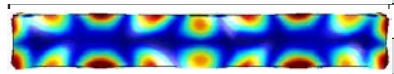		1623			
		3749			
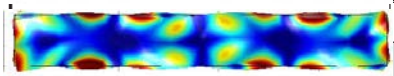		1947			
		4377			

Table 5.7 In-plane bending modes seen in isotropic and anisotropic models

in-plane bending modes

MODE FREQUENCY VS. GEOMETRY

TOP VIEW	END VIEW	SIMPLE PLANK	HOLLOW BOX	HOLLOW BOX WITH 2 SOUND HOLES	IDEALISED BOX
Anisotropic models					
Isotropic (E= 5 GPa) models					
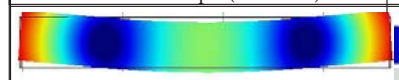		300	264	252	252
		304	304	298	295
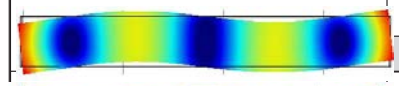		667	514	489	487
		762	733	711	706
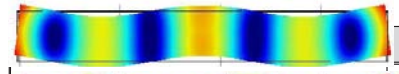		1067			
		1342	1216	1198	1188
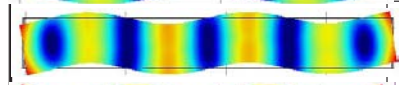		1463			
		1988	1681		1672
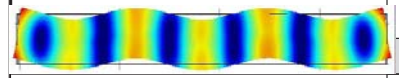		1858			
		2669			
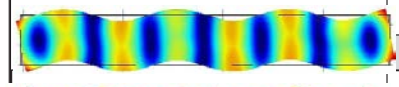		2236			
		3367			
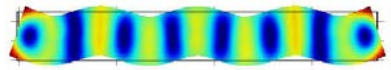					
		4066			
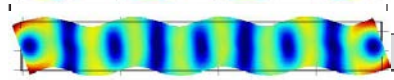					
		4735			

The difference between the same modes in isotropic and anisotropic modes is shown in Table 5.5, Table 5.6 and Table 5.7. Transverse bending modes are more closely similar between isotropic and anisotropic boxes than torsional and in-plane bending modes. Both isotropic and anisotropic planks have much higher mode frequencies than box models. All isotropic box models have relatively close mode frequencies to each other, regardless of sound holes and struts.

Up to this stage, comparison between isotropic and anisotropic models has been restricted to models without reference to physical data because no physical equivalent of these models exists. Therefore, two isotropic models of the plank were made with moduli of E= 5GPa and E= 1.2GPa, which is the geometric mean of the orthotropic properties available. The first 44 mode frequencies are compared with resonances found in the two transducer experiments and the LSV results from Chapter Four, as well as the anisotropic model. Figure 5.6 shows the alignment of the peaks from the physical experiments with the modes of the isotropic and anisotropic models.

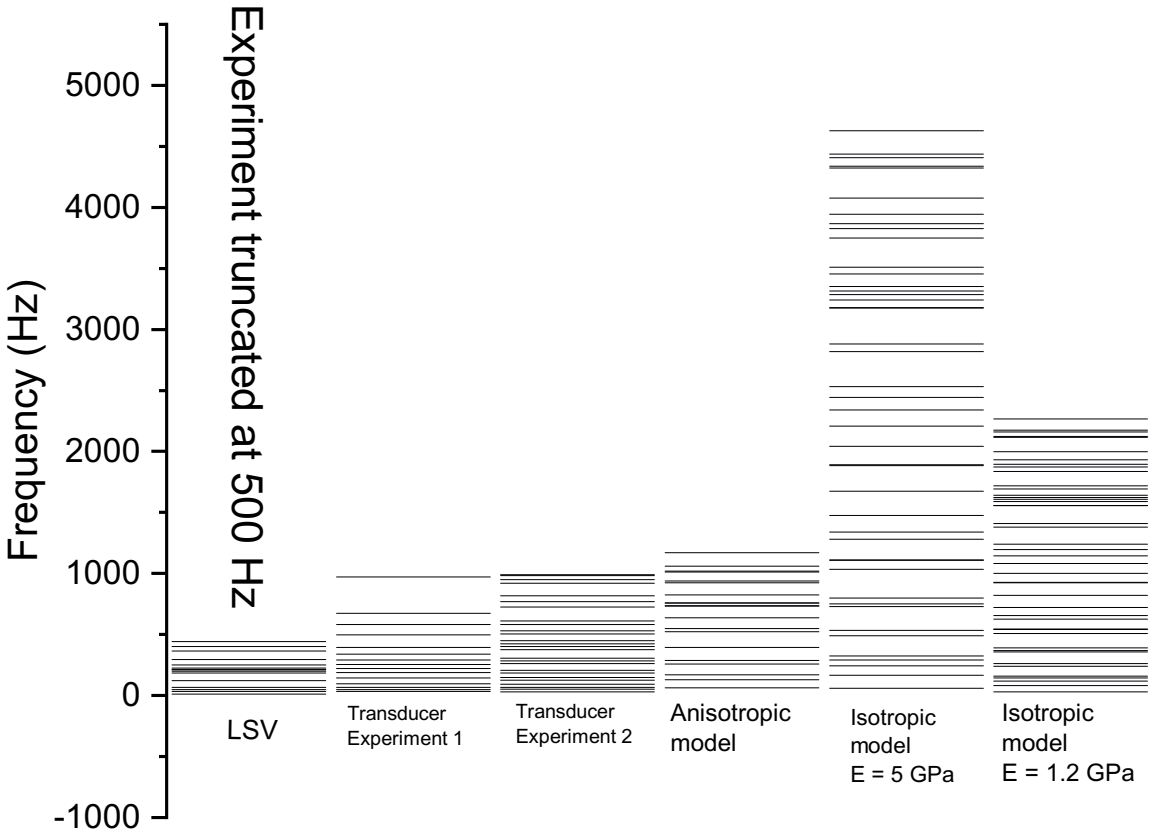

Figure 5.6 Isotropic and anisotropic models compared with physical experiments[4].

Figure 5.6 shows that the anisotropic model predicts many more of the mode frequencies observed in the physical experiments than the isotropic models do. The isotropic modulus of 5GPa is clearly inappropriate for modelling the wood. However, the isotropic model with the Young's modulus of 1.2 is closer to the anisotropic model in terms of frequency and so it may still be a viable replacement for the anisotropic properties. The LSV results are not as useful for frequency analysis because of the small range of frequencies studied with them. However, the LSV is the only experiment that has shown the mode shapes. Therefore, in Figure 5.7, the mode shapes for the first 500Hz are compared between the isotropic model (E=1.2 GPa), the anisotropic model and the LSV results.

[4] note LSV experiment was truncated at 500Hz by the external laboratory operator, stating that the required time for a larger frequency range was not available

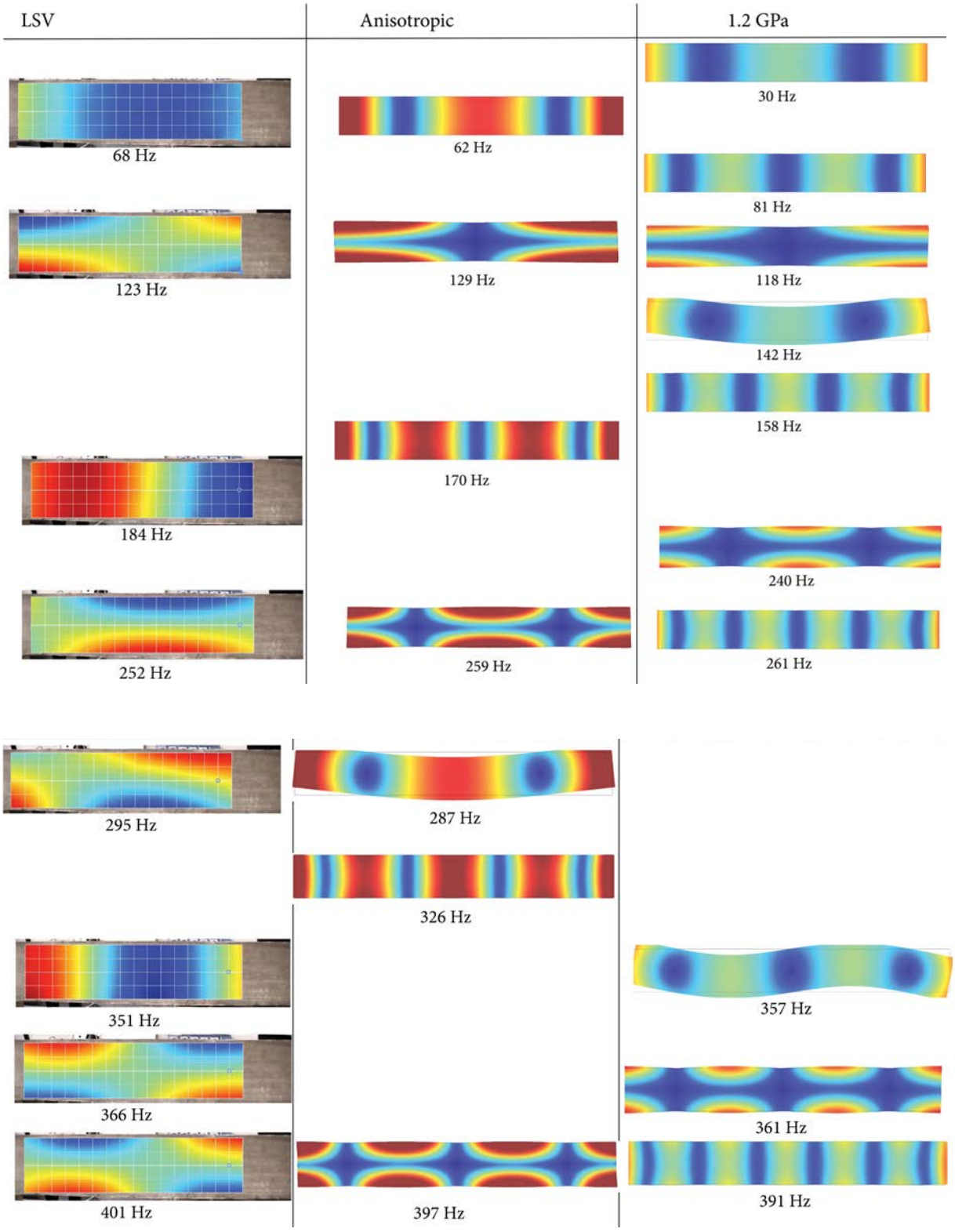

Figure 5.7 Isotropic model (E=1.2GPa) and the anisotropic model compared with LSV results of the plank

Figure 5.7 shows that the anisotropic results predict the majority of the modes seen with the LSV closely. Where the isotropic model predicts mode frequencies close to the LSV and anisotropic results, in all but one case the isotropic results model does not predict the correct mode shape. This observation shows that isotropic properties are incompatible with physical data; while the anisotropic properties are not ideal, the isotropic models have not improved the predictive power of the models.

Conclusion

In the anisotropic models, the first 44 modes are seen in a smaller frequency range. The components have a similar effect on the frequency range, but the effect is intensified with anisotropy combined. Anisotropy does not introduce (m,2), (m,3) and (m,4) modes generally, but if they exist in an isotropic wood with the same size and other properties, they appear outside the 'critical' range.[5] No ideal isotropic modulus has been found. The Young's modulus of 5GPa in isotropic models renders mode frequencies that are too high; the modulus of 1.2GPa gives closer eigenfrequencies but predicts a different mode shape to shapes predicted with the anisotropic model and observed using the LSV.

If the sample of wood that is tested was dry, seasoned and knot-free, the age and moisture content would not contribute to the physical properties as much as the relative density of each direction to the total density of the wood (Gibson and Ashby, 314). However, the plank used in this study is a young sample (it had been dried for 3 months and was about one year old at the time of purchase). It also seems that the sample is cut relatively close to the centre of the tree. The combined effect of these factors is that orthotropic properties struggle to replicate the responses captured in physical testing. With the isotropic moduli eliminated as an option for modelling, this exploration continues with attempts at improving the anisotropic moduli in the form of hybrid properties and optimisation of the available matrix of moduli.

[5] The critical range is 0-2kHz. These modes have not been found in the isotropic models of this study in frequencies up to 5000Hz.

Testing hybrid physical properties

The physical properties used in this work (see Methods chapter) were combined with properties from a FEM study of historical *qins*, (hereafter *qin* study properties), made available to the author as the Voigt matrix seen in Table 5.8 (Waltham, Coaldrake, Koster, Lan, 2017; Yang 2014). A set of hybrid properties were made as the geometric mean to test. If successful, the hybrid set can serve as a generic set of moduli for *paulownia* in heuristic studies. The Voigt matrix for all three sets of properties is shown in Table 5.8.

Table 5.8 CW.2, qin study and hybrid Properties

CW.2 properties					
5.81E+09	3.23E+08	1.85E+08			
	7.03E+08	1.35E+08			
		2.89E+08			
			1.68E+07		
				3.70E+08	
					5.20E+08
Qin study properties					
5.16E+09	2.64E+08	6.82E+08			
	2.11E+08	2.27E+08			
		3.37E+08			
			3.30E+07		
				4.16E+08	
					5.59E+08
Hybrid properties					
5.45E+09	2.36E+08	5.62E+08			
	1.72E+08	1.61E+08			
		2.72E+08			
			2.58E+07		
				3.93E+08	
					5.40E+08

Eigenmodes were obtained with all three sets of properties shown in Table 5.8. Mode shape and eigenfrequencies were compared between physical data from the LSV and the simulations with each of the three sets of properties. Table 5.9 shows the frequencies of all of the mode types discussed in all three sets of anisotropic properties; where LSV results exist, frequencies observed from the laser are also included in the comparison. Frequencies are shown in Hertz.

Table 5.9 Mode frequencies in each anisotropic modulus and in the LSV

Mode	LSV	CW.2	*Qin* study properties	Hybrid properties
Transverse bending				
(2,0)	68	63	48	54
(3,0)	184	170	134	148
(4,0)	352	326	259	286
(5,0)		524	450	469
(6,0)		759	645	680
(7,0)		1020	875	922
(8,0)		1304	1134	1190
(9,0)		1604	1416	1479
(10,0)		1917		
Torsion				
(1,1)	123	129	133	131
(2,1)	252	259	264	262
(3,1)	366	397	399	398
(4,1)		550	544	546
(5,1)		731	709	717
(6,1)		940	891	911
(7,1)		1181	1124	1139
(8,1)		1448	1360	1386
(9,1)		1730	1624	1657
(10,1)		2033		
(m,2)				
(0,2)		738	339	376
(1,2)		760	394	437
(2,2)		827	577	595
(3,2)		925	783	784
(4,2)		1059	998	987
(5,2)		1223	1217	1199
(6,2)		1409	1441	1416
(7,2)		1625		1646
(8,2)		1863		
In-plane bending				
IPB 1		287	221	253
IPB 2		636	512	575
IPB 3		1013	829	926
IPB 4		1383	1136	1268
IPB 5		1751	1425	1594
IPB 6		2102		
Hybrid/Unknown mode shape				
hybrid (1,1)			786	988
hybrid (2,1)			796	993
hybrid (3,1)			871	1053
hybrid (4,1)			1006	1180
hybrid (5,1)			1203	1379
hybrid (6,1)			1446	1629

Table 5.9 shows that although there are not many bending modes found from the laser data, a strong correlation is seen between the modes identified and the transverse bending modes

in COMSOL. The *qin* study properties and hybrid properties show curved nodal lines in lower frequency modes than the CW.2 properties set does. In the comparison of the frequencies between these modes, strong similarity is seen throughout. The torsional modes in Table 5.9 show less variation across the properties used. In-plane bending modes do not seem to be as affected as the other mode types. In Table 5.9, there is some mode shape change as the modes progress. In in-plane bending modes and (m,2) modes are omitted from this analysis because they were not clearly observed in the LSV and there is no physical counterpart to the predicted modes.[6] To expand the physical comparison, the peak frequency results from the validation attempts are compared with the three sets of properties available in Table 5.10. The mean frequency for each peak from all of the simulations and from the physical experiments are shown in the two columns on the far right. The mean, standard deviation, and the variance across each set of results is shown at the bottom of the table. Frequencies are all shown in Hertz.

[6] However, unusual and unexplained mode shapes appear in the hybrid properties and the *qin* study properties. These modes have nodal lines similar to those of torsional modes but their movement is in-plane, which is visible from the end view. These modes are not included because there is no frame of reference for them elsewhere in this work.

Table 5.10 Comparison of peak frequencies observed in validation with results from anisotropic models

transducer experiment 1	transducer experiment 2	LSV	CW.2 properties	*Qin* study properties	Hybrid properties	Mean of physical experiments	Mean of simulations
		13					
32	31	35				33	
50	52	50		47	54	51	51
65	66	68	62			66	62
97	93					95	
	125	123	129	132	131	124	131
144	146				148	145	148
187	185	184	170			185	170
	207	200				204	
		211				211	
		215				215	
222		225		221		224	221
255		252	259	259	253	254	257
	261			264	262	261	263
293	282	295	287		286	290	287
	305					305	
340		351	326	339		346	333
	374	366			376	370	376
395	403	401	396	399	398	400	398
	423					423	
	451	441		449	437	446	443
496	506			511	469	501	490
	530		524			530	524
			549	544	546		546
582	583			576	575	583	576
	611		636		595	611	615
675					680	675	680
				709			
	724		731		717	724	724

				738				738
				759		784		771
	778	771		760	782		775	771
		817		826	829		817	828
	869						869	
		919		925		911	919	918
		949		940		922	949	931
	971	983			978	926	977	952
		990		1012	1006	934	990	984
				1019	1021	987		1009
				1059		988		1023
				1172		993		1083
Mean	379.47	431.88	227.80	530.41	469.27	498.47	424.21	489.00
StDev	300.03	298.65	126.29	286.56	270.52	274.62	287.44	279.78
Variance	90020.76	89194.36	15948.60	82116.51	73183.50	75414.21	82622.90	78274.70
n	17	26	16	21	17	23	33	31

Table 5.10 shows close correlation between the physical results and the simulations across the three anisotropic properties. Next, an independent unpaired two-tail t-test with assumption of homoscedasticity was done between the mean of the physical results and that of each of the properties as well as the mean of the simulated modes. The results are shown in Table 5.11.

Table 5.11 T-test results

	mean of physical experiments vs. mean of simulations	mean of physical experiments vs. CW.2 properties	mean of physical experiments vs. *qin* study properties	mean of physical experiments vs. hybrid properties
t-value	0.136	0.034	0.315	0.095
p-value	0.446	0.486	0.378	0.462

The critical p-value is set at 0.05. From the above t-test, it can be deduced that the CW.2 anisotropic properties are not significantly different from physical experiments. However, the *qin* study properties and hybrid properties are significantly different. Therefore, these two sets of properties are not optimal for use in this project. The correlation between the CW.2 results and that of the mean of physical results shows a weak correlation. Ascertaining the mode shapes of the measured peaks is necessary for further clarification.

To run a paired t-test between these sets of data, the physical results can be considered the pre-treatment set, and the simulations as the post-treatment set. This assumption sets the modelling properties as the 'treatment'. There is no material available outside the results of this study on *paulownia* that can be used as the pre-treatment set. In such a setup, the t-values rise considerably. The CW.2 properties can also be considered a different pre-treatment set and the other two properties post-treatment. The results for both of these considerations are documented in Table 5.12:

Table 5.12 Paired t-test

paired t-test: set 1:				
pre treatment	mean of physical experiments	mean of physical experiments	mean of physical experiments	mean of physical experiments
post treatment	mean of simulations	CW.2	*Qin* study	Hybrid
t-value	0.07	0.93	0.10	0.03
p-value	0.944	0.362	0.925	0.976
set 2:				
pre treatment	CW.2	CW.2		
post treatment	*Qin* study	Hybrid		
t-value	0.22	0.04		
p-value	0.88	0.96		

In this paired t-test, p-values showed that the results are not significantly different between the properties.

Findings

This validation process shows that these hybrid properties do not improve the physical properties. It also shows some of the changes in mode shape across the matrices used. These moduli are all of *paulownia* or derived as an average of the known data. A range of possible mode shapes is observed within the confined scope of *paulownia* properties available. At this stage, the only other option was to try and optimise the physical properties available.

Optimising physical properties

Investigations to find alternative isotropic and anisotropic moduli for *paulownia* wood were unsuccessful to this point in the study. These investigations did not improve the results for modelling this wood from those obtained with the CW.2 properties, which were validated in Chapter Four. Therefore, an optimisation attempt was undertaken to improve the CW.2 properties used for modelling *paulownia.* This optimisation uses the eigenmodes of the plank model and aims to improve the elastic moduli available so that the alignment between the predicted and measured modes is increased. The benchmark physical data is the peaks from the second transducer experiment in Chapter Four. This optimisation tries to calculate what elastic moduli would result in the peaks observed with the physical experiment.

For this analysis, the five elastic constants of the CW.2 properties are varied systematically. A balanced fractional factorial design was used with a high and low value for each elastic constant. This means that each modulus is tried at a low value (80% of its original value) and a high value (120% of its original value). The combinations of all variations for the high and low values of the moduli gives 32 iterations. In this set of permutations, no combination of high and low values for each of the five elastic constants has a higher weighting than the others. The systematic variation used a balanced group set adapted from *The CRC Handbook of Tables for Probability and Statistics* (1966, 69).

The eigenmodes are obtained with each variation. Linear regressions are then undertaken for each mode shape across all variations of the elastic constants to improve the predicted eigenfrequencies. These frequencies are individually compared with the corresponding result from the physical experiment. The aim of the optimisation is to minimise the total difference between the predicted and recorded modes. The sum of the difference between the predicted modes and the peaks from the physical experiment is then calculated as the objective function, which is minimised to give the optimised elastic constants.

Figure 5.8 shows an example page from the systematic variation of the CW.2 properties. On the right-hand side, the frequencies at which each mode (each row) is observed is shown for the first eight variations. The associated mode shape is shown on the left-hand side of Figure

5.8.

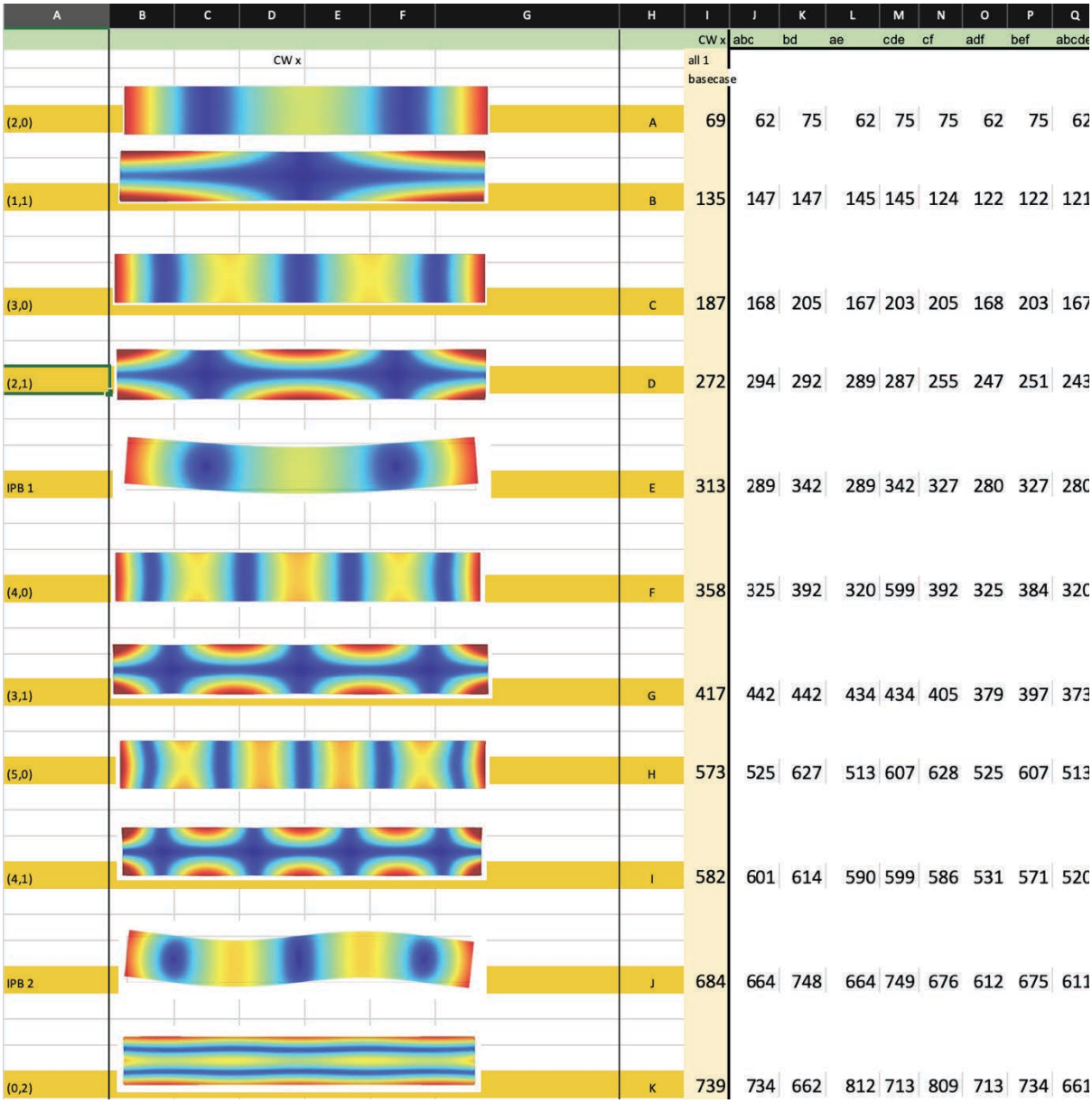

	CW x	abc	bd	ae	cde	cf	adf	bef	abcde
A	69	62	75	62	75	75	62	75	62
B	135	147	147	145	145	124	122	122	121
C	187	168	205	167	203	205	168	203	167
D	272	294	292	289	287	255	247	251	243
E	313	289	342	289	342	327	280	327	280
F	358	325	392	320	599	392	325	384	320
G	417	442	442	434	434	405	379	397	373
H	573	525	627	513	607	628	525	607	513
I	582	601	614	590	599	586	531	571	520
J	684	664	748	664	749	676	612	675	611
K	739	734	662	812	713	809	713	734	661

Figure 5.8 Example page from varying the physical properties for optimisation

After the variation of the elastic moduli and the regressions for each identified mode, Microsoft Excel's Solver function improved multipliers for the elastic moduli.[7] This output matrix, though showing the lowest objective function found, was still problematic. Firstly, the new moduli were extremely low. Secondly, they yielded results incompatible with physical measurements;

[7] Since the optimisation efforts in this study, newer versions of COMSOL Multiphysics include sophisticated optimization tools. These tools were not available at the time of this analysis and may be preferable to using the Excel Solver function in future studies

the mode shapes were not observed in the physical experiment and so, it is not possible to confirm that the modes aligned between the predicted and measured peaks are in fact the same eigenmode.

To battle the first issue, the lowest moduli predicted from the optimisation manually kept at their original values. These moduli are the longitudinal Young's modulus (EL) and the radial-tangential shear modulus (GRT). The simulation returns values much closer to the measured data by the exclusion of EL and GRT from optimisation. In Table 5.13, the results from both attempts at optimisation (with and without El and GRT) are compared with the original CW.2 properties.. In the table, each row shows one mode type. The frequencies for both sets of optimisation are shown for each row. For example, the (3,0) mode is seen at 39Hz when all moduli are changed. This mode is predicted at 161Hz when EL and GRT are manually kept at pre-optimisation values. This mode is found at 170Hz with the original CW.2 properties

Table 5.13 Comparison of two optimisation attempts, with and without manual control of EL and GRT

	Mode Frequency (Hz)		
Mode type	Solver Optimisation with all moduli	Manual EL and GRT	Pre-optimisation
(2,0)	14	62	63
(3,0)	39	161	170
(1,1)	41	44	129
IPB 1	67	178	287
(4,0)	76	295	326
(2,1)	80	107	259
(3,1)	116	204	397
(5,0)	125	448	524
(4,1)	153	332	550
IPB 2	161	289	636
(6,0)	185	613	759
(5,1)	196	481	731

Table 5.13 shows that, especially in higher order modes, both optimisation attempts are unsuccessful. At the present date, the author believes that the failure of optimisation is due to the assumption that in each of the tangential, radial and longitudinal directions, the properties are uniform and can be linearly extrapolated. Thus, although the physical properties (CW.2)

are not an exact match, they are the most useful properties. The most important reason for using the CW.2 properties is that they predict the resonances of the wood within a useful margin for this study (as shown in the Chapter Four). These CW.2 properties were obtained from physical measurements and not purely from numerical estimates and are still better than the unverified optimised values.

An important difference between the results is likely that of the origin in the wood samples; the simulations rely on information on North American *paulownia,* Coaldrake's *koto* is from *paulownia* grown in Japan, and the plank is from *paulownia* grown in Australia. Their elastic moduli are almost certainly different. The optimisation of physical properties for a general case was not successful. For the remainder of this study of the *koto*, the CW.2 properties continue to be used because they are the best-available properties and have been shown (in Chapter Four) to predict relatively close modes to those measured.

Concluding remarks

This chapter reviewed existing work on isotropic modelling of wooden musical instruments. It also compared isotropic and anisotropic models of *paulownia* using the best data available and approximation methods used by others in isotropic studies. The isotropic and anisotropic models of planks and *koto*-sized boxes were compared, and plank models were compared with experimental data. This chapter has found that there are few similarities between isotropic and anisotropic models. Other scholars have suspected issues with isotropic models. This study has shown that while the anisotropic models do not show a perfect match for the physical data, they are nevertheless more appropriate than isotropic models for the study of *paulownia*. This conclusion is based on the following three reasons:

1. Isotropic models do not predict the correct mode shape (see Figure 5.7) even when predicting the frequency accurately.
2. Isotropic box models predict widely different frequencies for the same modes than anisotropic models do (Table 5.5, Table 5.6, Table 5.7)
3. To successfully model the wood as isotropic, the assumption needs to be that it is cut sufficiently far from the core of the tree. It cannot be ensured that the sample of wood

used in this study has been cut in this fashion to allow for a reasonable isotropic approximation.

Therefore, although isotropic models have been useful for other studies, they are inappropriate in the study of the *paulownia*. It is likely that isotropic moduli are also problematic for similarly light and highly anisotropic woods. This study will continue with the orthotropic properties available for *paulownia*. However, future work on the *koto* will benefit from additional attempts at refining the available data on the physical properties of *paulownia.*

In Part One of this study, the methods of finite element modelling were discussed. The methods, physical properties and models were validated. Following, the use of isotropic and anisotropic moduli was explored further in this chapter. At this stage, this study has refined the tools used for analysis and discussed considerations and limitations present on the study. In Part Two, the methods are used for the discovery of the acoustical characteristics of the *koto* with the heuristic finite element models. Part Two starts with the finite element modelling of a *koto*-sized plank.

Part Two

Using Heuristic Models for the Study of the Japanese *Koto*

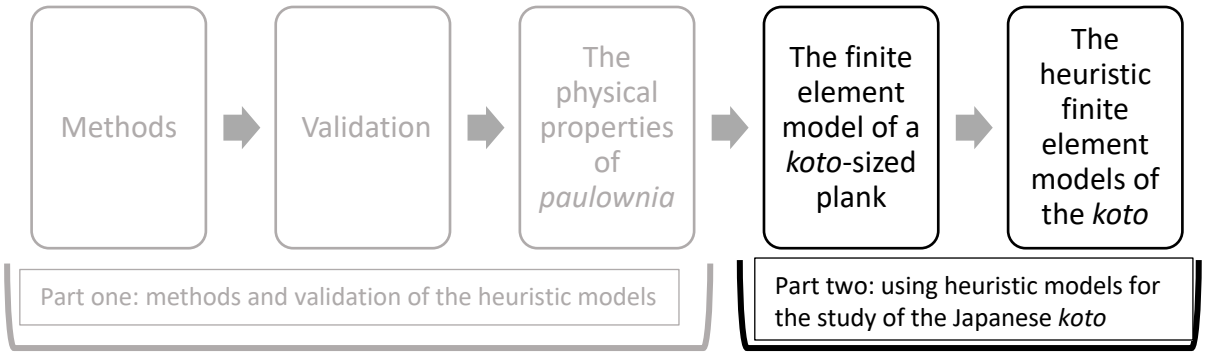

Part One of this thesis outlined the methods used for finite element modelling of the *koto* using heuristic models. It showed the validation of the methods, models and physical properties, and with further analysis showed the importance of modelling anisotropy in the study of the resonances of a body made of *paulownia* wood. This part applies the methods with the use of the heuristic models to the *koto*, not only to evaluate the usefulness of the methods in general but also for each model in particular. This part also investigates the characteristics of the sound of the *koto* using studies of the heuristic models in the three modal, frequency and time domains. This part starts with the simplest form of the model, which is a *koto*-sized plank of *paulownia* (Chapter Six). In Chapter Seven, the *koto* models are discussed.

First, the resonant modes of each model are obtained. With this analysis in the modal domain, the relationship between the basic components of the *koto* body and its resonances is clarified. Then, with a smaller group of important models, the next step of analysis is conducted. Air is added to selected box and lofted models to examine how the wood and the air interact to add or change resonances. This analysis, in the frequency domain, shows the importance of the internal air cavities. With these first two domains, the role of the wooden body and the air are characterised. Finally, time is added to the studies with the transient response of the lofted model. The transient response represents the dissipation and transmission of sound from the instrument body to the surrounding air, over a period of time. Therefore, it is musically paramount to the study of the sound of the instrument. The transient response can be characterised with the understanding of the resonances of the body and the connection between the wood and the air obtained from the other two domains. The lofted model of the instrument is excited at either end of the top shell and at the bridge points. Extensive analysis of the decay of sound from the instrument is undertaken to show how the decay of sound changes depending on where the instrument model is excited. This analysis is combined with the findings from the modal and frequency domain to characterise the basic acoustical response of the *koto* and the role of the components of its wooden body in the sound of the instrument. The findings of the study of the *koto* help to show which heuristic models are useful for the study of this instrument and what can be gained from analytical models.

Chapter Six focuses attention on the characteristics of a *koto*-sized *paulownia* plank. This chapter adds a study that uses the analytical methods of this work for a simple model, thereby

showing the use of the methods without the complex geometry of the *koto.* This chapter also gives a baseline for examining the *koto* models. Chapter Seven details the discoveries about the *koto,* made using the heuristic models.

This part of the thesis relies on the analysis of a large dataset of primary data. This data has been summarised in Volume II. The datasets are prepared to be helpful to the reader in the discussion of the observations in the text and best viewed on a large screen or a large page. These datasets are presented separately to comply with the thesis format restrictions at the University of Adelaide and limitations of the A4 page size. Some comparisons have needed to be made with reference to the datasets to deliver the data. It is assumed that the reader has access to an A3 printed version of the appendices or a soft copy of the material for magnification of necessary data.

Chapter 6
Finite Element Model of a *Koto*-Sized Plank

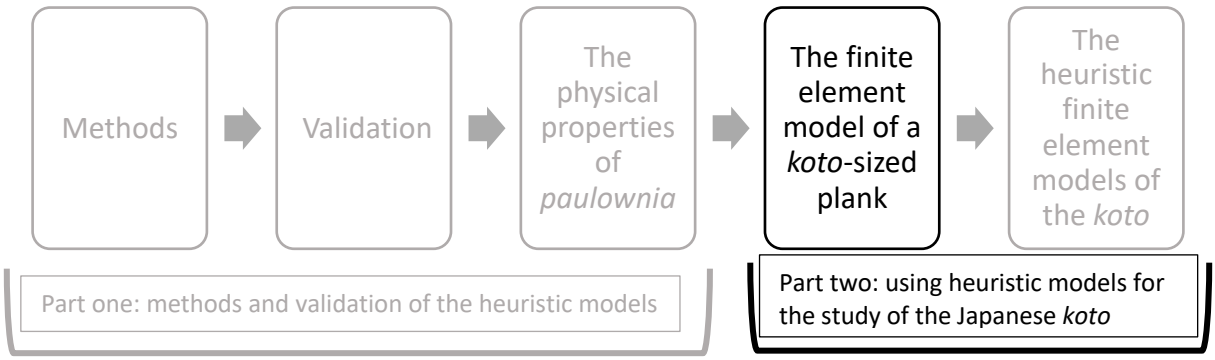

Overview

The validation process and the studies of the physical properties showed that the resonances of the *koto* are strongly affected by the physical properties of the wood in Part One. However, this process left many unanswered questions because as noted, there are few previous studies of *paulownia* and further information was required. An independent analysis of the wood without the complications of *koto* geometry was therefore designed to gain further insights, refine methods and parameter values required for input into the *koto* model's simulations. This chapter thus lays the framework for the analysis of the heuristic models of the *koto* by testing the methods and refining tools with a simpler model than that of the *koto.* The *koto* and the heuristic models of it are still complex geometries and the finite element models produce a wealth of data. A simpler model of the wood is necessary in this study so that it can provide an entry point for analysis of the more complex models and to create a baseline of understanding of the subject. It also gives a roadmap to the analysis of other subjects with the example of a simple shape.

This baseline for analysis, which is obtained with the plank model, provides three outcomes for the remainder of this work: it provides new information about a *koto*-sized plank of the wood without the geometric complexities of the body, which in turn allows for directly observing the role of the wood within the geometry; it sets up a template for the analysis and understanding of the complex resonances of the *koto*; it is used to refine methods of the study by being the simplest form of the model possible. The *koto*-sized plank model in this chapter uses the CW.2 physical properties, as detailed in the Chapter Three. In this chapter, eigenmodes of the *koto*-sized plank model are derived and a template for categorising modes is setup. The second section details frequency scans of a model of the plank in a sphere of air. This scan adds the resonances within the air and is used for understanding the radiation pattern of resonances of the body and the air. Finally, two transient studies are done with the plank in the air which test a periodic and a single piecewise excitation. The results of the three sets of studies are compiled and show the overall response of the plank, which eigenmodes are excited, and what resonances exist from the air and plank coupling.

Predicted eigenmodes of *the koto*-sized simple plank

The eigenmodes of the *koto*-sized plank were obtained and are presented in Figure 6.1, organised by the number of nodal lines seen along and across the plank. In Figure 6.1, the number of nodal line along the body are shown vertically and those across the body shown horizontally. Each column shows one mode type. The end view and an example of the side view for each mode type is shown above the column.

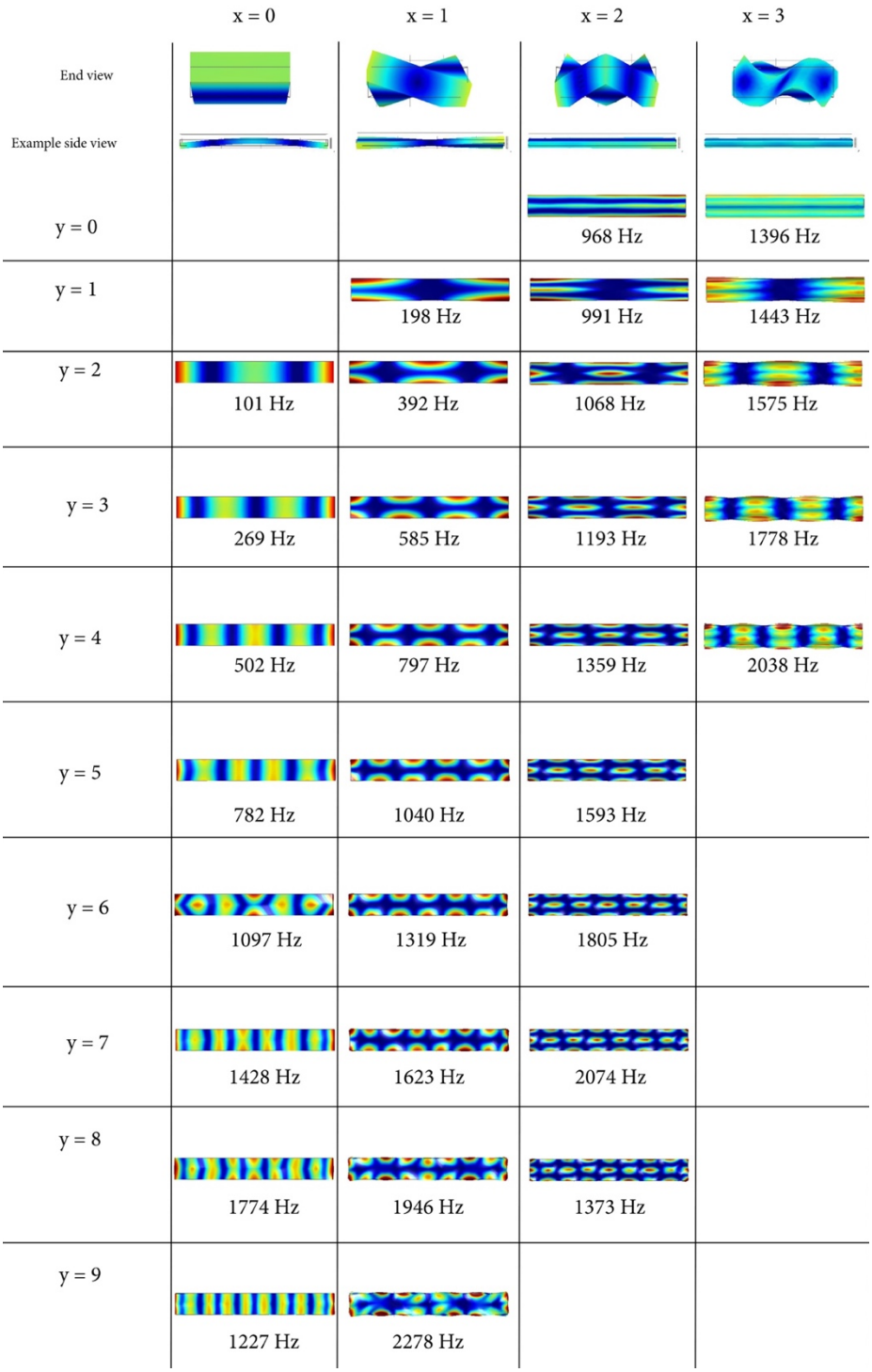

Figure 6.1 Mode chart of eigenmodes of the koto-sized plank

The modes seen in Figure 6.1, and any other modes identified as variations on these shapes are named (y,x) with y the number of nodal lines across the body (rows) and x the nodal lines along the body (columns). Frequencies at which each mode is found in the plank model is shown below the mode shape. The in-plane bending modes (IPBs) are excluded from the above

figure. These modes only have motion in the xy plane. They can also be classified under the first column (x=0). To avoid confusion, they are presented independently in Figure 6.2.

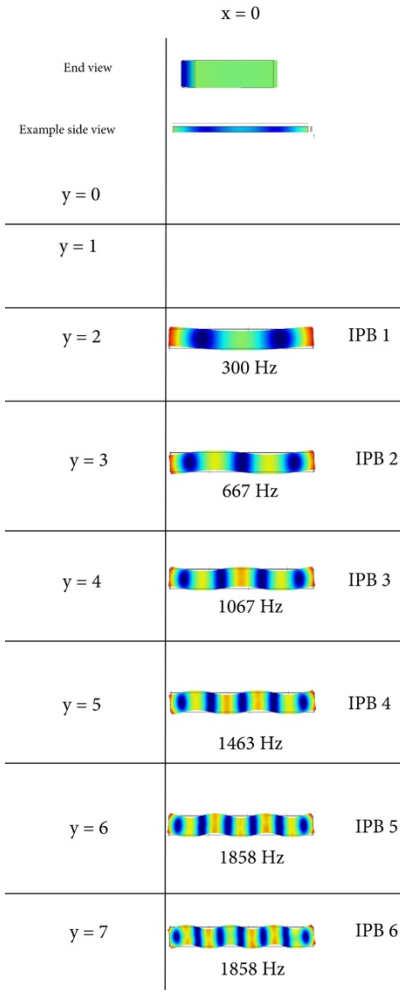

Figure 6.2 In-plane bending modes of the koto-sized plank

The modes shown in Figure 6.2 are labelled IPB n, with n being the index of the mode, which is one less than the number of nodal lines seen. The mode frequencies from the modes charted in **Figure 6.1** and **Figure 6.2** are shown in **Figure 6.3**, compared in terms of frequency across different mode types. It has not been possible to compare these modes with results from other authors, as no precedent study of this wood in this aspect ratio exists. Attempts at using other formulae to predict and compare the modes in an anisotropic plank were unsuccessful.

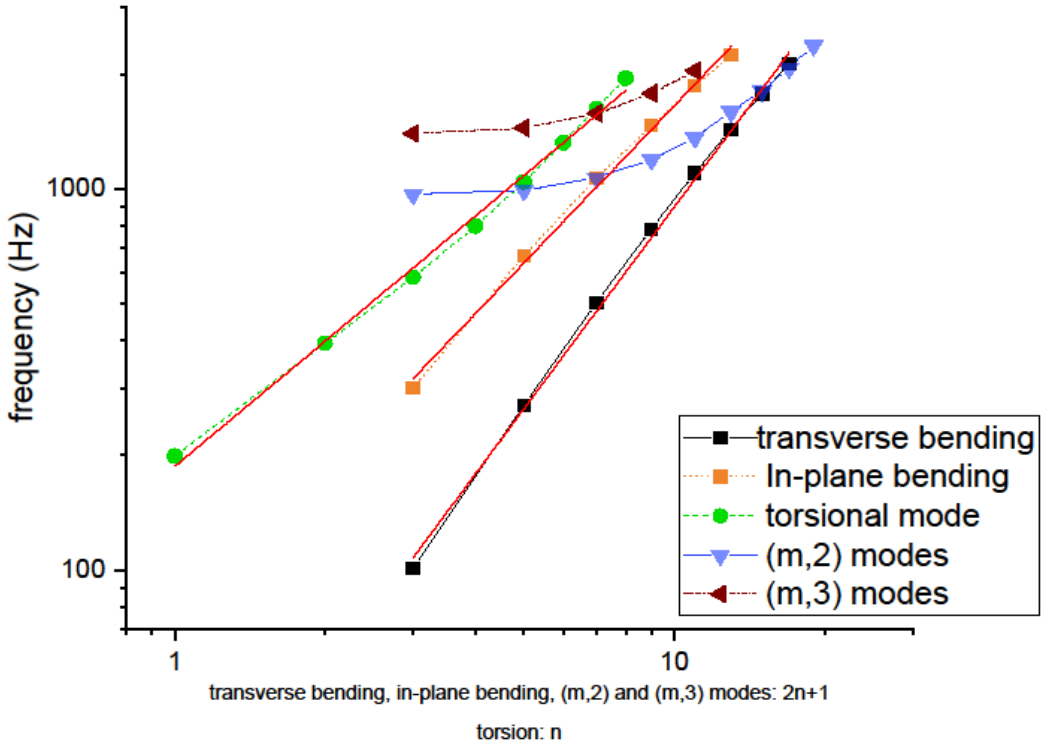

Figure 6.3 Mode frequencies in each mode type for a koto-sized plank

The slope for the in-plane bending modes in Figure 6.3 is 165. The transverse bending mode slope is 148 and the slope for the progression of the torsional modes is 207. The simple plank model shows very few in-plane bending (IPB) modes in the first 2500Hz range; the model predicts more (m,2) and (m,3) modes than IPBs. They exhibit additional non-linearity, currently not characterised. A number of these higher order modes occur at the same or very close frequencies to the transverse bending, in-plane bending and the torsional modes. In Figure 6.3, the index given all except torsional modes is 2n +1, where n is the number of nodes seen across the top of the simple plank (y-axis). For torsional modes, the index is n. This indexing follows Rossing and Russell's (1990) convention when comparing all modes.

Frequency scans using the plank model

The Methods chapter outlined the position of probes in the air surrounding the models. In Figure 6.4, the response of the plank, as observed above its midpoint, is shown for frequencies of 1-2500Hz.

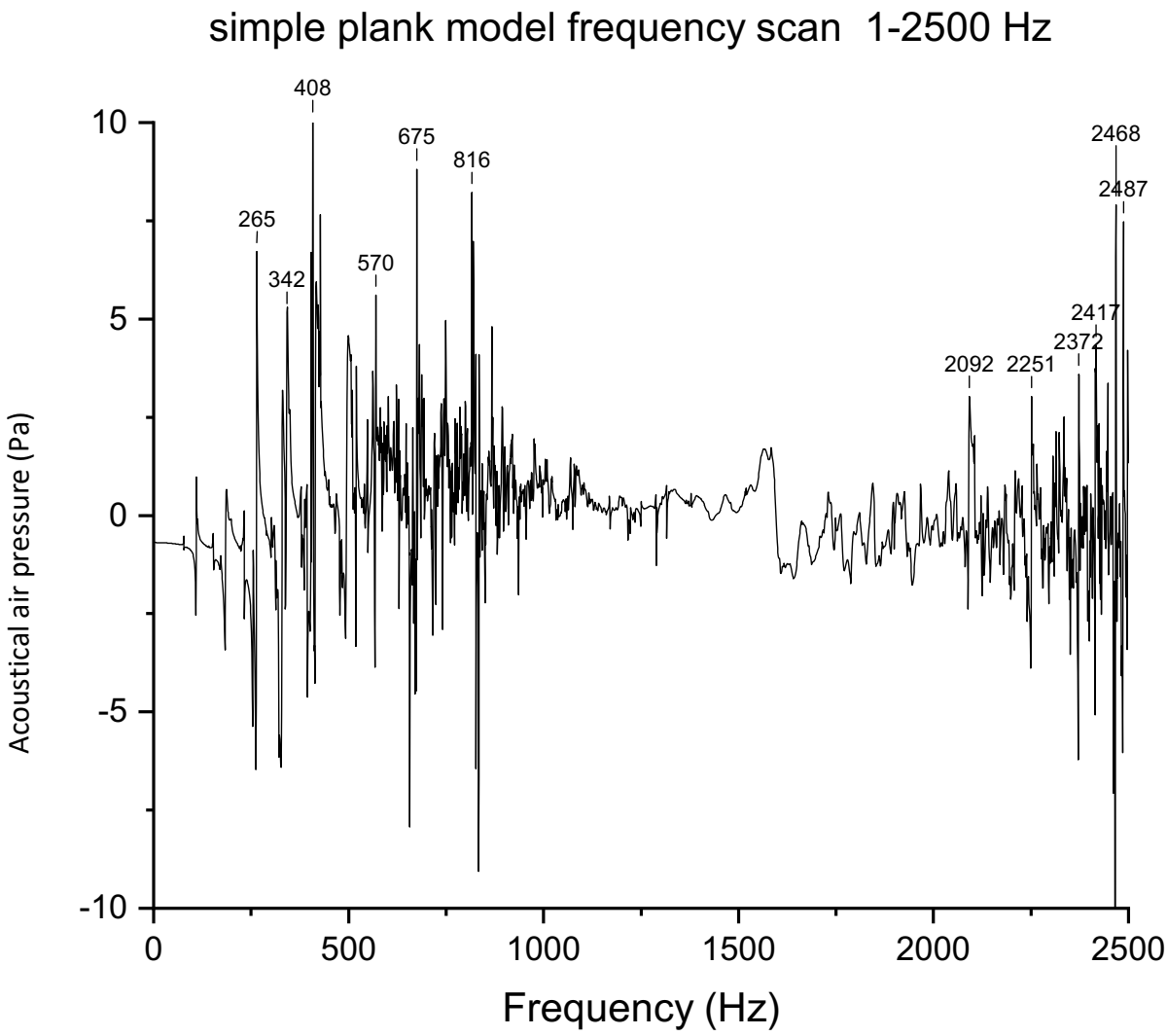

Figure 6.4 Frequency response of koto-sized plank above midpoint

In Figure 6.4, strong resonances are seen in the first 1000Hz and the last 500Hz of the scan range. These frequencies are compiled in Table 6.1. There is also a region of frequencies which the plank is non-responsive, found between 1250 and 1750Hz. From the response seen in Figure 6.4, the first 1000Hz is compared with the energy in the body of the plank and the eigenmodes observed in this range. Figure 6.5 shows this alignment. Displacement information could not be obtained within this frequency scan due to technical problems. In view of resource and time constraints, after significant unsolvable technical problems, obtaining displacement was noted as an area for future work.

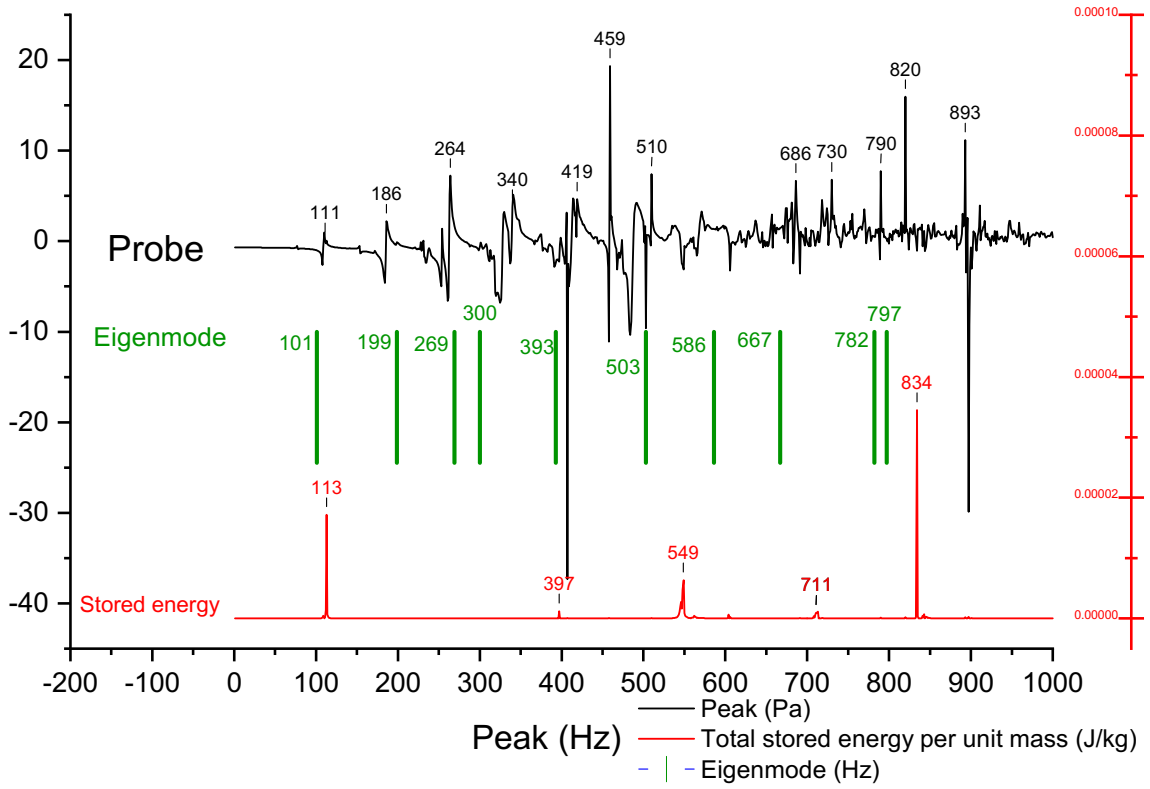

Figure 6.5 Alignment of eigenmodes with frequency response in the air and the body energy

In the alignment of peaks in Figure 6.5, it is shown that the stored energy in the plank body shows few peaks, with the clearest alignment between energy, eigenmodes and probes at slightly above 100Hz and close to 400Hz. The eigenmodes mostly align with peaks in the probe in the air, and it can be said that the eigenmodes in the first 1000Hz radiate strongly into the air. The largest energy peak in the plank is near 850Hz, but it is not seen as an eigenmode or a peak in the frequency scan.

For frequency peaks observed in Figure 6.5, the radiation pattern of the sound in the air sphere was extracted. In **Figure 6.6**, an example is shown of the radiation pattern of these peak frequencies in all three side, end and top views. In Figure 6.6, the plank is visible as the rectangle in the centre of the sphere.

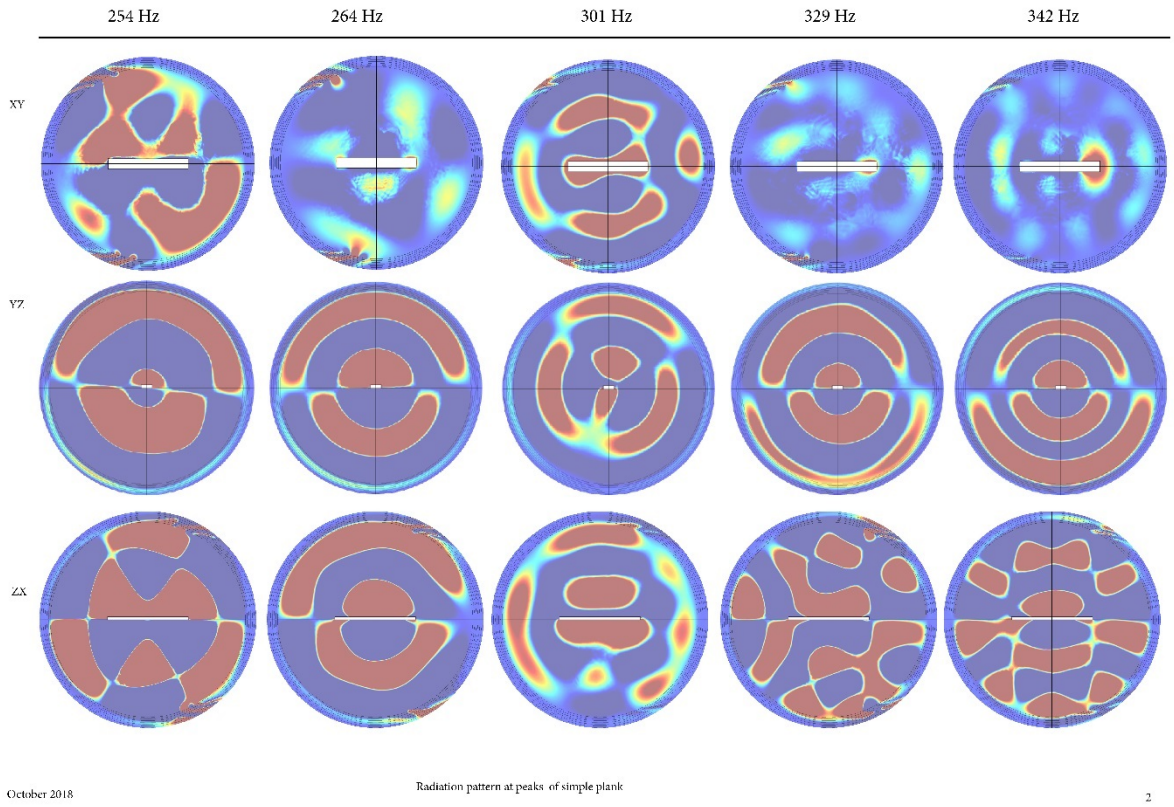

Figure 6.6 Radiation pattern at peaks observed in the probe above the midpoint

No particular pattern has been identified from these radiation patterns at this stage. The radiation is mostly spherical. This is expected given that the load energy input is positioned at the centre of the top of the plank with the increase of frequencies beyond 600Hz, the radiation pattern is too complex to discern.

Radiation at eigenmodes

In **Figure 6.7**, the radiation pattern at each eigenmode is shown for the simple plank. The frequency is shown at the top of the figure. The first row shows the top view of the plank model in the sphere of air; the second row shows the end view; the third row shows the side view. The eigenmode corresponding with the radiation pattern is shown at the bottom.

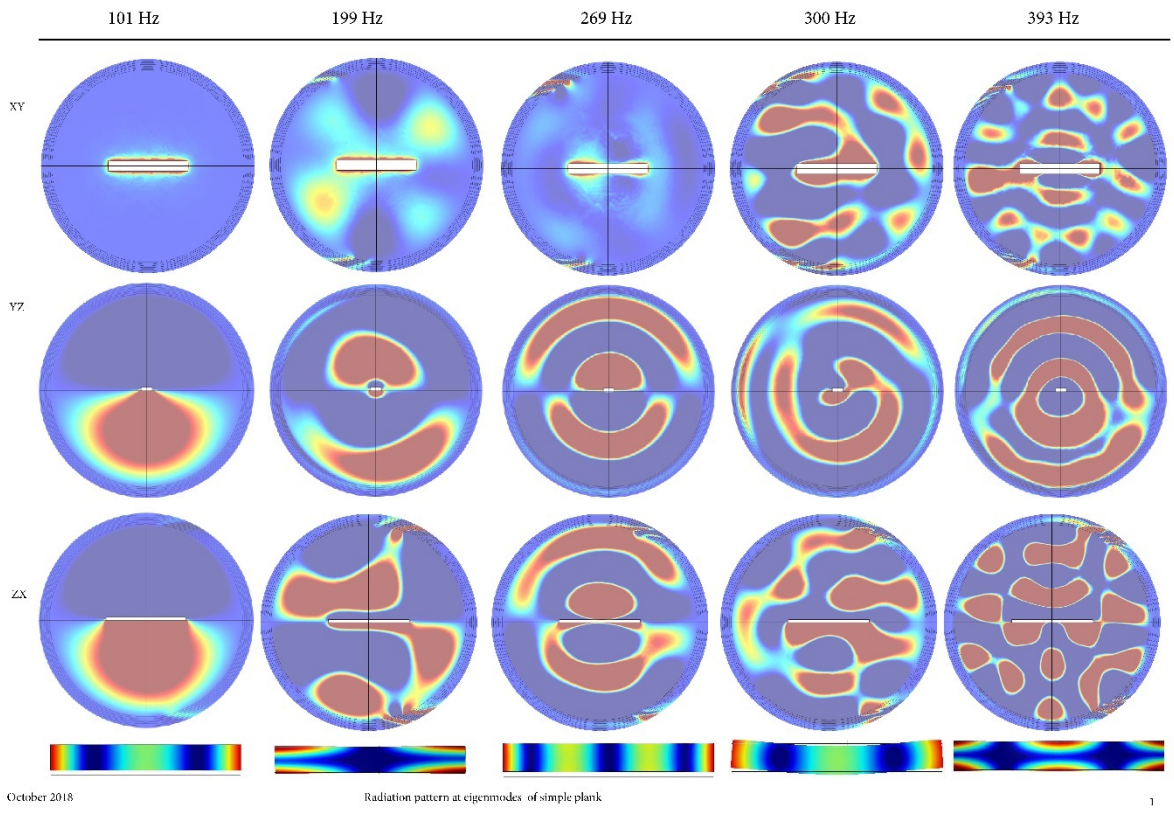

Figure 6.7 Radiation patterns in the air at eigenmodes of the plank

Similarly to peak frequencies, no particular pattern is visible beyond the addition of rings around the *koto*-sized plank and complex patterns from 600Hz.[1] Mode shapes do not correlate to the radiation pattern seen in the spheres in **Figure 6.7**. In Appendix 1, these radiation patterns are shown in comparison with the radiation pattern at peak frequencies.

Radiation patterns are clearest in the lower frequencies. The first transverse bending mode is entirely radiated through the bottom of the plank; the first torsional mode shows some diagonal dispersion of sound. In contrast, the first in-plane bending mode has a broader radiation pattern to the surrounding sphere. Comparing these modes individually, within their own mode type, it seems that there was an observed connection to the radiation pattern. The comparison showed that the nuances observed were likely caused by the radiation pattern of

[1] To explore whether radiation patterns are related to the type of movement or eigenmode, the same radiation is considered individually for each mode type across multiple models in the chapter 7.

the frequency, through analysis of the radiation at eigenmodes, rather than the mode shape. The reason the first transverse bending mode is radiated down is likely due to the point load being pointed down at the centre.

Comparison of frequency peaks and eigenmodes

To examine the peaks and eigenmodes closer, radiation pattern of the peaks are shown in **Figure 6.8**. Modes and peaks that align closely are shown in the same column. Here, only the side and end views are shown for radiation. The modes are shown above their radiation pattern. **Figure 6.8** shows an example page of this analysis. The full comparison within the first 1000Hz can be found in Appendix 1.

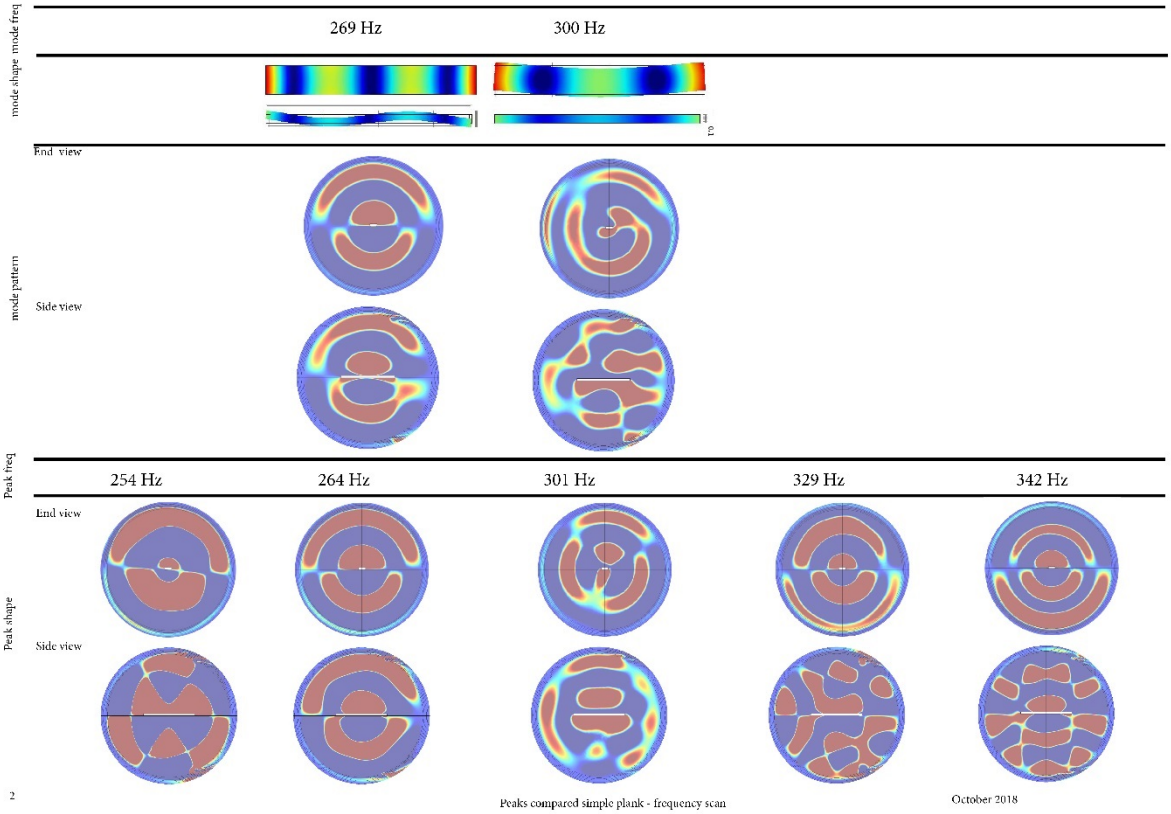

Figure 6.8 Comparison of radiation at peaks and eigenmodes in the plank

Comparison of radiation at peaks and eigenmodes shows that many eigenmodes are observed close to peaks in radiation and exhibit similar radiation patterns, as seen near 100, 199, 264, 300Hz. In this model, most modes except (5,0), (0,2) and (1,2) correspond to a close peak in

the frequency response. A phase change is seen in the radiation pattern at peak frequencies but is not seen when the eigenfrequency is radiated. This observation gives two possible clues about the resonance of the body and the interaction with air:

1. Sinusoidal movement of the body does not cause the largest amount of air pressure.
2. If the air and wood system is considered as one, the presence of air is 'modulating' the whole system's resonances.

If the first possibility is the case, it is likely that the coupling of air and the plank model are giving a new set of peaks. In this case, eigenmodes are not the only important feature of the resonances of the model. If the second possibility is the cause, changing the air can cause a change in the response of the model. It is likely that both of the possibilities happen in tandem within the response. The air surrounding the plank model can be considered a modulating filter, which emphasises some of the existing resonances and shifts the frequency at which they are heard, while restricting other resonances. Following, changes in the air such as altitude, humidity, temperature, would cause a change in resonances observed.

Transient studies of the plank model

In transient studies, the plank was placed in a cylinder of air with a height of 3.6m and a radius of 2.3m. The body was first observed for a duration of 1 second with the piecewise pulse and then with a periodic extrapolation of the same pulse. The waveform of the periodic extrapolation of the excitation force is shown in Figure 6.9.

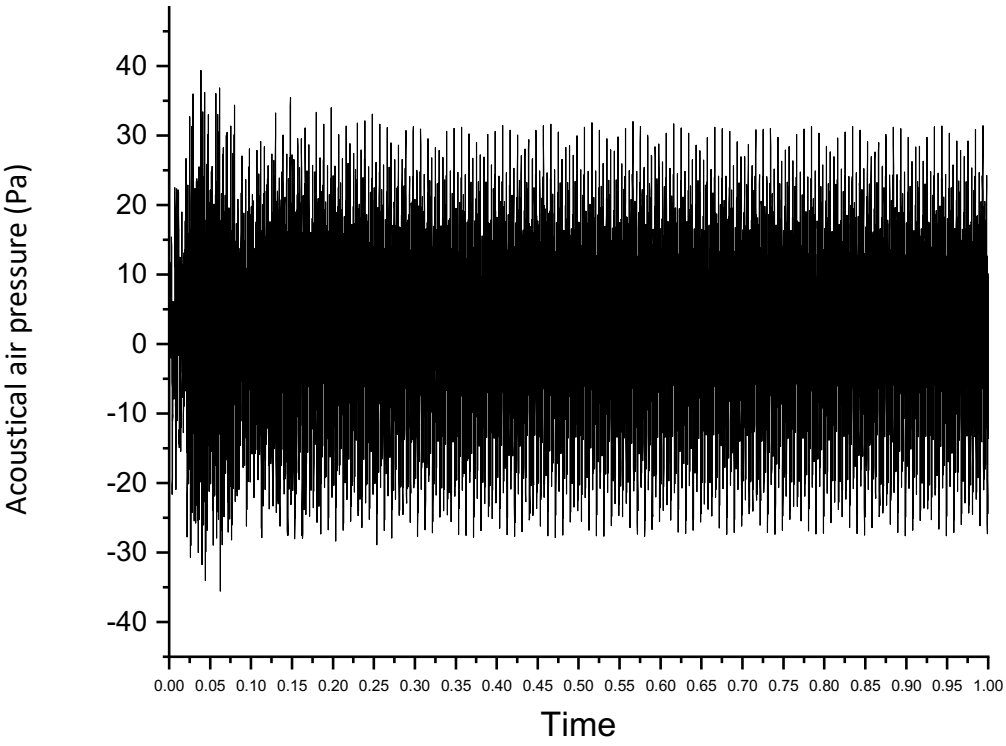

Figure 6.9 Periodic excitation of the koto-sized plank

The waveform of the pulse excitation is shown in **Figure 6.10**:

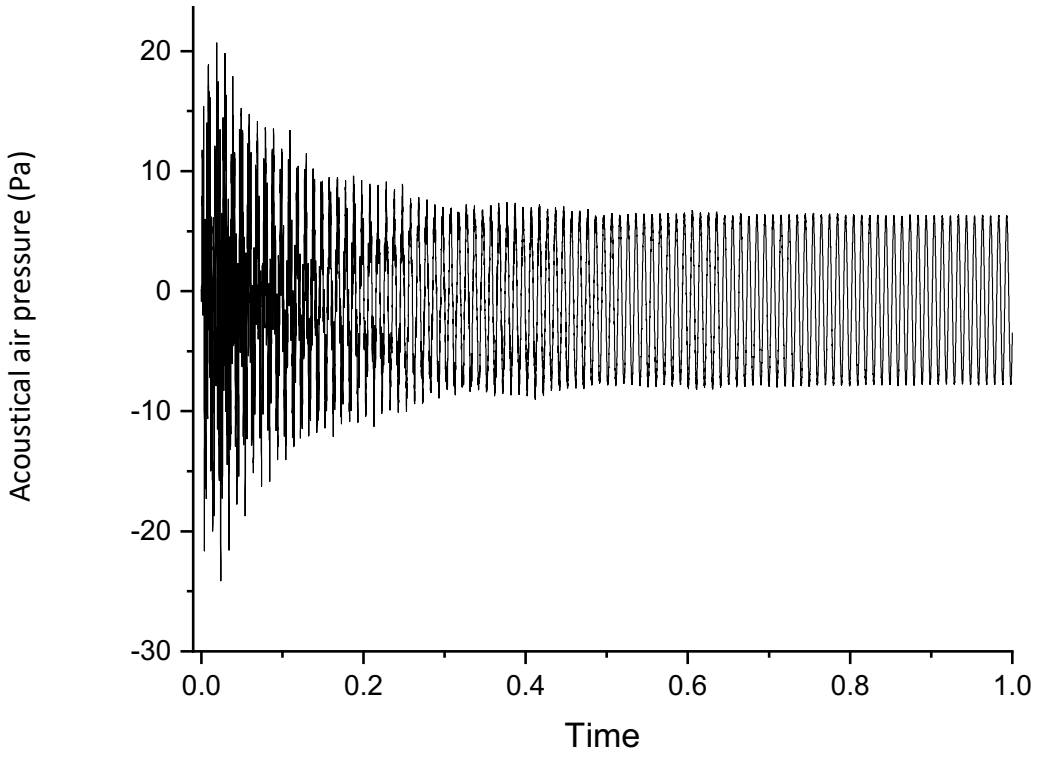

Figure 6.10 Pulse excitation of the koto-sized plank

The periodic excitation leads to a steady-state response in the body. The pulse excitation does not show a clear decay; it may be possible that a standing wave is present at the probe point or without the PMLs, the decay is not absorbed and stays within the cylinder.

Spectral analysis of the results

Spectral analysis in the plank included both frequency representation and time-frequency representations in the form of STFTs.

Short-term Fourier transforms

In Figure 6.11, the first row shows the STFT for the duration of the signal in this study's frequency range, which is 0-2000Hz. The second row shows the first 200 milliseconds of data for the same frequency range, and the third row shows the comparison within the first 100Hz for the first 200ms. The waveforms corresponding to the length of time in the STFTs are shown on the left of the corresponding STFTs. The first three rows are analysis of the periodic excitation and the last three rows are the pulse excitation of the plank.

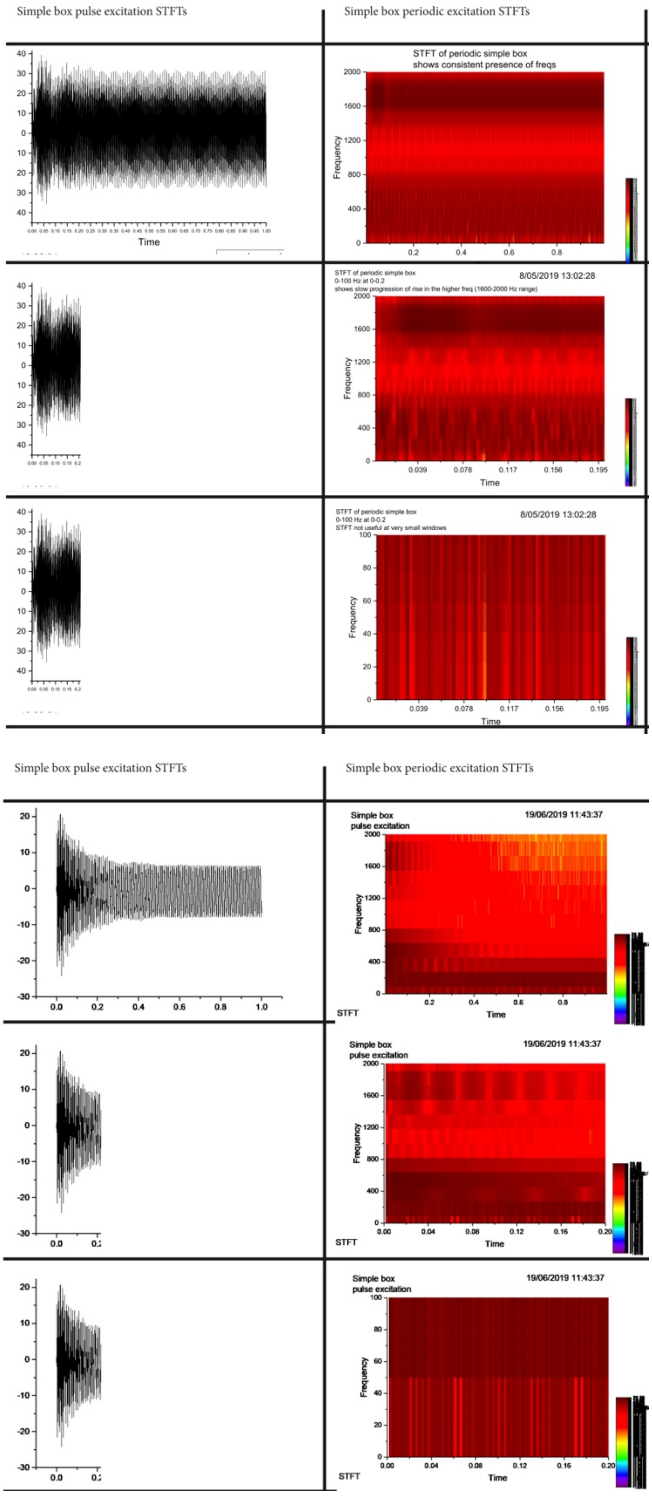

Figure 6.11 STFT of periodic and pulse responses in the plank

The fast decay of high frequencies within the range of this analysis (1800-2000Hz) is seen in the pulse response and a relative steady presence of these frequencies is observed in the periodic excitation. In the first 200ms of the pulse excitation, an almost steady pattern of

appearance and disappearance is seen in the presence of these frequencies. Bader (2013) observed similar presence in the studies of the guitar with the similar finite difference methods. It is observed in Figure 6.11 that the STFT, beyond an initial observation of presence of frequencies, does not offer strong conclusions.

FFTs of changing time ranges

In Figure 6.12, the first and third column show the waveforms produced by the periodic and pulse excitation, with the corresponding FFTs of that particular time region in the adjacent second and fourth columns.

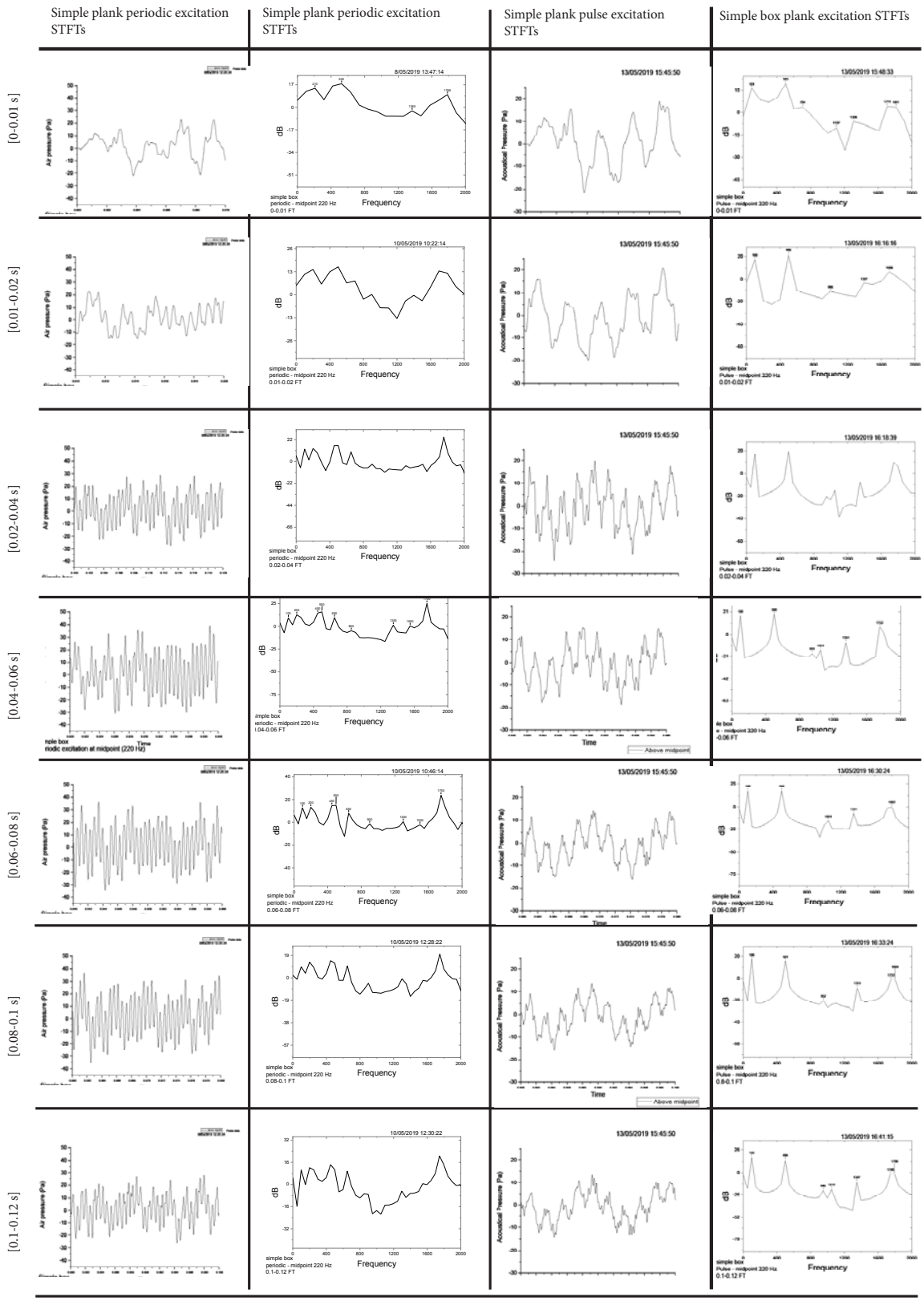

Figure 6.12 FFTs of intervals within the pulse and periodic responses of the plank

The intervallic FFTs presented in Figure 6.12 show where the response changes at different points in the initial section of the signal. However, all of the intervals used in the above analysis fall within the initial 200ms of the decay, which corresponds to the first part of the decay of sound in the pulse excitation. An additional analysis of the interval (0.4-0.42)s was done in both the periodic and pulse excitations. To compare the earlier FFTs to a later part in the signal, the FFTs from the time period (0.4-0.42) is shown in Figure 6.13.

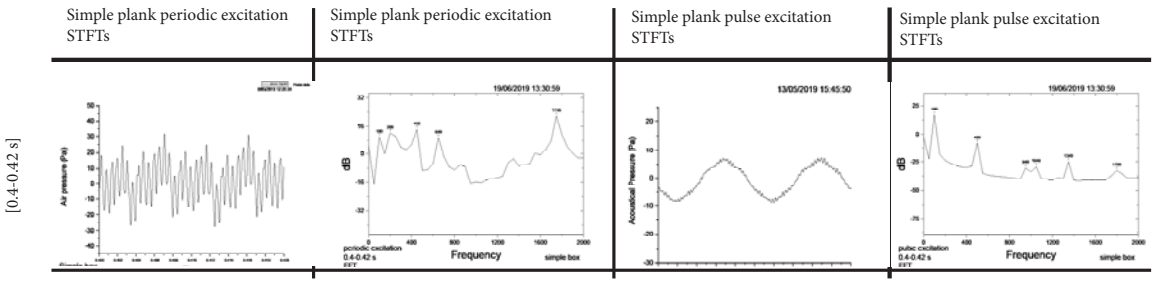

Figure 6.13 FFT of pulse and periodic excitation of the plank in the time range of (0.4-0.42)s

In the periodic excitation, the same response is seen as in the previous ranges. In the pulse excitation, by this later stage in the signal, the response in the small in all present peaks other than the first peak, which occurs at 100Hz.

The small window size of the time intervals means that the frequency response (FFT) is crude. To see the strength of the frequencies (although seen similarly across the intervals) across the range of time, building up to the whole 1 second of response, a cumulative set of FFTs was done within this 200ms range. This analysis was followed by a comparison with the 1s FFT.

Cumulative FFTs

The cumulative FFTs of the signals from both the periodic and pulse excitations of the plank are seen in Figure 6.14. These intervals of FFTs each increase in length and thereby include a larger portion of the signal without omitting the time-frame of the previous row. The firs trow shows the (0-0.02)s interval and the next three rows add 0.02s to the window of analysis. The final row shows the waveforms and FFTs of the full signal.

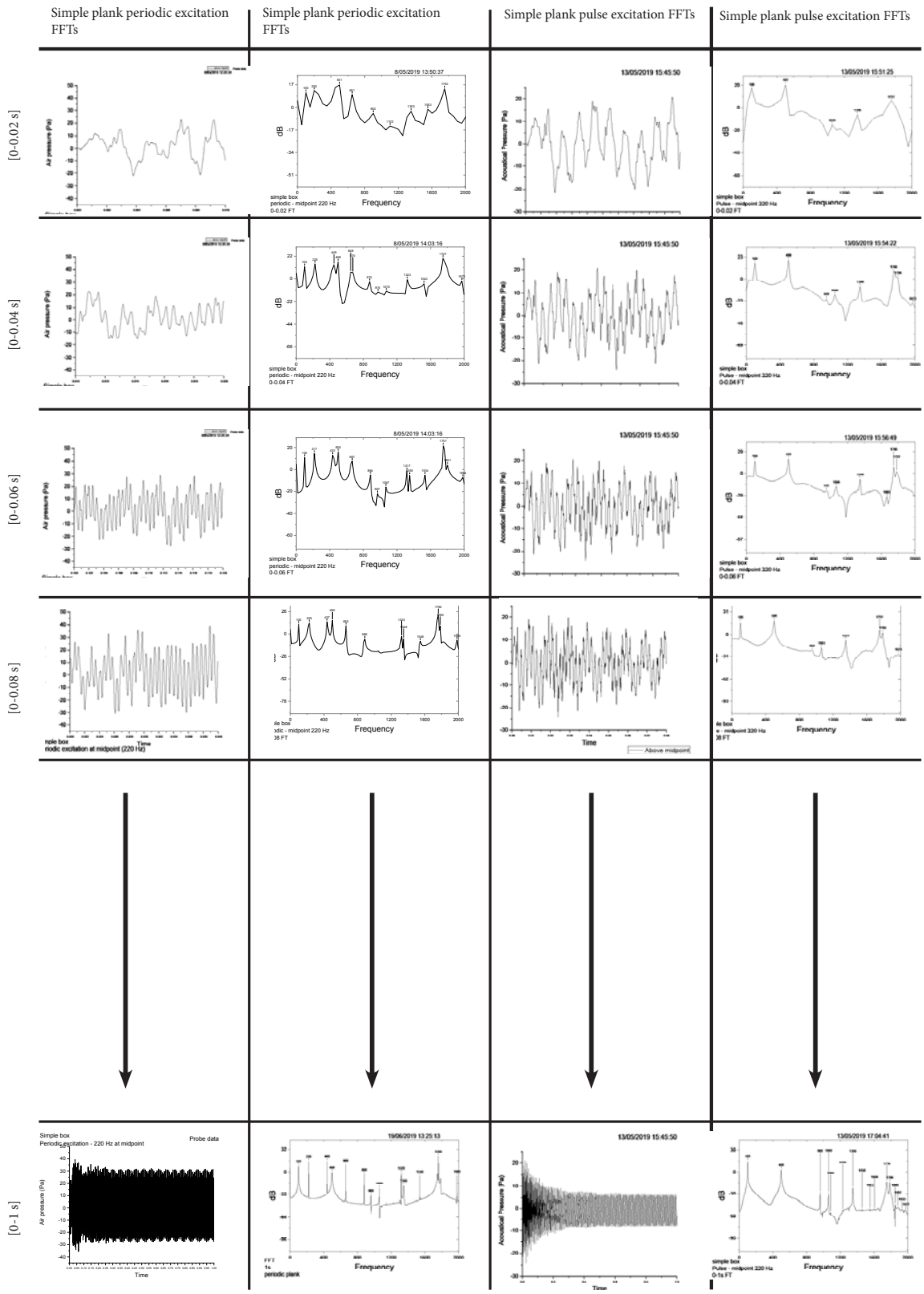

Figure 6.14 Cumulative FFTs of the periodic and pulse responses in the plank

Figure 6.14 shows that the spectrum does not change much in the timescale and frequency range considered in this study, regardless of extrapolation. In the spectral analysis, the periodic excitation adds the 220 and 440 peaks throughout the waveform, but does not show much other variation in the resonances observed from the pulse excitation. Since the pulse was extrapolated periodically at 220Hz, these peaks are expected as the fundamental frequency and the first octave harmonic. Form the comparison of intervallic FFTs, cumulative FFTs and FFT of the full second, it is shown that the full 1 second FFT is a reliable source for spectral analysis within the scope of this project. It is deduced that periodic excitation is not necessary to observe the instrument models' basic response at within the scope of this project. Therefore, for the analysis of transient responses of heuristic *koto* FEMs, STFTs are used to obtain general observations; FFTs are conducted for the full 1 second transient response to obtain spectral data, and the time-series (waveforms) are used for observations around amplitude and decay. In terms of refining study methods, the analysis of the plank results showed that STFTs, intervallic FFTs, and cumulative FFTs give insights for the time and frequency scale of this work; they thus are only used in preliminary analysis of the results of the *koto* chapter.

Compiled response of the plank: the three domains of analysis

The frequency response of all probes is compared in Table 6.1 with known eigenfrequencies of the plank. The peaks from the FFT of the transient response are compared with the eigenmodes and frequency scan results to give a compiled response of the plank in three domains. The transient peaks are found from the full 1s response of the pulse excitation of the plank.

Table 6.1 Compiled response of the simple koto-sized plank in terms of eigenmodes, frequency scan results, and the transient response

simple plank							
Eigenmode	frequency scan		transient response (pulse)	Eigenmode	frequency scan		transient response (pulse)
	Peaks from outside probe	Energy peak (J) at frequency	Peaks from outside probe		Peaks from outside probe	Energy peak (J) at frequency	Peaks from outside probe
1-1500Hz				1500-2500Hz			
101	111	113	101		1584		
199	186						1604
269	264			1623			
300	329						1750
	341			1774			
393	406	397		1779			1786
	414			1805			
	459			1858	1844		1849
503	510		498				1882
	535						1933
		549		1947			
		562			1967		1977
586							2019
	571			2038	2039		
		604			2058		2055
667				2074			
	686				2092	2090	
		713			2105		
	730			2128	2139		2134
782				2168			2161
797	790			2189	2183		2283
	820				2209	2198	
		834			2218		
		843		2236	2227		
	893	897			2251	2250	
969	969		960	2257	2256		
	976				2265		
995	990			2278	2274		
	999					2299	2298
	1004				2306	2302	
	1009				2311		
	1022				2314		
1041					2322		2324
1067		1063	1060	2334	2335		
1069	1069				2341		2341

	1079			2374	2372		2367
	1084		1086	2376			
1097	1090				2385		
1194	1100				2388		
	1104			2391	2394		
1230			1228		2417		
1319	1315				2421	2421	
	1327				2425		
	1336				2429		
1359			1348		2433		2432
1396					2444		
1428					2447		2450
1444					2468	2477	
1463			1458		2487		2484
	1520				2498	2498	2450
	1531						
1564	1564		1553				
	1567						
1575							

Table 6.1 shows the alignment of a large number of peaks across the spectrum of the study. In the next table, this alignment is re-examined based on the 'strength' of the resonances. As discussed in the methods chapter, the frequencies that show more alignment between eigenmodes, body energy, and response observed in the air are considered higher priority.[2] In the next table, the details of the alignment are shown in the leftmost column.

[2] These resonances are considered more important than those that show and alignment between frequency scan and the transient response for two reasons: first, the frequency scan is a time-averaged response and does not consider radiation over a period of time; time is an essential part of this study because the ultimate interest of this work is the radiation of sound in time. The second reason is that frequency scan peaks that are not eigenmodes are caused by the addition of air or are caused by the excitation pulse, the second possibility being less likely; these resonances are not integral to the body itself as much as eigenmodes are.

Table 6.2 Alignment of peaks between three domains of study

simple plank				
	Eigenmode	frequency scan		transient response
		Outside Probe	Energy peak (J)	Outside probe
	Hz	Hz	Hz	Hz
transient + frequency scan + eigenmode + energy	101	111	113	101
transient + frequency scan + eigenmode	503	510		498
	1564	1564		1553
	1858	1844		1849
	2128	2139		2134
	2189	2183		2283
	2374	2372		2367
	969	969		960
transient + eigenmodes	1230			1228
	1359			1348
	1463			1458
	1779			1786
transient + frequency scan		1967		1977
		1084		1086
		2058		2055
		2322		2324
		2341		2341
		2433		2432
		2447		2450
		2487		2484
transient + energy + eigenmode	1067		1063	1060
		2498	2498	2450
transient + energy			2299	2298

The other peaks seen in either of the three domains do not necessarily align with transient peaks and are omitted from Table 6.2.

Concluding remarks: finite element modelling a *koto*-sized plank

The study of the resonances of the simple plank showed few in-plane bending modes. The frequency scan of the plank in air showed a close alignment of peak frequencies in the surrounding air with eigenmodes but gave less insight in terms of radiation of sound. The transient response did not show a strong change in the spectral output of the model between the periodic and pulse excitation. The comparisons of the spectrum output at each interval and in the full length of the response between a periodic and a pulse excitation showed that the periodic extrapolation of the excitation pulse does not add a new set of resonances. The periodic excitation of the plank also obscures temporal observations about the sound envelope. The pulse excitation in the time domain showed an as-yet unexplained steady tail; because the periodic excitation does not allow for the observation of the sound decay, it restricts such anomalies. Periodic input of energy to the model is seen to be unnecessary to use in the context of the *koto* studies at this stage. Many features observed in the plank response (e.g. semi-periodic tail at pulse excitation) cannot be confirmed yet because of the simplicity of the plank model. These observations are further examined in the *koto* models. Their appearance in the plank model is useful in having a stand-alone observation of these events beyond the *koto* models.

The comparison of the three domains gave a compiled set of resonances of the plank. This analysis of the plank model was useful to observe how the wooden plank of *paulownia* responds acoustically. The resonances compiled provide a baseline for the analysis of the *koto* body and a starting point for comparison of different levels of geometric complexity in the models. With this baseline, changes in modelling can be compared against the simplest abstraction of the *koto* body. This plank is entirely different from the *koto* body, and it is not expected that any of the observations of its resonances will necessarily carry through to the instruments. Where resonances are observed in *koto* models and this plank model, it can be said that these resonances arise from to the aspect ratios of the outer shell and the material itself.

Chapter 7

Heuristic Finite Element Models of the *Koto*

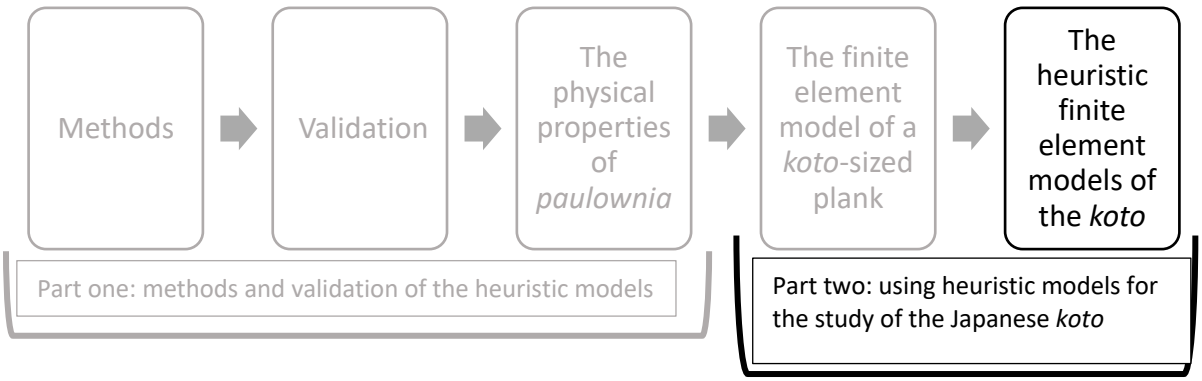

Introduction

This chapter aims to characterise the basic sound envelope of the *koto* by a series of studies using heuristic models. First, the basic resonances of the body are obtained in the modal domain. The role of the components of the *koto* on these basic resonances is studied using a variety of models of the instrument body as well as separate models of the *koto*'s top shell and base plate. Ando also studied the two plates separately in his 1996 and 1986 publication; his findings were discussed in Chapter Four. Ando's results have been questioned (Fletcher and Rossing, 289), especially as he was unable to observe the torsional modes of the body. The substructure coupling study here has replicated Ando's method of studying the plates separately. This analysis of the separate shells is combined with the analysis of the assembled body also helps to clarify Ando's findings. Additionally, the study of the substructures expands on the understanding of the role of geometric features of the top shell by testing variations in the model of the shell. In the modal domain, studies are often done with a smaller number of variations. Given the complexity of the *koto* and the few precedent studies in its acoustical response, more variations were tested in the models of the body and its individual shells.

Secondly, frequency scans were done of a smaller set of models from those studied in the modal domain. These models helped to clarify the effect of the internal air cavities of the instrument on its frequency response. Finally, with a basic understanding of the resonant modes of the *koto* and its interaction with the surrounding air, the transient response of the instrument was investigated using the lofted model. The insights from the modal and frequency domain were used in the time domain analysis; the lofted model was excited at different points along and across the top shell and changes in the decay of sound and in the spectral response inside and outside the body were predicted.

This chapter will show that the resonances of the *koto* are largely derived from the geometry of the top shell. The interaction between the body and the surrounding air results in a slight modulation of the resonant frequencies. Exciting the instrument across the top curvature of the body changes the distribution of energy between the top plate and the air inside the body; excitation points closer to the position of middle strings on the instrument across the top curvature emit a louder sound from the top shell. Movement along the dragon's spine on the

lofted model indicates that the arched top shell of the body has a strong impact on the response of the internal air chamber, which acts as a resonator by limiting the amplification of the frequencies within the 800-1000Hz range. The decay tail of the sound emitted from the sound holes is increased with changes in the response of the small chamber.

In this chapter, results are presented and discussed in each of the domains; the results are connected between domains at the end of each section. First, the results of studying the resonant modes of the *koto* and its substructures is discussed.

Modal Domain: Eigenmodes of the heuristic *koto* models

In this domain, geometric features are changed in the models, the deformation in the shape and modulation in the frequency of modes is noted. These two aspects of the modes are used to compare different models. Including mode shapes in the analysis helps to ensure that the same resonance is traced between the models. This analysis provides an understanding of the basic resonances of each simple model of the *koto* or its individual shells.

The analysis of the mode shapes

The deformation of identifiable mode shapes is documented in this analysis.[1] It is necessary to compare mode shapes because the mode shapes represent the first stage in understanding the resonances of the body. These mode shapes show the deformation of the body in each resonance. As shown in the validation chapter, correct alignment of the mode shapes is necessary for the study the modes. In this section the modes of the models of the full body are compared first. In this comparison, the modes of the simple plank (from chapter 6), the idealised box and the lofted model are shown, with the results from Coaldrake's CT scan model in the final column. This set shows the main stages of variations within the full-body models. A larger set of box models were compared in terms of modes, including those with changing numbers of struts. The results from the simple plank are different from those of the *koto* models, but they provide the basic undeformed mode shape and provide a baseline for the analysis. Figure 7.1, Figure 7.2 and Figure 7.3 display the deformation in the transverse bending, torsional and in-plane bending modes of the models. In these figures, each row shows one mode, with the labels on the left side of the figure. The frequency of each mode is shown underneath each mode shape.

[1] In modal domain and frequency domain studies of the *koto* models, because there exists a model variation, the simple plank (also called simple box) model results are shown alongside the *koto* models' results to provide a baseline for observing changes in mode shape and frequency responses.

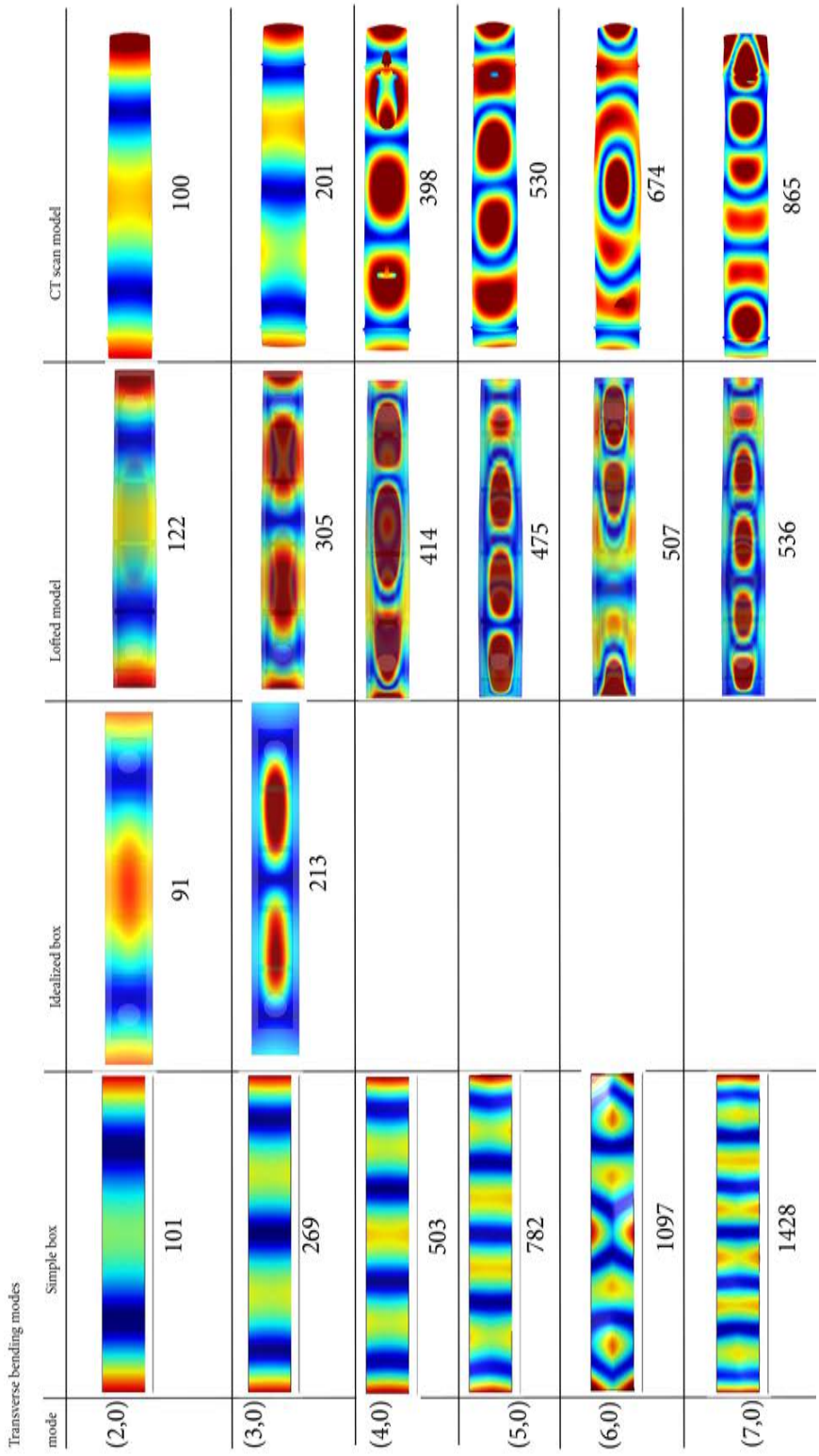

Figure 7.1 Transverse bending modes compared between simple models and the Coaldrake CT scan model

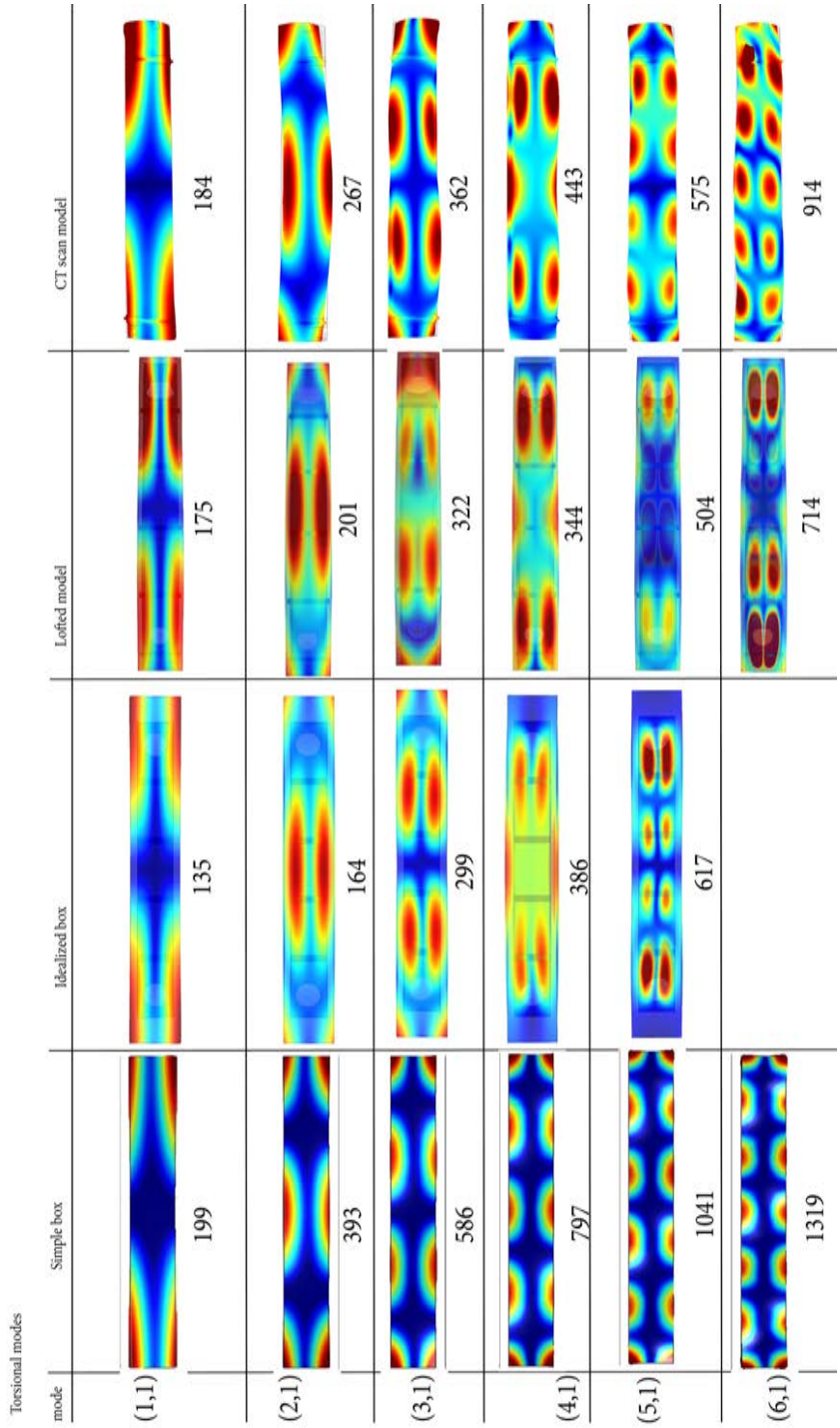

Figure 7.2 Torsional modes compared between simple models and the Coaldrake CT scan model (Note the deformation of torsional modes. Especially observed in the (4,1) mode, the middle nodal lines are inverted and overlapped)

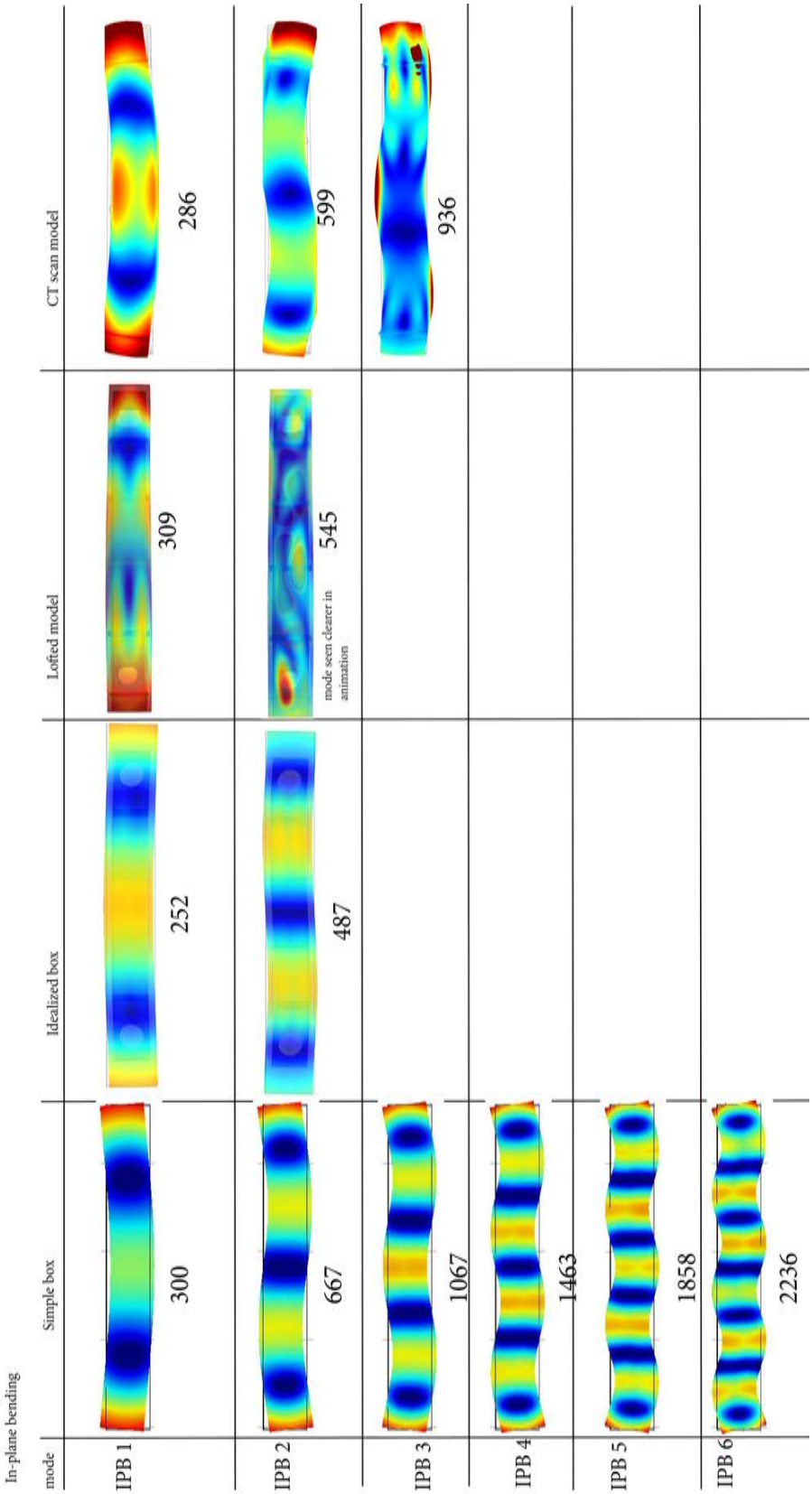

Figure 7.3 In-plane bending modes compared between simple models and the Coaldrake CT scan model

Torsional modes are deformed from the second torsional mode (Figure 7.2) The fourth torsional mode (4,1) shows the two middle nodes inverted and combined in the idealised box. The lofted model and CT scan model also show this inversion, but the nodes are less overlapping. The same effect was seen in the (5,1) mode in these models. [2]

Box models are included in this study to assess whether the lofted or the idealised box models is an appropriate heuristic model. In Figure 7.1 to Figure 7.3, in modes that both the box and lofted model predict, the lofted model shows no increased accuracy. However, the lofted model does show more mode shapes that are found in the CT scan model, especially in the transverse bending modes. The lofted model is determined as a more useful heuristic model because more modes are aligned between this model and the CT scan model. After the mode shape analysis, the progression of the frequency of modes in each of the mode types is compared between models.

Mode frequency analysis

Among the 44 modes found for the full body models, many are not easily identifiable as one of the mode types. Therefore, the findings of the mode comparisons are constrained to the mode types of torsion, in-plane bending and transverse bending. The slopes of the regression for these mode types are compared in Table 7.1.

[2] Extensive analysis was done to identify these modes. The mode were compared against all other modes of each model; the modes depicted in Figure 7.2 were the more likely option for the (4,1) and (5,1) within the predicted modes.

Table 7.1 Lines of best fit compared between mode types and models

In-plane Bending Modes			
Plot	simple plank	idealised box	lofted model
Intercept	-294.7	-100.6	-45.1
Slope	195.0	117.5	117.9
R-Square (COD)	0.99	1	1
Adj. R-Square	0.99	--	--
Transverse Bending Modes			
Plot	simple plank	idealised box	lofted model
Intercept	-466.1	-92.0	132.0
Slope	147.6	61.0	31.0
R-Square (COD)	0.98	1	0.87
Adj. R-Square	0.98	--	0.85
Torsional Modes			
Plot	simple plank	idealised box	lofted model
Intercept	-44.5	24	51
Slope	207	88.8	84
R-Square (COD)	0.97	0.95	0.94
Adj. R-Square	0.96	0.91	0.92

Table 7.1 demonstrates that the identified modes are reliable for this study; the R^2 values for the regression show a strong correlation between the modes in each type. However, the R^2 values from modes identified in the idealised box are unreliable. In this box, only two of each mode is identified and so the R^2 value is meaningless. The slope and intercept values from the box model can only be used to give a general idea of progression of modes in each mode type. The analysis of in-plane bending modes in the lofted model is also not reliable, because only two in-plane bending modes were found in the model (see Figure 7.3).

Additionally, there is some rise in mode frequencies from the boxes to the loft model in the torsional modes (see Figure 7.2). The CT scan model and the lofted model do not seem to be closely aligned in the torsional and transverse bending mode types. Because few modes are identified in many cases, the analysis results remain limited. With the general understanding of the modes in the simple models of the *koto* body, the individual plates are examined next.

Variation on the top shell and base plate substructures of the koto

A full summary of the results from mode frequency analysis can be found in Dataset 2. Each mode shape is traced in Dataset 2 through variations in base plate, variations in top shell, box model and the lofted model in each column, from top to bottom. The orange sections denote modes that are not observed, such as the fifth torsional mode in the box models and the sixth torsional mode in the box models and the lofted model. Reading along each column shows which modes are seen in all models and which are only observed some of the models. The fourth torsional mode is an example of a mode that is observed in both plates and in the full-body models; this mode occurs at 344Hz in the lofted model. In this analysis of resonant modes, the addition of arching on the top plate shows the clearest effect on the torsional modes of the top shell. Unlike the top shell, the modes of the base plate did not show a clear change (see Dataset 2).

Torsional modes are not affected by changes of a plate's attributes when it is not connected to the full body as much as transverse bending modes; these modes are affected more by the joining of the two plates.

It has been found that torsional modes are mostly reliant on the full body of the instrument, and less influenced by the individual plates; the fourth torsional mode is seen in the flat top shell at 439Hz, in the arched and tapered top shell at 456Hz, and in the top shell with arching, tapering and the 'ears', at 456Hz; this mode is seen at a much lower frequency of 344Hz in the lofted model. In contrast, transverse bending modes are heavily affected by the arched nature of the top shell (see Dataset 2). There were not enough in-plane bending, (m,2) and (m,3) modes observed across the models to draw a conclusion on the trend in these modes.

Arching and tapering have also been seen to increase the frequency of modes, especially in transverse bending modes. As an example, the third transverse bending mode, (3,0), is predicted at 157Hz on the flat top shell (without arching or tapering); this mode is seen at 255Hz on the arched shell. Tapering does not have as much of an effect on the increase of mode frequency, as the same mode, (3,0), is seen at 180Hz in the tapered but not arched plate.

It is clear that each component of the body of the *koto,* if examined alone, has its own set of resonances. The fully assembled instrument has different resonances to the individual components. Nevertheless, some modes are recognisable between the top shell and the full-body models; an example of this observation is the first four torsional modes in the lofted model observed at 175, 201, 322, 344 and 504Hz respectively. This analysis has allowed for creating some distinctions between the assembled simple models of the *koto* body and the models of the individual plates. However, the mode shape and mode frequency analyses have not given a clear understanding of the connection between the two plates and the full body. To investigate these resonances further, the total stored energy of the models was compared next.

Total energy analysis

The analysis of the stored energy in the body reveals the total energy of the body, which when in vibration, is transferred between modes. The lowest stored energy shows the substructure that is least resistant to vibration. As discussed in Chapter Three, the body with the lowest stored energy is considered the most stable. Therefore, the total stored energy of the body from the sum of all modes observed in each body was compared. The sum of the stored energy from 44 modes was used instead of the stored energy for individual modes to make the energy analysis independent from the frequency and mode shape. The stored energy in modes rises exponentially with the rise of frequency, and therefore, the same mode observed across multiple bodies would have different energy amounts. Changing mode frequencies are combined with the deformation of mode shape across substructures, which has made many modes impossible to identify. Almost half of the modes found for each substructure are as of yet unidentified. The sum for all of 44 modes is a way to include these unidentified modes in the analysis. Given that the mass of the substructures is different, the total stored energy per unit mass (J/kg) was used instead. Figure 7.4 illustrates the energy analysis for all models.

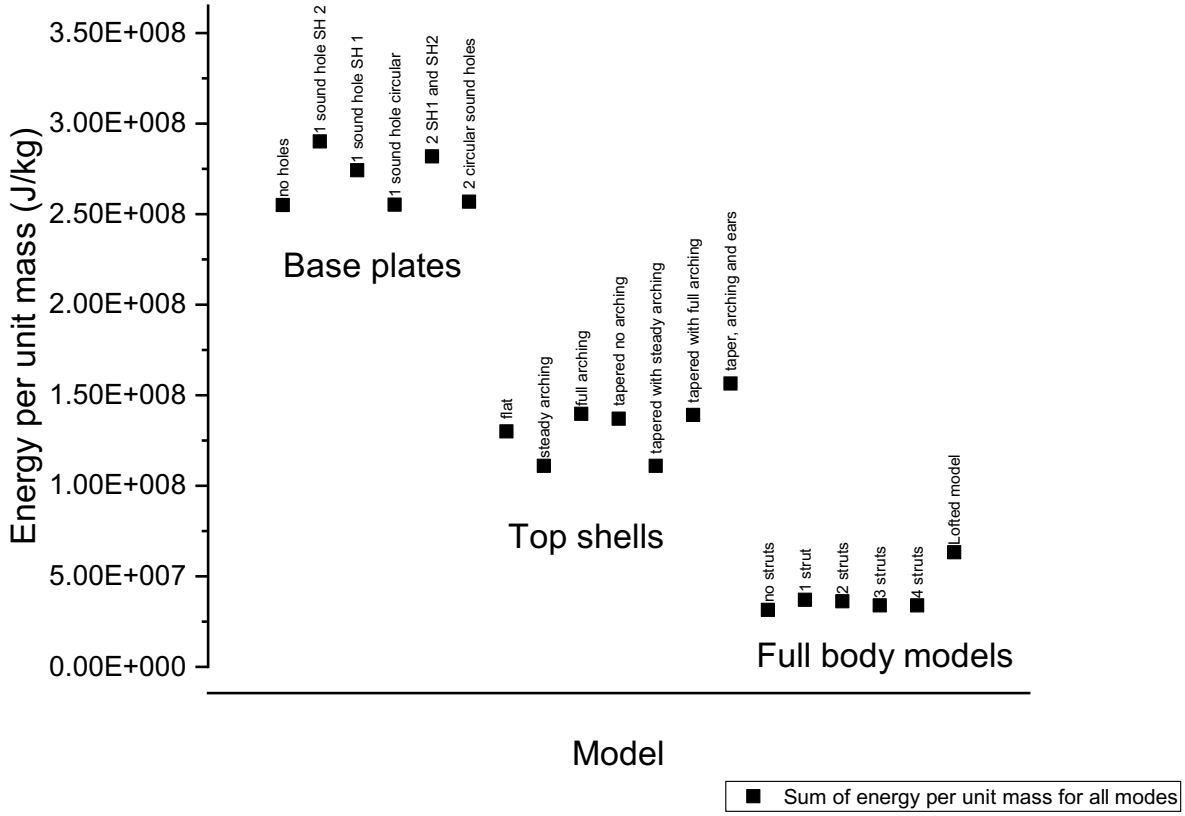

Figure 7.4 The sum of energy per unit mass (J/kg) for all 50 predicted modes in each variation of the shells and the full-body models. Note that the energy values are not the value for an individual mode. The values currently seem high to the author. The author has not been able to find any second experiment to provide additional energy values for the substructures and the data is entirely reliant on the simulations. No erroneous source has been found by the author at this stage.

Figure 7.4 demonstrates that the full body models have less stored energy per unit mass than the individual substructures, and that the top shell has a lower energy per unit mass than the base plate. This minimisation of energy in the full body models shows that the assembled body is more stable than individual plates with respect to the amount of energy used to produce sound. The models with a lower amount of total stored energy require less energy to vibrate. The box models have a lower energy than the lofted model, which implies that the geometric complexities in the body raise the total stored energy. Further exploration to verify the prediction that the assembled box is more stable can compare the Q factors of each

substructure and the full-body models. However, without physical specimens, this comparison is currently not possible within the scope of the thesis.

Comparison between Dataset 2 and Figure 7.4 illustrates that unidentified modes of the full-body models are likely the modes that reduce the body energy. In all cases, identified modes are seen to have a higher frequency in the full-body models than in the substructures (see Dataset 2) and with the rise of frequency, the energy rises. This difference signifies that although the full body model is lower in energy than individual plates' substructures; modes that carry through from the substructure to the full body are not lower in energy. Therefore, the lowering of frequency in the full-body models is likely due to the lowering of mode frequency in the as-of-yet unidentified modes. The unidentified modes were not usable in the analysis of mode shape and mode frequency but were an integral part of clarifying the relationship between the separate plates of the *koto* and the assembled body. Next, the effect of each plate and variations in it is discussed as the final part of the analysis in the modal domain.

The role of components in the eigenmodes of the *koto*

Variations in the individual shells and the full-body models of the *koto* have helped to clarify the role of individual components in the resonances of the *koto.* In the study of the resonant modes of these shells, geometric variations were added individually to the models to assess their effect on the resonant modes. This section discusses effects of the struts, the base plate, and the three curvatures of the top shell of the *koto* on its resonant modes; the curves on the top shell are the arching along the top of the top shell (along the dragon's spine), the top curvature across the body, and the tapering along the body. Table 7.10 documents the effect of each component on the eigenmodes of the *koto.* These results are derived from the material presented in Dataset 2, where examples provided in the third column can be found.

Table 7.2 Summary of the effect of each component on the eigenmodes of the koto body

Component	Effect on eigenmodes	Observations	Interpretation	Comments and limitations
Arching of the top shell	This feature raises the frequency of bending modes. Arching also adds to raise in frequency of the (m,2) and (m,3) modes caused by tapering.	(2,0) is found at 86Hz without arching, at 104Hz with arching; at 104Hz with arching and taper as found on the instrument.	Arching has the dominant effect on the modes of the top shell, both in terms of frequency and shape. A plate with no arching behaves similarly to a flat plate, even if it is tapered.	In this analysis, the lofting process means that the arching used along the dragon's spine determines the amount of curving along and across the shell. This design means that the effect of curvature across and the arching along the body cannot be separated yet.
Tapering along the top shell	Causes some deformation of nodal lines in (m,2) and (m,3) modes. Mode frequencies stable	(1,2) mode at 207Hz in the arched and tapered top shell.	Tapering is not a clear contributor to eigenmodes of the *koto*[3]	Varying the amount of tapering along the body was not tested, so additional possible effects are not documented.
Sound holes	In-plane bending modes drop in frequency with addition of extra sound holes; Many of the modes remain steady across the models of the base plate. Some modes are not identified in models with more	IPB 1 drops from 313 to 296Hz with the addition of sound holes. IPB 2 drops from683 to 603Hz with the addition of sound holes. The (1,2) and (7,0) modes were not identified in models with the sound holes	Torsional modes in the base plate showed negligible variations with the inclusion of sound holes, regardless of shape. The introduction of the sound holes did not have a clearly observed effect on the mode frequencies and shapes.	More work is necessary to separate the effect of the position and shape of the sound holes from the amount of mass they remove from the plate on the eigenmodes.

[3] According to Waltham, harps that are "much more tapered than those of *guzhengs* and *kotos,* the tapering has the effect of moving the most mobile part of the soundboard toward the treble end as the mode frequency increases" (2014, 378). Waltham states that this is needed in the harp, but not in the *koto,* because in the harp the higher pitched strings need the taper, but having movable bridges means the *koto* does not require as much tapering (ibid.).

	complex sound holes.	shaped as found on the instrument. These modes were expected near 250 and 280Hz respectively.		
Internal struts	No effect between models with change in the number of struts More modes identified in models with struts than models without.	IPB 1 mode observed at 252Hz in all box models;(2,0) mode at 92Hz in all box models; (1,1) mode at 135Hz in all box models. The largest difference caused by changing the number of struts, between the frequencies of the same mode, is 3Hz, which is too small to be considered a real effect in this study.	The addition of struts stabilises the box model but the number of struts is not a strong factor in the resonant modes of the box.	Only the box models were used to test changing the struts, and the effect may be different in the lofted model. Struts are placed symmetrically in the box, which may be obscuring the effect of their position along the body. It has been seen that in the violin the position of the sound post has a considerable effect (Gough 2015, 1220). However, the relevance of this effect in the *koto* remains to be studied.

The observations presented in Table 7.2 regarding each geometric feature remain limited in their scope. Still, these effects provide an initial point of analysis for the study of the heuristic models in the more complex domains of frequency and time. These results indicate the curves of the top shell are critical to the resonances of the instrument because they affect the response of the top shell, which in turn shows the clearest connection to the resonances of the assembled body. Therefore, the effects of the curves along and across the top shell are further examined in the transient response.

The Findings of the modal domain

The modal domain analysis has given results for both the methods of finite element modelling the *koto* and the basic resonances of the instrument. In terms of methods, box models are considered useful in identifying complicated mode shapes in the lofted model. However, these models themselves do not predict mode frequencies or mode shapes found in the higher resolution models. It was found that while the box model with flat plates helped to observe some features of the resonant modes of the instrument, the body is changed too much by the addition of arching for a flat model to remain predictive of the response of the instrument. Even so, box models were useful in testing the effect of internal struts on the resonant modes.

With the addition of struts, more modes are identifiable in the box models. In this study, struts were added one by one to the box models; sensitivity to number of struts was not seen in the modelling of 3 to 5 struts, suggesting that the craftsperson's choice of 4-5 struts (Johnson 2004, 62) does not change the resonant frequencies. Despite their limitations in this project, box models may be useful in future studies of earlier versions of the *koto* from the eras before the Nara period (710 – 784 C.E.), when the *koto* was box shaped (Johnson 2004, 169); the use of struts in the body may have been different in earlier zithers. It is possible that that the strengthening role of the struts in the current design is different than the role of the struts in pre-Nara period instruments.

The modal domain results have shown the importance of arching as the dominant geometric feature of the resonances of the top shell. Tapering and 'ears' have shown less effect on the resonant modes of the top shell in the heuristic models. The resonant modes of the top shell in turn translate closely to the modes of the lofted model of the instrument; the resonances of the base plate translate less to the modes of the assembled body.

This domain has also helped to clarify Ando's results. It is possible that Ando's approach did not show clear results with torsional modes because of the response in the torsional modes is highly affected by the assembly of the two plates. Torsional modes are found to be more reliant on the full body being assembled, meaning that the plates' separate torsional modes do not translate clearly to the frequencies of the full body modes. These torsional modes are less

affected by the particularities of the plates, such as sound holes or arching. By comparison, transverse bending modes are more reliant on the modes of the individual plates. This study has found that many of the transverse bending modes of the full body are similar to the modes of the top shell. Ando's method has worked better with these modes the transverse bending modes because of their relative independence from the assembly of the body. Without access to rapid model variations available now, clarifying how different mode types respond to the body assembly and addition of components would have been more difficult for Ando.

The aim of this analysis in the modal domain has been to create simple models of the *koto* so that the complexities of the instrument body can be examined. The goal was to create as simple a model as possible, while maintaining enough complexity to have a model that could be used to understand the instrument's acoustical response. From this point, the substructure models and the variations in the box models are not necessary and are omitted from the next two stages of analysis. Next, the frequency response of the heuristic models in a sphere of air is obtained using frequency domain analysis. The idealised box and the lofted model used in the frequency domain and are compared to the simple plank and Coaldrake's CT scan model.

Frequency domain: Frequency response of the heuristic *koto* models

The coupling of the air and the body are investigated in this domain using the idealised box and the lofted models. This coupling is important to understand so that the core resonances from the *koto* and those from its interaction with the air can be separated in the study of its decaying tail. This domain also allows for obtaining an overview of the response of the internal chambers of air and the sound holes. The sound holes of the instrument are also important in its interaction with the surrounding air, and in this heuristic study, this interaction cannot be tested in the modal domain only. Therefore, a new box model was made without sound holes; this model serves as a negative control experiment for examining the effect of the sound holes. The results from the frequency scans of the plank model are used as a baseline for analysis in the frequency domain. Figure 7.5 shows the frequency responses of the models used in this domain, along with the prominent peak frequencies in each response.

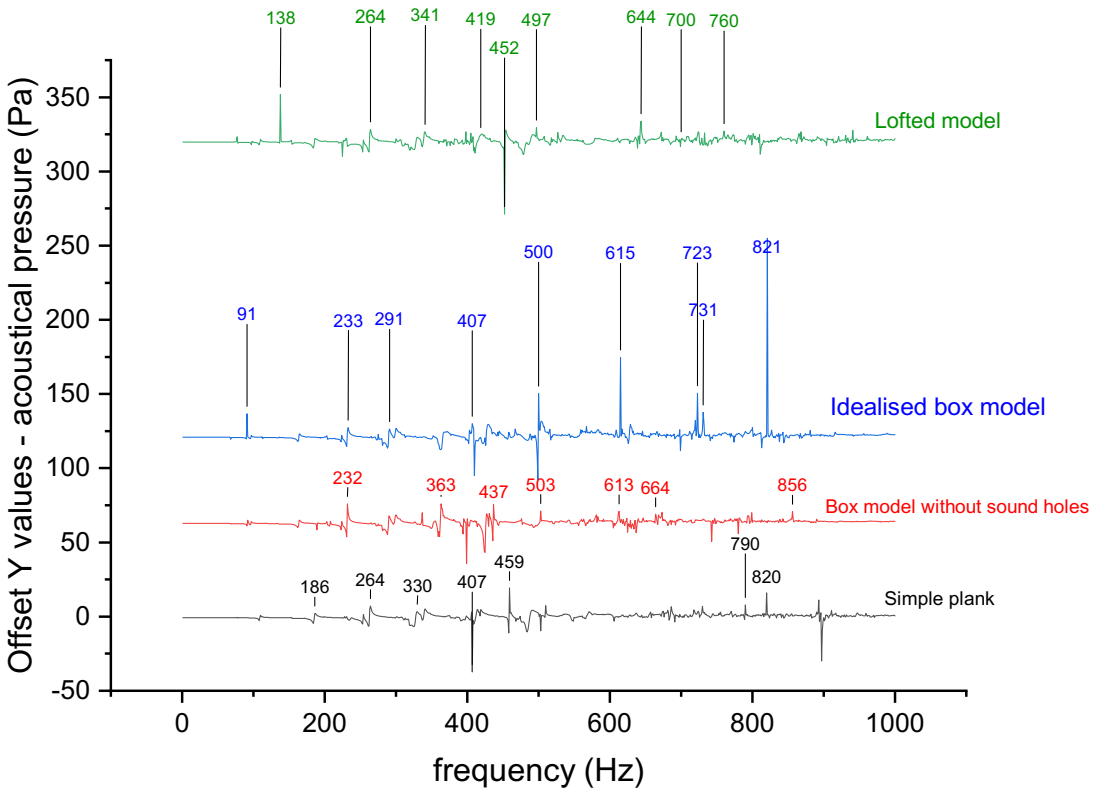

Figure 7.5 Frequency responses of the heuristic models

Figure 7.5 shows that the resonances of the body are not uniform across the plank, box and lofted models. Additionally, the resonances in the box model without sound holes (red line) show a partial alignment with the idealised box.

The frequency scan studies indicate both the amplitude and radiation of sound from the body at each frequency. The idealised box model has four clear strong resonances (500, 615, 723, and 821Hz) and another set of smaller peaks (91, 233, 249, 291, 407, and 731Hz). The lofted model has seven clearly observable resonances (138, 264, 419, 452, 497, 644, and 700Hz) and a more varied response across the spectrum. The plank model has six strong resonances (330, 407, 459, 790, 820 and 897Hz). These peaks are considered the core frequency resonances of the model coupled with the air. The remainder of the frequency domain section examines the frequency responses from these four models closely.

At these peak frequencies, the radiation patterns can be used to analyse where the sound radiates most from the body at each frequency. A compilation of the radiation patterns at peak frequencies and at the eigenmodes of the body can be found in Dataset 3 for the idealised box and Dataset 4 for the lofted model.

Radiation pattern analysis

The eigenmodes of the lofted model align closely with peak frequencies observed in the air surrounding the body; examples include the mode at 122Hz and the frequency peak at 107Hz, the modes at 175, 199, and 201Hz and the peaks at the 225 and 253Hz, the mode at 322Hz and the peak at 317Hz, and the mode at 305Hz and the peak at 301Hz. This alignment is shown in Dataset 2. These are likely to be the eigenmodes that carry through the air in the lofted model. The slight drop in the frequency of the peak between an eigenmode and the aligned peak observed in the surrounding air supports the hypothesis of the air as a downward modulator of the frequency.

Radiation at modes and peaks

The radiation patterns for peak frequencies and eigenmodes were compiled into Dataset 3 in the idealised box and Dataset 4 in the lofted model. There, the peaks and eigenmodes are aligned based on frequency. This alignment shows the two areas of interest in the frequency domain: whether the eigenmodes and frequency peaks appear in similar frequencies and whether the patterns of the radiation of sound are the same between the eigenmodes and frequency peaks is a sample of this comparison (see Datasets 3 and 4). This analysis showed that most eigenmodes are found a few Hertz above peak frequencies, as seen in the example of the first bending mode and the third torsional mode of the lofted model at 122 and 322Hz respectively (see Dataset 4).

Peak frequency analysis

Next, the frequency response is compared between the four models studied in this domain. Table 7.3 presents a comparison of the peaks from the main three models compared. Where the peaks align (within a 10Hz range) across the three models, the row is highlighted.

Table 7.3 Comparison of peak frequencies between the simple plank, idealised box and the lofted model

Simple plank (Hz)	Idealised box model (Hz)	Lofted model (Hz)	Simple plank (Hz)	Idealised box model (Hz)	Lofted model (Hz)	Simple plank (Hz)	Idealised box (Hz)	Lofted Model (Hz)
77	68	77		329		615		616
	91	97		342		628		627
111	113	107	367		360		637	642
		138	406	406	397		656	
153		153	426	420			674	
	165		430				681	
		185	458	459	452	698		699
203			467	472		723	718	725
224	231	225	500		497	731	730	
233				510	520			760
	254	253			528	780		779
	264	265		537			790	
291			567	571	562			811
300	301	301		597		821	820	
313								868

Table 7.3 shows that there are eight closely shared peak frequencies across all three models (green rows: 77, 111, 224, 300, 406, 458, 567, and 723Hz in plank). This is an overall description of strong modes and peaks; no peak analysis function has been used. From the seven aligned resonances, only the resonance at 300Hz corresponds to a mode in every model; however, in each model the corresponding mode is a different shape. Therefore, either the resonances have shifted in frequency and these aligned resonances are not actually the same resonance or the mode shape has changed because of the changes in the geometry. In the other resonances that align between all three models, in the lofted model, the resonances at 225, 397, 452, and 562Hz also align with an eigenmode. In the box mode, the resonances at 313 and 406Hz align with resonant modes of the box, and in the plank, the resonances at 111 and 406Hz align with a resonant mode each. Because these resonances align with an eigenmode,

each is considered the resonant mode of the model that is transferred to the air. However, they do not appear in all three models. Therefore, it is deduced that these resonances disappear with the addition on the complexity of the geometry. No peak in this alignment between the three models corresponds to the same mode shape in all three. Therefore, these are not the same resonance. The resonances of the plank, the idealised box and the lofted model are considered entirely separate sets. The resonances that do not carry through to the lofted model are not predicted to be modes of the *koto,* but tracing these resonances across models makes it possible to gain a general understanding of how changing the geometry affects the resonances of the body.

This comparison of resonances between the models shows that though many eigenmodes are shared between the box and lofted models (Figure 7.1, Figure 7.2, Figure 7.3), the lofted model interacts with air differently. The difference in reaction is due to the lofted and box models responding differently to excitation and to the surrounding air. Both of these points of difference may be caused by the arched top shell. Therefore, the arching of the top shell is reinforced in its importance in terms of radiation; thus, the box model is less valuable to continue with as a heuristic instrument model. To examine the role of the sound holes further, future studies could use extra probes close to the sound holes to better observe any artefacts caused by the changing shape of the sound holes.

The physical properties of *paulownia* and the outer aspect ratios of these models are their only similarity and are deemed the only possible causes of these alignments. Where peaks only align with the idealised box and lofted model, they are attributed to the hollow air cavity inside the body, and not by the arching along the dragon's spine of the *koto*.

Modulation of peaks observed outside the instrument body in this domain can be clarified in future studies, using simulations and physical experiments that test the response at different temperatures, altitudes, and with other material such as helium placed in the sphere instead of air.

Sound holes

The extent to which sound pressure is propagated from inside the hollow body to the surrounding air was assessed using the comparison between the models with sound holes (idealised box, lofted model) and the box model without sound holes. First, the box model is compared with and without sound holes. Figure 7.6a shows the box model without sound holes and Figure 7.6b shows the idealised box model (with sound holes). In each, the red line shows the frequency response observed inside the model and the black line shows the response observed in the surrounding air.

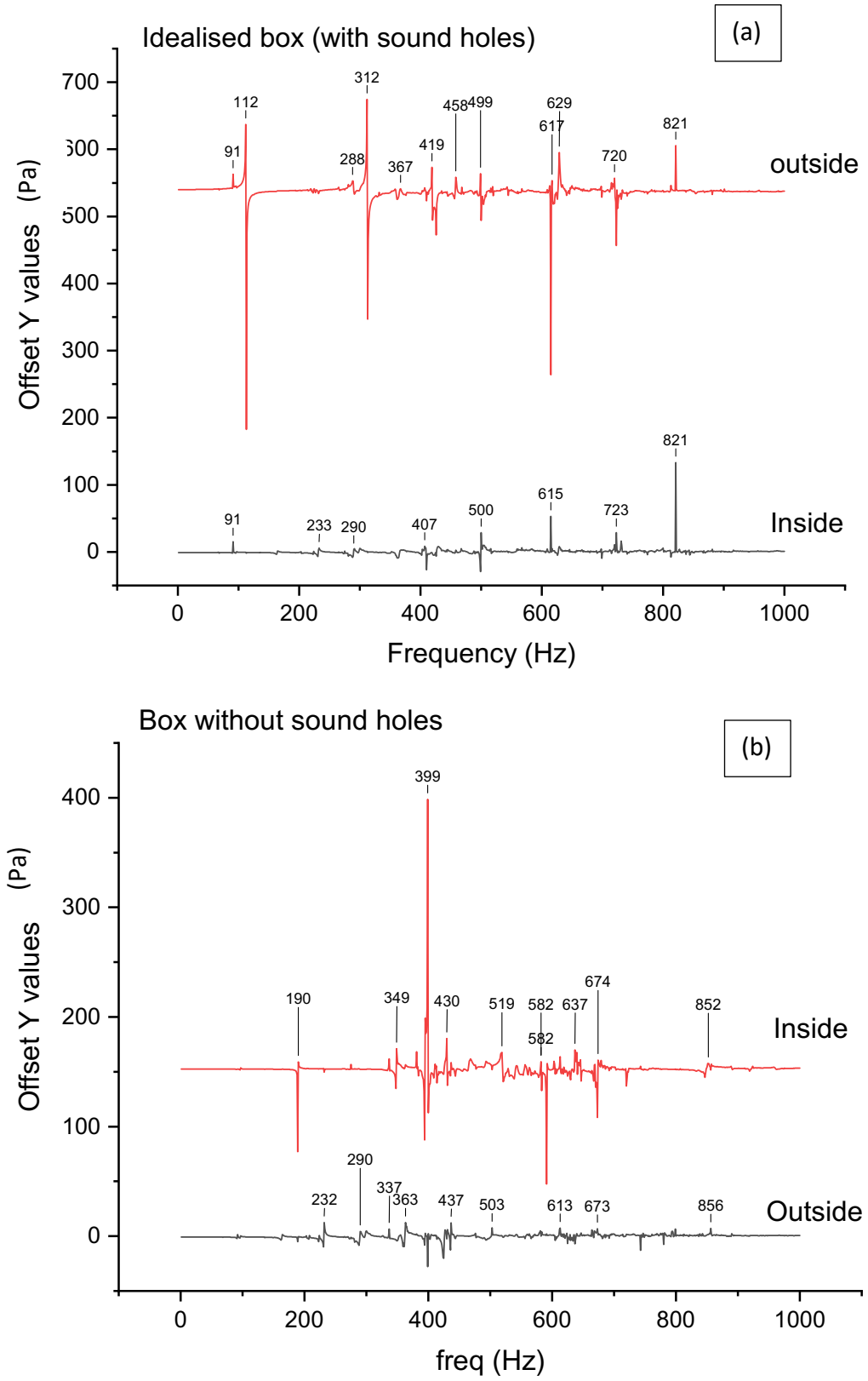

Figure 7.6 Response outside vs. inside the box models with and without sound holes

Figure 7.6 illustrates that with the addition of sound holes (Figure 7.6b), new resonances are formed inside the box. Also, the sound dissipated out of the body is louder; the amplitude of the frequency response outside the body in is higher in Figure 7.6b than in Figure 7.6a because the peaks in Figure 7.6b are higher.

Figure 7.6 shows that without sound holes, most of the air pressure inside the body is not transferred to the surrounding air. In Figure 7.6b resonances from inside the body do not translate to peaks outside, except for the range of 200-500Hz. The difference in air pressure inside and outside is as expected, because the air cavity inside the body is much smaller than the sphere of air surrounding it. Adding sound holes, the responses inside the body and outside change. in Figure 7.6a, strong resonances are seen outside of the body of the idealised box (spikes at 500, 600, and 800Hz); these resonances transfer through the sound holes. Resonances that are seen both in the idealised box model and the model without sound holes can only be transferred to the air via the shell of the instrument.

This comparison shows that the idealised box model has a very different response inside the hollow shell of the body than the box model without sound holes. The only difference between the two box models is the inclusion of sound holes and it is observed that these extra resonances, at 97, 139, 225, 274, and 360Hz are caused by the movement of air in and out of the instrument. These resonances do not carry through to the lofted model (as per earlier discussion of Table 7.3), suggesting that the additional geometric complexity in the lofted model modulates or eliminates these resonances. With this overview of the role of the sound holes and the main air cavity, the analysis of the frequency response in the small chamber follows.

Small internal chamber of lofted model

The lofted model is the only model with the small internal chamber. In Figure 7.7, the frequency response in this small chamber is compared with the response in the main air cavity of the lofted model.

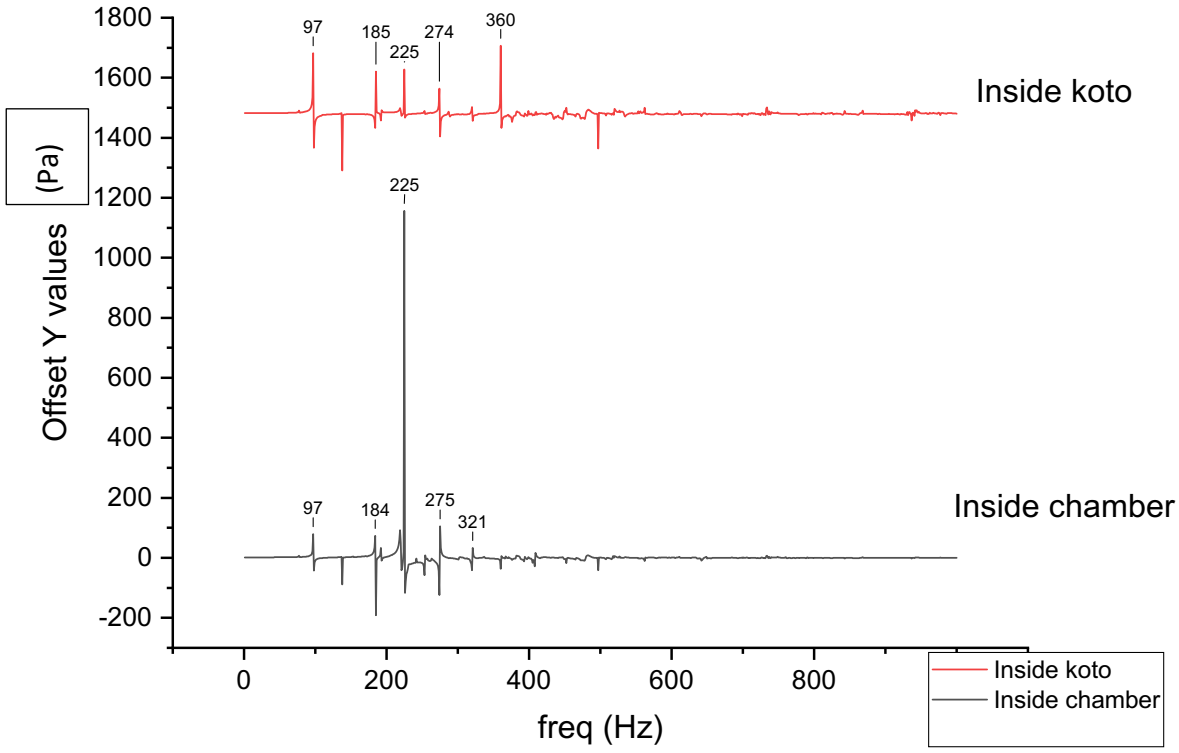

Figure 7.7 Frequency response inside the main air cavity and in the small chamber of the lofted model

In Figure 7.9, a clear peak exists at 225Hz inside the chamber, with an almost 1000Pa increase in pressure. The small chamber does not affect most other frequencies in the 0-1000Hz range. This peak is also observed outside the instrument (see Table 7.3) with a much smaller amplitude. There is an eigenmode at 225Hz which may explain the large peak observed inside the chamber. It is possible that in the instrument, this frequency is an eigenmode that is amplified and modulated slightly in the chamber. As in the modal domain, the peaks themselves do not give a clear understanding of the response of the body and the use of comparing peaks is mostly confined to distinguishing the responses between models. For a clearer understanding of the response in the heuristic lofted model, the energy of the body at each frequency is compared with the eigenmodes and the frequency response in the air.

Comparison with the modal domain

In the frequency domain, total stored energy of the body at a particular frequency refers to how much the body is responding to excitation at a particular frequency; here, increase in the energy equates to increase in the response of the body.[4] Figure 7.8 shows the total stored energy in the lofted model for each frequency in this frequency scan (1-1000Hz).

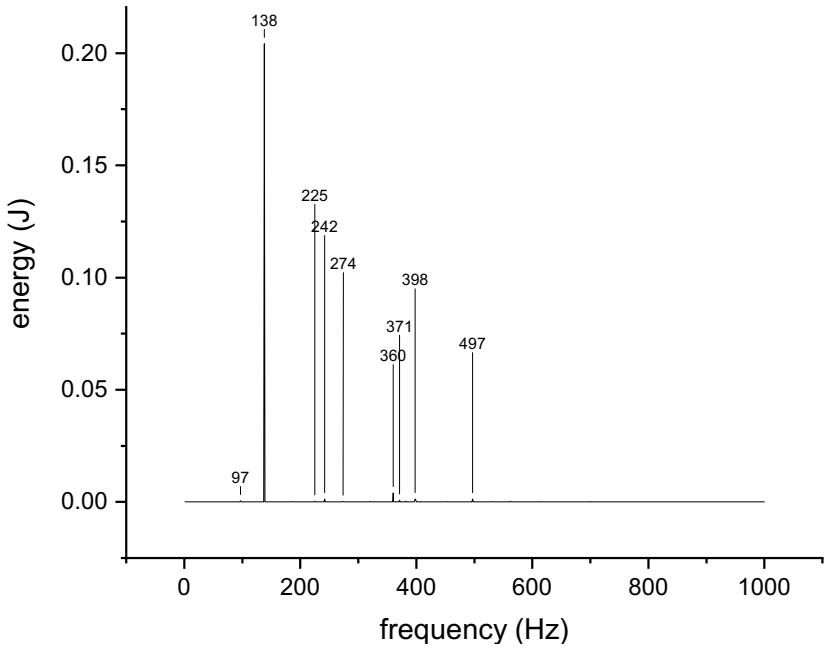

Figure 7.8 Lofted model total stored energy in body (1-1000Hz)

Figure 7.8 shows that in the lofted model, there stored energy is minimal at all frequencies, except for the nine peaks at 97, 138, 225, 242, 274, 360, 371, 391 and 497Hz. These are

[4] The difference between total stored energy in the body in the modal domain and frequency domain is as follows: in the modal domain, the lowest energy indicates a more 'stable' body and in the frequency domain, the highest energy shows a major peak. In the modal domain, the instrument is examined without excitation, instead the total energy in the body per unit mass is studied. The body is most 'stable' if it has the least amount of energy stored in it, because that means that entropy is higher in that body across its first 50 resonant modes. This lower stored energy means that at resonant frequencies, the total energy in the body is lower, so when the body is excited, more energy will be emitted from it. In the frequency domain, where excitation is present, the total energy of the body (kinetic and potential) is analysed, as it responds to excitation at a particular frequency; the more total energy it has at a frequency allows us to see that it has more displacement at that frequency. In the frequency domain, comparison is between energy in one model across 1000 frequencies; where there is more energy, there is more displacement.

frequencies at which at which the lofted model responds efficiently (loudly). These frequencies are likely to be important peak frequencies in the response of the heuristic model within the air. Thus, Figure 7.9 compares this energy response with the eigenmodes of the body and the frequency response measured by peaks.

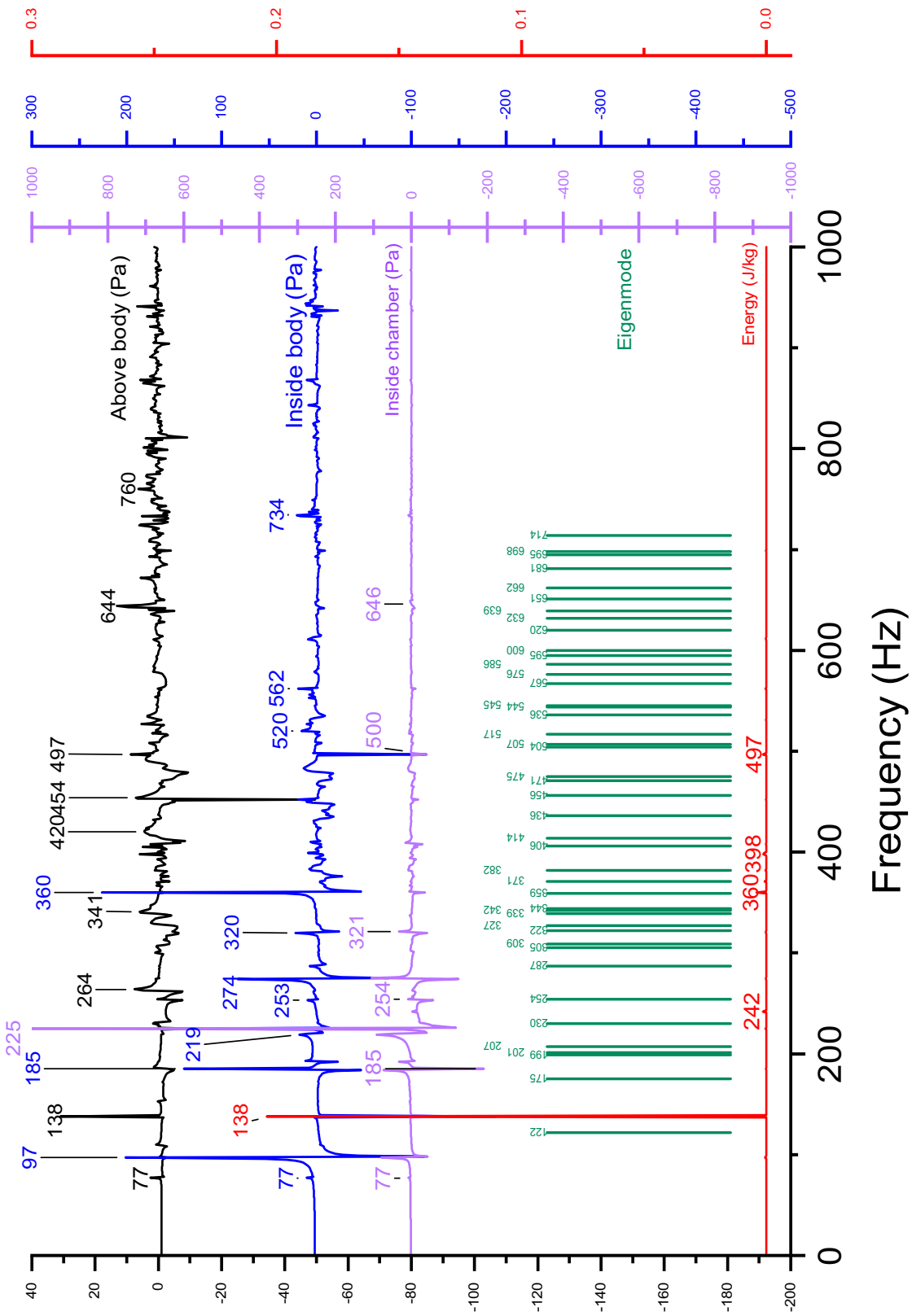

Figure 7.9 Lofted model stored energy, eigenmodes and frequency response

Figure 7.9 shows that more resonances inside the main air cavity of the lofted model align well with the energy peaks and eigenmodes observed. The strongest energy peak is found at 138Hz; it does not align with an eigenmode or any peaks inside the body but is seen as a peak outside the model. This peak does not translate out of the instrument. The eigenmodes below 600Hz show an alignment with peaks observed inside the body most clearly but only some of these modes are observed out of the body. For example, the strongest peak inside the chamber is at 225Hz and corresponds to an eigenmode; this mode does not project out of the body. By contrast, the peaks at 371 and 504Hz translate to resonances outside of the body. This comparison means that the higher frequency eigenmodes project out of the body better than lower frequency modes. However, this is a time-average response, which means that it is unclear when in the decay of sound from the body these resonances would appear. Although the effect of the small chamber cannot be clearly seen yet, the resonances within the main air cavity (see Figure 7.9 blue line) translate well outside the body.

In Figure 7.9, a peak is observed in all probes at 77Hz, but it does not appear as an eigenmode. This peak shows activity inside the body in Dataset 4. It is likely that 77Hz is the first Helmholtz resonance predicted with the heuristic lofted model. This resonance is observed at 85Hz in Coaldrake's CT scan model (2019).

Compared to the box model, there was more activity observed inside the lofted model. Radiation in this model is more separated between the two sound holes and closely resembles a dipole shape (see Dataset 4). With frequencies up to 700Hz, most of the radiation happens from the bottom of the instrument. The air inside and outside the instrument was found to be in-phase at these peaks, which suggests that the base plate is not hindering the motion of air or is moving in-phase with it.

The findings of the frequency scans

In this domain, box models and the lofted model were used to obtain an understanding of the interaction between the wooden body and the air inside and outside the *koto.* It was found that the addition of sound holes introduces new resonances to the frequency response (97, 139, 225, 274, and 360Hz). However, this analysis found that the eigenmodes of the box

models do not translate into the surrounding air in the same way as those of the lofted model. Therefore, box models are considered unsuitable for the remainder of the analysis. If no clear link exists between the response of the box and lofted models, they cannot be considered informative in the study of the *koto*'s acoustics as a set. Box models have been useful in determining the effect of changing basic components of the body. However, they are not validated models. By comparison, the lofted model is validated as much as possible against physical measurements and is considered a reliable heuristic model. Therefore, only the heuristic lofted model is used in the transient studies. The results from the frequency scans also suggest that the small internal chamber acts as a resonator.

The small internal chamber shows a strong resonance at 225Hz. Due to this being a relatively low frequency, the chamber's amplification of it may be giving the instrument extra depth in tone. In his discussion of Ando's work and the *koto*, Fletcher and Rossing state that modes may be expected but not yet observed at "integral multiples of a fundamental near 100Hz" and that the mode near 400Hz should vibrate efficiently and show up as a spike in a frequency response (Fletcher and Rossing 1991, 289 and 290). The 225Hz peak in the chamber and the 138Hz energy peak may be close approximations to the multiples expected. The small chamber likely serves in the design of the instrument to reinforce this frequency, similar to the design of ported loudspeakers. The response of the internal chamber is examined further in the transient studies.

Time Domain: transient response of the heuristic *koto* model

The transient response of the *koto* is the last part of its acoustical response and is examined in this study using the lofted model. The following section discusses the outcome of exciting the instrument at two cross-sections (which correspond to positions near the two fixed bridges at either end of the instrument) and at the bridge position for each of the thirteen strings in *hirajōshi* tuning starting from E; these excitation positions are detailed in the Methods

chapter.[5] These excitations were used to examine how the transient response was affected by and the position of the excitation along and across the body. First, qualitative observations were made of all waveforms from the 39 simulations, which was followed by spectral analysis of the initial observations. Decay analysis was the final analysis. The compilation of these different analyses showed that the initial response of the body from the top shell is determined by the position of excitation across the body (string number), whereas the initial response captured below the body is affected by the position of excitation along the body. The separate response of the internal cavities and the top shell converge in the final decay of the body to a uniform decay tail. These findings provide the necessary starting point for understanding the acoustical response that results in the complex tone of the *koto*.

The first analysis of the time domain results was the qualitative observations of all waveforms. The lofted model was excited at three points along the body for each of the thirteen string positions (at two cross-sections on either end of the body and at the bridge position). The waveforms output from the probes were compared between these 39 excitations and between all probes in each excitation. The probes above the midpoint, below the first sound hole, inside the main air cavity and inside the small chamber were selected as those used for further analysis. The FFT spectra were also compared between the probes and between the different excitation positions. Table 7.4 summarises the findings of the qualitative observations. The observations are used in the analysis and interpretation of the results through the remainder of this chapter. The raw data analysed in Table 7.4 can be found in Dataset 5 and Dataset 6.

[5] The 13 strings are not evenly spaced across the arc of the cross-section. The excitation points are positioned at the point where the string sits atop the body when no bridge is in place. This slight shift of some excitation points from even spacing to string space has little effect on the amplitude both inside and outside the body and on the frequency response outside the body. In the main air cavity, this slight shift in position causes a change in the frequency response which is seen in the FFTs inside the main air cavity.

Table 7.4 Summary of qualitative observations of the waveforms from exciting the lofted model

Observation	Clarification	Position across the top curvature (string number)	Position along the body	Probes	Interpretation
Booming	An additional section in the tail of the transient response where the amplitude rises again and falls. Without this effect, the amplitude steadily falls from the initial excitation onwards.	Outer strings (1-3 and 11-13)	Dragon's tail (minimum arching) and bridge positions	Above the midpoint and in both internal chambers in the dragon's tail and bridge positions. Below the sound hole in dragon's tail.	The energy in the outer strings is not directly dissipated out of the top shell after the initial excitation. Energy is transferred through the wood inside the body and the small chamber, dissipating out of the body slowly; the booming effect is highlighted at strings 12 and 13 with a red box labelled A in Dataset 5.
Higher initial amplitude	The higher amplitude of the first 0.2s of the waveform	Middle strings; initial amplitude increases towards middle strings from the outer strings.	All three sets	Above the midpoint	Excitation placed away from the outer walls leads to a larger amplitude in the sound dissipating in the immediate 0.2 seconds after excitation. The effect is caused by the position across the top curvature of the body and not along the body.

The unresponsive region of frequencies and the change in its size	A region of frequencies in the FFT where the response is flat and low; this region is measured as the distance between the two peaks surrounding it; it is also referred to as a band gap in other studies (Bader 2019, 3091).		All three sets	Probe inside the small chamber	Initially, it seems that this effect is related to the change in the excitation position. This region is further studied in the spectral analysis. This effect is discussed later and presented in Dataset 7.
Semi-periodic state	A period from 0.5 to 1s in the waveform where the amplitude does not drop and visually resembles a periodic waveform. [6]	All strings, but more in inner strings. [7]	Dragon's tail, bridge positions.	Above the midpoint.	This effect was also observed in the plank (see Chapter 6). It is likely caused by the slow release of energy from the body or reflections in the air. [8] effect is highlighted at string 7 with an orange box labelled B in Dataset 5.

In Table 7.4, the booming of sound affects the decay analysis. Working around this booming is discussed in the decay analysis section. The amplitude of the response is increased in the excitations located at the inner strings. This effect is observed at both cross-sections and at the bridge positions and is a starting point for observing the effect of moving the excitation point across the 13 strings. All simulations showed a clear decay within the first 0.2 seconds (see Dataset 5). A semi-periodic state is seen in the second half of the response tail in these strings,

[6] As a way to approximate the semi-periodic state, the mean of the absolute value for the amplitude of the tail was obtained. This value is used in the compilation of observations to clarify the response of the instrument.
[7] At the bridge position, this semi-periodicity is largest in string 2, which is also the string with the smallest unresponsive region in this excitation set.
[8] The herringbone pattern seen below the sound holes of some *koto* is not included in the model (Johnson, 62). It may have an effect on this booming and further research could clarify its acoustical role in terms of the sound hole as booming of sound observed.

observed above the body. At the maximum arching cross-section, uniform decays are observed (see Dataset 6). These initial observations show that both the position of the excitation along the body -i.e. string number – and the position of excitation along the arched top shell affect the response. The features of the transient response are identified with this qualitative analysis and can be examined in detail with spectral and temporal analysis.

Spectral analysis of the results

The frequency spectrum in each transient response was obtained using a fast Fourier transform (FFT). The spectrum observed outside the body was largely uniform across all excitations, with the exception of the response inside the small chamber. Figure 7.10 gives an example of the uniform spectrum observed outside the lofted model, with the main peaks annotated.

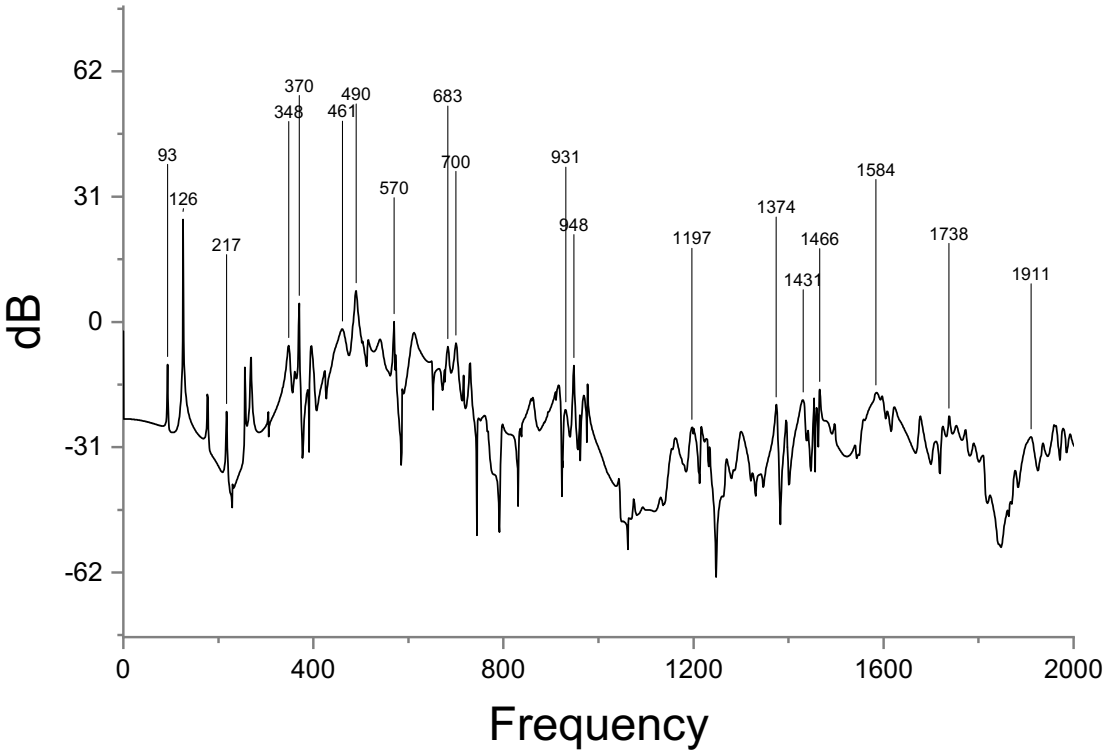

Figure 7.10 The spectrum of response observed outside the lofted model

Figure 7.10 shows the response above the body, when it is excited at the standard position of string 7 in *hirajōshi* tuning. This response, with prominent peaks at 93, 126, 490, 948, 1584Hz, is observed similarly in all 39 simulations. This means that the general frequencies present from

the instrument are likely to be the same regardless of where it is struck. By comparison, clear differences were found between the spectra from different excitations in the small internal chamber, with a range of frequencies that were unresponsive frequencies within the spectrum; this range changed through the 39 excitations. The following section summarises the main analysis of this region.

The unresponsive frequency range in the small internal chamber

The small chamber is unresponsive to a range of frequencies. Bader et al. have observed a similar band of unresponsive frequencies in the study of a frame drum, which they refer to as a 'band gap' (Bader et al. 2019, 3091). Frequency scan of the simple plank (in Chapter Six) also showed a similar region of unresponsive frequencies in the range of 1250 – 1750Hz.[9] The size of this range was found by measuring the distance between the two outer peaks at the edges of this range. The size of the region changes in all three sets across the 13 strings. The FFTs from the waveform inside the small chamber are presented in Dataset 7. In the dataset, the general area of the unresponsive range is shown in the dashed red lines. Table 7.5 details the starting and ending frequency and the size of this region at all excitation points.

[9] However, this region was observed outside the plank, in the surrounding air, and in a frequency domain study; in this study, this unresponsive range was observed most clearly inside the small chamber. Though the two sets of results between frequency scans and frequency analysis of the transient response cannot be equated, the connection of results invites further study.

Table 7.5 The size of the unresponsive region of frequencies (Δf) observed inside the small chamber at three points along all 13 strings

	Dragon's head (maximum arching)			*Bridge positions*			*Dragon's tail (minimum arching)*		
String number	From f (Hz)	To f (Hz)	Δf (Hz)	From f (Hz)	To f (Hz)	Δf (Hz)	From f (Hz)	To f (Hz)	Δf (Hz)
1	1058	1176	118	830	1550	720	938	1324	386
2	1021	1245	224	987	1321	334	938	1318	380
3	1019	1244	225	1020	1208	188	934	1282	348
4	1021	1401	380	1020	1299	279	976	1233	257
5	993	1401	408	976	1269	293	987	1184	197
6	1027	1403	376	993	1301	308	1044	1184	140
7	959	1402	443	947	1301	354	1044	1185	141
8	955	1288	333	1023	1273	250	1045	1181	136
9	984	1287	303	1011	1298	287	1045	1180	135
10	1051	1198	147	1028	1273	245	985	1179	194
11	1020	1241	221	999	1274	275	935	1314	379
12	1060	1178	118	999	1271	272	938	1314	376
13	1059	1177	118	1096	1180	84	938	1360	422

Table 7.5 shows that the chamber responds to the motion across the body (string number) differently depending on the position of excitation along the arched top shell. At the dragon's head (maximum arching), the gap is largest in middle strings (gap of 443Hz in string 7) and smallest in outer strings (gap of 118Hz in strings 1 and 13). An opposite response in seen in dragon's tail; the gap is largest in outer strings (422Hz gap in string 13) and smallest in inner strings (gap size is 141Hz in string 7). Excitations at the bridge positions show an almost consistent gap size of nearly 300Hz in strings 2-12. It can be deduced that at each cross-section, there is a clear change in the response of the chamber. However, changing the bridge position means that the position of excitation simultaneously moves along and across the body, which means that even with the addition of the two cross-sections, the effect of moving the excitation along and across the top shell can only be separated in a generalised way. The clearest peaks from the responses above the midpoint of each cross-sections (Figure 7.10) are compared with the previous frequency and modal domain results.

Connection of the three domains of study

Table 7.6 shows the alignment of peak frequencies observed in each of the three domains of study. Frequencies are considered aligned where they are present within 10Hz of each other. In Table 7.6, resonances are organised on the basis of alignment with eigenmodes, stored energy in the *koto* body, and probe data. The hierarchy of peaks from top to bottom represents the importance of the peaks. Peaks aligning with the total body energy and an eigenfrequency are considered the main resonances of the body; peaks only aligning with the probe data in the frequency scan in the air are considered air-based resonances.

Table 7.6 Compiled response of the lofted model in three domains

	Lofted model					
	Modal domain	Frequency domain		Time domain		
	Eigenmode	Energy peaks (J) at frequency	Outside Probe peaks	Minimum arching transient response outside	Maximum arching transient response outside	Bridge (string) position string 7
	Hz	Hz	Hz	Hz	Hz	Hz
Transient + frequency scan + eigenmode + energy	230	225	231	220	220	217
	504	497	497	505	504	
Transient + frequency scan + eigenmode					402	
	414		420	415	428	
	456		454	460	466	461
	576		579	576		
	639		644	646		649
	662		672	670		
	695		693	691	692	
	714	708				716
Transient + energy + eigenmode	359	360		351		348
	371	371		371	372	370
Transient + energy + frequency scan		398	398	394		396
		97	98	94	95	93
Transient + eigenmodes	122			126	126	126
	175					177
	254	254				256
	322			318	316	
	436			439		
	475			481		490
	517					516
	544					540
	567					570
	545			545	550	
	595			593		
	632				631	
	651				659	
	681					683
	698					700
Transient + energy		274		272		
Transient + frequency scan			186	181	180	
			264	264	262	269
			527	525	533	
			611	617		612
			724	724		730
			733	731	744	

			761	754		761
			774	777	776	
			794			798
			840	847		
			865	875	879	862
			905	907		
			921		927	916
			941		939	948
Transient only				557		
				816	811	
				903		
				933		931
				965		969
				985	979	977

In Table 7.6, the eigenmodes at 230 and 504Hz are found to be the most important resonances of the heuristic lofted model. These frequencies are resonances of the *koto* body and translate out of the body at both ends of the instrument. The eigenmodes at 414, 456, 576 and 539 are examples of similarly strong eigenmodes. However, these modes do not show a strong peak in the energy from the frequency scans, which suggests that they are not as strong as the 230 and 504Hz modes. This analysis has traced the most important resonances of the body through three sets of studies to find the two resonances that strongly carry through. The following sections continue with the results of the temporal analysis to detail how the spectrum inside the body and the decay of sound are affected by the position of excitation.

Temporal analysis of all results

Decay analysis followed the qualitative observations of the transient response (Table 7.4) to provide a clearer understanding of how energy dissipates from the lofted model during the one second length of observation.

Decay analysis

The decay analysis used the response above the body, below the sound holes, and inside the two internal chambers. Each response at each probe was divided to multiple decay events within. The decays observed above the body were divided into three decay events. In the probe above the midpoint, the first decay was defined as t=(0-0.05)s; the second decay at t=(0.05-0.3)s, and the third decay at t=(0.25-1)s. The same intervals were used for the decays below the sound holes. However, in these probes, the period (0.25-1)s was divided to (0.25-0.5)s and (0.5-1)s to mitigate the effect of 'booming' observed in the response (see Table 7.4 and Dataset 5).

The probes inside the body are useful because the motion of energy is most likely through the air in the small chamber to the main are cavity to the surrounding air outside the instrument body. The expected length of the presence of sound from these locations is calculated because it allows the study to approximate how long the sound tail is likely to last with the help of the decay from the air inside the *koto* body moving to the surrounding air. Having the decay rates inside also helps clarify the movement of energy within this system in the form of sound.

Inside the body only the final decay is of interest. The aim of this decay analysis is to observe the duration of the decay of sound from the instrument. Any transfer of energy from the internal chambers in the initial part of the response would be embedded in the response observed outside the body, or it would have been absorbed within the wooden shell. Therefore, it is only the energy inside the air cavities of the body at latter part of the signal that is not already transferred out of the body and into the surrounding air. The initial decays in the internal chambers do not contribute to the total duration of the final decay of sound and thus were omitted from this decay analysis. Additionally, these decay periods show the 'booming' effects ((see Table 7.4 and Dataset 5); given that this effect is not clarified, the skewed decays from it could not be included in this investigation.

The interval t=(0.5-1)s was chosen for the decay analysis studied from the probes in the two internal air chambers; only the final decay of sound from the internal probes was of interest in this study. Also, the initial parts of the response from the probes inside the body frequency

showed booming (see Dataset 6), which would have skewed the analysis. Initially, to obtain the decay constants, asymptotic fits ($y=a-bc^x$) were tested. This fit was considered inappropriate for this study because beyond visual cues there was not enough evidence to support an asymptotic decay in the signal. Instead, a different approach was taken to obtain an exponential decay, using the natural logarithm of the initial waveform. The absolute value of the probe data was obtained ($|A|$). The moving average of the value was calculated ($|\bar{A}_{mov}|$), with 100 steps backward and 100 steps forward, equal to 0.002s in either direction. The natural logarithm of ($|\bar{A}_{mov}|$) was then calculated, ($\ln(|\bar{A}_{mov}|)$); finally, a linear fit of the waveform made from this ($\ln(|\bar{A}_{mov}|)$) gave the decay constant. Figure 7.11 shows an example of the three decay constants observed above the instrument model, using the linear fit of the semi-log data: ($\ln(|\bar{A}_{mov}|)$).

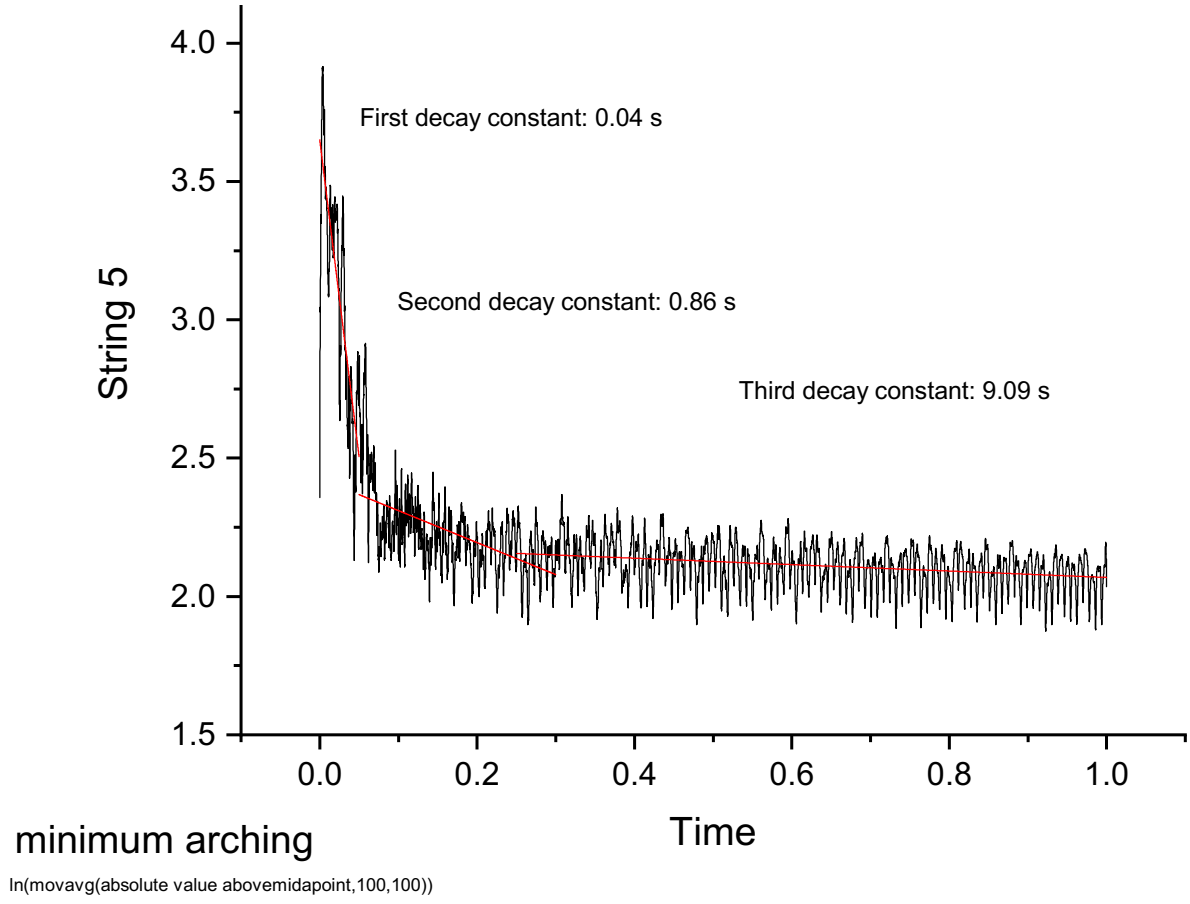

Figure 7.11 Example of the exponential decay constants using string 5 at the dragon's tail (minimum arching)

The example in Figure 7.11 shows the three decay events observed and the general time stamp for each. Table 7.7 shows the compiled set of the first and second decay constants obtained from probes outside the body in the three sets of excitations.

The time range of the decays were defined using observations from the case study of strings 1 and 5 and can be considered an estimate for the three decay events observed in the 139 waveforms of the 39 excitations of this study. Identical time ranges for the decays are not appropriate for all excitations, as it is likely that each decay is slightly faster or slower, shortening or extending the point in time where the decay occurs. However, in this heuristic study, it is more appropriate to find decays within the same time range across excitations. Below the sound hole, the third decay seen above the midpoint was divided to two decays: t=(0.25-0.5)s and t=(0.5-1)s. This same time-stamp, t=(0.5-1)s is used in the two probes inside the small and main air cavity of the body as the final decay.

Table 7.7 Exponential decay constants outside the body for all strings and positions

Outside probes						
String	max arching Above midpoint	bridge position Above midpoint	min arching Above midpoint	max arching Below SH 1	bridge position Below SH 1	min arching Below SH 1
First decay constant (s)						
1	0.05	0.11	0.13	0.17	0.13	0.12
2	0.05	0.19	0.11	0.05	0.16	0.09
3	0.04	0.05	0.07	0.10	0.06	0.10
4	0.04	0.03	0.05	0.06	0.07	0.13
5	0.04	0.04	0.04	0.05	0.07	0.15
6	0.04	0.06	0.04	0.05	0.06	0.16
7	0.04	0.06	0.04	0.05	0.05	0.15
8	0.04	0.07	0.05	0.05	0.13	0.11
9	0.04	0.07	0.05	0.06	0.17	0.08
10	0.04	0.05	0.06	0.08	0.15	0.07
11	0.04	0.04	0.08	0.10	0.07	0.09
12	0.05	0.05	0.12	0.05	0.08	0.17
13	0.05	0.05	0.13	0.04	0.10	0.17
Second decay constant (s)						
1	0.20	3.45	3.03	2.13	0.79	2.86
2	0.18	3.85	2.44	0.17	1.35	1.35
3	0.20	0.68	1.92	0.20	0.41	1.09
4	0.21	0.32	1.33	0.23	0.21	0.70
5	0.22	1.25	0.87	0.24	0.35	0.49
6	0.23	1.35	0.65	0.24	0.40	0.36
7	0.22	1.59	0.60	0.24	0.47	0.31
8	0.21	1.54	0.66	0.23	0.37	0.32
9	0.21	1.39	0.88	0.22	0.35	0.38
10	0.21	1.49	1.43	0.21	0.39	0.54
11	0.20	1.41	2.50	0.20	0.48	0.94
12	0.20	0.22	3.70	0.19	0.17	1.67
13	0.20	0.31	4.17	0.21	0.15	2.08

In Table 7.7, the first decay above and below the body event ranges from 0.03 to 0.13 second across all positions of excitement. The second decay is slower in both positions, with decay constants of up to 4 seconds in duration observed in the outer string positions (minimum arching, above midpoint in Table 7.7) and the rate of the decay of sound slows down after the initial decay. This observation suggests that there are multiple decays after the first exponential decay. Following the first two decays, Table 7.8 shows the final decays inside and

outside the body in all excitation points. In these analyses, the maximum decay time observed would be the final decay time of the entire system; the final decay is not the sum of the decay in all probes, but the longest decay time observed from each excitation. The additional decay from other probes likely translates to the loudness or richness of the sound in its final decay.

Table 7.8 Final exponential decay constants in all probes inside and outside body, at all positions and strings

	Final decay constants - all probes (s)											
String	Above midpoint Maximum arching	Above midpoint Bridge position	Above midpoint Minimum arching	Below SH 1 Maximum arching	Below SH 1 Bridge position	Below SH 1 Minimum arching	Inside main air cavity Maximum arching	Inside main air cavity Bridge position	Inside main air cavity Minimum arching	Inside small chamber Maximum arching	Inside small chamber Bridge position	Inside small chamber Minimum arching
1	3.45	8.33	9.09	2.22	6.25	2.94	0.90	2.27	1.28	1.16	2.00	1.23
2	2.63	8.33	9.09	2.38	7.14	3.70	0.98	5.88	1.25	1.64	N/A	1.22
3	1.54	7.69	9.09	2.27	3.33	4.76	1.27	1.85	1.12	1.49	1.92	1.10
4	1.19	5.26	9.09	1.49	3.13	5.88	1.05	1.08	0.95	1.56	2.17	0.93
5	1.03	7.69	9.09	1.67	6.67	8.33	0.93	1.72	0.81	1.54	1.54	0.75
6	0.96	7.69	9.09	1.92	6.94	10	0.89	3.33	9.09	1.54	1.89	0.65
7	0.94	7.69	9.09	2.22	7.69	8.33	0.88	5.88	1.89	1.52	1.92	0.91
8	0.95	7.69	9.09	2.38	8.33	6.67	0.89	8.33	N/A[10]	1.52	1.52	1.69
9	1.02	7.14	9.09	2.50	8.33	5.56	0.92	9.09	2.27	1.52	1.96	2.86
10	1.14	6.67	9.09	2.44	7.14	4.55	1.00	6.67	1.49	1.47	1.96	1.64
11	1.54	6.25	9.09	2.27	6.67	3.33	1.27	3.70	1.22	1.49	2.04	1.28
12	2.38	2.00	9.09	2.13	3.57	2.50	1.61	1.59	1.10	1.47	1.92	1.14
13	3.45	4.55	0.94	1.85	4.76	2.22	0.89	2.08	1.08	1.16	1.28	1.11

In Table 7.8, the final decay of sound above the instrument stays constant at 9 seconds in length in the minimum arching cross-section (the dragon's tail) with the exception of string 13, which shows an inexplicably quick final decay. At the dragon's tail, as the excitation point moves across the top shell, the sound continues to decay evenly from the top shell. The range

[10] At this position, the booming effect has skewed the final decay to a rise and there is no decay rate.

of decay times is lower in maximum arching (dragon's head), where the longest decay is observed in the outer strings at 3.45 seconds. This analysis shows that the final decay outside the instrument is longest at the dragon's tail, and generally faster at the dragon's head end of the body, which also affects the length of the decays at the bridge positions since the bridges extend across the entire distance between the two cross-sections (Table 7.8 data column 2 – decays ranging from 2 to 9 seconds). Up to this stage, the results of each decay event had been analysed separately.

Contour maps were used for the analysis of the decay constants to assist comparisons of excitation parameters. In Figure 7.12, the final decay constants are shown in relation to the position of excitation across the top curvature (string number, y axis) and the position of the excitation along the arched shell (distance from the small chamber at the dragon's head, Δx).

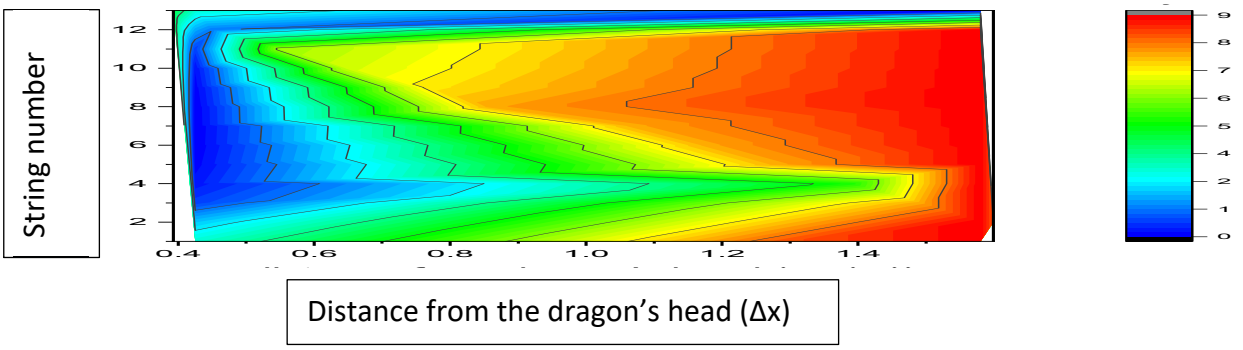

Figure 7.12 Contour plot comparing the long decay time constants observed above the body with the position of excitation across and along the top shell.

Figure 7.12 shows that the final decay observed above the body decreases with moving closer to the dragon's head. All excitations closer to the dragon's head (maximum arching) have shorter decay constants (blue). The excitations at the dragon's tail (minimum arching) show the highest decay constants (red), and a stable decay is seen across the thirteen bridge positions of excitation, with a value between the two extremes (green – four to six seconds in duration). This parameter (Δx) showed the clearest separation between the three sets of excitations because the because Δx is constant in the two cross-sections. The findings of this analysis help to discretise the effect of each parameter. Other contour plots were made that compared the decay constants with the other parameters of excitation and are shown in Figure 7.13.

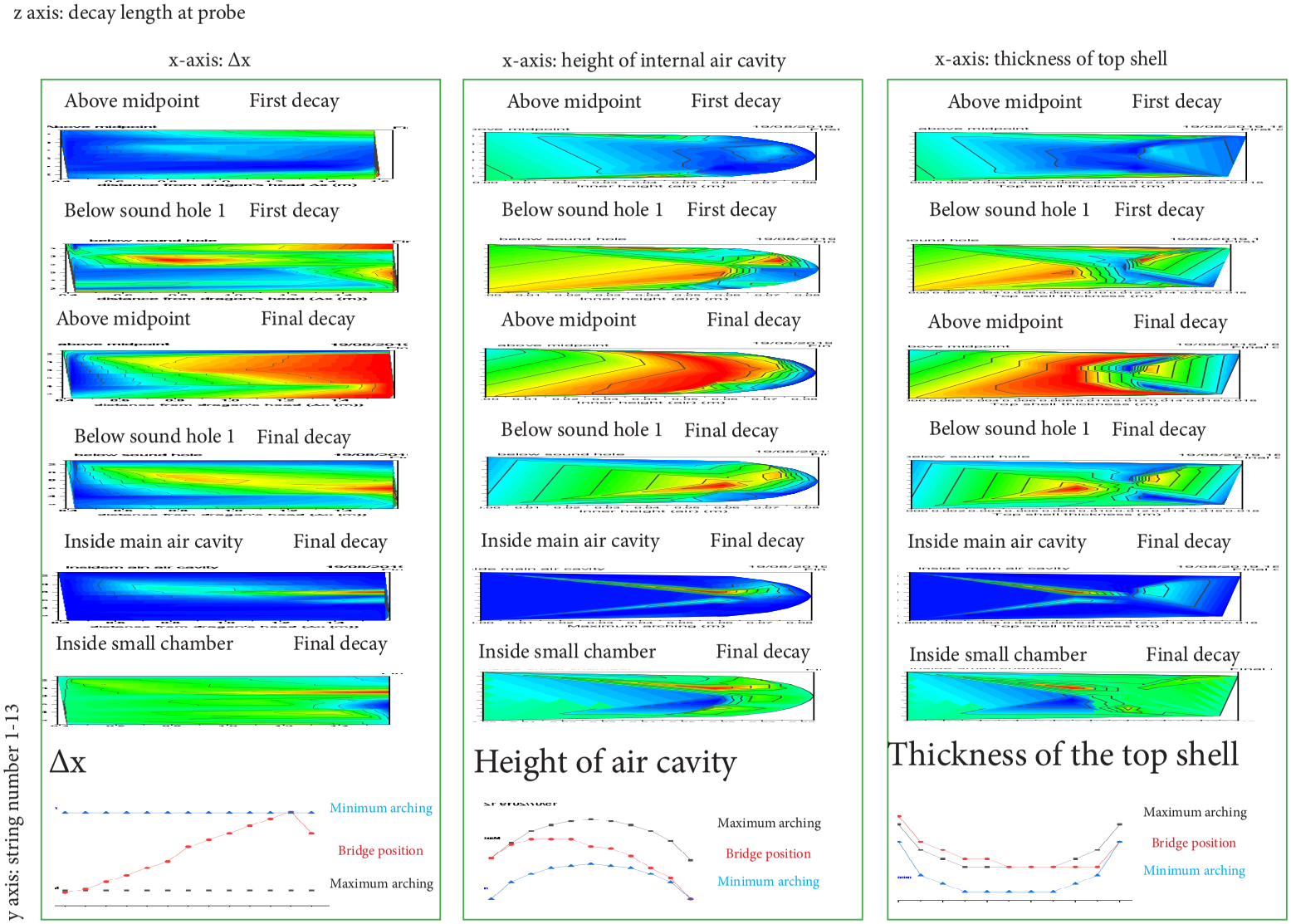

Figure 7.13 Contour plot comparisons between parameters of excitation and decay constants

The findings of this contour plot analysis (Figure 7.13) help to discretise the effect of each parameter. Table 7.9 compiles the details from each decay event in each set of excitations to refine the findings in terms of the decay of sound from the body and not as individual excitation points.

Findings of the transient studies

The time domain analysis has shown that the decay of the sound changes depending on the position of excitation. There are also discrete decay events in the sound of the instrument. In this study, three approximate decay events were found. Table 7.9 summarises the findings of each decay.

Table 7.9 Summary of observations from the decay constants

Decay	Excitation position		
	Minimum arching (dragon's tail)	**Bridge position**	**Maximum arching (dragon's head)**
First	First decay time is shorter in middle strings above and below the body.	After string 2, fluctuations are small in the probe above midpoint; below the sound hole, large fluctuations are seen, with a booming in stings 8-11.	Decay time is shorter in middle strings similarly to the minimum arching cross-section. Decay time variation is smaller and the decays are shorter than the shortest at minimum arching
Middle decays	Second decay drops in inner strings. The third decay is problematic due to booming side effects, as discussed earlier. The second decay is reliant on position across body.	Fluctuation of response above the body is small. Both above and below body show longer decays in strings 7-10, with this increase in decay time seen clearer in probe above midpoint.	The second decay is lower in maximum than minimum arching, and variation across string points is small. Decay time rises in middle strings above midpoint and below the sound hole. [11.] Variation is large between the cross-sections in middle strings.
Final decay	Above the body, final decay time is constant at 9 seconds, except for in string 13.[12] Below the body, decay time increases in middle strings to 10 seconds at string 6 and is seen at 3 seconds in outer strings. Inside probes all decay within 3 seconds, except for anomalies.	In strings 6-11, a rise and fall of decay time is seen in the chamber. These strings that are placed directly atop the shell are furthest away from both ends and the outer side walls The length of the decay changes in the same way above and below the body. Inside the body, in the small chamber and the main air cavity, the response is not clearly connected to any parameter. The bridge position shows smaller variance between the strings, with a slow decrease of the final decay constant with the progression of strings.	Final decay time above drops in middle strings; highest level in outer strings is 4 seconds. Inside and below, a steady and short decay time of less than 3 seconds is observed. At the dragon's tail, the final decay tail above is not reliant on position across the top curvature, but decay tail below is increased in middle string points.
Deductions: final decay			
	Final decay largely comes from the top shell, complimented by the response from the sound holes. Inside, the response fluctuates but is decayed within 3 seconds.	Consistent decay time, but source of decay time changes.[13]	Consistent and low final decay time.

[12] The reason for this anomaly has not yet been determined.
[13] The string 2 anomaly may owe to it being placed on an 'ear', which creates an additional tube of air directly below the string.

The three sets of excitations have some similarities but are distinct from each other. The duration of the final decays was longer when excitation was more distanced from the dragon's head. The movement of the excitation across the top shell only effects the initial decay time (Table 7.7), and does not have a clear effect on the final decay; at both cross-sections, the final decay time is relatively steady across the 13 bridge points (Table 7.8 and Table 7.9). Therefore, either the arching along the body and or proximity of the excitation to the small chamber have the strongest effect on the decay of sound from the body.

Table 7.8 and Table 7.9 show that at the bridge positions, the decay of sound from the top changes across the 13 bridge points ranging from 2-9 seconds. Nevertheless, at the bridge positions, the final decay remains steadily between 6-8 seconds across the 13 strings because the probe which accounts for this decay time changes between the probes outside and the probe inside the main air cavity. Table 7.7 shows that at the bridge positions, in strings 1-4, the longest decay is seen in the probe above the body; the decay tail is then detected from the sound holes in strings 5-7, 10 and 11; the longest decay tail is seen inside the main air cavity in string 8 and 9. In strings 12 and 13, the decay time is low in all probes at the bridge positions, which indicates that the proximity to the small chamber or the outer walls is likely shortening the decay time. The decay is generally the same across all bridge points, but in excitations where the decay from the outside of the instrument is reduced, there is additional energy remaining inside the main air cavity, which dissipates out slowly, giving additional decay time that stabilises the total decay. This means that the uniform length of decay at the standard bridge position is achieved in the instrument model by a balance between the top and the bottom of the instrument; the decay of sound is likely to be heard uniformly if the instrument is tapped at different points, but this consistent decay is created by sound transmitting through different parts of the body.

The analysis has shown the effect of moving the excitation points in a general way. However, it had been impossible to clearly correlate the observations from each decay with specific changes in the positions of excitation. To address this problem, the excitation points were compartmentalised into the following parameters: distance of the excitation from the dragon's head end of the instrument (Δx), thickness of the top shell (h_t), height of the air inside the body

below the excitation point (h_a), and the thickness of the base plate at the excitation point.[14] With specific parameters, all observations and measurements from the transient studies were compiled (see Dataset 8). In Dataset 8, each decay is compared between all excitations and the parameters of the excitation point. These parameters are shown in the final row in Dataset 8. Table 7.10 details the relationship found in Dataset 8 between the first and the final decays and the parameters of the excitation point.

Table 7.10 The effect of study parameters on decay time

Parameters increasing decay time	Parameters decreasing decay time
First decay	
Distance from dragon's head (Δx)	Height of air cavity (h_a)
	Thickness of top shell (h_t)
Final decay	
Distance from dragon's head (Δx)	
$3cm \leq h_a \leq 6$ cm	Height of air cavity (h_a) outside the optimal range
$2cm \leq h_a \leq 10cm$	Height of air cavity (h_a) outside the optimal range

The thickness of the top shell and the height of the air cavity (h_a and h_t) affect the first and final decays separately (Table 7.10). With larger values for these parameters, the initial decay time is shorter (Dataset 8 – first column). In comparison, the final decay time is extended with larger values for both parameters, but only if these two parameters are within the particular range detailed in Table 7.10. Outside this range, the final decay constant was found to be lower. This fact indicates that the thickness of the top shell and the size of the *koto* are critical to the decay of sound from the body. It reinforces the important contribution of the shape of the top shell to the acoustical response of the instrument.

Discussion of results from the transient studies and the role of the geometric features of the heuristic lofted model on the decay of sound

It is now possible to discuss the role of individual parts of the body on its acoustical response because of the distinctions that were established between different parameters. The response

.

of the *koto*'s wooden shell has been characterised in this work in terms of the different parts of the decay tail and the components of the body. This characterisation is achieved by the excitation of the lofted model of the *koto* at two cross-sections at either end of the body and at a set of bridge positions derived from *hirajōshi* tuning.[15] The uniform spectral response observed outside the body at the three cross-sections shows that the top shell of the *koto* radiates a consistent spectrum at different excitation points. Moving the position of excitation along the body determines the response of the chamber and affects the sound radiation out of sound holes; moving across the top affects how much sound is radiated out above the top shell.

The two internal chambers contribute to the decay of sound from the instrument. The differing role of these two chambers is shown in Table 7.11.

Table 7.11 The role of the two internal air chambers in the transient response

	Small internal chamber	Main internal air cavity
Response affected by	Proximity of excitation to the small chamber most important factor in response, then response changes with distance of the excitation point from the side walls.	1. Height of cavity directly below excitation point 2. Distance of excitation point from side walls
Role in the transient response	1. Resonates at lower frequencies and shows an unresponsive region of frequencies around 800-1200Hz. 2. Has a loud but fast decay of sound	1. Extends decay duration 2. Acts as a pipe and directs sound through to the sound holes

[15] Given the resource-intensive nature of time dependent studies using finite element methods, it was not possible to explore different tuning systems within the scope of this thesis. *Hirajōshi* tuning was chosen as a commonly used tuning system and the arrangement, starting from E4, allowed for maximising the range of excitations along the body and thus obtaining an overview of the response of exiting the *koto* body at different positions along and across the curved top shell.

The third row in Dataset 8 shows increased decay time inside the main air cavity with increased height in the air cavity, especially at the bridge positions (red).The response inside the main air cavity depends on the height of the air cavity directly below the excitation point and the volume of air near that point, with the distance from the outer walls also impacting the response. By comparison, the small internal chamber acts as a resonator in the initial part of the decay of sound from the instrument, having a loud but fast decay of sound itself (Dataset 6; Table 7.8). A larger unresponsive range inside the chamber equates to more energy in specific frequency bands, which decay faster. When this range of frequencies increases, in the maximum arching cross-section (dragon's head), energy is focused into the lower frequency range. The addition of energy causes the lower frequencies to be louder. This lower frequency range may be contributing to the bass-frequencies heard in the *koto* and is likely a design choice. The small chamber acts as a bass booster by removing a range of frequencies within 800-1200Hz.

All excitations at the middle strings decay faster. It is possible that the internal main chamber in the body is acting as a pipe, with the velocity decreasing as excitation moves closer to the boundary. Thus, the top shell gives the resonances of the *paulownia* shell and the sound holes give the response of the air inside the body and the internal geometry, seen in the distribution of decays and amplitude features. This observation is also made by Coaldrake (2018) that the 100Hz eigenmode is radiated from the top and the 85Hz Helmholtz resonance is radiated through the bottom of the body.[16]

This study has not simulated the strings of the *koto* in the FEMs. Actual strings input energy to the body at three points: the two fixed bridges and the moveable bridge point. As discussed in the Methods chapter, the positioning of the two maximum and minimum cross-sections is

[16] It would be interesting to investigate the response more formally in terms of a transfer function. However, this is a closed system, therefore the total energy in the system moves between air and wood in form of sound, displacement of body, potential energy and heat. Obtaining total stored energy of the shell as a function of time and total stored energy in air as function of time should show where the deficits occur as amplitudes rise in air.

close to the position of the fixed bridges of the *koto*. These results are useful for understanding how much these three points, relative to each other, contribute to the input of energy from the string. The response from energy input by a string is hypothesised to be a combination of the findings for each string at the three positions of this study.

Figure 7.14 presents the summary of the understanding of the decay of sound from the *koto,* as obtained by using the heuristic lofted model. It uses an abstraction of a decaying waveform to show the three stages of the decay of sound.

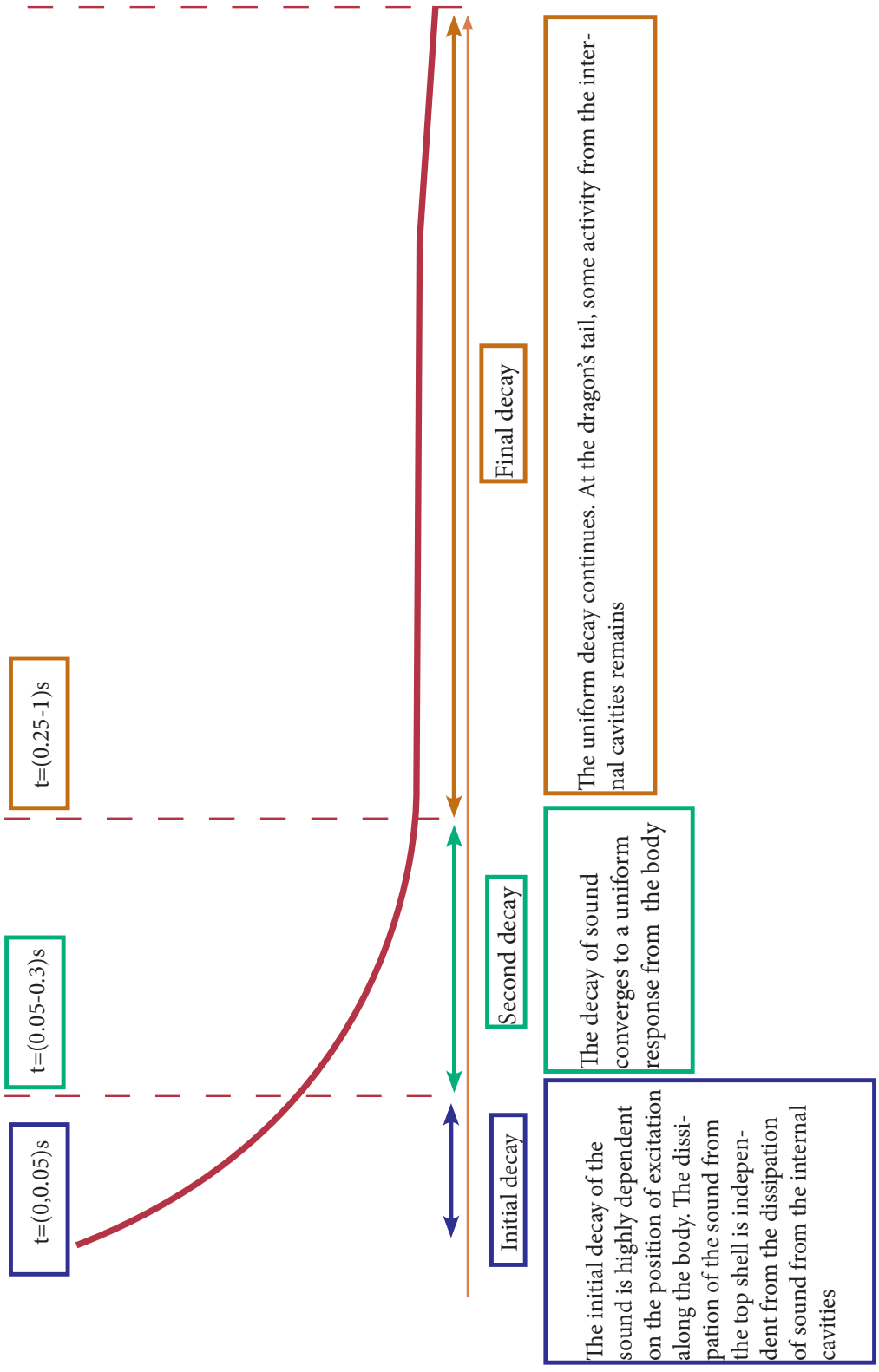

Figure 7.14 The stages of the decay of sound from the koto

Figure 7.14 illustrates that the main decay events of the instrument are each impacted by a different feature of its geometry. During the initial decay, the top shell radiates sound independently from the base plate and the internal air cavities. The initial decay of sound above the body is reliant on the position of excitation across the top curvature (string number). The initial decay below the body is reliant on the position of excitation along the body (distance from the small chamber). These components converge to a uniform decay in the second to final decays.[17] As the decays converge, the sound output from the top and bottom of the instrument becomes more uniform. In a reverberant instrument with a long decay tail such as the *koto*, this feature may ensure that the tail of the sound stays coherent.

Concluding discussion on the finite element modelling of the *koto* with heuristic models

This chapter started with the studies of the eigenmodes of the *koto* and its separate shells. Through the substructure coupling, the box and loft models, some of the effect of changing the geometry of the instrument were found. The eigenmodes showed that the top shell had the most impact on the eigenmodes of the body. These modal domain studies also showed that the total stored energy of the body is minimised by joining the two plates (Figure 7.4). Frequency scans of box and lofted models followed, which helped to clarify the connection between the wood and the air. The frequency scans indicated that the small internal chamber is acting as a resonator (Figure 7.9). The transient studies followed with the excitation of the lofted model at thirteen bridge points and across two cross-sections at either end of the top shell. The transient studies showed that the decay of sound from the body of the *koto* is faster at the dragon's head end of the instrument than the dragon's tail (Figure 7.12). Table 7.12 presents the findings of the acoustical response of the *koto* from the studies detailed in this chapter.

[17] In these decays, a semi-periodic waveform is seen at the dragon's tail and at the bridge positions, which extends the final decay time. This semi-periodicity seems to be integral to the response of the body, because the decay time observed with the semi-periodicity is the same as the decays that have been observed by expert performers (Personal Communications with Coaldrake 2019). The data suggests that the semi-periodicity is what causes the additional decay time, since this decay time has not been observed at maximum arching where the semi-periodic decay is not present.

Table 7.12 The findings of studies using the heuristic finite element models of the koto

Findings	Summary of evidence
1. The resonant modes of the *koto* are strongly affected by the anisotropic elasticity of the wood.	1. Anisotropy was found to be integral to the validation of the model and the exploration of using different physical properties for modelling.
2. The resonant modes of the assembled instrument are most similar to those of the top shell.	2. The modes of the top shell translate closely to those observed in the lofted model in the substructure modelling
3. The assembly of the top and based plates minimises the total stored energy of the body, making it more stable.	3. The sum of the total stored energy in the body showed the minimisation of energy in assembled models.
4. The small internal chamber near the dragon's head acts as a resonator, amplifying the lower resonances and extending the duration of the decay of sound from the body.	4. Frequency scans and the spectral analysis of the time-dependent response in the small chamber showed the additional response in the chamber unresponsive range.
5. The transient response of the instrument starts as two separate events but converges to a uniform response.	5. The analysis of the decays inside, above and below the body show the convergence to a uniform response.
6. The geometric detail which has the most effect on the sound envelope of the *koto* is the arching along the dragon's spine.	6. Moving the excitation point along the dragon's spine towards the dragon's head end of the instrument reduces the length of the decay.

The findings detailed in Table 7.12 have a number of important implications in terms of understanding the sound of the *koto:*

1. The highly porous and asymmetrical nature of *paulownia* is integral to the resonances of the *koto* and further research is necessary to understand the complexity of this wood.

2. The complex resonances of the *koto* are dependent on the shape of the top shell. Changing the shape of the top shell is likely a strong contributor to changing the resonances of the instrument.

3. The assembly of the *koto* stabilises the instrument and helps it radiate sound more loudly.

4. This small chamber contributes to the complexity of the tail of the sound from the *koto* and is an important part of shaping the resonances heard from the instrument; it changes the resonances of the air inside the instrument.

5. The way the instrument is creating and dissipating sound changes throughout the decay of sound from the *koto* body, adding complexity to the initial sound heard from the body and a distinct tail in the sound.

6. The combination of the two fixed and one moveable bridge is most likely creating uniformity between the length of decays from the thirteen strings

Changing the arching of the body down the length of the instrument itself seems to contribute to major changes in the resonances heard. The *koto* used in this study for the basis of the heuristic model is a *Yamadagoto.* It is more arched than the *Ikutagoto* design (Johnson 2004, 40-41). This study has shown the effect of arching on the decay of sound from the body. It is likely that some of the sonic differences between the sound of the *koto* in the two schools of practice, *Ikuta* and *Yamada*, is caused by the difference in arching. This is an important avenue for future discovery using the method established in this study.

At the bridge positions of excitation, the effects of individual components are balanced to give a uniform decay of sound across the 13 strings. This result has performance implications in terms of tuning of the *koto.* Firstly, the evenness allows flexibility for performers to make judgments for performances and adjust tuning to account for the needs of the composition

and the performance space. The moveable *do* system of tuning for the *koto* is well-suited to allow for this flexibility. The geometry of the instrument in turn supports the needs of the tuning system. Furthermore, the scores for *koto* music are written in tablature, meaning that the adjustment to the tuning is considered separately from the string. The performer can adjust the tuning of a string but perform from the same score unlike pitch-based notation which generally dictates the pitch desired and not the string with which the pitch should be executed.

This thesis has only examined the body of the *koto* using heuristic models. It has been outside of the scope of this study to include the assessment of the other parts of the *koto* such as plectra, bridges, and the various stands used for positioning the instrument. Fletcher and Rossing (1991, 289-290) state that the floor would have an effect on the response, with additional reflections from the hard surface; in traditional practice, *koto* are performed on a *tatami* mat, which is a dense woven mat. As discussed earlier, a decay time of close to 7 seconds has been observed by expert performers (Personal Communications with Coaldrake 2019). This decay time has been seen in simulations in the minimum arching and at bridge positions. It is likely that the long decay tail of the *koto* sound is designed so that it can withstand the damping caused by the mat and still project sound to the audience. Without the extended decay time, the sound of the decay tail would be absorbed by the mat and would not relay to the audience. Without the mat, the extended decay is likely to cause a build-up of resonances in the room, reducing clarity of the sound of individual notes as the reverberation and the long decays continue.

This chapter started with the eigenmodes of the shells of the *koto,* followed by frequency scans of heuristic models of the full-body of the instrument, and finally, examined the transient response of the instrument using the heuristic lofted model. This study and the study of the plank (Chapter Six) make up Part Two of this volume, where the methods of the study were applied to the investigation of the *koto* and a *paulownia* plank. The next chapter concludes this study and offers broader comments about the study of the *koto* and heuristic finite element modelling of East Asian zithers.

Chapter 8

Conclusion

This study had two focal points: the methods of analysis and the study of the *koto*. Part One presented the development of heuristic finite elements models from first principles. Simplicity of models and clarity of methods have been the tenets of this work. The series of simple finite element models were designed to analyse the vibration characteristics of the wooden body of the Japanese *koto*. The models of this instrument were then validated against the limited existing literature and new physical experiments. Table 8.1 presents a summary of findings regarding the methods of the study. This work has identified the characteristic interactions between different components of the instrument body and revealed how the resonances of this instrument manifest in its sound envelope. Overall the lofted model has proven to be the simplest valid abstraction since the lofting technique used to construct the model gives versatility and strength. Nevertheless, the investigations highlight that, unlike some other woods used for musical instrument studies, it is not appropriate to model the *koto* with isotropic moduli.

Table 8.1 A summary of the findings on the methods of this study

Findings	Summary of evidence
1. Orthotropic properties of the wood, even where an incomplete fit with measured data, are more useful in modelling the koto than isotropic properties.	1. The validation and exploration of the physical properties showed issues with isotropic models.
2. Box models are too simple for modelling the acoustical response of the koto	2. Box models did not predict important features in the resonances of the koto.
3. Heuristic lofted models are the simplest valid abstraction of the instrument.	3. Basic features of the acoustical response of the koto were successfully obtained with the lofted model.
4. Ando's method of separating the plates can be useful in new studies with finite element modelling because it allows for the researcher to observe the response of individual plates as well as the assembled body.	4. Substructure coupling in this study successfully showed new important details about the resonances of the koto and its individual shells.

This work has also shown that although previously considered problematic, Ando's method of studying the individual plates (1986 and 1996) is useful for exploratory studies of the *koto*; new technologies such as finite element modelling can clarify and refine this method for use in the *koto* family. With modelling, the response of individual shells can be studied, and full instrument models can be prototyped with ease. Additionally, with modelling, resonances can be observed more easily in large instruments than they can be with physical experiments.

Limitations of working with Chladni patterns on large plates may be mitigated using software such as COMSOL, but only if the models are validated using other tests.

This work has used visual representation of data as a tool for analysing the results. It shows that alongside the numerical tools of analysis, insights can be gained by employing the expansive visualisation tools available; COMSOL is an ideal software for this purpose. Importantly, these visual analysis techniques broaden the accessibility of finite element models within musicology, which can allow for greater integration of sound studies, organology, and musical acoustics.

Thus we now may conclude that this work can provide a roadmap for the study of other Asian zithers using heuristic finite element models. A lofted model is the simplest valid abstraction of the *koto* for heuristic modelling. Moreover, as noted, the lofting process gives versatility and strength to simple finite element models and enables transfer of the techniques to other case studies such as modelling other East Asian zithers. It also suggests that the lofting process has potential for modelling other under-studied instruments.

Part II focused on the study of the *koto*. Chapter Six provided a baseline for this the analysis of the resonances of the *koto* with a finite element model of a *koto*-sized plank. This chapter also demonstrated the integrated method of this study with a geometry simpler than the *koto* body. Chapter Seven discussed the findings of the study of the *koto*. In this work, the basic resonances of the body of the *koto* have been found. The heuristic model of the *koto* estimates the first eigenmode at approximately 100Hz. It has been shown that the arched top shell of the instrument determines these resonances to a large degree. This is seen through the modes that carry through from the model of the top shell to the full-body lofted model. The assembly of the body of the instrument also stabilises it, by minimising the stored energy in the body. The small internal chamber found at the dragon's head end of the instrument was found to act as a resonator. This chamber contributes to the long decay of sound from the *koto*. It was also shown that the decay of sound is slower at the dragon's tail end of the body.

Future work

This study investigated the methods for analysis of the *koto*'s acoustics using heuristic models, from which an important issue emerged for future studies of the *koto* or other wooden zithers. As noted in Chapter Five, a gap remains in the available data on the physical properties of *paulownia*; with refined properties, heuristic models of the instrument will likely show much closer results to the physical measurements of the instrument.

Improvements in model design are also important. Future lofted models of the *koto* or similar instruments would benefit from a loft cross-section near each bridge point, so as to make obtaining the angle of incidence for the force from the pulse more direct; having thirteen more lofts would also refine the shape of the top arch captured in the model. With additional lofts, the effect of changing top curvature can be compared better with the decay constants. However, such an expansion would require high computation power and computation time, especially in the transient studies. Similarly, the combined effect of arching, tapering, and the small chamber currently cannot be made fully discrete using one lofted model. Variations of the model of the *koto* can expand on the findings for example in terms of tapering, the position of the small internal resonating chamber, and the arching of the body, by creating variations on these models where the relative placing of these geometric elements is different. A model with the chamber at the dragon's tail end of the body can be the first step in separating these effects. The results from the radiation patterns in the frequency scans will likely also improve with more variations in the heuristic models.

Another area emerging in finite elements studies of musical instruments in general is relevant here. This relates to the modelling of strings. This research used excitation at three points along each string position. The next step in using the same heuristic study would be to excite the models at many more points along each string; doing so would help to clarify the effect of moving the excitation along the instrument's arched top. Future research can also expand on the excitation of the instrument in the addition of strings to the model. More detail in terms of the transfer of energy from the strings to the model can also be incorporated without the addition of strings themselves to the model. Similarly, the addition of the 13 strings and components such as fixed bridges to the lofted model would likely change the response from the body; *paulownia* being a soft and viscoelastic wood, it is likely that new detail will be found

in terms of its resonance under the string tension. Existing work on other stringed instrument groups will be useful for informing this future study.

The performer's interaction with the body of the *koto* is another avenue for future exploration. It is likely that the findings of the performer interaction with the body will further enlighten research on the excitation of the instrument, as it has with existing research. In terms of modelling this interaction, the force and direction applied to the string is a next step for analysis, both for verifying the range of force applied by performers and how changing the amount of force applied to the instrument affects the output sound from the body. Future studies can quantify the absorption of energy by the body before sound is produced. These studies could also be done in tandem with changing the excitation force on the body.

In terms of the three types of studies, a larger range of frequencies (up to 5000Hz) would also prove useful in the study of other zithers. The critical range of the frequency response of instruments is generally considered to be 2000Hz (Giordano 2016). However, the artefacts seen in the transient response and the higher harmonics heard in the sound of the *koto* may be an area of interest with future scans. In addition, to obtain the transient response of the *koto* models, a pulse is input onto the top plate as a way to excite the body. In reality, a plucked string is not just one pulse that is input to the body, but a continuous excitation with diminishing amplitude. In general, more extensive transient studies in future should refine our understanding of the instrument's acoustics.

The methods and heuristic finite element models developed and applied to study of the *koto* have contributed to the understanding of the characteristics of the sound of this instrument. In the future they may contribute to similar studies of other East Asian zithers and other under-studied instruments. Connecting the knowledge thereby gained with existing information from the broader discipline of musicology will help to build the interdisciplinary musical and cultural understanding of the *koto* and other Asian instruments.

Glossary

Chladni patterns

Developed by Ernest Chladni, these patterns are derived from the vibration of objects and show the types of vibration at a specific frequency. At a resonant frequency, the entirety of the object e.g. a plate (nodes), will be moving in-sync, with particular areas of the object remaining stationary. These nodes can be traced by adding a layer of material that shakes into place easily such as grains of sand or salt or glitter. By exciting a plate that has been covered with such a material, the parts that are moving shake the material off and it gathers around the nodal lines. This technique is used by instrument makers to check resonances during the construction process (UNSW, n.d.).

Eigenmode

An eigenmode of a vibrating system is a mode at which the entire system is vibrating sinusoidally. It is the natural mode of vibration for the system. The mode has a phase, frequency and mode shape. The shape of the vibration of the structure at an eigenvalue is its mode shape. These mode shapes are often complex in real-life objects. Simple geometries result in recognisable shapes. Chladni first visualised mode shapes by sprinkling salt and sand on thin plates and exciting them. His work was expanded by Waller, who provided tables and charts of mode shapes for plates of differing shapes. Known types of motion are torsional, bending and longitudinal. Bending modes can be in-plane or transverse. For isotropic materials, Blevins' 1976 book is useful in predicting mode shapes and frequencies.

Eigenfrequency

The frequency of an eigenmode is the eigenfrequency. The eigenfrequencies of the resonating body are observed in the excitation of the instrument and are affected by the

type of excitation and constraints on the object. Eigenfrequencies can be observed with excitation of the body in a physical experiment such as frequency sweep or tapping.

Excitation

The input of energy to the object (model, instrument etc.), in instruments aimed at creating a sound output. Bowing a string, hitting a membrane with a mallet, and striking a bell by causing the motion of a clapper all constitute physical methods for excitation. input of energy to a model by the input of a sine wave is another form of excitation.

Finite element methods

Finite element methods (FEM) are tools for understanding the behaviour of complex objects. In FEM, the complex geometry of an object is broken into small triangles, called elements. These simple geometries are then recombined (meshed) together to make up the main object under study. (Akin 2010, 2).

This process uses elementary physical equations to simulate a complex interaction, such as that of an instrument producing a tone. Due to the number of small parts involved in this method of modelling, it requires a high amount of computation power.

There are five conceptual stages to modelling with the finite element method, which are here summarised as:

1. Drawing
2. Mathematical equations
3. Meshing
4. Solving
5. Post-processing (Zimmermann, 8).

Post processing is defined as the follow-up examination of the output (of a model) for a meaningful interpretation of the results, and to measure the theoretical errors in the study (Zimmermann, 8; Akin, 17).

Fourier analysis

The decomposition of a function (wave) to simple waveforms (sine and cosine trigonometric functions). Fourier transforms in audio analysis are used to find the frequencies present in a sound.

Frequency sweep or frequency scan

A physical or simulated test that measures how much a system (e.g. instrument) responds to a range of frequencies. This method can be used to characterise the frequency response of an acoustical system. It is often for the frequency responses of speakers.

Impulse response

An impulse response is an experiment that measures the response of a system or object to a pulse. If a system shows a peak at a frequency, it resonates at that frequency. These scans are often done with a range of frequencies input to a system with energy. The pulse is often created using a quick excitation such as a tap or balloon pop. The response over a period of time is recorded and decoded to capture frequencies present in the response and how the sound projects and decays. Within a space, this test is done to capture the reverberations within that space.

Physical properties of materials

Materials that show equal stiffness in all directions are considered isotropic and have one value for each property. Materials that show different stiffness in each direction are anisotropic and have a different modulus for each direction. Between isotropy and full anisotropy, many materials show approximate symmetries in stiffness in three dimensions and are classified depending on how many axes of symmetry they have. If there are three planes of symmetry in an anisotropic material, it is referred to as orthotropic. Many woods exhibit orthotropic symmetry at a cellular level and their

physical properties are approximated as orthotropic (Bodig and Jayne 87). Material properties relevant to this study are the following:

1. Poisson's ratio

The ratio of transverse strain to axial strain in the material or the ratio of transverse expansion to axial compression.

2. Shear modulus

The radio of shear stress to shear strain. This modulus in each direction shows how much the material is deformed when pressure is put to it parallel to that direction.

3. Young's modulus

The measure of the stiffness or elasticity of a material.

Sound envelope

For the purpose of this project, the sound envelope of the signal is defined as the duration that starts with the excitation of the physical instrument or model. This sound envelope includes the dynamic envelope and the spectral content. The dynamic envelope shows the changes in the amplitude of the sound over time, and the spectral content, which shows the frequencies present. Time-frequency analysis shows an approximation of individual frequency bands and how their amplitude changes over time.

1. Dynamic envelope

The change the amplitude of an audio signal or a sound from the start of displacement of energy to the end of the decay of the sound.

1.1 Attack

In a dynamic envelope of sound, the initial part, where the amplitude of sound starts from minimum (or equilibrium or background noise) to the maximum, is called the attack. This attack is most clear with transient sounds. Plucked notes on an instrument clearly show the attack portion. Psychoacoustically, the attack is significant in the recognition of the source.

1.2 Decay

In audio practices, decay is discussed as the portion of a transient dynamic envelope following the attack, where the amplitude of sound drops to the sustained level. In acoustical studies, and in most vernacular, the decay refers to the trailing off of sound back to equilibrium or background noise, which equates to the tail of the note.

Radiation pattern

The directional patterns of wave propagation observed through the movement of waves in a medium.

Resonance

When an object is excited at an eigenfrequency, the amplitude of the resultant sound is higher than the same excitation at a different frequency. This louder sound is caused by the object amplifying the frequency because of its natural tendency to vibrate at that frequency. Resonance of objects is changed by the geometry, materials and construction process as well as environmental factors.

Bibliography

Abel, Johnathan, John W. Rick, Patty P. Huang, Miriam A. Kolar, Julius O. Smith and John M. Chowning. 2008. 'On the Acoustics of the Underground Galleries of Ancient Chavín de Huántar, Peru' *The Journal of the Acoustical Society of America* 123(5): 3605.

Acoustics and Audio Group at University of Edinburgh. *MusICA Seminars.* http://www.musica.ed.ac.uk/ Accessed 15 May 2019.

Adriaanz, Willem. 1973. *The Kumiuta and Danmono Traditions of Japanese Koto Music.* Los Angeles: University of California Press.

Akin, John Edward. 2010. *Finite Element Analysis Concepts Via SolidWorks.* Singapore: Mainland Press Pte Ltd for World Scientific.

Altman, Douglas and Martin Bland. 1996. Statistics Notes: Comparing Several Groups Using Analysis of Variance' *BMJ* 312. Accessed 31 December 2016. DOI: http://dx.DOI.org/10.1136/bmj.312.7044.1472

Almeida, Giana, Francoise Huber and Patrik Perré. 2014. 'Free Shrinkage of Wood Determined at the Cellular Level using an Environmental Scanning Electron Microscope' *UFRO.*

Anagnost, Susan. 2017. 'Scanning Electron Images of Wood Cubes' N. C. Brown Centre for Ultrastructure studies. https://ncbrownultrastructure.wordpress.com/2017/04/13/scanning-electron-microscope-images-of-wood-cubes/ Accessed 19 July 2018.

Ando, Yoshinori. 1986. 'Acoustics of Sohs ("koto"s)' *Proceedings of the 12th International Congress on Acoustics* 3: K1-5. Toronto.

Aramaki, Mitsuko Henri Baillères, Loïc Brancheriau, Richard Kronland-Martinet and Sølvi Ystad. 2007. 'Sound Quality Assessment of Wood for Xylophone Bars' *The Journal of the Acoustical Society of America* 121: 2407.

Arroabarren, Ixone and Alfonso Carlosena. 2004. 'Vibrato in Singing Voice: The Link Between Source-Filter and Sinusoidal Models' *Journal on Advances in Signal Processing* 7:1-14.

Ashby, Michael F. 1992/2000. *Material Selection in Mechanical Design.* Oxford: Butterworth Heinemann.

AV Info. 'Reverberation Time' http://www.bnoack.com/index.html?http&&&www.bnoack.com/acoustic/RT_meeting rooms.html Accessed 26 August 2019

Avitabile, Peter. 'Experimental Modal Analysis' *Sound and Vision* 2001. January.

Bader, Rolf. 2018. *Springer Handbook of Systematic Musicology*. New York: Springer.

_____. 2018. 'Impact of Internal Damping on Forced Vibrations of Piano Soundboards' *The Journal of the Acoustical Society of America* 143: 1908.

_____. 2013. *Nonlinearities & Synchronization in Musical Acoustics*. Berlin, Heidelberg: Springer-Verlag.

Bader, Rolf, ed. 2009. *Current Research in Systematic Musicology Volume 1: Sound – Perception – Performance.* Heidelberg: Springer.

_____. 2008. 'Modeling of Musical Instruments' *Signal Processing in Acoustics* 419-446. Berlin: Springer-Verlag.

_____. 2006. 'Finite-Element Calculation of a Bass Drum' *The Journal of the Acoustical Society of America* 119: 3290.

_____. 2005. *Computational Mechanics of the Classical Guitar.* Heidelberg: Springer-Verlag.

Bader, Rolf, Christiane Neuhaus and Ulrich Morgenstern eds. 2010. *Concepts, Experiments and Fieldwork: Studies in Systematic Musicology and Ethnomusicology*. Frankfurt am Main: Peter Lang.

Bader, Rolf, Jost Fischer, Malte Münster and Patrick Kontopidis. 2019. 'Metamaterials in Musical Acoustics: a Modified Frame Drum', *The Journal of the Acoustical Society of America* 145 (5): 3086 – 3094.

Beauchamp, James W. 2007. *Analysis, Synthesis and Perception of Musical Sounds.* New York: Springer.

Bécache, Eliane, Antoine Chaigne, Gregoire Derveaux and Patrick Joly. 2005. 'Numerical Simulation of a Guitar' *Computers and Structures* 83: 107-126.

Becker, Judith. 2012. 'Response to 'Consilience Revisited'' *Ethnomusicology* 56 (1): 112-117.

_____. 2009. 'Ethnomusicology and Empiricism in the Twenty-first Century' *Ethnomusicology* 53 (3): 478–501.

_____. 2009. 'Religious Ecstatics, 'Deep Listeners,' and Musical Emotion' *Empirical Musicology Review* 4(2): 49-70.

Bel, Bernard and Bernard Vecchione. 1993. 'Computational Musicology' *Computers and the Humanities* 27: 1-5.

Benade, Arthur H. 1987. 'Musical Acoustics' *Encyclopedia of Physical Science and Technology* 620-649.

Blevins, Robert D. 2001. *Formulas for Natural Frequency and Mode Shape* (reprint ed.). Malabar, FL: Kreiger.

Brown, Judith. C. 1996. 'Frequency Ratios of Spectral Components of Musical Sounds' *The Journal of the Acoustical Society of America* 99 (2): 1210-1218.

Besnainou, Charles, Joel Frelat and Kurijn Buys. 2010. 'A New Concept for String-Instrument Sound Board: The Splitting Board' *Proceedings of the 20th International Symposium on Music Acoustics* Sydney. August.

Bielski, Paweł and Marcin Kujawa. 2017. 'Nonlinear Modelling in Time Domain Numerical Analysis of Stringed Instrument Dynamics' *AIP Conference Proceedings Scientific Session of Applied Mechanics IX* 1822.

Bilbao, Stefan. 2009. *Numerical Sound Synthesis: Finite Difference Schemes and Simulation in Musical Acoustics.* West Sussex: John Wiley and Sons.

_____. 2012. 'Time Domain Simulation and Sound Synthesis for the Snare Drum' *The Journal of the Acoustical Society of America* 131: 914-925.

Bissinger, George. 2008. 'Structural Acoustics of Good and Bad Violins' *The Journal of the Acoustical Society of America* 105: 1942-1950.

Brétos, Jose, Carlos Santamaría and J. Alonso Moral. 1999. 'Vibrational Patterns and Frequency Responses of the Free Plates and Box of a Violin Obtained by Finite Element Analysis' *The Journal of the Acoustical Society of America* 124: 1764-1773.

Braasch, Jonas. 2018. 'Convolution, Fourier Analysis, Cross-Correlation and Their Interrelationship' *Springer Handbook of Systematic Musicology*, edited by Rolf Bader. New York: Springer 273-284.

Broughton, S. Allen and Kurt Bryan. 2009. *Discrete Fourier Analysis and Wavelets: Applications to Signal and Image Processing.* Hoboken NJ: Wiley & Sons.

Bucur, Voichita. 2016. *Handbook of Materials for String Musical Instruments*. Basel: Springer.

_____. 2006. *Acoustics of Wood*. Berlin: Springer.

Burgess, John C. 2008. 'The FFT and Tone Identification' *Handbook of Signal Processing in Acoustics*, edited by David Havelock, Sonoko Kuwano, Michael Varländer. New York:

Springer 53-64.
Candy, James V. 2006. *Model-Based Signal Processing*. New York: Wiley-IEEE Press.
Campbell, Murray. N.d. 'Timbre' *Oxford Music Online.* Accessed 21 November 2016. http://www.oxfordmusiconline.com/subscriber/article/grove/music/27973
Cantrell, Cherise, Joshua Vawdrey, Jeffrey O'Flynn and Bonnie Andersen. 2018. 'Comparing Clarinet Grunt and Squeak Notes to Transitions in Coupled Oscillators' *The Journal of the Acoustical Society of America* 143: 1908.
Campbell, Murray. N.d. 'Timbre' *Oxford Music Online.* Accessed 21 November 2016. http://www.oxfordmusiconline.com/subscriber/article/grove/music/27973.
Case, Jade, Lauren Neldner and Thomas Moore. 2019. 'Nonlinear Generation of Sum Frequencies in Sitka Spuce' *The Journal of the Acoustical Society of America* 145: 1709.
Le Carrou, Jean-Loic, Quentin Leclere and Francois Gautier. 2010. 'Some Characteristics of the Concert Harp's Acoustic Radiation' *The Journal of the Acoustical Society of America* 127 (5): 3203-3211.
Chabassier, Juliette, Antoine Chaigne and Patrick Joly. 2013. 'Modeling and Simulation of a Grand Piano' *The Journal of the Acoustical Society of America* 134: 648.
Chaigne, Antoine. 2002. 'Numerical Simulation of Stringed Instruments – Today's Situation and Trends for the Future' *Catgut Acoustical Society Journal* 4 (5): 12-20.
Chakraborty, Soubhik, Guerino Mazzola, Swarima Tewari and Noujhuri Patra. 2014. 'The Role of Statistics in Computational Musicology' *Computational Musicology in Hindustani Music*. New York: Springer 15-24.
Chatzionannou, Vasilis. 2019. 'Reconstruction of an Early Viola da Gamba Informed by Physical Modeling' *The Journal of the Acoustical Society of America* 145 (6): 3435-3442.
Cheng, Bing, Yang Zhang, Keita Tanaka, Robert S. Schlauch and Toshiaki Imada. 2018. 'Neural Coding of Perceptual Temporal Asymmetry for Sounds with Rising vs. Falling Intensity Envelopes in Non-Attentive and Attentive Listening Conditions' *The Journal of the Acoustical Society of America* 143: 1746.
Chowning, John. 1980. 'Computer Synthesis of the Singing Voice' *Sound Generation in Wind, Strings, Computers* 4-13. Stockholm: Royal Swedish Academy of Music.
Clark, Grace A. 2016. 'Smart People Behaving Foolishly: Lessons from a Career in Scientific Research' *Acoustics Today* Fall: 22-30.
Clough, Peter and Cathy Nutbrown. 2002. *A Student's Guide to Methodology.* London: Sage Publications.
Clynes, Manfred. 1995. 'Microstructural Musical Linguistics: Composer's Pulses are Liked Most by the Musicians' *Cognition* 55: 269-310.
Coaldrake, Kimi. 2019. 'Finite Element Modelling of the *Koto*: Problems and Some Solutions' *Proceedings of the 23rd International Congress on Acoustics*. Aachen, September. 7549-7556.
_____. 2018. 'Construction and Validation of a High Resolution Finite Element Model of the *Koto*' *The Journal of the Acoustical Society of America* 144: 1891.
_____. 2015. 'Construction of a Finite Element Model of the Japanese *koto* and its Comparison with the Reference Instrument' *The Journal of the Acoustical Society of America* 138: 1937.
_____. 2012a. 'Towards a New Method for the Evaluation of the Tonal Colouring of the Japanese *Koto* using COMSOL Multiphysics' *Proceedings of COMSOL 2012.*
_____. 2012b. 'Simulation Schema in COMSOL', unpublished.
_____. 2012c. 'Extending the Musical Understanding of Timbre in the Japanese *Koto*

through COMSOL Multiphysics Simulation' *Proceedings of COMSOL 2012*.Tokyo.
Coaldrake, Kimi and Iran Sanadzadeh. 2019. 'Timbral Analysis' *The SAGE International Encyclopedia of Music and Culture* edited by Janet Sturman 2191-2192.Thousand Oaks, CA: SAGE Publications. DOI: http://dx.doi.org/10.4135/9781483317731.n729.
Cogan, Robert.1984. *New Images of Musical Sound.* Cambridge, MA: Harvard University Press.
Cogan, Robert and Pozzi Escot. 1976. *Sonic Design: The Nature of Sound and Music.* Englewood Cliffs, NJ: Prentice-Hall Press.
Cottingham, James P. 2019. 'Initial Transients in Free Reed Instruments: A Survey of Experimental Results' *The Journal of the Acoustical Society of America* 145: 1676.
COMSOL. 2016a. 'The Company' Accessed 27 May 3016. https://www.comsol.com/company
COMSOL. 2016b. *Introduction to COMSOL Multiphysics Version 5.2a.*
COMSOL. N.d. *Introduction to LiveLink for Excel in 18 Minutes.* Accessed 10 May 2019 https://www.comsol.com/video/the-basics-of-livelink-for-excel-with-comsol-in-18-minutes
Cook, Perry. 2014. 'Computer Music' *Springer Handbook of Acoustics* 747-778*.* Berlin, Heidelberg: Springer-Verlag.
Cremer, Lothar. 1984. *The Physics of the Violin.* Cambridge, MA: MIT Press.
Coutinho, Eduardo, Marcelo Gimenes, Joao M. Martins and Eduardo Reck Miranda. 2005. 'Computational Musicology: An Artificial Life Approach' *Proceedings of the Portugese Conference on Progress in Artificial Intelligence* 85-93. Covilha.
Daltrop, Shira, Andrzej Kotlicki and Chris Waltham. 2010. 'Vibro-Acoustic Characteristics of an Aoyama Amphion Concert Harp' *The Journal of the Acoustical Society of America* 128 (1): 466-473.
Dawe, Kevin. 2002. 'The Cultural Study of Musical Instruments' *The Cultural Study of Music,* edited by Martin Clayton, Trevor Herbert and Richard Middleton 195-205. New York and London: Routledge.
Delprat, N., P. Guilleman and R. Kronland-Martinet. 1990. 'Parameter Estimation for Non-linear Resynthesis Methods with the Help of a Time-Frequency Analysis of Natural Sounds' *Proceedings of the 1990 International Computer Music Conference* 88-90. Glasgow.
Datta A., Solanki S., Sengupta R., Chakraborty S., Mahto K., Patranabis A. 2017. 'Signal Analysis of Hindustani Classical Music' *Signals and Communication Technology.* Singapore: Springer.
De Poli, Giovanni, Aldo Piccialli and Curtis Roads, eds. 1991. *Representations of Musical Signals.* Cambridge, MA: MIT Press.
Dolan, Emily. 2013. 'The Idea of Timbre' *The Orchestral Revolution: Haydn and the Technologies of Timbre.* Cambridge: Cambridge University Press 53-89.
Dubnov, Shlomo and Xavier Rodet. 2003. 'Investigation of Phase Coupling Phenomena in Sustained Portion of Musical Instruments Sound' *The Journal of the Acoustical Society of America* 113 (1): 348-359.
Dunlop, J. I. 1989. 'The Acoustics Properties of Wood in Relation to Stringed Musical Instruments' *Acoustics Australia* 17(2): 37-40.
Ege, Kerem and Xavier Boutillon. 2010. 'Synthetic Description of the Piano Soundboard Mechanical Mobility' *Proceedings of the 20th International Symposium on Music Acoustics* Sydney. August.

Elejabarrieta, María Jesús, Amaya Ezcurra and Carlos Santamaria. 2002. 'Coupled Modes of the Resonance Box of the Guitar' *The Journal of the Acoustical Society of America*. 111 (2): 2283–2292.

Elie, Benjamin, François Gautier and Bertrand David. 2012. 'Macro Parameters Describing the Mechanical Behavior of Classical Guitars' *The Journal of the Acoustical Society of America* 132: 4013.

Elster, John. 1989. *Nuts and Bolts for the Social Sciences.* New York: Cambridge University Press.

Emmerson, Simon and Denis Smalley. 2016. 'Electro-Acoustic Music' *Grove Music Online*. *Oxford Music Online*. Accessed 10 August 2016. http://www.oxfordmusiconline.com/subscriber/article/grove/music/08695

Evens, Aden. 2005. 'Fourier Analysis and Other Techniques' *Music, Machines and Experience.* Minneapolis: University of Minnesota Press.

Explorable.com n.d. *ANOVA.* Accessed 10 May 2019 https://explorable.com/anova

Ewins, D.J. 1986. *Modal Testing: theory and practice*. Research Studies Press LTD.

Fales, Cornelia. 2002. 'The Paradox of Timbre' *Ethnomusicology* 46 (1):56-95.

Faraci, Philip P., John A. Case, Jillian M. Farrell, Eoin A. King and Robert Celmer. 2018. 'Dynamic Characterization of Grand and Upright Piano Action' *The Journal of the Acoustical Society of America* 144: 1753.

Feng. S. -Y. 1984. 'Some Acoustical Measurements on the Chinese Musical Instrument P'iP'a' *Journal of the Acoustical Society of America* 7: 599-602.

Ferrer, Rafael and Tuomas Eerola. 2011. 'Semantic Structures of Timbre Emerging from Social and Acoustic Descriptions of Music' *EURASIP Journal on Audio, Speech and Music Processing* 11. Accessed 1 August 2015. http://asmp.eurasipjournals.com/content/2011/1/11

Fischer, Jost L. and Rolf Bader. 2018. 'Switch of Synchronization States of Aeroacoustical Coupled Organ Pipes' *The Journal of the Acoustical Society of America* 143: 1908.

Fletcher, Neville H. 2010. 'Inverse Problems in Musical Acoustics' *Proceedings of the 20th International Congress on Acoustics*. Sydney.

_____. 1998. 'Nonlinearity, Complexity and the Sounds of Musical Instruments' *The Journal of the Acoustical Society of America* 103(5): 3603.

Fletcher, Neville H. and Thomas D. Rossing. 1991/1998. *The Physics of Musical Instruments.* New York: Springer-Verlag.

Fletcher, Neville H., William J. Strong and R. K. Silk. 1982. 'Acoustical Characterisation of Flute Head Joints' *The Journal of the Acoustical Society of America* 71(1): 1255–1260.

Florenz, Jean-Loup and Claude Cadoz. 1991. 'The Physical Model: Modeling and Simulating the Instrumental Universe'. *Representations of Musical Signals*, edited by Giovanni De Poli, Aldo Piccialli and Curtis Roads. Cambridge, MA: MIT Press.

Fox, John and Sanford Weisberg. 2011. *Companion to Applied Regression.* Los Angeles: SAGE Publication.

French, Mark. 2007. 'Structural Modification of Stringed Instruments' *Mechanical Systems and Signal Processing* 21: 98-107.

Fritz, Claudia, Joseph Curtin, Jacques Poitevineau, Palmer Morrel-Samuels and Fan-Chia Tao. 2012. 'Player Preferences among New and Old Violins' *Proceedings of the National Academy of Sciences of the United States of America* 109 (3): 760-63.

Gabriel, Jack D. and Whitney L. Coyle. 2018. 'Studying the Clarinet with an Artificial Mouth: Comparison of Playing Frequencies Between Model and Measurement' *The Journal of*

the Acoustical Society of America 144:1891.
Garnett, Guy E. 1991. 'Music, Signals and Representations: A Survey' *Representations of Musical Signals Representations of Musical Signals,* edited by Giovanni De Poli, Aldo Piccialli and Curtis Roads. 325-370. Cambridge, MA: The MIT Press.
Gardiner, Michael and Joyce Lim. 2014 'The Chromatopes of Noh: An Analysis of Timbral Progressions in the Introductions to Three Plays' *Asian Music* 45 (2): 84-128.
Garfias, Robert. 1975. *Music of a Thousand Autumns: The Togaku Style of Japanese Court Music.* Los Angeles: University of California Press.
Gibson, Lorna and Michael F. Ashby. 1997. *Cellular Solids.* Cambridge: Cambridge University Press.
Giordano, Nicholas. 2019. 'Transients in Wind Instruments Modeled with the Navier-Stokes Equations' *The Journal of the Acoustical Society of America* 145: 1677.
_____. 2018a. 'Some Observations on the Physics of Stringed Instruments' *Springer Handbook of Systematic Musicology*, edited by Rolf Bader. New York: Springer 105-119.
_____. 2018b. 'Physical Modeling of a Conical Lip Reed Instrument' *The Journal of the Acoustical Society of America* 143 (1): 38-50.
_____. 2016. 'Simulation Studies of the Flute' *5th Joint Meeting of the Acoustical Society of America and the Acoustical Society of Japan* 3254.
_____. 2016. *Physics of the Piano.* New York: Routledge.
_____. 1997. 'Simple Model of a Piano Soundboard' *The Journal of the Acoustical Society of America* 102: 1159.
Glottopedia. 2016. 'Analysis by Synthesis' Accessed 27 May 2016. http://www.glottopedia.org/index.php/Analysis-by-synthesis
Godøy, Rolf Inge. 2018. 'Sonic Object Cognition' *Springer Handbook of Systematic Musicology*, edited by Rolf Bader. New York: Springer 761-777.
González-Concepción, Concepción, María Candelaria Gil-Fariña and Celina Pestano-Gabino. 2017. 'The Relationship Between Spanish Economic Variables: Evidence from the Wavelet Techniques' *Proceedings of the Wold Academy of Science, Engineering and Technology Conference* 1956-1956*.* Paris.
Gough, Colin. 2018. 'The violin bridge-island input filter' *The Journal of the Acoustical Society of America*. 143 (1): 1- 12.
_____. 2017. '*Violin acoustics – An introduction and recent developments' MusICA Seminars at the University of Edinburgh.* https://www.musica.ed.ac.uk/archive/2017/colin-gough/
_____. 2016. 'Violin Acoustics' *Acoustics Today* 12 (2): 22-30.
_____. 2015. 'Violin Plate Modes' *The Journal of the Acoustical Society of America*. 137 (1): 139-153.
_____. 2015. 'A Violin Shell Model: Vibrational Modes and Acoustics' *The Journal of the Acoustical Society of America*. 137 (3): 1210-1225.
_____. 2014. 'Musical Acoustics' *Springer Handbook of Acoustics,* edited by Thomas D. 567-701. Berlin: Springer-Verlag.
_____. 2013. 'Vibrational Modes of the Violin Family' *Proceedings of the Stockholm Music Acoustics Conference* 66-74. Stockholm.
_____. 2010. 'Acoustical Cavity Modes of a Traditional La Gruyère Violin' *Proceedings of Meetings on Acoustics (POMA)* 9. Published Online 2015. https://asa.scitation.org/DOI/pdf/10.1121/2.0000043?class=pdf

Gilbert, Jöel. 2017. 'Stepwise Regimes in Elephant Trumpet Calls: Similarities with Brass Instrument Behavior' *The Journal of the Acoustical Society of America* 141: 3724.
Guyader, Jean-Louis. 2006. *Vibrations in Continuous Media.* London: ISTE Ltd.
Hartmann, W.M. 1998. *Signal, Sound, Sensation.* Woodbury, N. Y.: AIP Press.
Havelock et al. 2008. *Handbook of Signal Processing in Acoustics*. Berlin: Springer-Verlag.
Helmholtz, Hermann. 1863/1954. *On The Sensations of Tone as a Physiological Basis for the Theory of Music,* Translated by Alexander J. Ellis. London: Dover.
Hind, Nicky. N.d. 'Physical Modelling Synthesis' *Centre for Computer Research in Music and Acoustics.* Accessed 21 November 2016.
Hirota, T. ed. 1994. *Nihon Koto no Hajime* [*The Beginnings of the Japanese Koto*]. Hiroshima Kenritsu Rekishi Hakubutsukan. Fukuyama, Japan: Āto Insatsu.
Hooke, Robert. 1665/1961. *Micrographia*. New York: Dover.
Hornbostel, Erich M. and Kurt Sachs. 1914/1961. 'Classification of Musical Instruments: Translated from the Original German by Anthony Baines and Klaus P. Wachsmann' *The Galpin Society Journal* 14: 3-29.
Horner, Andrew and James W. Beauchamp. 2008. 'Instrument Modeling and Synthesis' *Handbook of Signal Processing in Acoustics* 357-397.
Hoston, Donald L. 2002. 'Dirac's Equation and the Sea of Negative Energy,' *infinite Energy* 43.
Hutchins, Carleen Maley. 1981. 'The Acoustics of Violin Plates,' *Scientific American* 170-186. October.
_____. 1962. 'The physics of Violins' *Scientific American* 78-93.
_____. N.d. 'New Violin Family' *Oxford Music Online.* Accessed 21 November 2016. http://www.oxfordmusiconline.com/subscriber/article/grove/music/51569
Hutchins, Carleen Maley and Virginia Benade. 1997. *Research Papers in Violin Acoustics* 1975-1993. Woodbury, NY: Acoustical Society of America.
Huron, David 1999. 'Lecture 3. Methodology: The New Empiricism: Systematic Musicology in a Postmodern Age' *The 1999 Ernest Bloch Lectures.* University of California, Berkley Department of Music. Accessed 27 June 2016. http://www.music-cog.ohio-state.edu/Music220/Bloch.lectures/3.Methodology.html
Jansson, Erik. 2009. 'On the Prominence of the Violin Bridge Hill in Notes of Played Music' *Journal of the Violin Society of America* 22(1): 169-176.
Jansson, Erik, N.-E. Molin and H. O. Saldner. 1994. 'On Eigenmodes of the Violin- Electric Holography and Admittance Measurements' *The Journal of the Acoustical Society of America* 95(2): 1100-1105.
Jayne, Benjamin and Jozsef Bodig. 1982. *Mechanics of Wood and Wood Composites.* New York: Van Nostrand Reinhold Company Inc.
Johnson, Henry. 2004. *The Koto: A Traditional Instrument in Contemporary Japan.* Amsterdam: Hotei Publishing.
_____. 1999. 'The Sounds of *Myuzikku:* An Exploration of Concepts and Classifications in Japanese Sound Aesthetics' *Journal of Musicology Research* 18 (4): 291-306.
_____. 1996/1997. 'A '*Koto*' by Any Other Name: Exploring Japanese Systems of Musical Instrument Classification' *Asian Music* 28 (1): 43-59.
_____. 1996a. 'The Koto: Musical Instrument, Material Culture' *Journal of the American Musical Instrument Society* 23: 56-93.
_____. 1996b. 'A Survey of Present-Day Japanese Concepts and Classifications of

Musical Instruments,' *Musicology Australia* 19 (1): 16-39.
_____. 1996c. 'Koto Manufacture: The Instrument, Construction Process and Aesthetic Considerations' *Galpin Society Journal* 49: 38–64.
Kac, Mark. 'Can One Hear the Shape of a Drum?' *American Mathematical Monthly* 73 (4): 1-23.
Kane, Brian. 2014. *Sound Unseen: Acousmatic Sound in Theory and Practice.* New York: Oxford University Press.
Kausel, Wilfried. 2018. 'Vibrations and Waves' *Springer Handbook of Systematic Musicology*, edited by Rolf Bader. New York: Springer 29-47.
Kaymakci, Alperen, Ibrahim Bektas and Bekir Cihad Bal. 2013. 'Some Mechanical Properties of Paulownia (*Paulownia Elongata*) Wood' *Proceedings of the International Caucasian Forestry Symposium* 917-919. October, Artvin.
Kennedy, Hugh. 2007. 'A New Statistical Measure of Signal Similarity' *Conference Proceedings of 2007 Information, Decision and Control* 112 - 117.
Kirk, Thomas, James Cottingham and Eric Sindelar. 2016. 'Modes of Vibration of a Sheng Reed' *5th Joint Meeting of ASA/ASJ* 3143.
Klapuri, Anssi and Manuel Davy eds. 2006. *Signal Processing Methods for Music Transcription.* New York: Springer
Kolar, Miriam. 2018. 'Aechaeoacoustics: Re-Sounding Material Culture,' *Acoustics Today* 14 (4):28-37.
Krishnamurthy, Rohan. 2016. 'Transforming Rhythmscapes' *5th Joint Meeting of ASA/ASJ* 3143. December, Honolulu.
Kronland-Martinet, Richard and Alex Grossmann. 1991. 'Application of Time-Frequency and Time-Scale Methods (Wavelet Transforms) to the Analysis, Synthesis and Transformation of Natural Sounds' *Representations of Musical Signals,* edited by Giovanni De Poli, Aldo Piccialli and Curtis Roads. 45-85. Cambridge, MA: The MIT Press.
Kronland-Martinet, Richard. 1988. 'The Wavelet Transform for Analysis, Synthesis and Processing of Speech and Music Sounds' *Computer Music Journal* 12 (4): 11-20.
Lau, B. A., Rolf Bader, Albrecht Schneider and P. Wriggers. 2010. 'Finite-Element Transient Calculation of a Bell Struck by its Clapper' *Concepts, Experiments and Fieldwork: Studies in Systematic Musicology and Ethnomusicology.* Frankfurt am Main: Peter Lang.
Lawson, Francesca. 2012. 'Consilience Revisited: Musical and Scientific Approaches to Chinese Performance' *Ethnomusicology* 56 (1): 86-111.
Le Carrou, Jean-Loic et al. 2010. 'Vibratory Study of Harp's Soundboxes' *Proceedings of the 20th International Symposium on Music Acoustics* Sydney. August.
Le Carrou, Jean-Loic, Quentin Leclere and Francois Gautier. 2010. 'Some Characteristics of the Concert Harp's Acoustic Radiation' *The Journal of the Acoustical Society of America* 127 (5): 3203-3211.
Leman, Mark, 2008. 'Systematic Musicology at the Crossroads of Modern Music Research'. In *Systematic and Comparative Musicology: Concepts, Methods, Findings* edited by Albrecht Schneider. 89-115.Frankfurt am Main: Peter Lang.
Lerch, Alexander. 2012. *An Introduction to Audio Content Analysis: Applications in Signal Processing and Music Informatics*. Online: John Wiley and Sons.
Levenson, Thomas. 1995. *Measure by Measure: A Musical History of Science.* New York: Touchstone.
Levine, Scott N. And Julius O. Smith III. 2007. 'A Compact and Malleable Sine + Transients +

Noise Model for Sound' in *Analysis, Synthesis and Perception of Musical Sounds,* edited by Beauchamp, J.W. New York: Springer.
Li, Peng and Juhachi Oda. 2007. 'The Flame Retardancy of Paulownia and its Mechanisms' *Journal of Material Science* 42: 8544-8550.
Li, Qi. 2009. 'An Auditory-Based Transform for Audio Signal Processing' *Proceedings of Applications of Signal Processing to Audio and Acoustics.* New Paltz, NY.
Libin, Laurence. 2001. 'Organology' *Oxford Music Online.* Accessed 20 August 2019.
Love, Augustus Edward Hough. 1892. *A Treatise on the Mathematical Theory of Elasticity*. Cambridge: Cambridge University Press.
Lysloff, René and Jim Matson. 1985. 'A New Approach to the Classification of Sound-Producing Instruments' *Ethnomusicology* 29(2): 213-236.
Madisetti, Vijay. 2009. *Digital Signal Processing Fundamentals.* CRC Press.
Maestre, Esteban, Gary Scavone and Julius O. Smith. 2018. 'Efficient Rendering of Saxophone Sound by Modal Synthesis and Wave Scattering' *The Journal of the Acoustical Society of America* 144: 1752.
Malm, William P. 1986. *Six Hidden Views of Japanese Music.*
_____. 1967. *Music Cultures of the Pacific, Near East and Asia.* Englewood Cliffs, N.J.: Prentice-Hall.
_____. 1959. *Japanese Music and Musical Instruments.* Tokyo: C.E. Tuttle Co.
Mansour, Hossein, Alireza Kasaiezadeh, Siamak Arzanpour and Mehdi Behzad. 2009. 'Finite Element Modeling of Setar, a Stringed Musical Instrument' *Proceedings of the ASME 2009 International Mechanical Engineering Congress & Exposition*. IMECE2009-13015. Florida.
Mathworks.n.d. *Measuring Signal Similarities.* Accessed 10 May 2019. https://au.mathworks.com/help/signal/examples/measuring-signal-similarities.html
McAdams, Stephen. 2013. 'Musical Timbre Perception' *The Psychology of Music,* 3rd edition, edited by Diana Deutsch. 35-67. Amsterdam etc.: Elsevier.
McCarty, Willard. 2004. 'Modelling: A Study in Words and Meaning' *A Companion to Digital Humanities*, edited by Susan Schreibman, Ray Siemens and John Unsworth. Malden, MA: Blackwell Publishing.
Merriam-Webster's Learner's Dictionary. 2016. 'Model'. Accessed 26 May 2016. https://www.comsol.com/community/forums/general/thread/30712/
Mofrey, Christofer L. 2001. *Dictionary of Acoustics*. London: Academic Press.
Molin, Nils-Erik. 2002. 'Visualizing Instrument Vibrations and Sound Fields – The State of the Art' *Catgut Acoustical Society Journal* 4 (5): 21-29.
Molin, Nils-Erik and Erik V. Jansson. 1989. 'Transient Wave Propagation in Wooden Plates for Musical Instruments' *The Journal of the Acoustical Society of America* 85: 2179-2184.
Molin, Nils-Erik anders O. Wåhlin and Erik V. Jansson. 1990. 'Transient Wave Response of the Violin Body' *The Journal of the Acoustical Society of America* 88(5):2479-2481.
Moore, Thomas and Whitney L. Coyle. 2019. 'Imaging of Transient and Steady-State Flow in Organ Pipes' *The Journal of the Acoustical Society of America* 145: 1677.
Moore, Thomas, Lauren Neldner and Eric Rokni. 2018. 'Are Phantom Partials Produced in Piano Strings?' *The Journal of the Acoustical Society of America* 144: 1890.
Moore, Thomas and Neville H. Fletcher. 2004. *Principles of Vibration and Sound.* 2nd ed. New York: Springer.
Morse, Janice M. and Linda Nierhaus. 2009. *Mixed Method Design: Principles and Procedures.* Walnut Creek, CA: Left Coast Press.

Navarro, Laurent, Gut Courbebaisse and Jean-Charles Pinoli. 2008. 'Continuous Frequency and Phase Spectrograms: A Study of their 2D and 3D Capabilities and Application to Musical Signal Analysis' *Journal of Zhejiang University SCIENCE A* 9(2):199-206.

Neilson, H. C., G. C. Everstine and Y. F. Wang. 1981. 'Transient Response of a Submerged Fluid-Coupled Double-Walled Shell Structure to a Pressure Pulse' *The Journal of the Acoustical Society of America* 70(6): 1776-1782.

Noreland, Daniel. 2003. 'Numerical Techniques for Acoustic Modelling and Design of Brass Wind Instruments' *Comprehensive Summaries of Uppsala Dissertations from the Faculty of Sciences and Technology* 862. Uppsala: ACTA Universitatis Upsaliensis Uppsala.

Obataya, E. T. Ono and M. Norimoto.2000. 'Vibrational Properties of Wood Along the Grain' *Journal of Material Science* 35: 2993-3001.

Obataya, E. N. Zeniya and K. Endo-Ujie. 2020. 'Effects of Seasoning on the Vibrational Properties of Wood for the Soundboards of String Instruments' *Journal of the Acoustical Society of America* 147-998.

Odaka, A. and Shigeru Yoshikawa. 2006. 'Acoustical Characteristics of Chinese Stringed Instruments and their Asian Relatives' *Journal of the Acoustical Society of America* 120: 3118.

Ohio State University. 2016. *Music Cognition at OSU.* Accessed 21 April 2016. http://www.musiccog.ohio-state.edu/CSM_lab.html

Ono, T. and H. Yano. 1996. 'Traditional Wood for Musical Instruments and the Future' *Journal of the Acoustical Society of America* 122: 568-573.

Oxford English Dictionary. 2016. 'Isotropy' *Oxford English Dictionary.* Accessed 25 August 2016. http://www.oed.com.proxy.library.adelaide.edu.au/view/Entry/100194?redirectedFrom=isotropy&

_____. 2011. 'Acousmatic' *Oxford English Dictionary.* Accessed 29 June 2016. http://www.oed.com/view/Entry/1691?redirectedFrom=%09acousmatic&

_____. 2002. 'Model' *Oxford English Dictionary.* Accessed 11 September 2016.http://www.oed.com/view/Entry/120577?rskey=nGKjvr&result=1&isAdvanced=false

Pantelic, Filip. 2017. 'Improvement of Method for Tone Wood Properties Examination Using the Very Near Field Sound Pressure Scanning for Mode Visualization' *The Journal of the Acoustical Society of America* 141: 3962.

Papadopoulos, Hélène and Matthieu Kowalski. 2013. 'Sparse and Structured Decomposition of Audio Signals on Hybrid Dictionaries Using Musical Priors' *The Journal of the Acoustical Society of America* 134(1): 666-685.

Paté, Arthur, Jean-Loïc Le Carrou and Benoît Fabre. 2014. 'Predicting the Decay Time of Solid Body Electric Guitar Tones' *The Journal of the Acoustical Society of America* 135: 3045.

Patel, Aniruddh D. 2008. *Music, Language and the Brain.* Oxford: Oxford University Press.

Preifle, Florian. 2016. 'Organologic and Acoustic Similarities of the European *Violin* and the Chinese *Erhu*' *5th Joint Meeting of ASA/ASJ* 3143.

Rahne, Torsten, Christine Rasinski and Kerstin Neumann. 2010. 'Measuring Timbre Discrimination with Cross-faded Synthetic Tones' *Journal of Neuroscience Methods*189 (2): 176-179.

Ravina, Enrico. 2010. 'Experimental Approaches on Vibratory and Acoustic Characterization of Harp-Guitars' *Proceedings of the 20th International Symposium on Music Acoustics* Sydney. August.
Baron Rayleigh [John William Strutt]. 2011/1894. *Theory of Sound*, volume 1. London and New York: Macmillan and Co.
Reck, David. 1977. *Music of the Whole Earth.* New York: Charles Scribner's Sons.
Ritchey, Tom. 1991. 'Analysis and Synthesis' *Systems Research* 8 (4): 21-41.
Roads, Curtis. 2001. *Microsound*. Cambridge, MA: MIT Press.
_____. 1995. *Computer Music Tutorial.* Cambridge, MA: MIT Press.
Rodgers, Oliver E. 1988. 'The Effect of the Elements of Wood Stiffness on Violin Plate Vibration' *Journal of the Catgut Acoustical Society* 2d. ser. 1 (5): 13-16.
Rose, Nicholas and Damien Holloway. 2012. 'Finite Element Modeling of Brass Musical Instruments' *Proceedings of Acoustics 2012: Acoustics, Development and Environment,* Fremantle.
Rossing, Thomas D. 2010. *Science of String Instruments.* New York: Springer.
_____. 2007. *Springer Handbook of Acoustics.* New York: Springer.
_____. 2007. *Science of Percussion Instruments.* New York: Springer.
_____. 2007. *Physics of Musical Instruments.* New York: Springer.
_____. 1990. *The Science of Sound*, 2nd ed. Reading, MA: Addison-Wesley Publishing.
Rossing, Thomas and Daniel Russell. 1990. 'Laboratory Observation of Elastic Waves in Solids' *American Journal of Physics* 58 (12): 1153-1162.
Rucz, Péter et al. 2016. 'Time Domain Simulation of a Novel Lingual Organ Pipe Construction' *5th Joint Meeting of ASA/ASJ* 3036.
Sage Journals. 2016. 'Empirical Studies in the Arts' Accessed 19 November 2016. http://www.art.sagepub.com
Sage Journals. 2016. 'Musicae Scientiae' *European Society for the Cognitive Sciences of Music.* http://www.msx.sagepub.com
Seidenburg, Kai. 2019.'Specifying the Perceptual Relevance of Onset Transients for Musical Instrument Identification' *The Journal of the Acoustical Society of America* 145: 1078.
Schneider, Albrecht. 2018. 'Systematic Musicology: A Historical Interdisciplinary Perspective' *Springer Handbook of Systematic Musicology* 1-24. Berlin, Heidelberg: Springer.
Schneider, Albrecht and Arne von Ruschkowski, eds. 2011. *Systematic Musicology: Empirical and Theoretical Methods.* Frankfurt am Main: Peter Lang.
Schneider Albrecht and Robert Mores. 2013. 'Fourier-Time-Transformation (FTT): Analysis of Sound and Auditory Perception' *Sound - Perception - Performance. Current Research in Systematic Musicology* edited by Rolf Bader 1: 299-329. Heidelberg: Springer.
Schrader, Barry. 1982. *Introduction to Electro-Acoustic Music.* Englewood Cliffs, NJ: Prentice-Hall.
Schumacher, Robert T. 1988. 'Compliances of Wood for Violin Top Plates' *The Journal of the Acoustical Society of America* 84: 1223.
Schumacher, Robert T. 1992. 'Analysis of Aperiodicities in Nearly Periodic Waveforms' *The Journal of the Acoustical Society of America* 91 (1): 438-451.
Selfridge-Field, Eleanor, ed. 1997. *Beyond MIDI.* Cambridge, MA: MIT Press.
Serra, Xavier. 1997. 'Musical Sound Modeling with Sinusoids plus Noise' In *Musical Sound Processing,* edited by C. Roads, S. Pope, A. Picialli and G. De Poli.

Shepherd, Micah R. and Stephen a. Hambric. 2016. 'Anticlastic Bending of Rectangular Plates and Inference of Poisson's ratio' *The Journal of the Acoustical Society of America* 139.

Shepherd, Micah R., Stephen A. Hambric and Dennis B. Wess. 2014. 'The Effects of Wood Variability on the Free Vibration of an Acoustic Guitar Top Plate' *The Journal of the Acoustical Society of America* 136 (5).

Slawson, Wayne. 1985. *Sound Color.* London: University of California Press.

Smalley, Denis.1997. 'Spectromorphology: Explaining Sound Shapes' *Organised Sound* 2 (2): 107-126.

_____. 1986. 'Spectro-Morphology and Structuring Processes' In *The Language of Electroacoustic Music*, edited by Simon Emmerson. Houndsmills etc.: Macmillan Press.

Smith, Julius. 2016. 'Physical audio Signal Processing'. *Centre for Computer Research in Music and Acoustics (CCRMA).* Accessed 25 July 2016.https://ccrma.stanford.edu/~jos/pasp/

_____. 2011. *Spectral Audio Signal Processing*. Online Book. Accessed 21 June 2019. https://ccrma.stanford.edu/~jos/sasp/

_____. 2010. 'Virtual Acoustic Musical Instruments: Review and Update'. *Centre for Computer Research in Music and Acoustics (CCRMA).* Accessed 28 April 2016. https://ccrma.stanford.edu/~jos/jnmr/

Smyth, Tamara and Marjan Rouhipour. 2013. 'Saxophone Modelling and System Identification' *Proceedings of Meetings on Acoustics (POMA)* 19.

Smyth, Tamara. 2011. 'Estimating the Clarinet Mouthpiece Reflection from Measurement and the Instrument's Produced Sound' *The Journal of the Acoustical Society of America* 130.

Sonologia. 2016. *Sonologia – Out of Phase: International Conference on Sound Studies.* Accessed June 27, 2016. http://www2.eca.usp.br/sonologia/

Statistics Solutions. 2013. *ANOVA.* Accessed 27 July 2016. http://www.statisticssolutions.com/academic-solutions/resources/directory-of-statistical-analyses/anova/

Tatugi, Tomoyasu and Yoshimasa Tohnai. 2001. 'Acoustical Analysis on the Sawari Tone of the Chikuzen Biwa' *Acoustical Science and Technology* 22(3): 199-207.

Terada, Torahiko. 1907. 'Acoustical Investigation of the Japanese Bamboo Pipe, Syakuhati' *Journal of the College of Science* 21 (10):1-34. Tokyo. Reprinted in *Scientific Papers* (1904-1909), 1(18): 81-85 and 31:211-232. Iwanami Syoten, Tokyo 1939.

_____. 1906. 'On Syakuhati' *Proceedings of the Tokyo Mathematics-Physics Society* 3:83-87.

The Arthur H. Benade Archive. *Writings on Acoustics by Arthur H. Benade.* Accessed 10 May 2019. https://ccrma.stanford.edu/marl/Benade/writings/80s.html

Thacker, Jared W. and Nicholas Giordano. 2019. 'Computational Studies of Flow in Flue Pipes' *The Journal of the Acoustical Society of America* 145: 1677.

Thompson, D'arcy. 1963 *On Growth and Form.* 3rd ed. London: Cambridge University Press.

Thompson, J. M. T. And H. B. Stewart. 1986. *Nonlinear Dynamics and Chaos.* Chichester: John Wiley and Sons.

Tiwari, Senkalp and Anurag Gupta. 2017. 'Effects of Air Loading on the Acoustics of an Indian Musical Drum' *The Journal of the Acoustical Society of America* 141(4): 2611-2621.

TMH: Speech, Music and Hearing. 2016. 'The Music Acoustics Group at KTH' *Speech, Music and Hearing.* Accessed 13 July 2016. http://www.speech.kth.se/music/music_about.html

_____. 2016. 'Publications: Doctoral Dissertations' *Speech, Music and Hearing.* Accessed 25 July 2016. http://www.speech.kth.se/publications/dissertations/

Trévisan, Benjamin, Kerem Ege and Bernard Laulagnet. 2017. 'A Modal Approach to Piano Soundboard Vibroacoustic Behavior' *The Journal of the Acoustical Society of America* 141: 690.

Underwood, Shane. 2017. 'Get to Know COMSOL Multiphysics' *Technics*. Course Material.

University of California, Berkeley. 2016. 'Introduction to Finite Element Modeling' *FEM Notes.* Accessed 26 April 2016.

University of New South Wales. 2016. *Music Acoustics.* Accessed 25 July 2016. http://newt.phys.unsw.edu.au/music/

University of New Sounth Wales. N.d. *Chladni Patterns for Violin Plates*. Accessed 30 October 2012. http://newt.phys.unsw.edu.au/jw/chladni.html

University of Southern California. 2016. '6. Methodology' *Organizing Your Social Sciences Research Paper.* Accessed 25 July 2016. http://libguides.usc.edu/writingguide/methodology

Välimäki, Vesa et al. 2006. 'Discrete Time-Modelling of Musical Instruments' *Reports on Progress in Physics.*

Van Trees, H. L. 1968. *Detection, Estimation and Modulation Theory, Part I: Detection, Estimation and Linear Modulation Theory.* New York: John Wiley and Sons.

Verge, M. P. A. Hirschberg and R. Caussé. 1997. 'Sound Production in recorder-like instruments. II. A simulation model' *The Journal of the Acoustical Society of America* 101(5): 2925-2939.

Wade, Bonnie. 1976. *Tegotomono: Music for the Japanese Koto.* Westport, Conn.: Greenwood Press.

Wainwright, S. A., W. D. Biggs, J. D. Currey and J. M. Gosline.1975. *Mechanical Design in Organisms.* London: Edward Arnold.

Waller, Mary Desireé. 1961. *Chladni Figures – A Study in Symmetry*. London: G. Bell and Sons LTD.

Waltham, Chris. 2015. 'Elastic Moduli of *Paulownia Tomentosa*' Unpublished report, University of British Columbia.

_____. 2014. 'An Acoustical Comparison of East Asian and Western String Instruments' *Proceedings of the International Symposium on Musical Acoustics* 375-380. Le Mans.

_____. 2013. 'String Instrument Measurements' *Proceedings of Meetings on Acoustics* 19. DOI: 10.1121/1.4799438.

_____. 2008. 'Vibrational Characteristics of Harp Soundboards' *The Journal of the Acoustical Society of America* 123 (3): 1774-1780.

Waltham, Chris and Laura Kim. 2018. 'Characterization and Modeling of the Erhu' *The Journal of the Acoustical Society of America* 144: 1753.

Waltham, Chris, Kimi Coaldrake, Evert Koster and Yang Lan. 2017. 'Acoustics of the Qin' *Studies in Musical Acoustics and Psychoacoustics* edited by Albrecht Schneider, volume 4 of *Current Research in Systematic Musicology*. Berlin and Heidelberg: Springer 49-74.

Waltham, Chris, Evert Koster, Nils Smit-Anseeuw and Aaron Zimmer. 2013. 'Acoustic Imaging of String Instrument Soundboxes' *ICA 2013,* Montreal June.

Waltham, Chris, Yang Lan and Evert Koster. 2016 'An Acoustical Study of the Qin' *The Journal of the Acoustical Society of America* 139: 1592-1600.

Waltham, Chris and Shigeru Yoshikawa. 2018. 'Construction of Wooden Musical Instruments' *Springer Handbook of Systematic Musicology*, edited by Rolf Bader. New York: Springer 63-79.
Wang, Chong. 2015. 'Modal Transmission Loss of a Single Leaf Panel: Effects of Inter-Modal Coupling' *The Journal of the Acoustical Society of America* 137: 3514.
Weinreich, Gabriel. 1993. 'Klopsteg Memorial Lecture (August 1992): What Science Knows about Violins – and What it Does Not Know' *American Journal of Physics* 61 (12) 1067-1077.
Wollman, Indiana, John Robert Smith and Joe Wolfe. 2010. 'The Low Down on the Double Bass: Looking for the Effects of Torsional Modes' *Proceedings of the 20th International Symposium on Music Acoustics* Sydney. August.
The Wood Database. 2015. *Paulownia (Paulownia Tomentosa).* Accessed 9 Feb 2016. http://www.wood-database.com/lumber-identification/hardwoods/paulownia
Wojtczak, Magdelena. 2011. 'The Effect of Carrier Level on Tuning in Amplitude Modulation' *The Journal of the Acoustical Society of America* 130 (6):3916-3925.
Yale University Statistics. N.d. *Experimentation.* Accessed 10 May 2019. http://www.stat.yale.edu/Courses/1997-98/101/expdes.htm
Yang, F.2014. 对不同材质古琴 琴体声学特性的有限元分析 (Guqin of Different Materials: Finite Element Analysis of the Acoustic Characteristics of the Qin Body). In Chinese. *Musical Instrument Magazine* 14-20.
Yang, F. 2015. 古琴震动体与共鸣体声学特性研究 (Research into the Vibration and Acoustic Characteristics of the Guqin). In Chinese. Beijing: Central Conservatory of Music Press.
Yoshikawa, Shigeru. 2017. 'Japanese Flutes and Their Musical Acoustic Peculiarities' *Studies in Musical Acoustics and Psychoacoustics* edited by Albrecht Schneider volume 4 of *Current Research in Systematic Musicology*. Berlin and Heidelberg: Springer 1-47.
_____.2010. 'Plucked String Instruments in Asia' *The Science of String Instruments,* edited by Thomas D. Rossing. London and New York: Springer.
_____. 2007. 'Acoustical Classification of Woods for String Instruments' *The Journal of the Acoustical Society of America* 122 (1): 568-573.
Yoshikawa, Shigeru, Masahiro Shinoduka, Takafumi Senda. 2008. 'A Comparison of String Instruments Based on Wood Properties: Biwa vs. Cello' *Acoustical Science and Technology* 29(1):41-50.
Yoshikawa, Shigeru and Chris Waltham. 2014. 'Woods for Wooden Musical Instruments' *Proceedings of the International Symposium on Musical Acoustics*. Le Mans 281- 286.
Youatt Andrew P. 2012. 'Analyzing Edgard Varese's Ionisation Using Digital Spectral Analysis' Ph.D diss. University of Arizona. Accessed 15 August 2016. ProQuest (UMI 1513382).
Young, Robert W. and H. K. Dunn. 1957. 'On the Interpretation of Certain Sound Spectra of Musical Instruments' *The Journal of the Acoustical Society of America* 29: 1070- 1073.
Zhang, Ailin and Jim Woodhouse. 2018. 'Playability of the Wolf Note of the Bowed String Instrument' *The Journal of the Acoustical Society of America* 144(5): 2852-2858.
Zhang, Jing, JIabin, Tian, Na Ta and Zhushi Rao. 2018. 'Transient Response of the Human Ear to Impulsive Stimuli: A Finite Element Analysis' *The Journal of the Acoustical Society of America* 143(5): 2768-2789.
Zheng, Su. 'Musical Instruments' *Garland Encyclopedia of World Music 7: East Asia: China, Japan and Korea.* Edited by Robert C. Provine, Yosihiko Tokumaro and J. Lawrence

Wilzleben. New York and London: Routledge.
Zhu, Wei and M. Victor Wickerhauser. 2013. 'Wavelet Transforms by Nearest Neighbor Lifting' *Excursions in Harmonic Analysis* 2: 173-192.
Zeimer, Tim. 2018. 'Wave Field Synthesis' *Springer Handbook of Systematic Musicology*, edited by Rolf Bader 329-347. New York: Springer.
Zimmermann, William B. J. 2006. *Multiphysics Modelling with Finite Element Methods.* Singapore: World Scientific.
Zivanovic, Miroslav and Johan Schoukens. 2009. 'Time-Variant Harmonic Signal Modeling by Using Polynomial Approximation and Fully Automated Spectral Analysis' *Proceedings of the 17th European Signal Processing Conference* 899-903. Glasgow.

The University of Adelaide

Elder Conservatorium of Music

Faculty of Arts

A Musicological Study of the Japanese *Koto* using Heuristic Finite Element Models

Submitted in fulfilment of the requirements for the degree of

Doctor of Philosophy

Iran Sanadzadeh

November 2019

Volume II: Datasets

The datasets presented in this volume comprise a summary of the core data used in this research. The amount of material necessary for each part of the analysis is large. Therefore, to assist the reader the datasets are presented separately to the discussion. Additionally, this material may be useful for future studies as raw material.

The datasets included in this volume are the resonant modes of the heuristic models, the radiation of these modes and peak frequencies in the plank, box and lofted models, and the materials and analysis of the transient response of the lofted model using 39 excitation points.

These datasets are organised in order of their analysis in the main discussion. Annotations on the dataset are presented to assist the reader in following the discussion using Volume II with access to the core materials of the observations.. The content of the datasets is summarised in Table 1.

Table 1 The datasets in this volume

Dataset	Contents
Dataset 1	A compilation of the radiation patterns at the eigenmodes and peak frequencies of the model of a *koto*-sized plank.
Dataset 2	All eigenfrequencies from the substructures and the models of the *koto* body, along with the graphs comparing the progression of each mode type.
Dataset 3	A compilation of the radiation patterns at the eigenmodes and peak frequencies of the idealised box model.
Dataset 4	A compilation of the radiation patterns at the eigenmodes and peak frequencies of the model lofted model.
Dataset 5	Shows all waveforms from probes in the air cylinders in the transient responses used in this study.
Dataset 6	Includes all waveforms from probes in the internal air chambers of the *koto*'s lofted model in the transient responses used in this study.
Dataset 7	Includes the FFTs of the probe inside the small chamber in all three sets of excitations, showing the range of unresponsive frequencies at the dragon's head, the dragon's tail and the bridge positions.
Dataset 8	Summarises the analysis of the observations of the transient responses, decay analysis and comparison of the results with the parameters of the excitation point.

Dataset 1

The radiation patterns of the plank model

mode freq

101 Hz

199 Hz

mode shape

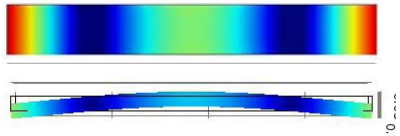

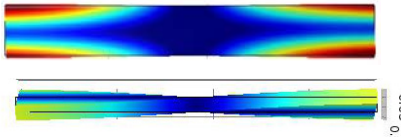

mode pattern

End view

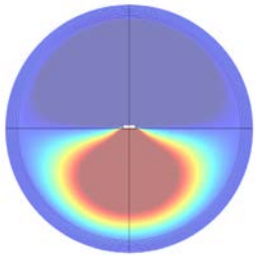

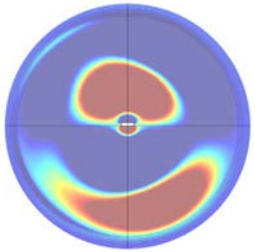

Side view

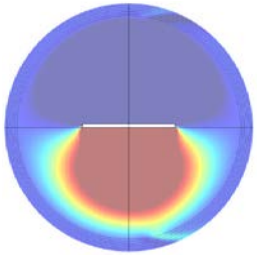

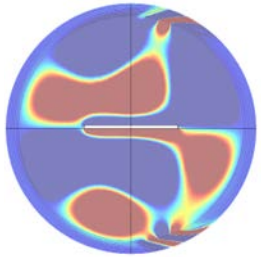

237

Peak freq

77 Hz

111 Hz

153 Hz

186 Hz

231 Hz

Peak shape

Side view

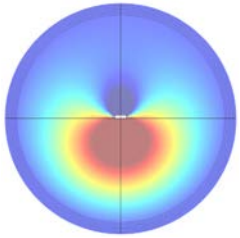

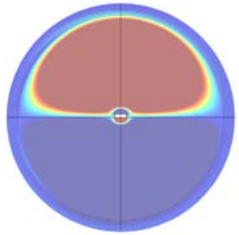

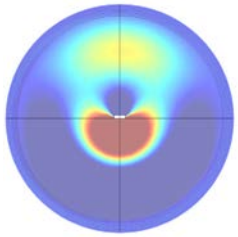

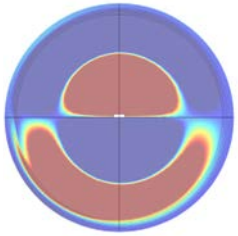

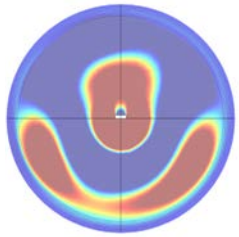

End view

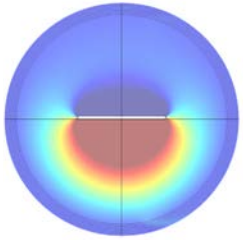

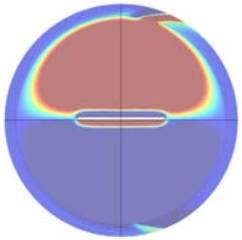

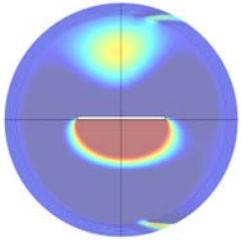

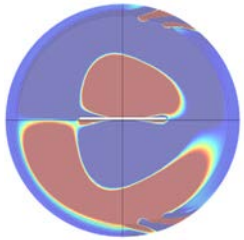

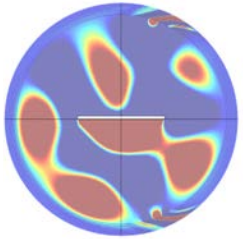

mode shape mode freq

269 Hz

300 Hz

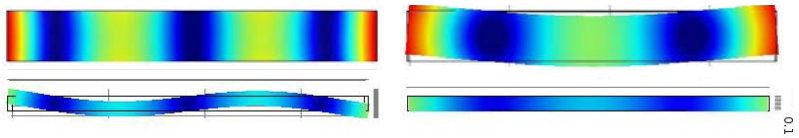

mode pattern

End view

Side view

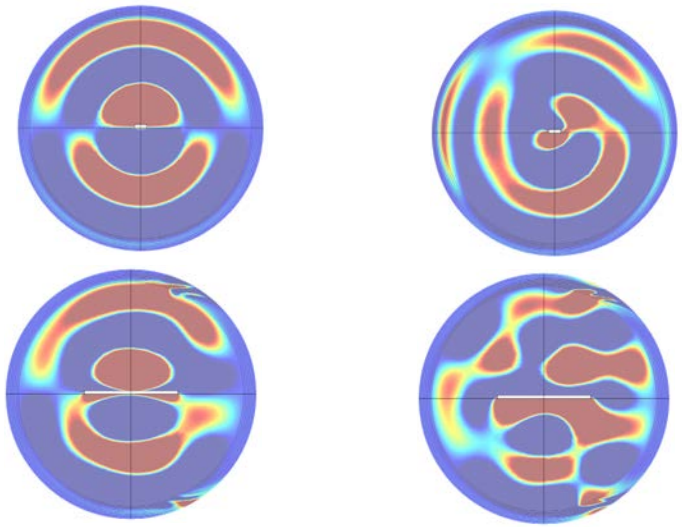

Peak freq

254 Hz

264 Hz

301 Hz

329 Hz

342 Hz

Peak shape

End view

Side view

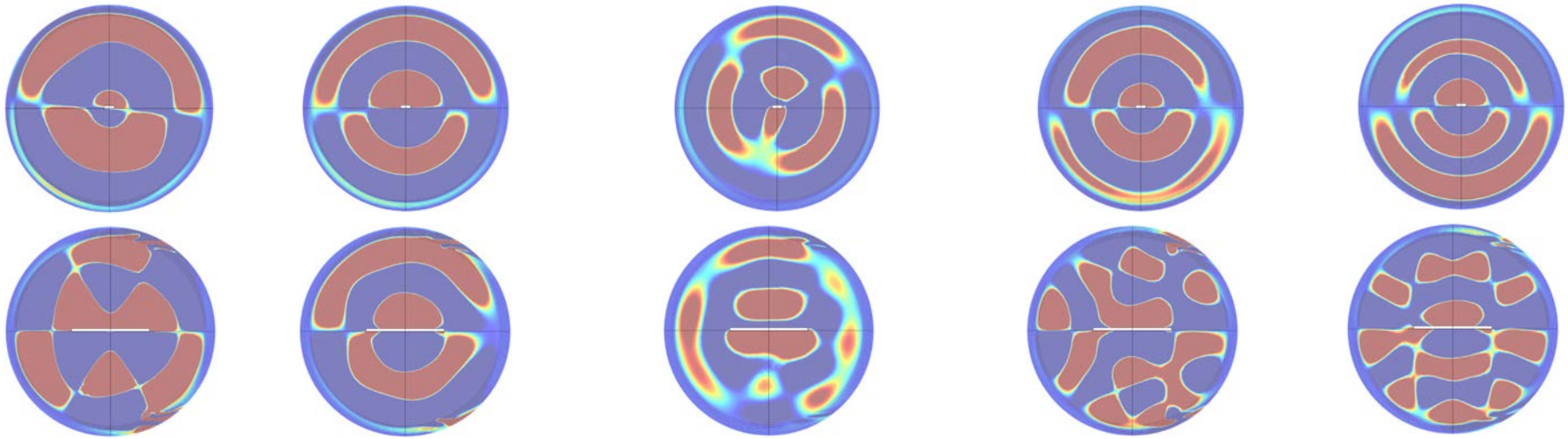

Peaks compared simple plank - frequency scan

mode freq

393 Hz

mode shape

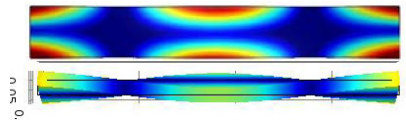

End view

mode pattern

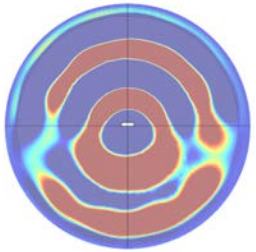

Side view

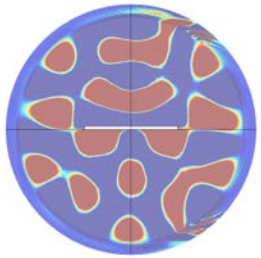

Peak freq

374 Hz | 406 Hz | 415 Hz | 420 Hz | 459 Hz

Side view

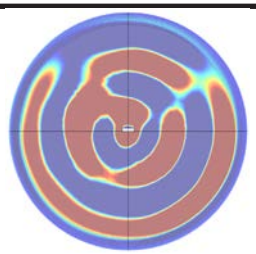

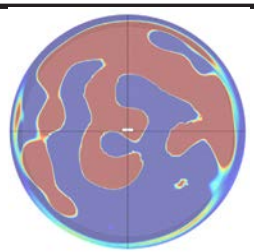

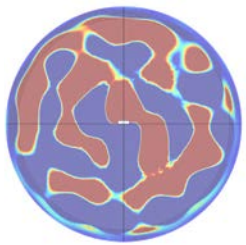

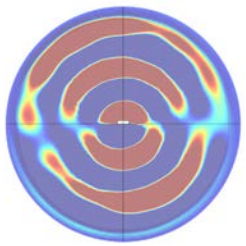

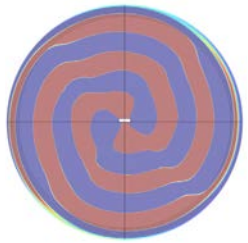

Peak shape

End view

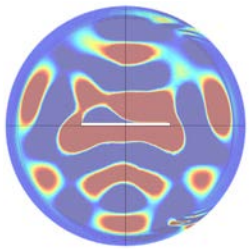

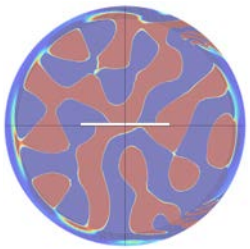

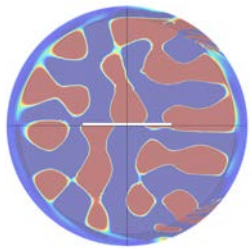

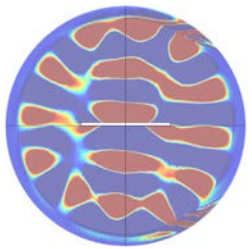

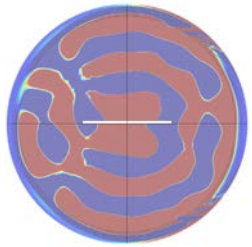

mode shape mode freq

503 Hz

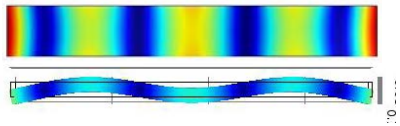

mode pattern

End view

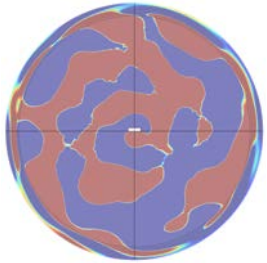

Side view

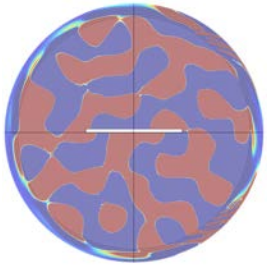

Peak freq

472 Hz | 490 Hz | 510 Hz | 537 Hz | 571 Hz

Peak shape

End view

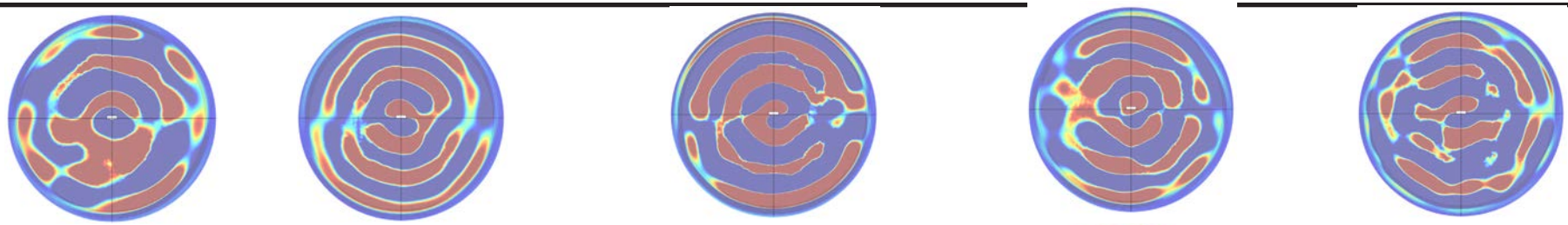

Side view

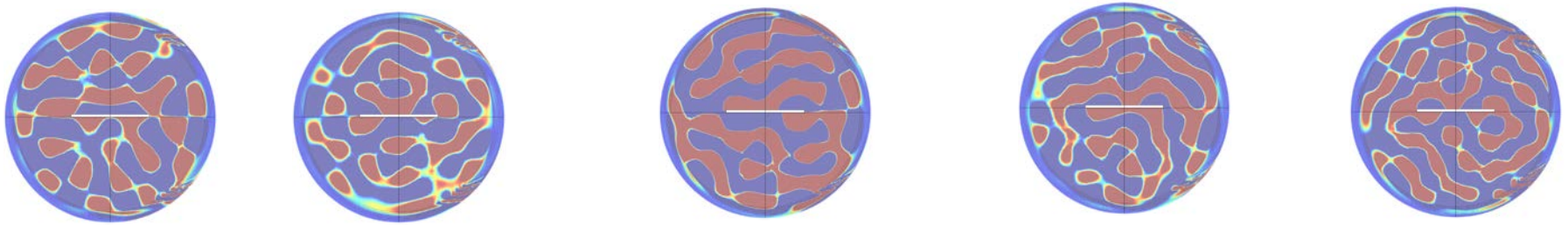

Peaks compared simple plank - frequency scan

mode freq

586 Hz

667 Hz

mode shape

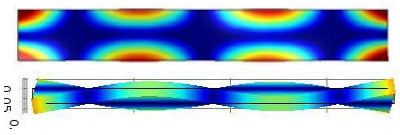

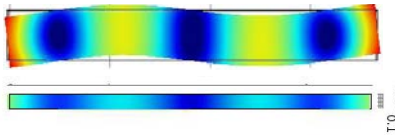

mode pattern

End view

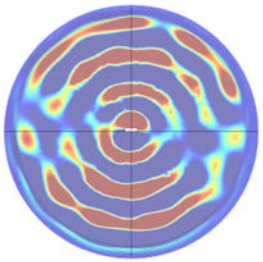

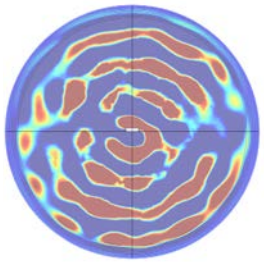

Side view

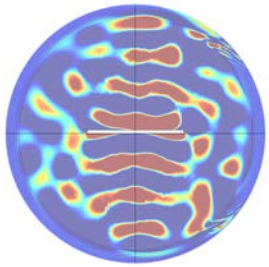

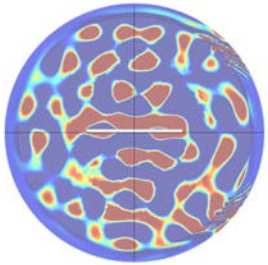

Peak freq

597 Hz

637 Hz

656 Hz

674 Hz

681 Hz

Peak shape

Side view

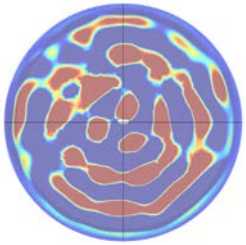

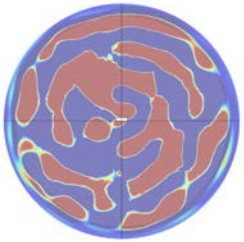

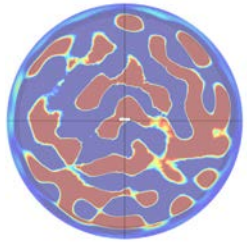

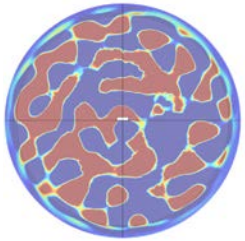

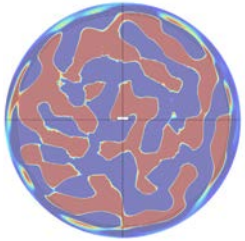

End view

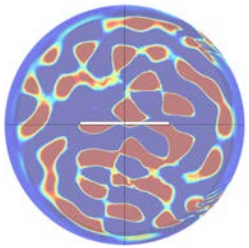

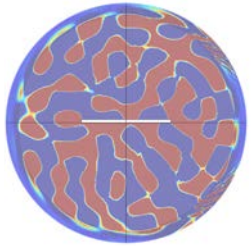

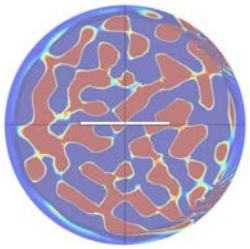

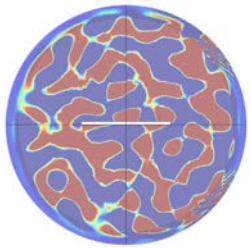

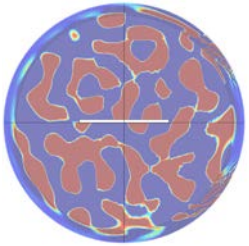

mode shape mode freq

782 Hz

797 Hz

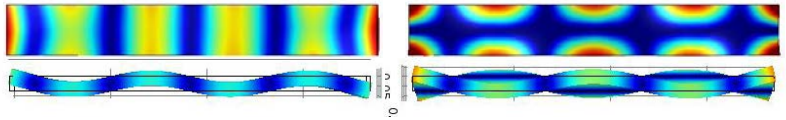

mode pattern

End view

Side view

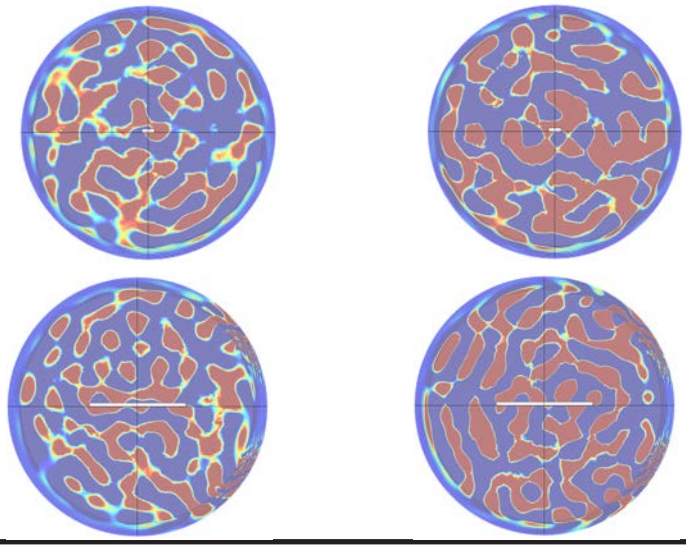

Peak freq

718 Hz

730 Hz

790 Hz

820 Hz

Peak shape

End view

Side view

Peaks compared simple plank - frequency scan

mode freq

969 Hz

995 Hz

mode shape

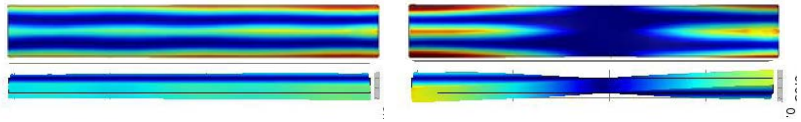

mode pattern

End view

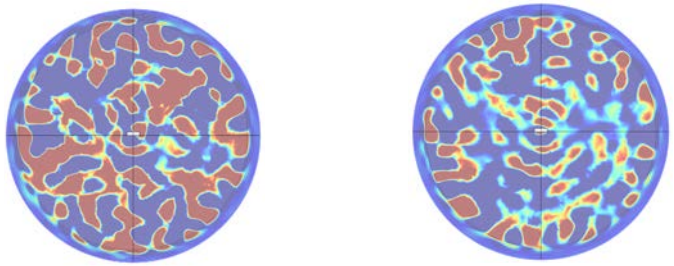

Side view

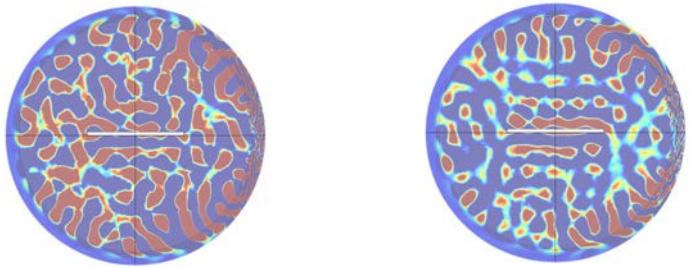

Peak freq

893 Hz

911 Hz

Peak shape

Side view

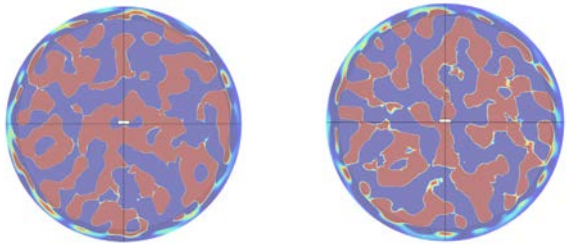

End view

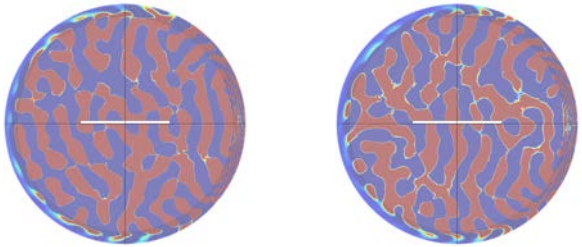

Dataset 2

The eigenmodes of the models of the *koto* and its substructures

BASE PLATE

Frequencies

Mode	(1,1)	(2,1)	(3,1)	(4,1)	(5,1)	(6,1)
Base plate	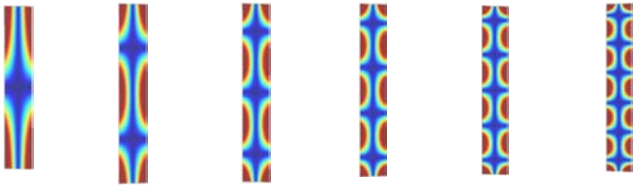					
Flat	32	66	106	153	209	277
sound hole 1 shape	34	68	107	153	210	278
sound hole 2 shape	34	69	108	156	213	281
2 sound holes	34	68	105	151	207	275
1 sound hole (circular)	32	65	102	149	206	274
2 sound holes (circular)	32	64	100	146	204	271

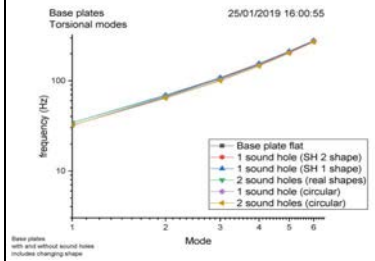

sound holes do not affect the mode frequency; sound hole shape does not affect mode frequency

<< sound holes shape of the first hole
<< sound hole shape of the second hole
<< both sound holes shaped as found on instrument

TOP SHELL

Mode	(1,1)	(2,1)	(3,1)	(4,1)	(5,1)	(6,1)
Top shell	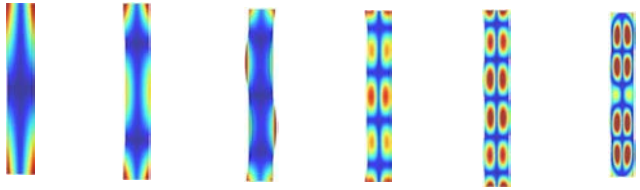					
Flat	26	109	248	439	577	668
Full Arching	44	111	234	543	595	753
Steady arching	28	108	288	455	601	710
Tapered no arching	30	108	249	428	580	586
Taper with steady arch	29	107	291	456	593	
Arched and Taper	45	112	233	375	598	
Arched and taper + ears	45	112	235			

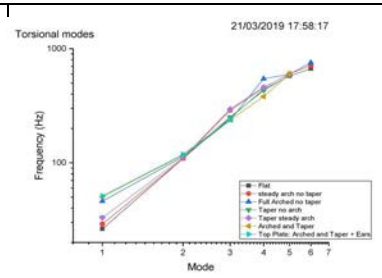

Effect of arching, tapering and ears is not clearly observed with changes in the plates. Modes are harder to identify here.

BOX MODELS

Mode	(1,1)	(2,1)	(3,1)	(4,1)		
Box models	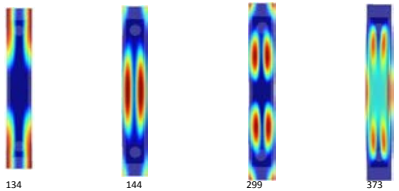				MODE NOT OBSERVED	MODE NOT OBSERVED
0 struts	134	144	299	373		
1 strut	135	157	296	381		
2 struts	135	159	298	384		
3 struts	135	162	298	385		
4 struts	135	164	299	386		

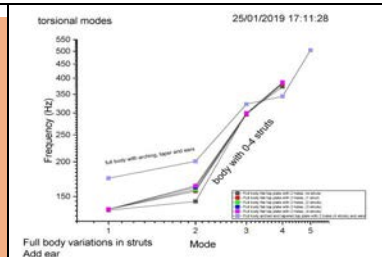

little difference is seen across models with varying struts. Struts are not seen to make a difference in mode frequency. The frequencies of modes slighly lower than in the lofted model.

LOFTED MODEL

Overview Compiled

Mode	(1,1)	(2,1)	(3,1)	(4,1)	(5,1)	
Image XY (includes top and base plate views)	Top View|| Base view	Top View|| Base view	Top View|| Base view	Top View|| Base view	Top View|| Base view	
Full lofted model	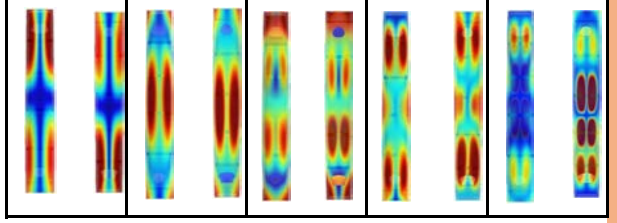					MODE NOT OBSERVED
	175	201	322	344	504	

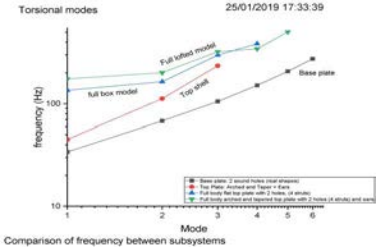

Torsional modes are most affected by the full body being assembled. They are not affected by the modes of the individual plates. Lofted model modes are closest to the body modes.

BASE PLATE

Frequencies

Mode	(0,2)	(1,2)	(2,2)	(3,2)	(4,2)	(5,2)
Base plate	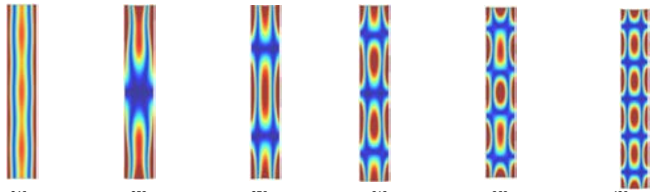					
Flat	246	253	276	313	360	420
sound hole 1 shape	260*		300	331	375	425
sound hole 2 shape	263		301	338		440
2 sound holes	263		297	332	372	415
1 sound hole (circular)	238	249	273	308	351	416
2 sound holes (circular)	237	237	271	305	338	405

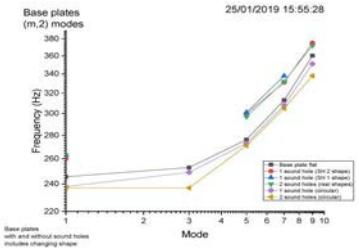

No strong observation of changes with the addition and shaping of holes.
(1,2) modes not identified in models with 'real' hole shapes

TOP SHELL

Mode	(0,2)	(1,2)	(2,2)	(3,2)	(4,2)	(5,2)
Top shell	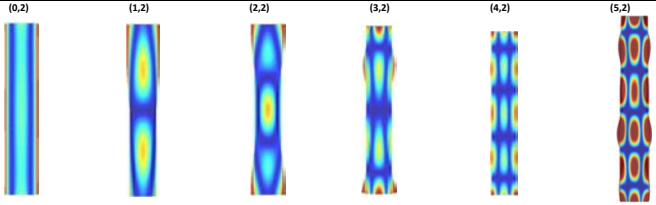					
Flat	139	146	184	428	593	
Full Arching	161	200	232	449	732	
Steady arching	89	101	369	432	609	
Tapered no arching	160	178	203	468	597	885
Taper with steady arch	89	102	--	436	612	
Arched and Taper	161	207	235	674	740	
Arched and taper + ears	159	206	232	645	710	

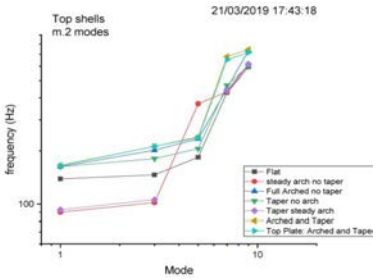

arching and tapering are seen to increase mode frequency

BOX MODELS

Mode					(4,2)	
Box models	MODE NOT OBSERVED	MODE NOT OBSERVED	MODE NOT OBSERVED	MODE NOT OBSERVED	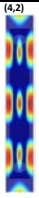	MODE NOT OBSERVED
0 struts					490	
1 strut					505	
2 struts					497	
3 struts					507	
4 struts					509	

Not enough modes seen for comparison

LOFTED MODEL

Overview Compiled

Mode		(1,2)	(1,2) or (2,2)			
Image XY (includes top and base plate views)		Top View|| Base view	Top View|| Base view			
Full lofted model	MODE NOT OBSERVED	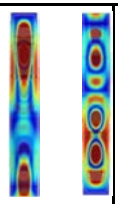	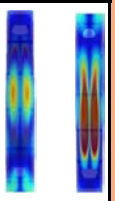	MODE NOT OBSERVED	MODE NOT OBSERVED	MODE NOT OBSERVED
		436	517			

Not enough modes observed for comparison

BASE PLATE

Frequencies

Mode	(2,0)	(3,0)	(4,0)	(5,0)	(6,0)	(7,0)	(8,0)	(9,0)	(10,0)
Base plate	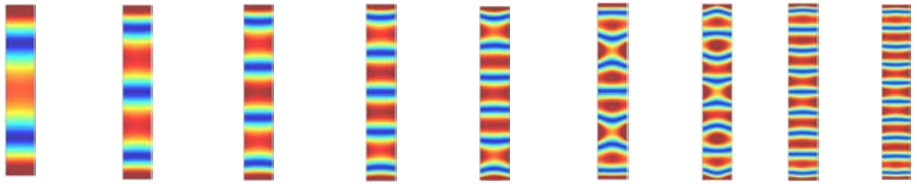								
Flat	15	42	82	136	203	284	377	482	600
sound hole 1 shape	15	41	78	127	191		362	459	549
sound hole 2 shape	15	42	80	131	196			469	573
2 sound holes	16	41	76	123	184		356	456	545
1 sound hole (circular)	15	41	79	130	196	278	363	457	566
2 sound holes (circular)	15	40	75	125	189	273	359*	441	537

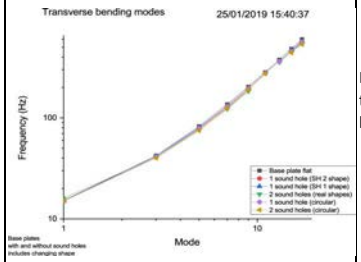

Base plate modes are not affected by sound holes much. In the models with the real sound hole shapes, the 6th bending mode was not observed.

TOP SHELL

Mode	(2,0)	(3,0)	(4,0)	(5,0)	(6,0)	(7,0)	(8,0)	(9,0)	(10,0)
Top shell	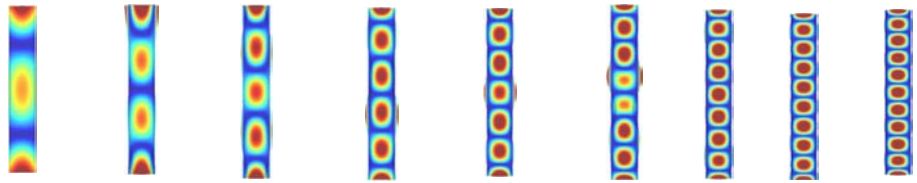								
Flat	86	157	208	258	324	399	490	591	705
Full Arching	104	255	360	431	545	704	816	944	
Steady arching	118	180	246	322	391	524	588	679	770
Tapered no arching	82	157	224	273	345	426	520	629	749
Taper with steady arch	122	180	248	325	495	587	681	772	--
Arched and Taper	104	258	366	476	595	701	874	944	
Arched and taper + ears	104	254	358	428	539/586	644/686	797	924	

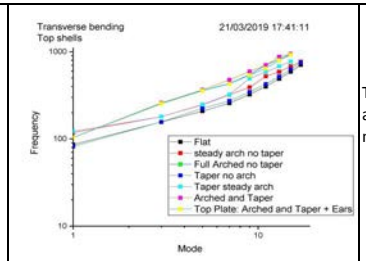

Top shell transverse bending modes increased by the addition of arching, but the amount of arching does not make a real difference.

BOX MODELS

Mode	(2,0)	(3,0)							
Box models	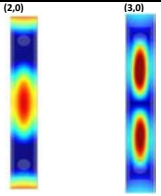		MODE NOT OBSERVED	MODE NOT OBSERVED	MODE NOT OBSERVED	MODE NOT OBSERVED	MODE NOT OBSERVED	MODE NOT OBSERVED	MODE NOT OBSERVED
0 struts	92	not identified							
1 strut	92	219							
2 struts	92	217							
3 struts	92	215							
4 struts	92	214							

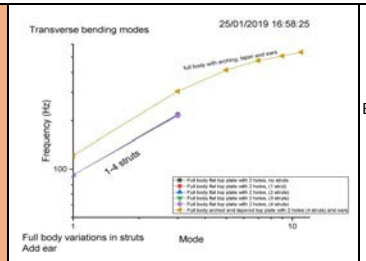

Box models fail to show transverse bending modes clearly

LOFTED MODEL

Mode	(2,0)	(3,0)	(4,0)	(5,0)	(6,0)	(7,0)			
Image XY (includes top and base plate views)	Top View| | Base view	Top View| | Base view	Top View| | Base view	Top View| | Base view	Top View| | Base view	Top View| | Base view			
Full lofted model	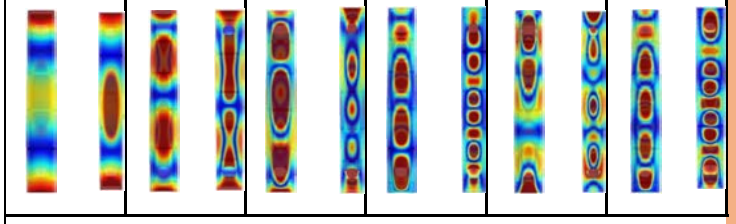						MODE NOT OBSERVED	MODE NOT OBSERVED	MODE NOT OBSERVED
	122	305	414	475	507	536			

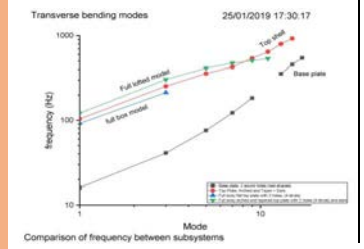

Overview Compiled

transverse bending modes are highly dependent on the arching of the top shell.

BASE PLATE

Mode	(0,3)	(1,3)	(2,3)	(3,3)
Base plate	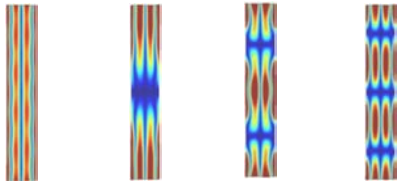			
Flat	626	632	649	681
sound hole 1 shape			710	740
sound hole 2 shape	664		710	741
2 sound holes	666		705	736
1 sound hole (circular)	598	627	645	677
2 sound holes (circular)	598	599	642	673

Frequencies

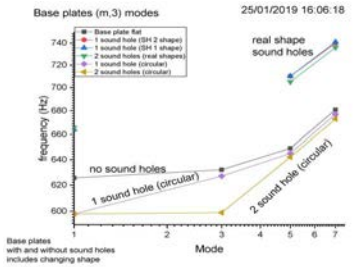

no strong conclusions. Clear changes are difficult to

TOP SHELL

Mode	(0,3)	(1,3)	(2,3)	(3,3)
Top shell	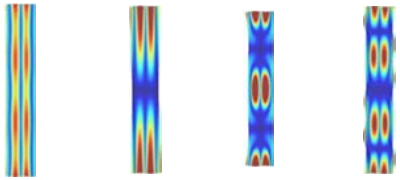			
Flat	656	659	676	706
Full Arching			884	815
Steady arching	626	636	657	692
Tapered no arching	709	730	760	782
Taper with steady arch	622	669		
Arched and Taper				
Arched and taper + ears	850	907		

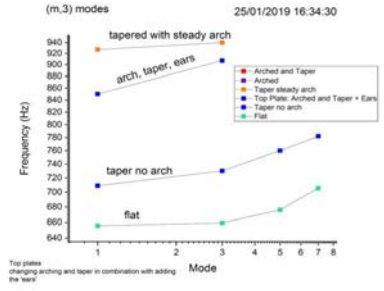

BOX MODELS

Mode				
Box models	MODE NOT OBSERVED	MODE NOT OBSERVED	MODE NOT OBSERVED	MODE NOT OBSERVED
0 struts				
1 strut				
2 struts				
3 struts				
4 struts				

not enough modes are observed across models for strong conclusions

LOFTED MODEL

Mode				
Image XY (includes top and base plate views)				
Full lofted model	MODE NOT OBSERVED	MODE NOT OBSERVED	MODE NOT OBSERVED	MODE NOT OBSERVED

Modes not observed in models of full body clearly.

BASE PLATE

Mode	IPB1	IPB 2
Image XY	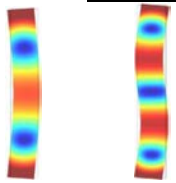	
Flat	313	683
1 sound hole(shaped 2)	297	621
1 sound hole (shaped 1)	298	642
2 sound holes (shaped)	296	603
1 sound hole (circular)	306	646
2 sound holes (circular)	301	613

Frequencies

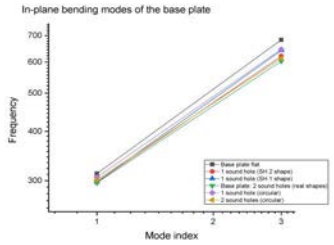

Not enough modes observed for a strong conclusion.

TOP PLATE

Mode	(2,1) and IPB 1 mix	IPB 2
Image XY		
Flat	241	
Full Arching	320	758
Steady arching		
Tapered no arching	282	779
Taper with steady arch	427	
Arched and Taper	330	
Arched and taper + ears	326	767

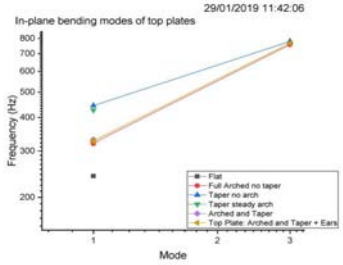

Not enough modes observed for a strong conclusion.

BOX MODELS

Mode	IPB 1	IPB 2
Image XY		
Full body flat top plate with 2 holes, no struts	252	489
Full body flat top plate with 2 holes, (1 strut)	252	494
Full body flat top plate with 2 holes, (2 struts)	252	489
Full body flat top plate with 2 holes, (3 struts)	252	488
Full body flat top plate with 2 holes, (4 struts)	252	487

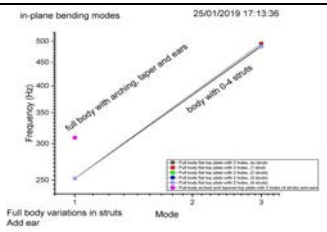

Not enough modes observed for a strong conclusion.

LOFTED MODEL

Mode	IPB 1
Image XY (includes top and base plate views)	Top View | | Base view 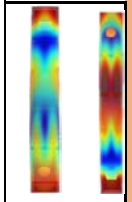
Full body arched and tapered top plate with 2 holes (4 struts) and ears	309

MODE NOT OBSERVED

Not enough modes observed for a strong conclusion.

Dataset 3

The radiation patterns of the idealised box model

mode freq

91 Hz

135 Hz

164 Hz

mode shape

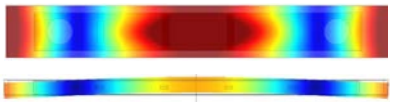

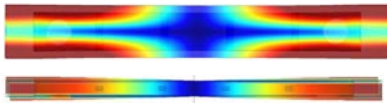

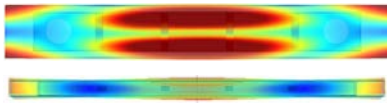

mode pattern

End view

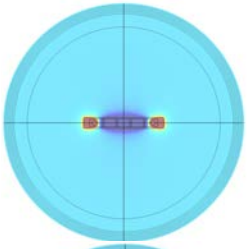

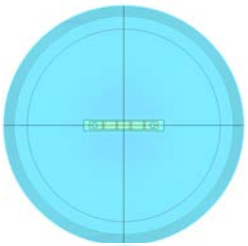

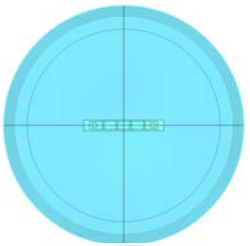

Side view

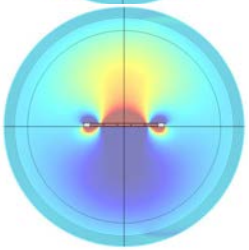

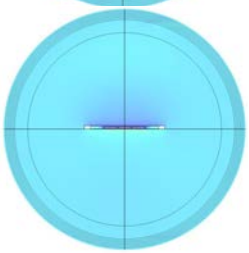

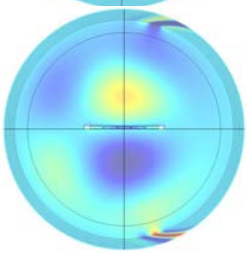

Peak freq

68 Hz

91 Hz

113 Hz

165 Hz

Side view

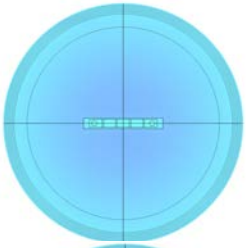

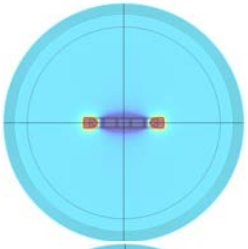

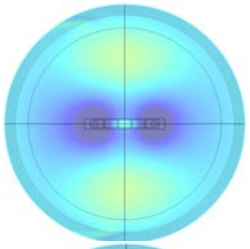

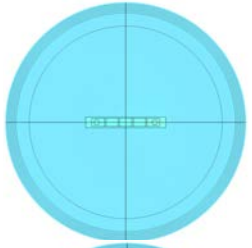

Peak shape

End view

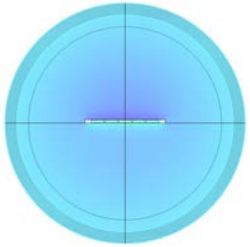

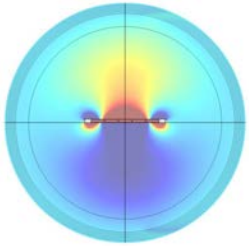

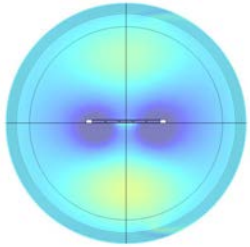

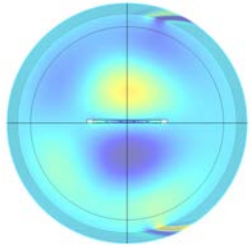

mode freq

213 Hz

251 Hz

mode shape

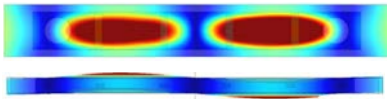

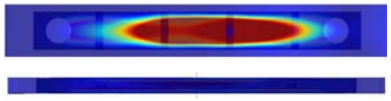

End view

mode pattern

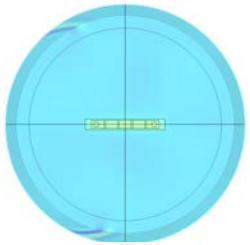

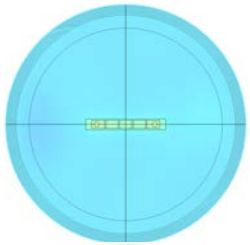

Side view

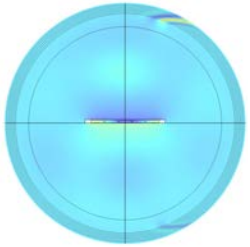

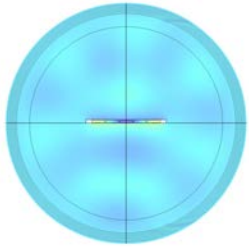

Peak freq

203 Hz

224 Hz

233 Hz

End view

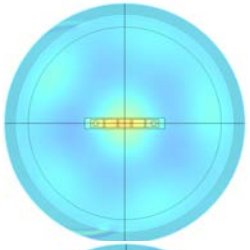

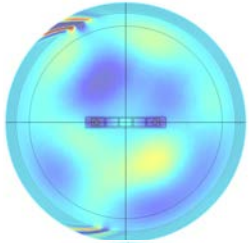

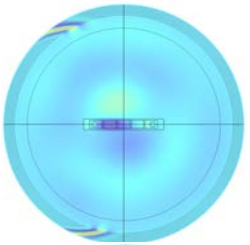

Peak shape

Side view

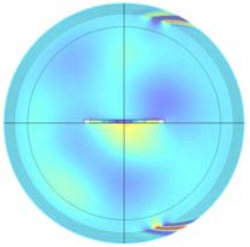

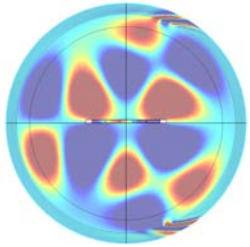

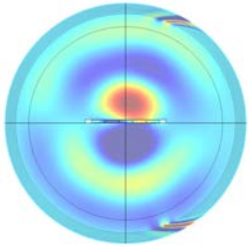

Peaks compared idealised box - frequency scan

mode freq

252 Hz | 254 Hz | 264 Hz | 268 Hz | 280 Hz

mode shape

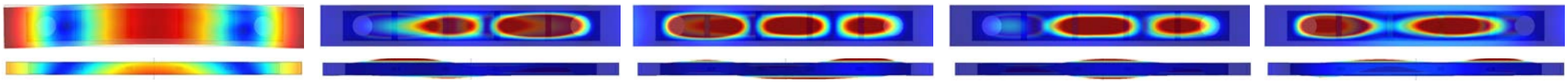

End view

mode pattern

Side view

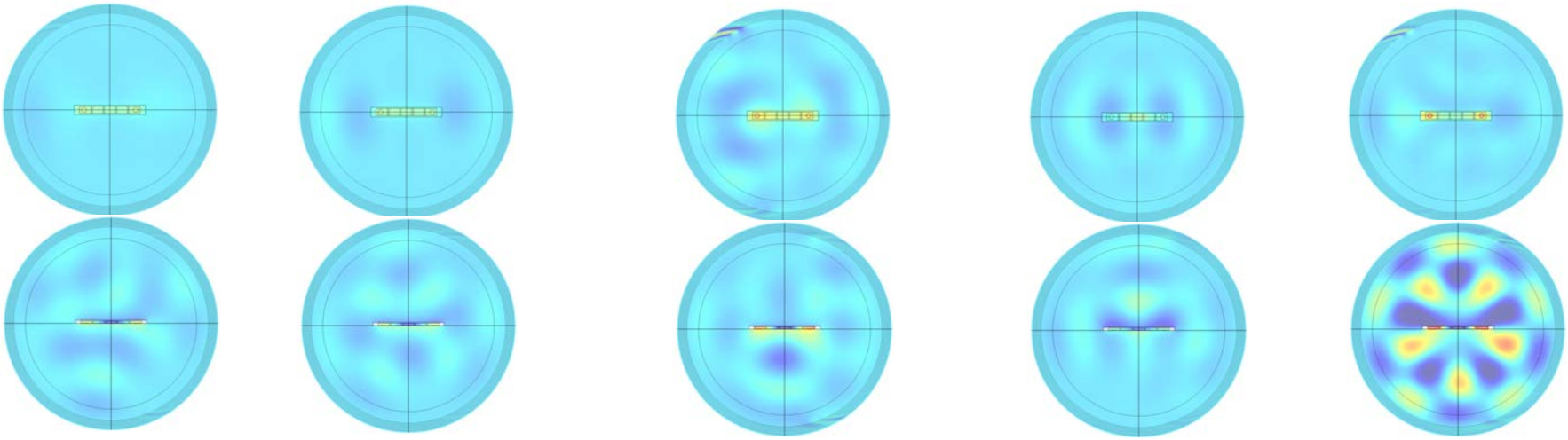

Peak freq

Side view

Peak shape

End view

mode shape mode freq

283 Hz | 288 Hz | 299 Hz | 314 Hz | 323 Hz

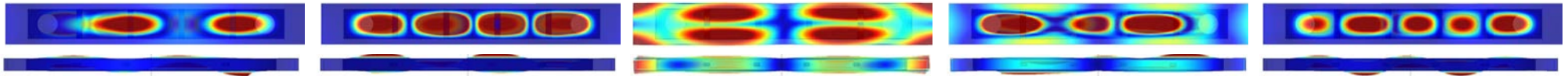

End view

mode pattern

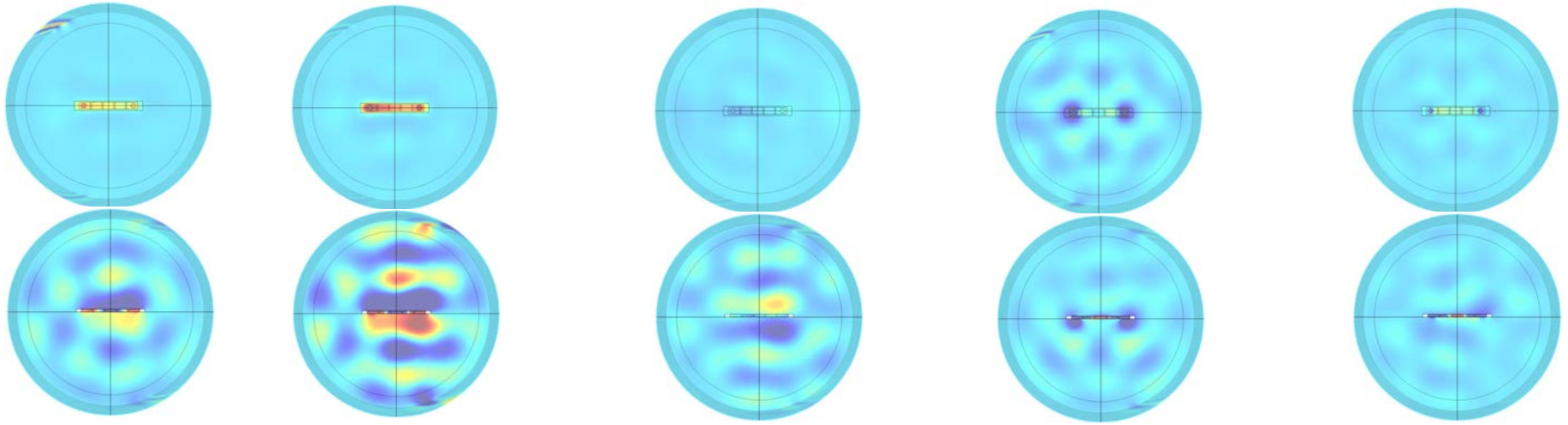

Side view

Peak freq

291 Hz | 300 Hz | 313 Hz

End view

Peak shape

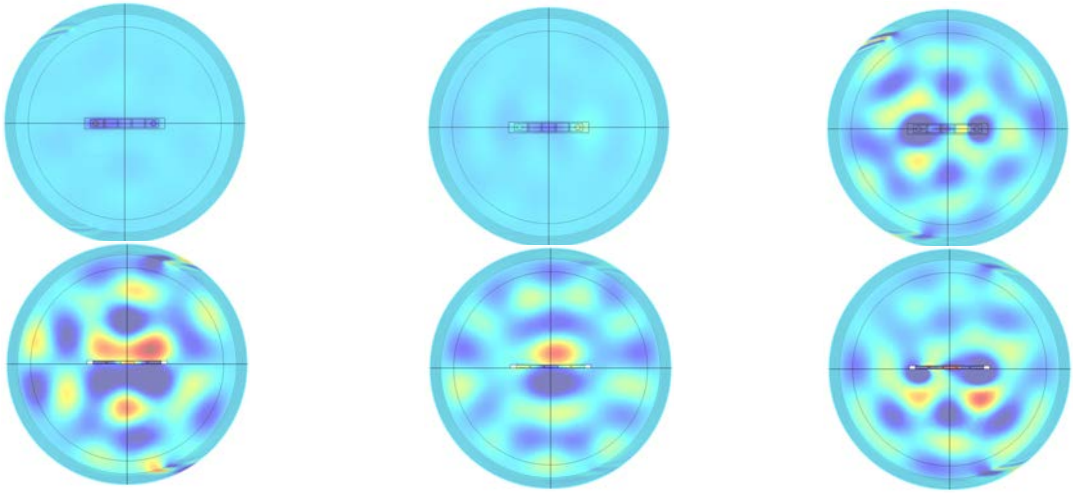

Side view

Peaks compared idealised box - frequency scan

mode freq

328 Hz | 361 Hz | 365 Hz | 386 Hz | 408 Hz

mode shape

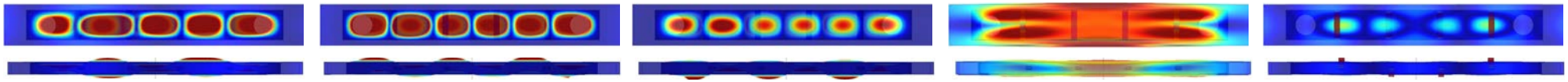

End view

mode pattern

Side view

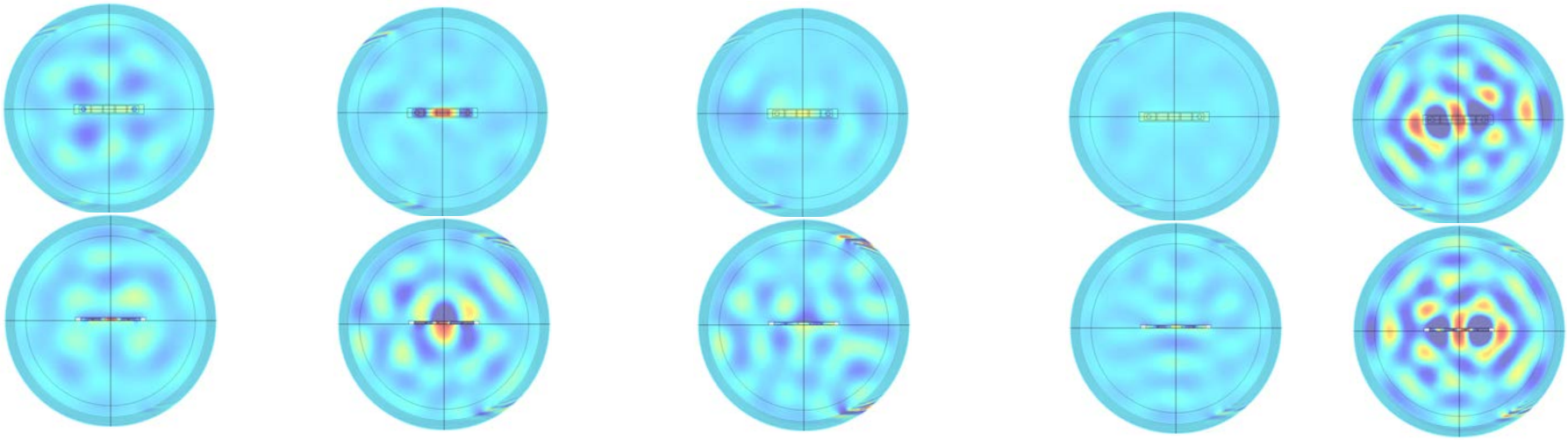

Peak freq

359 Hz | 367 Hz | 406 Hz

Side view

Peak shape

End view

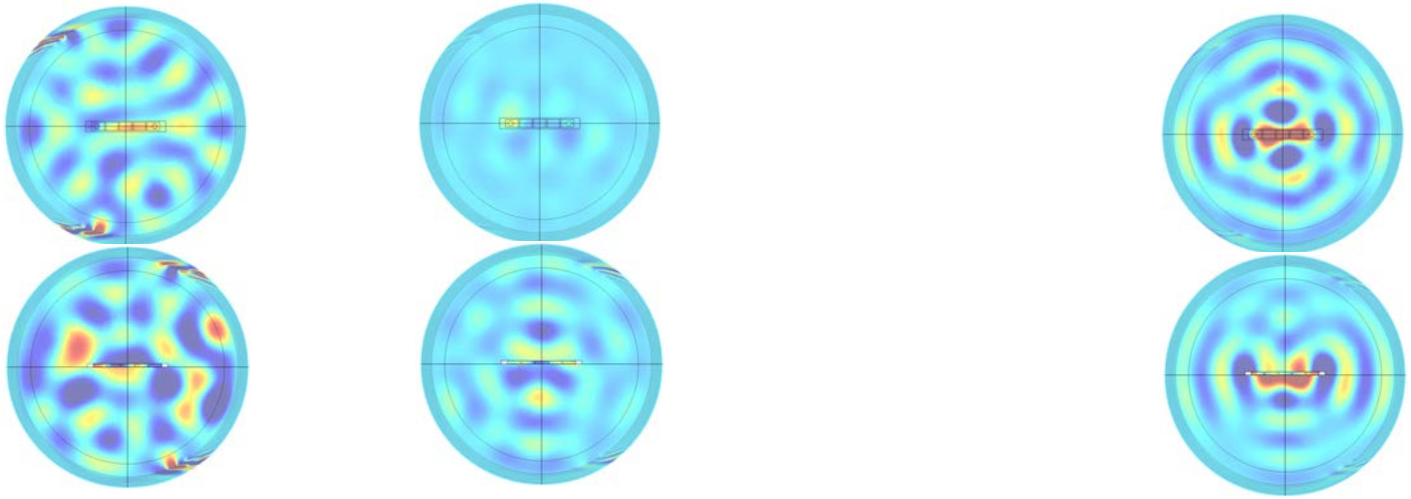

mode shape mode freq

410 Hz | 416 Hz | 421 Hz | 426 Hz | 430 Hz

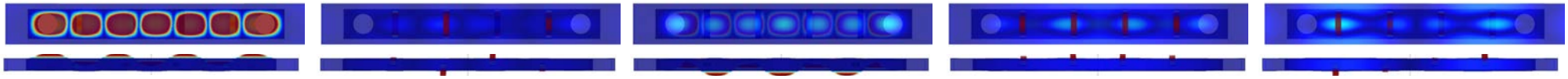

End view

mode pattern

Side view

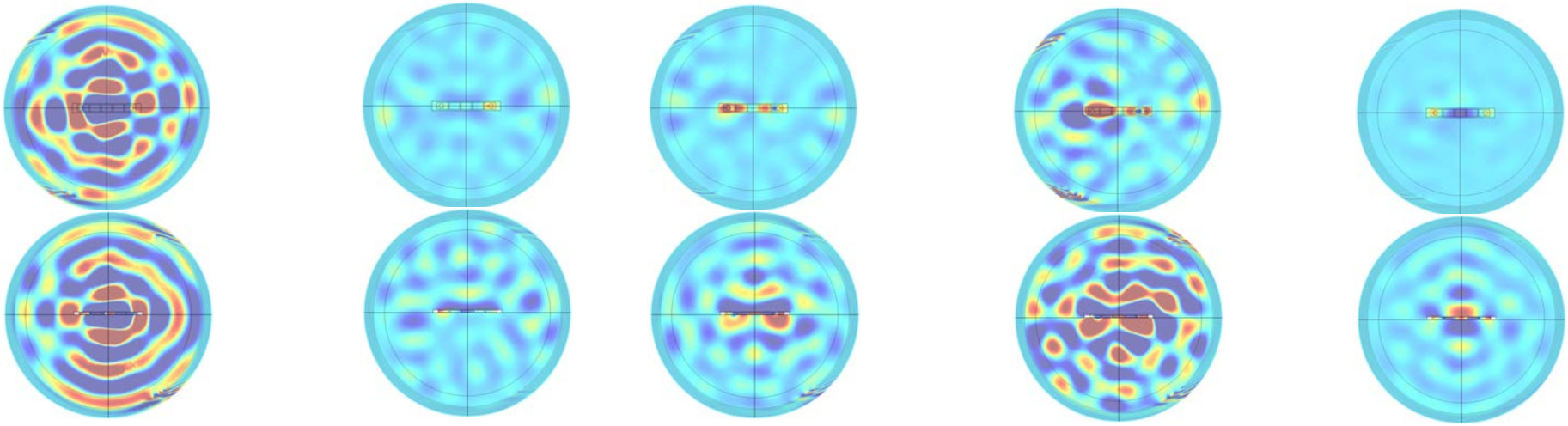

Peak freq

426 Hz | 430 Hz

End view

Peak shape

Side view

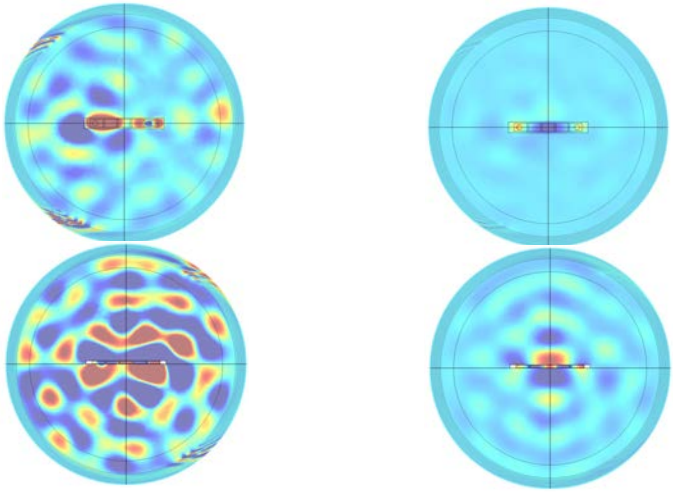

mode freq

473 Hz | 487 Hz | 490 Hz | 494 Hz

mode shape

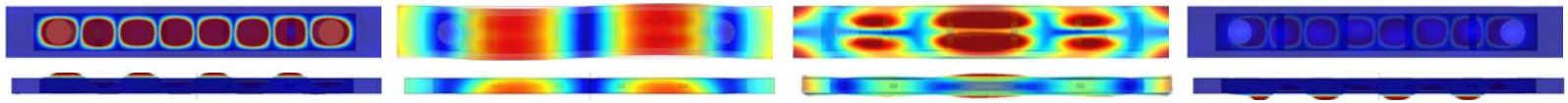

End view

mode pattern

Side view

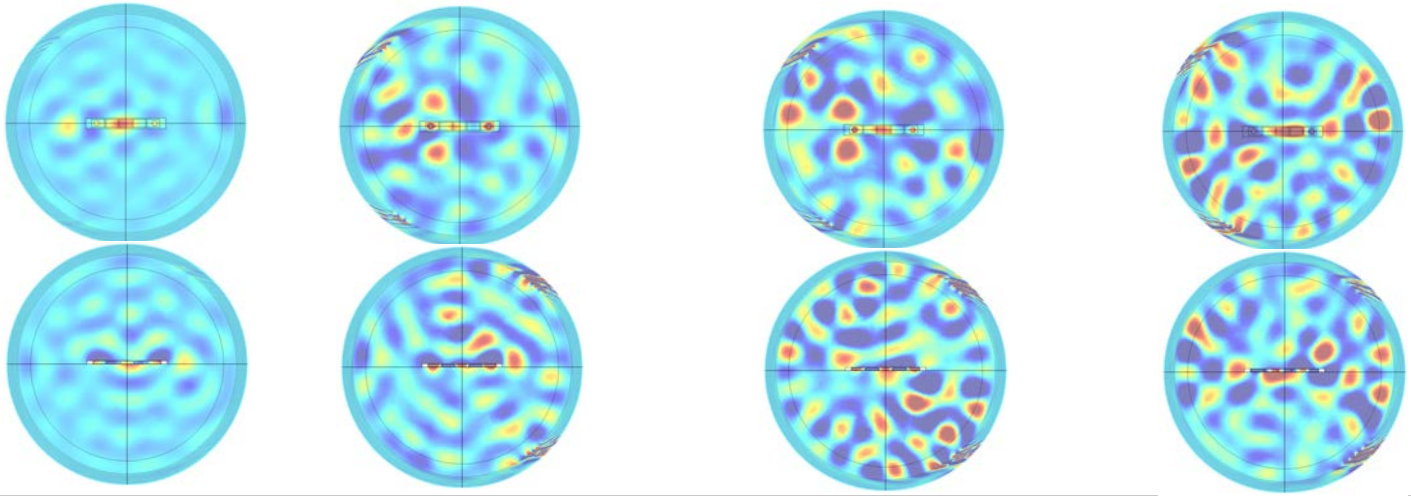

Peak freq

458 Hz | 467 Hz | 500 Hz

Side view

Peak shape

End view

mode shape mode freq

509 Hz | 541 Hz | 585 Hz | 617 Hz | 623 Hz

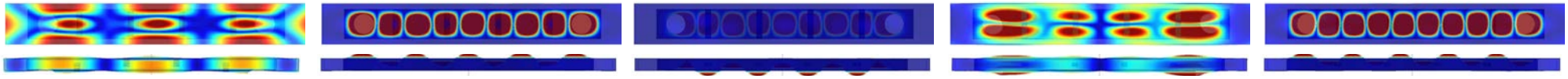

End view

mode pattern

Side view

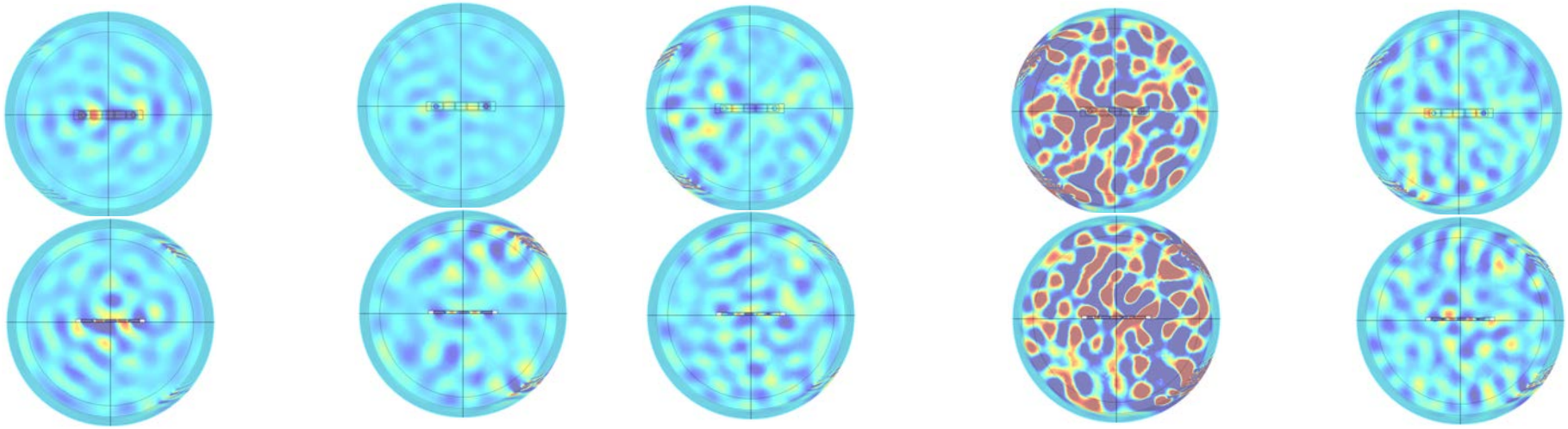

Peak freq

615 Hz | 628 Hz

End view

Peak shape

Side view

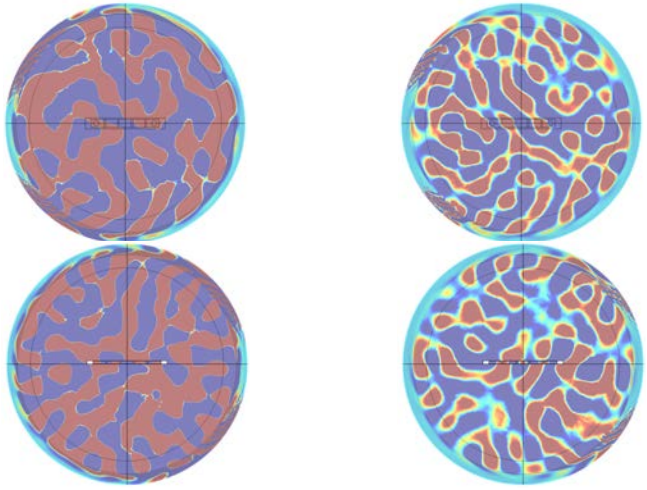

mode freq

666 Hz | 684 Hz | 686 Hz | 690 Hz | 699 Hz

mode shape

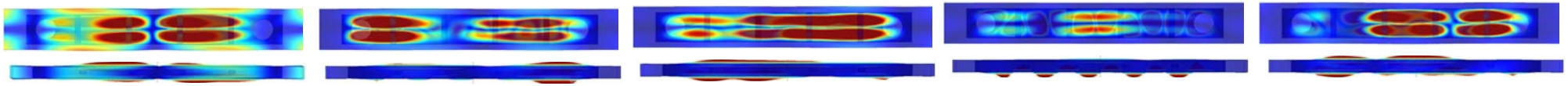

End view

mode pattern

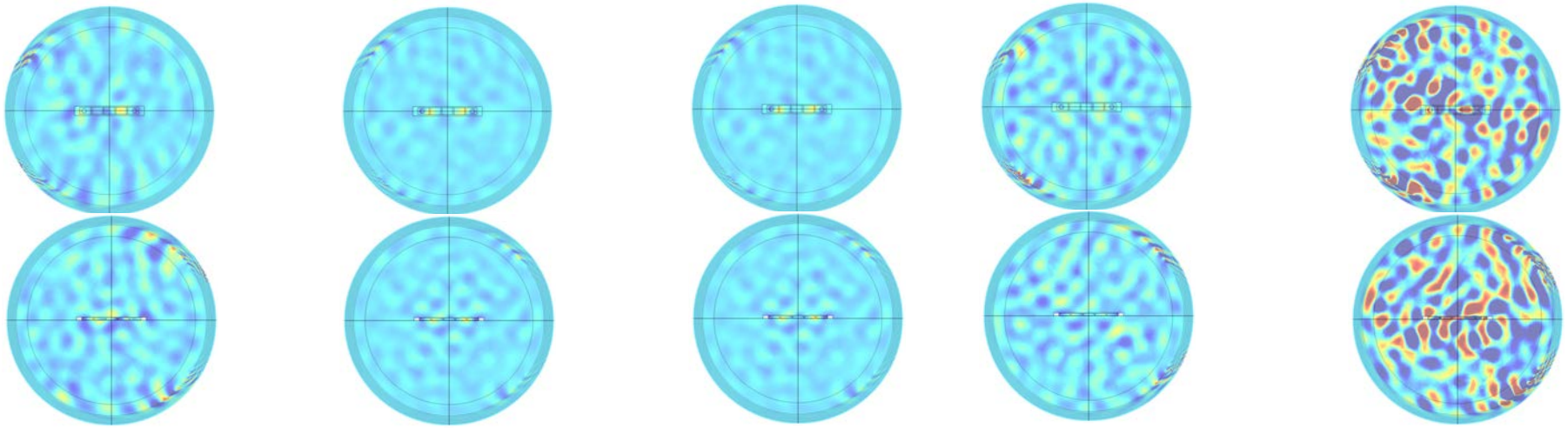

Side view

Peak freq

698 Hz

Side view

Peak shape

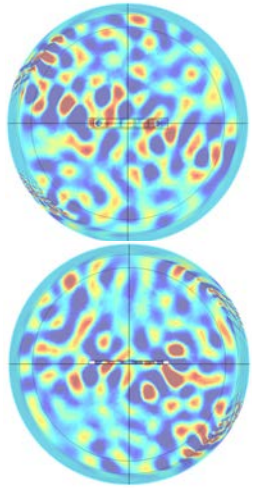

End view

mode freq

711 Hz

712 Hz

724 Hz

739 Hz

750 Hz

mode shape

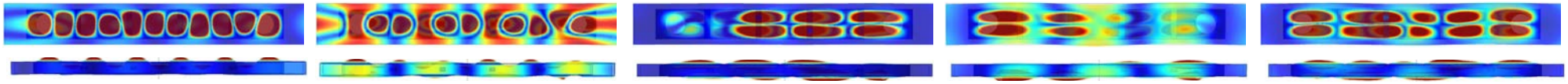

mode pattern

End view

Side view

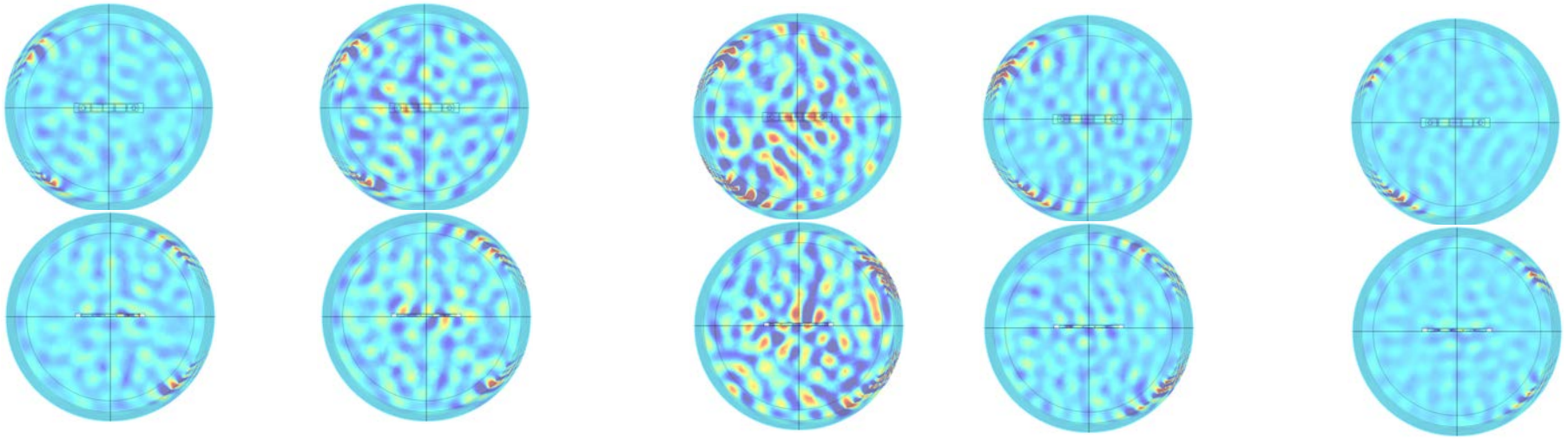

Peak freq

723 Hz

731 Hz

Peak shape

End view

Side view

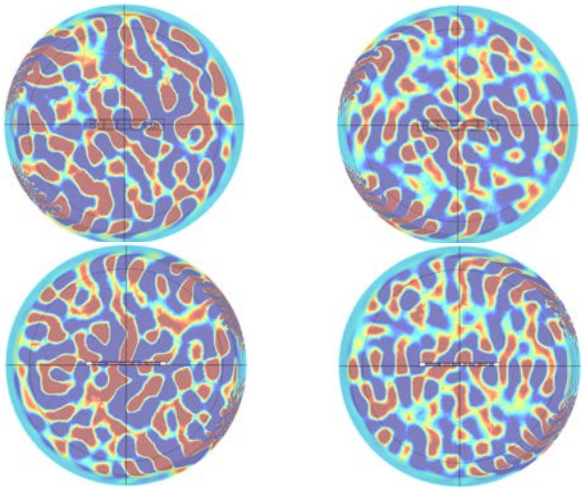

mode freq

mode shape

End view

mode pattern

Side view

Peak freq

780 Hz

821 Hz

Sic

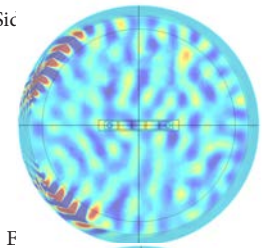

F

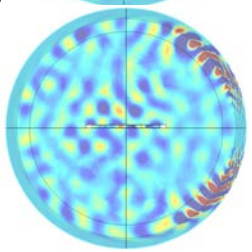

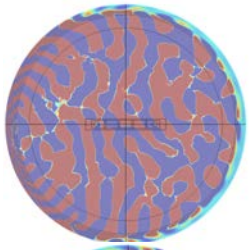

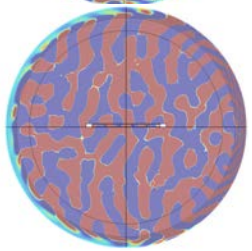

Peak shape

Dataset 4

The radiation patterns of the lofted *koto* model

mode freq

122 Hz

mode shape

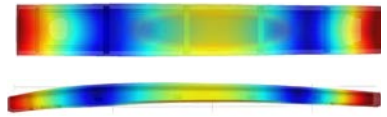

mode pattern

End view

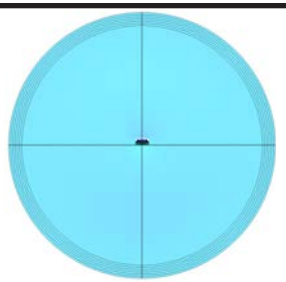

Side view

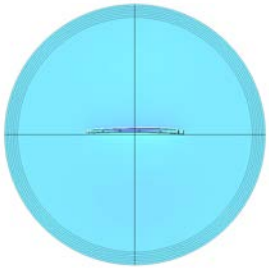

Peak freq

77 Hz | 97 Hz | 107 Hz | 138 Hz

Peak shape

Side view

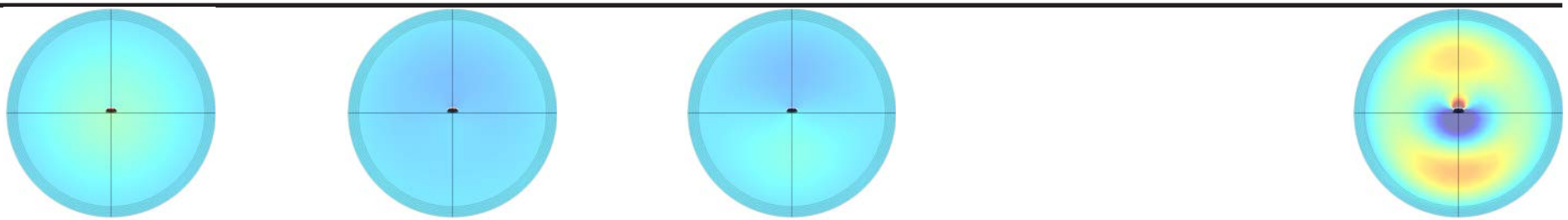

End view

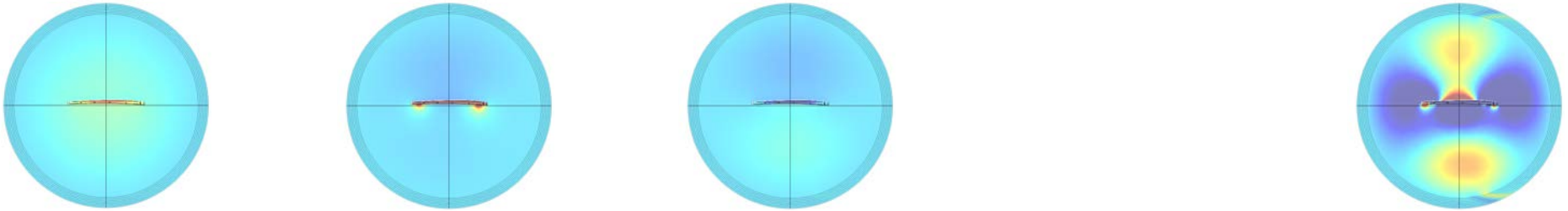

Radiation patterns at eigenmodes and peak frequencies in the lofted model

mode shape mode freq

175 Hz

199 Hz

201 Hz

mode pattern

End view

Side view

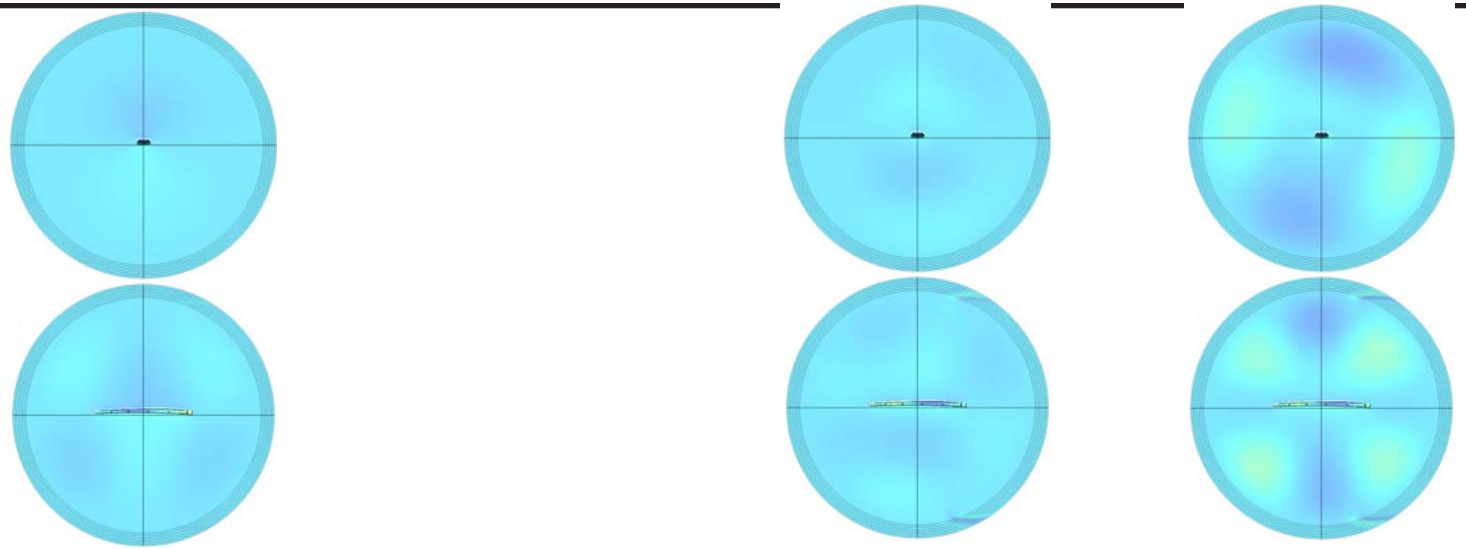

Peak freq

153 Hz

185 Hz

Peak shape

End view

Side view

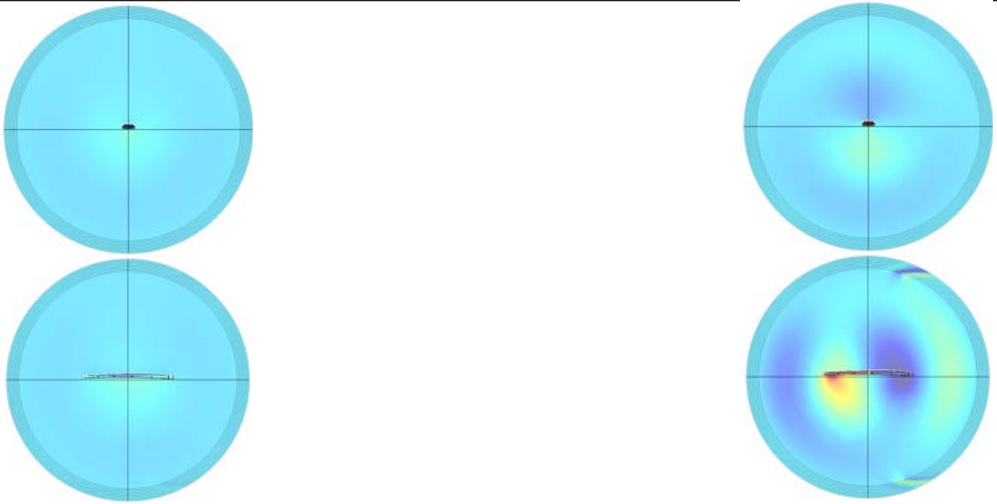

Radiation patterns at eigenmodes and peak frequencies in the lofted model

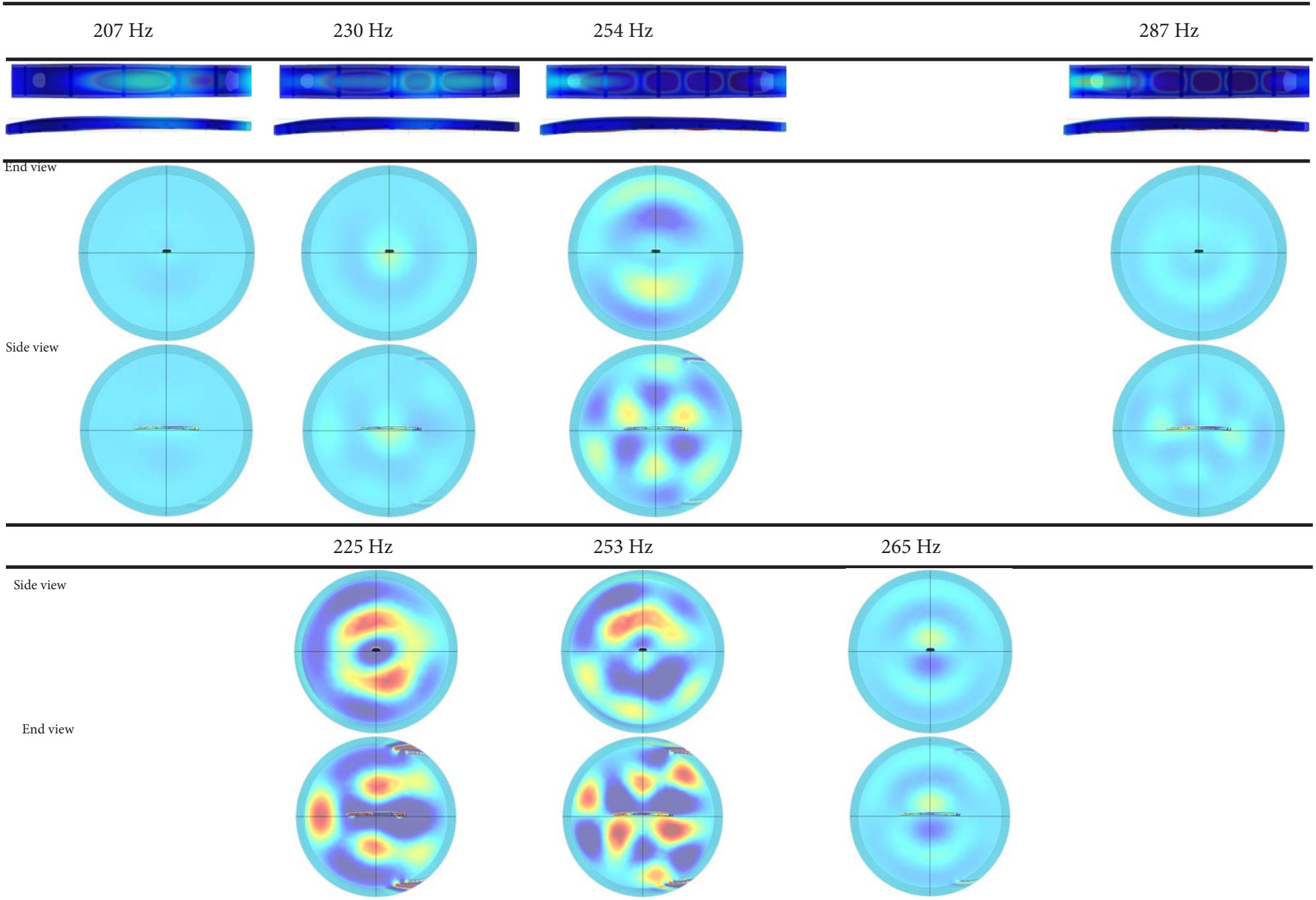

Radiation patterns at eigenmodes and peak frequencies in the lofted model

mode shape mode freq

305 Hz | 309 Hz | 322 Hz | 327 Hz | 339 Hz

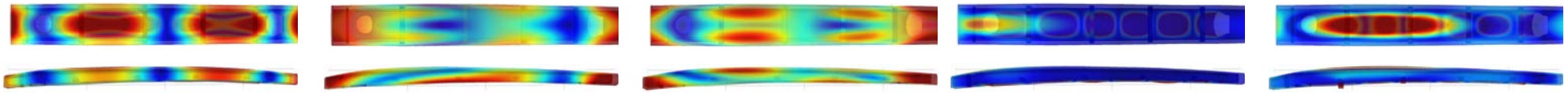

mode pattern

End view

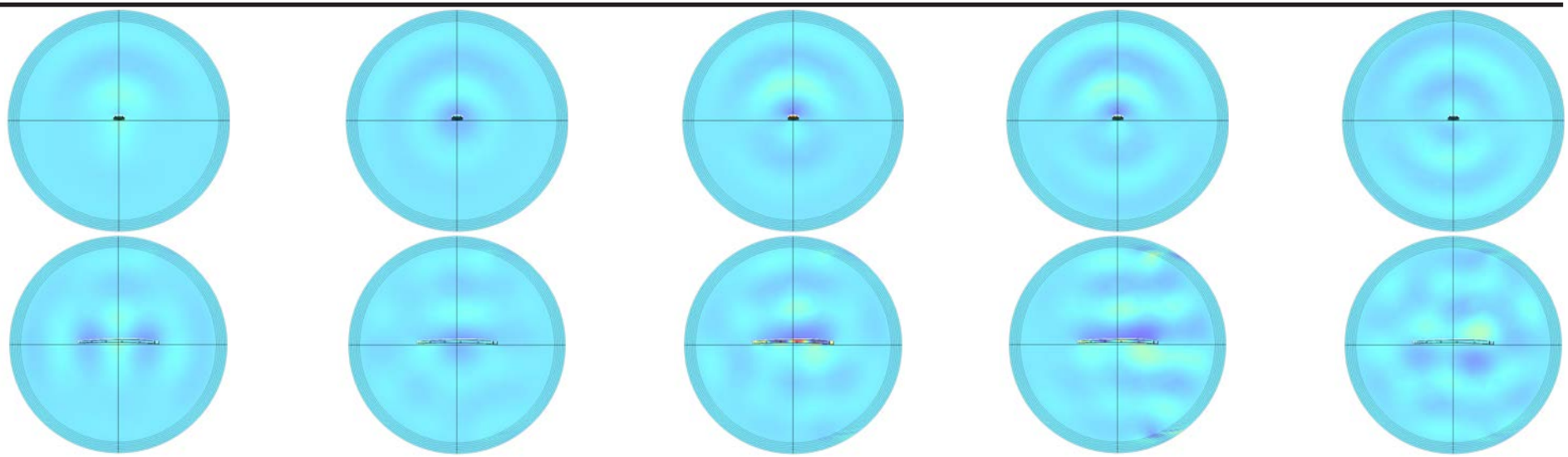

Side view

Peak freq

301 Hz | 317 Hz

Peak shape

End view

Side view

Radiation patterns at eigenmodes and peak frequencies in the lofted model

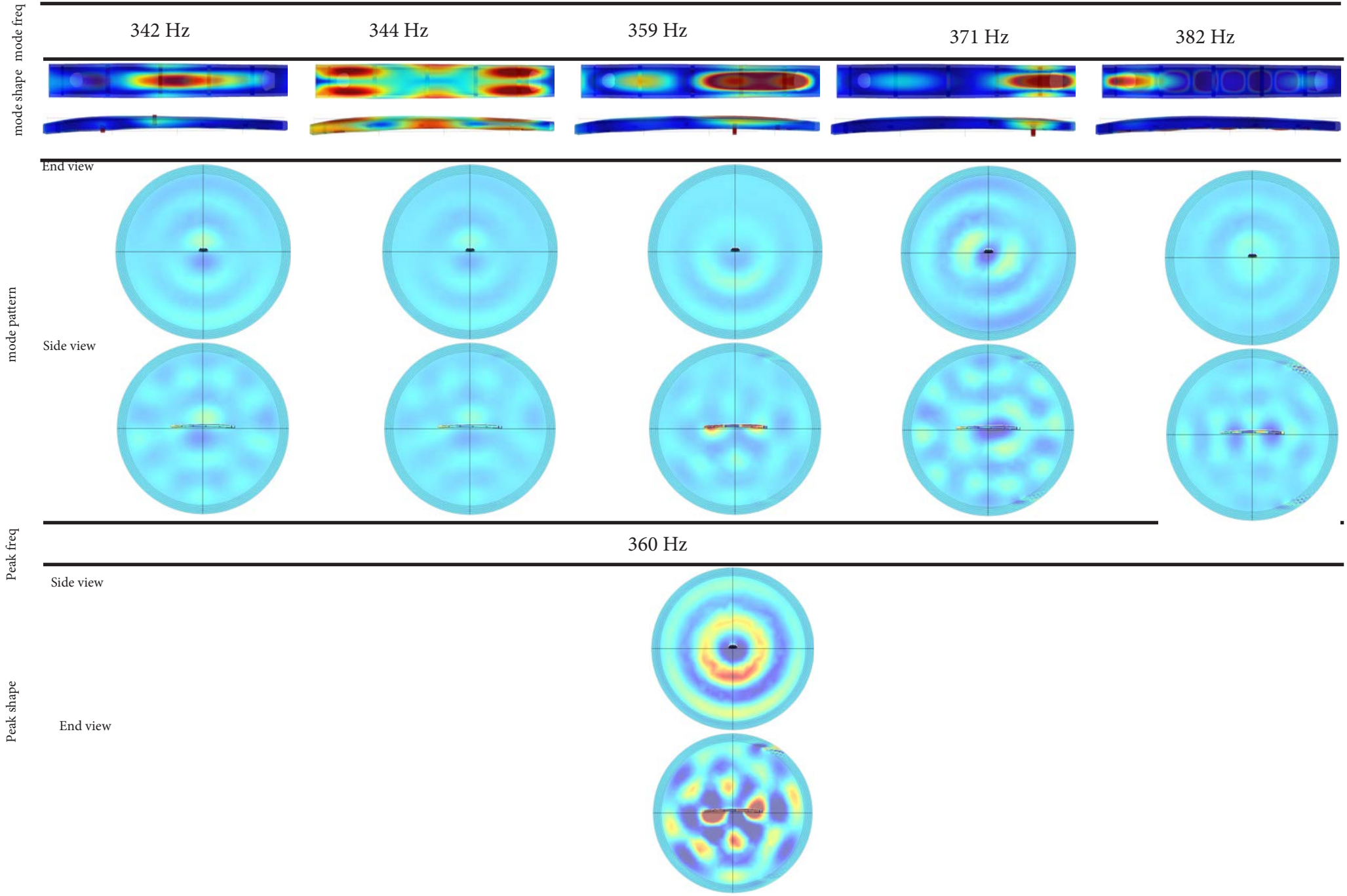

Radiation patterns at eigenmodes and peak frequencies in the lofted model

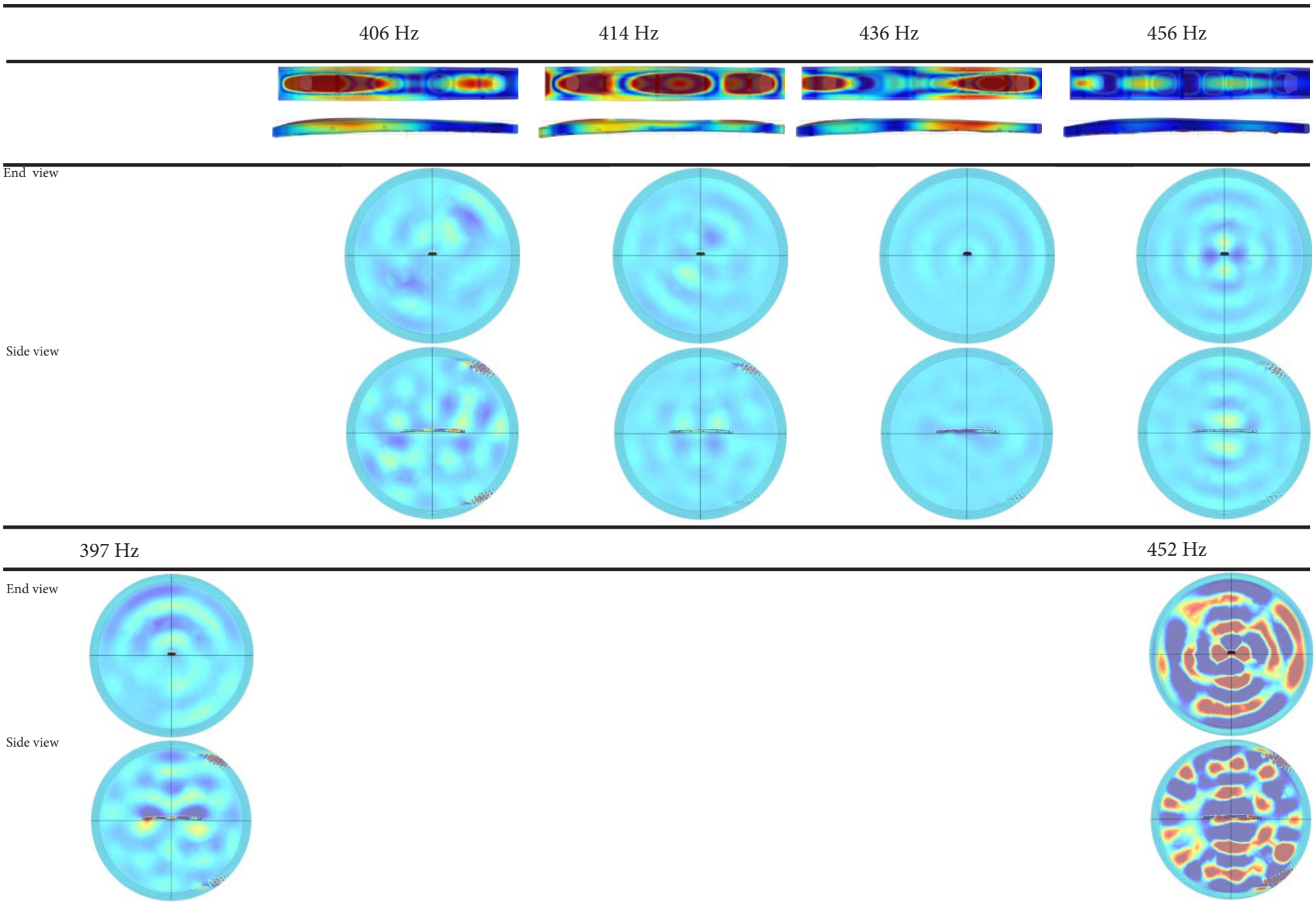

Radiation patterns at eigenmodes and peak frequencies in the lofted model

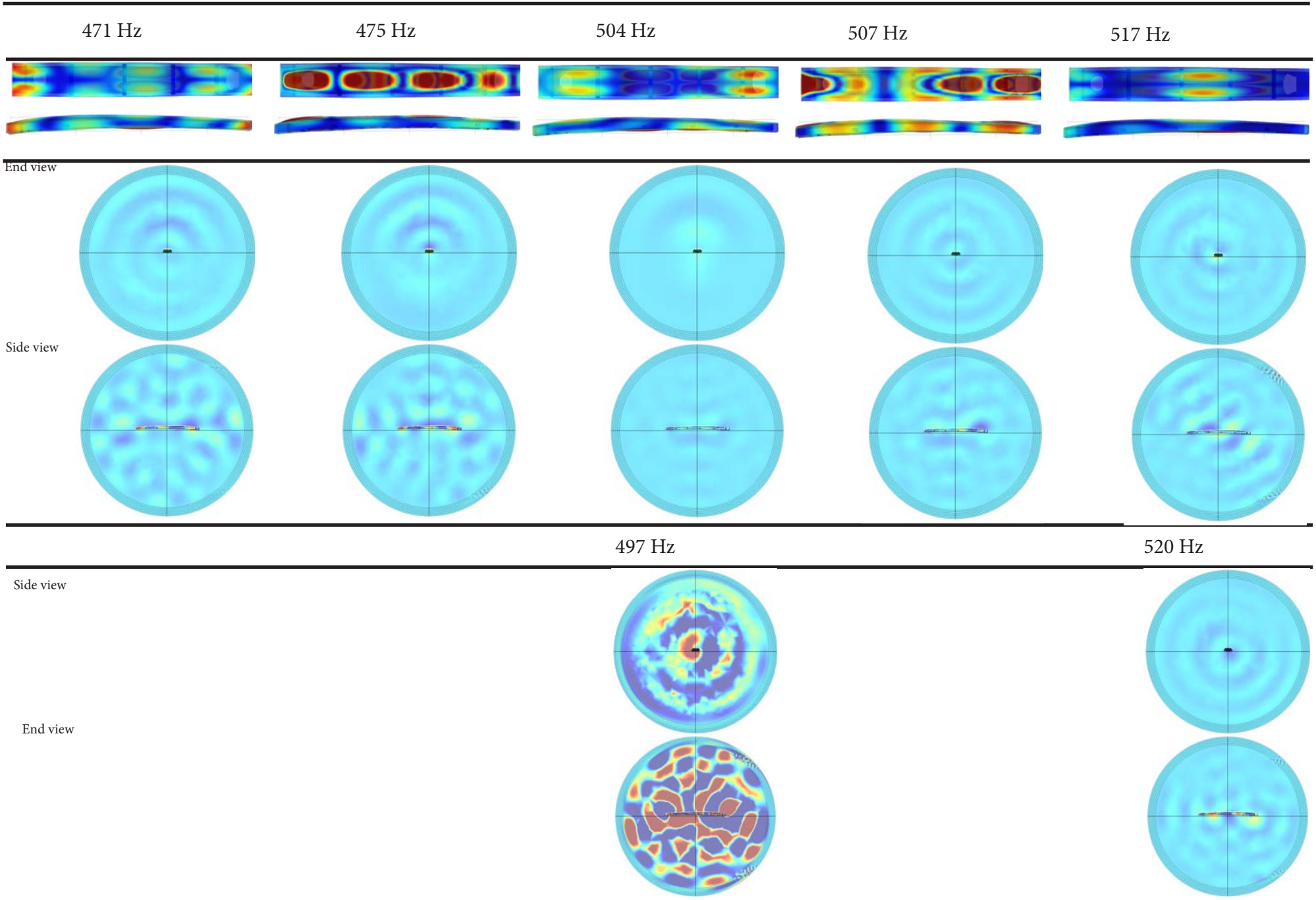

Radiation patterns at eigenmodes and peak frequencies in the lofted model

mode shape mode freq

536 Hz | 544 Hz | 545 Hz | 567 Hz

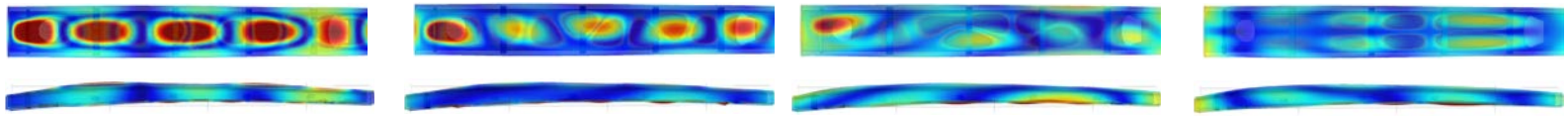

mode pattern

End view

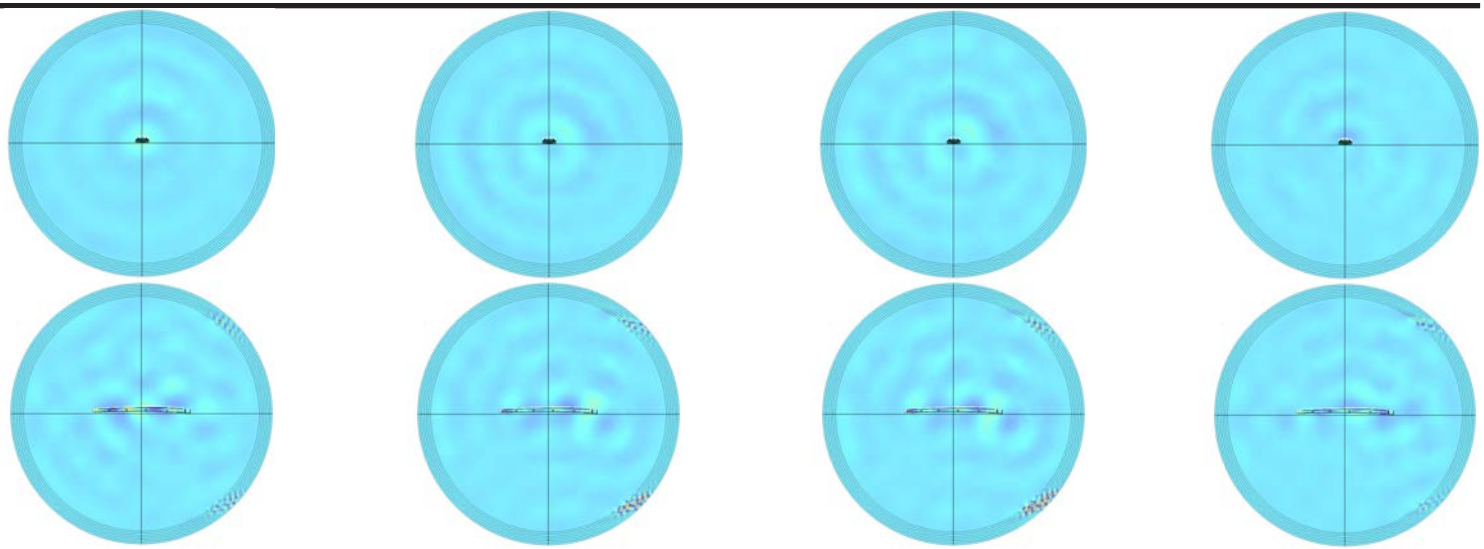

Side view

Peak freq

528 Hz | 562 Hz

Peak shape

End view

Side view

Radiation patterns at eigenmodes and peak frequencies in the lofted model

mode freq

576 Hz | 586 Hz | 595 Hz | 600 Hz

mode shape

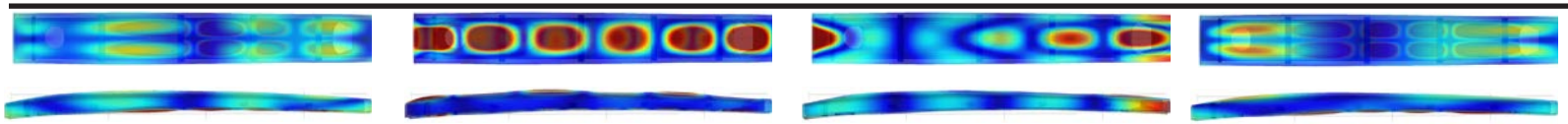

mode pattern

End view

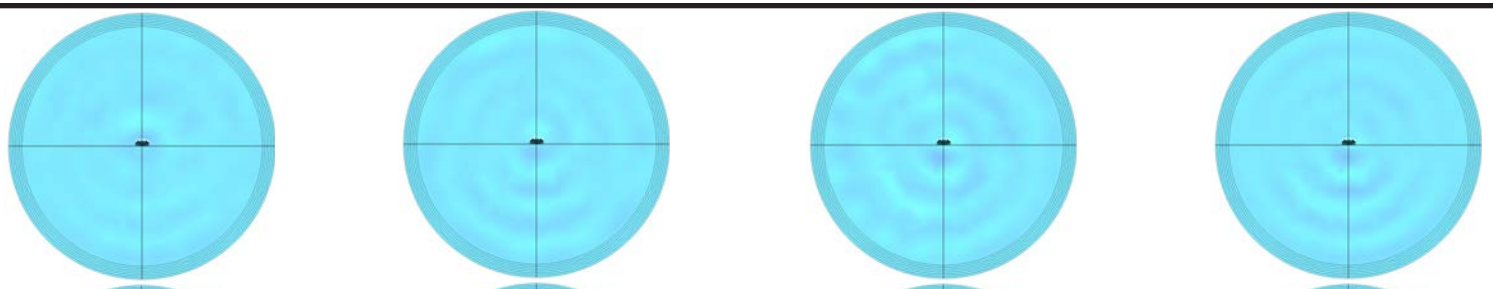

Side view

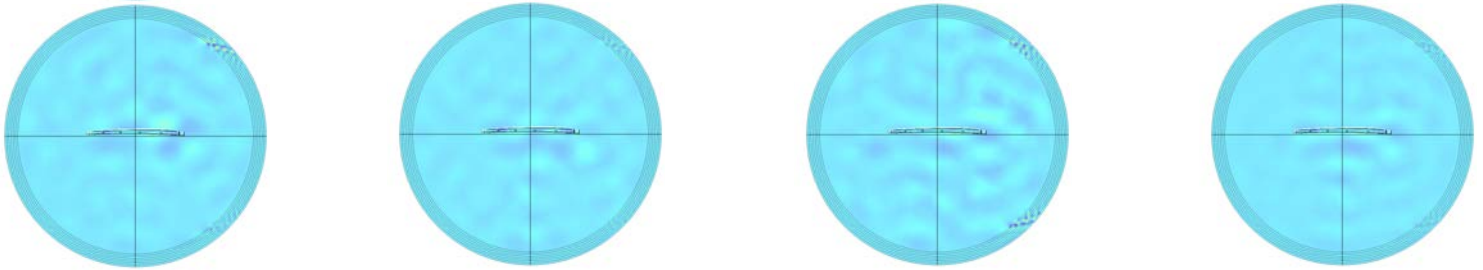

Peak freq

611 Hz

Side view

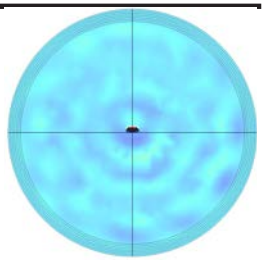

Peak shape

End view

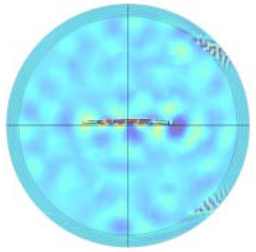

Radiation patterns at eigenmodes and peak frequencies in the lofted model

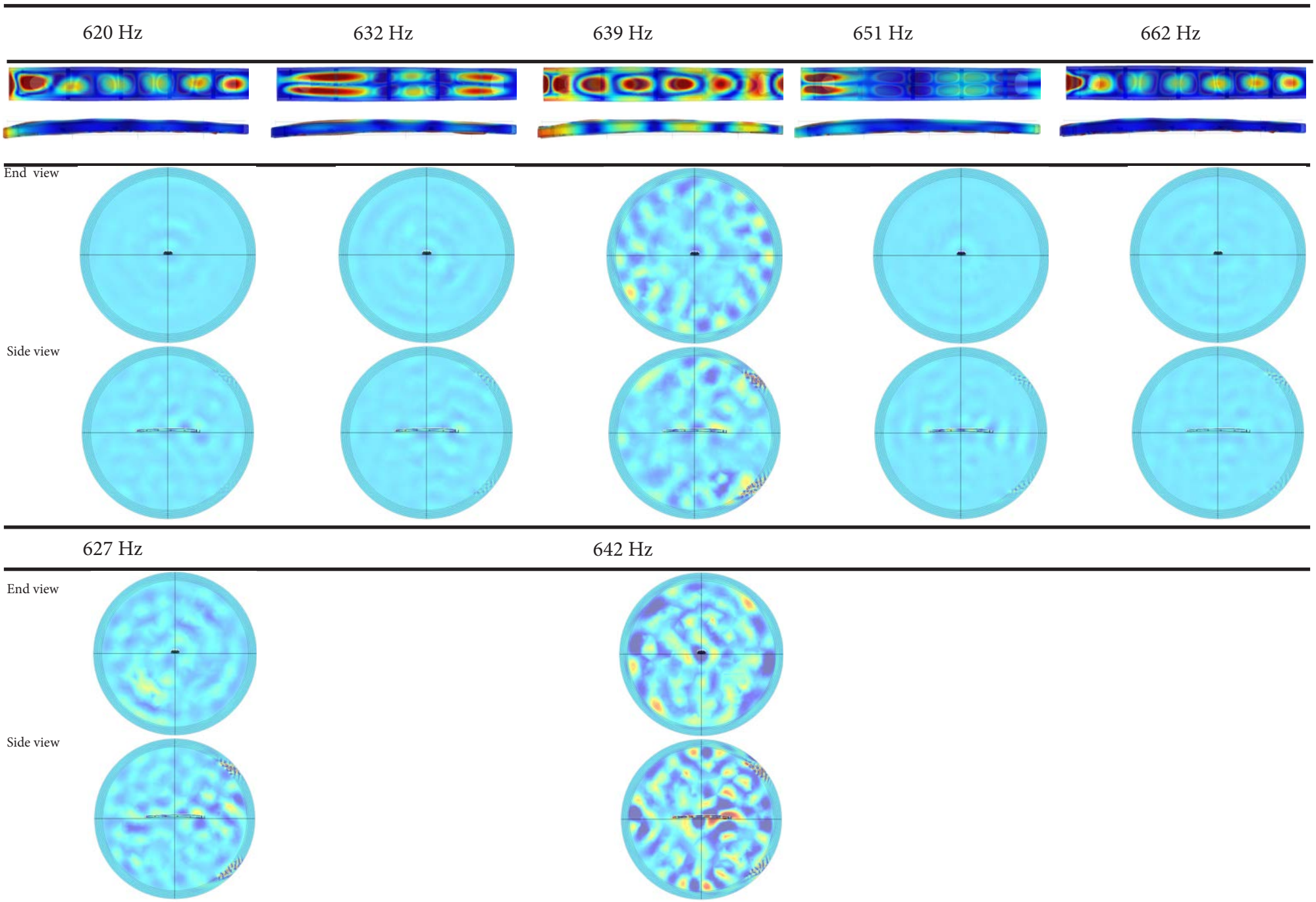

Radiation patterns at eigenmodes and peak frequencies in the lofted model

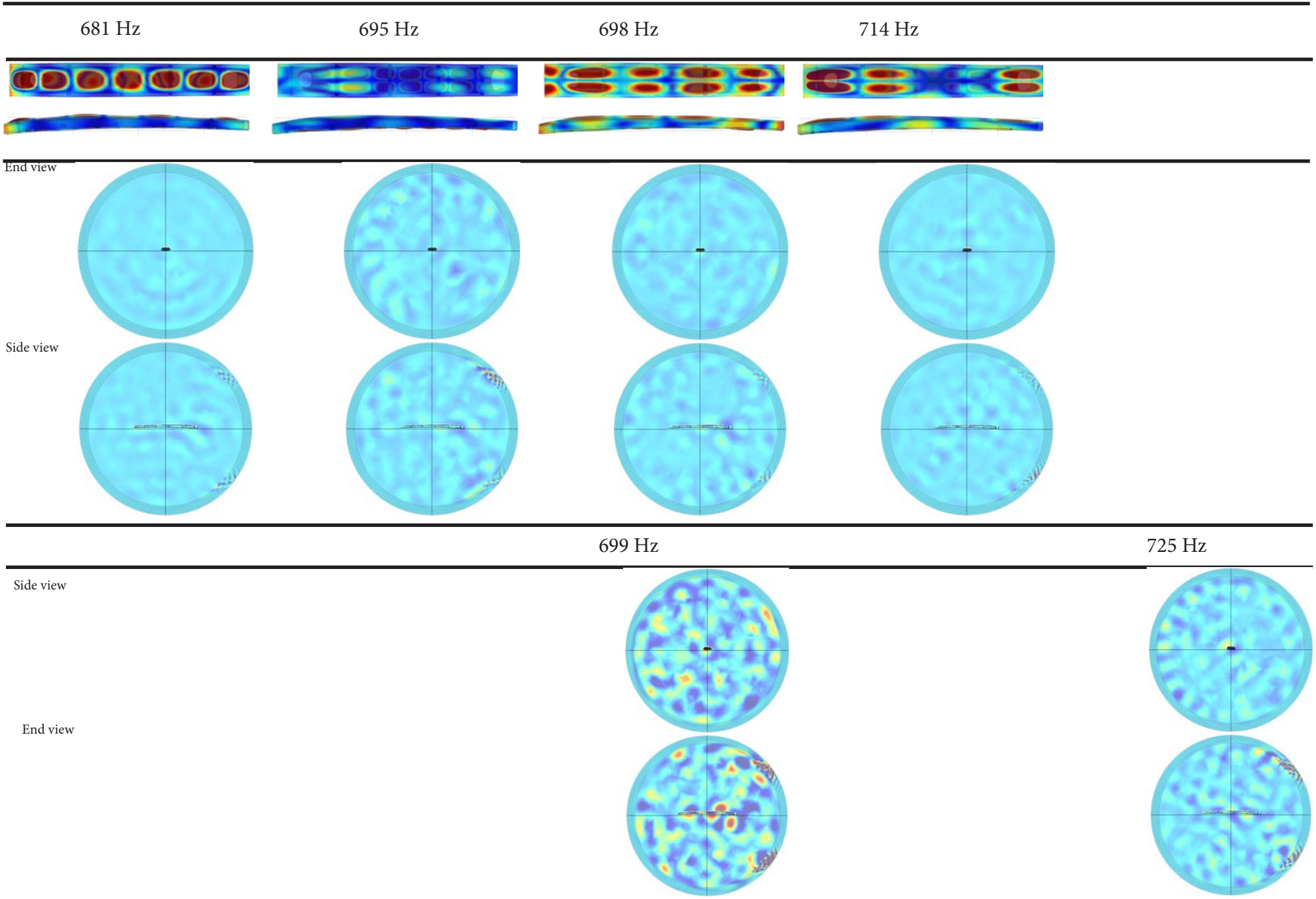

Radiation patterns at eigenmodes and peak frequencies in the lofted model

mode shape mode freq

End view

mode pattern

Side view

Peak freq

760 Hz | 779 Hz | 811 Hz | 868 Hz | 937 Hz

End view

Peak shape

Side view

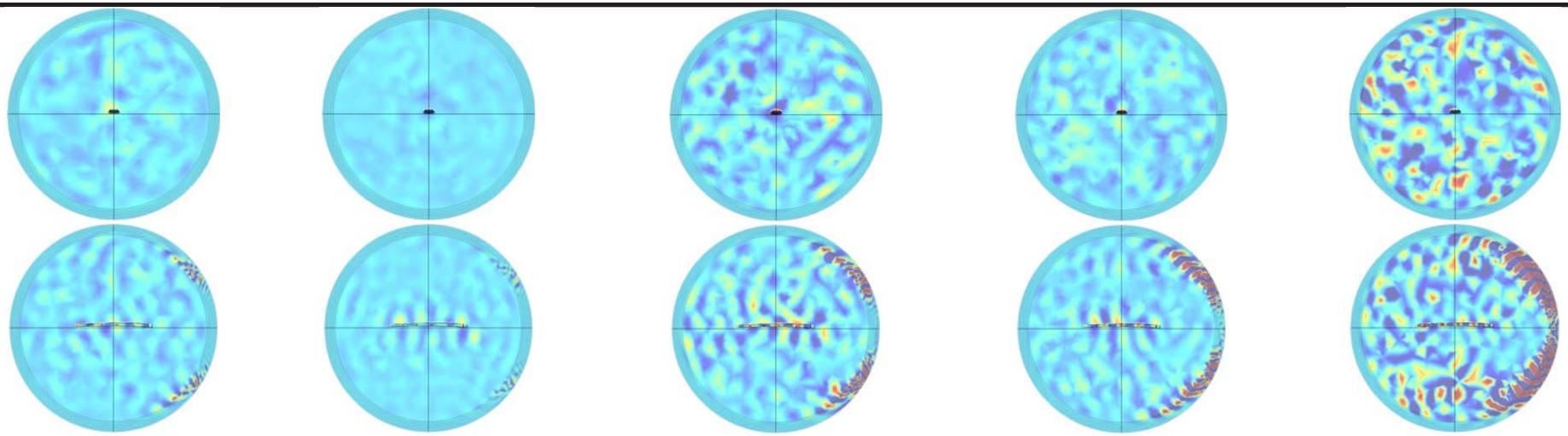

Radiation patterns at eigenmodes and peak frequencies in the lofted model

Dataset 5

Waveforms in the air cylinder

in the transient responses of the lofted model

All probes outside body stacked

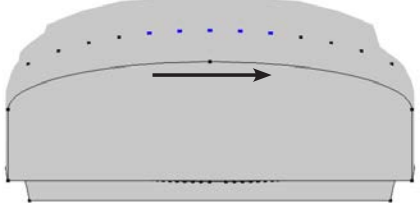

Cross-section 2 - maximum arching

String position - changing arching and tapering

Cross-section 1: minimum arching

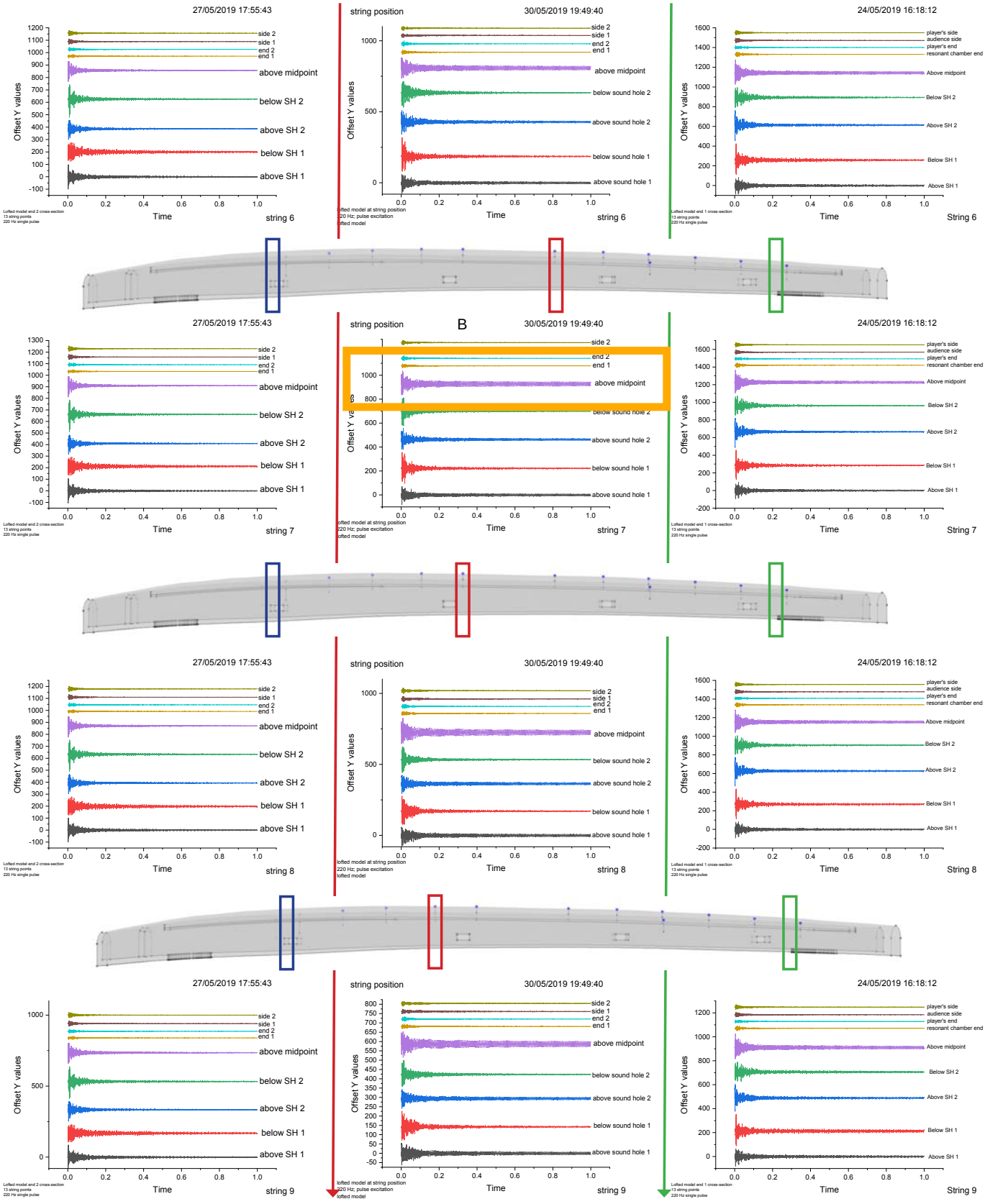

All probes outside body stacked

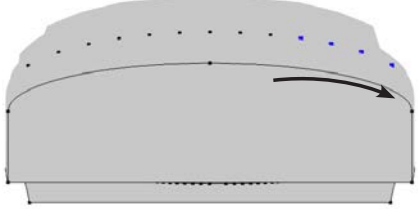

Cross-section 2 - maximum arching

String position - changing arching and tapering

Cross-section 1: minimum arching

27/05/2019 17:55:43

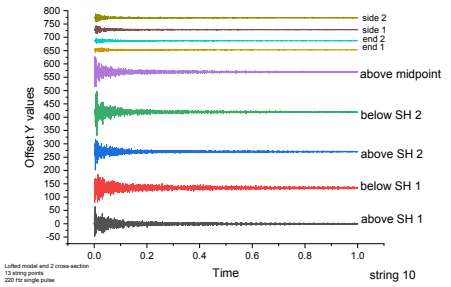

string position 30/05/2019 19:49:40

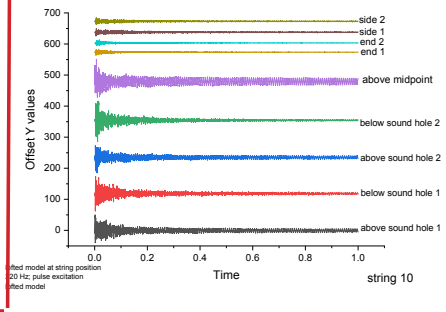

24/05/2019 16:18:12

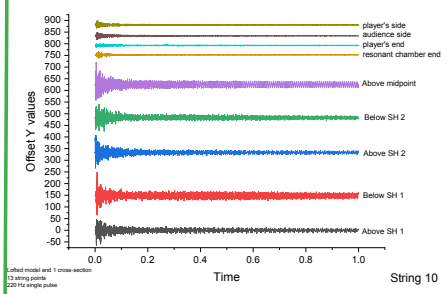

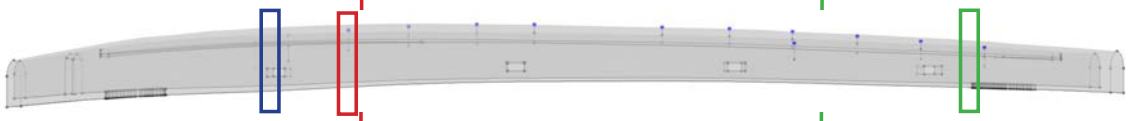

27/05/2019 17:55:43

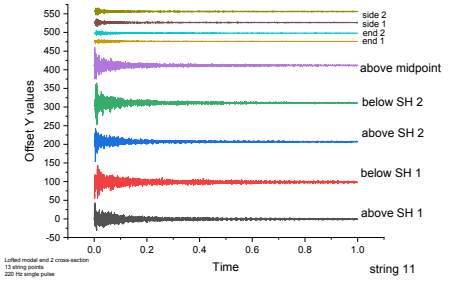

string position 30/05/2019 19:49:40

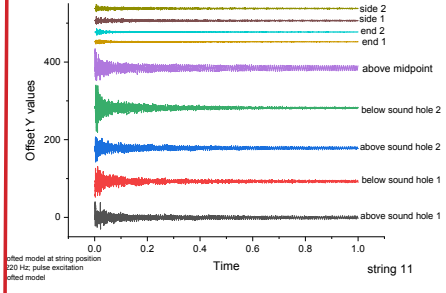

24/05/2019 16:18:12

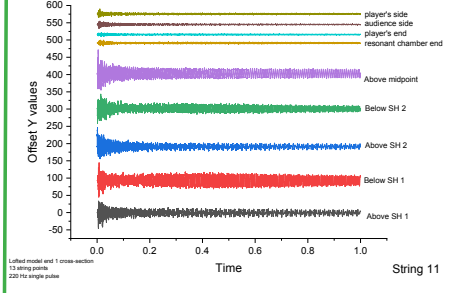

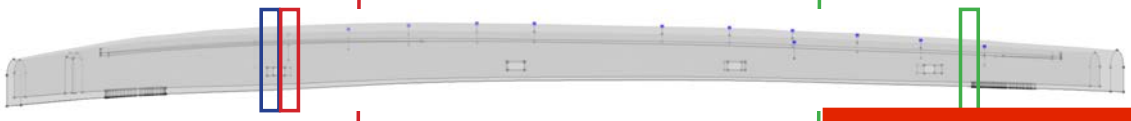

A

27/05/2019 17:55:43

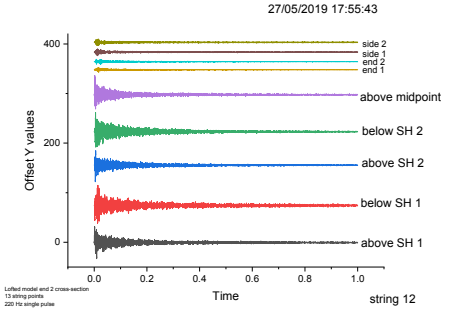

string position 30/05/2019 19:49:40

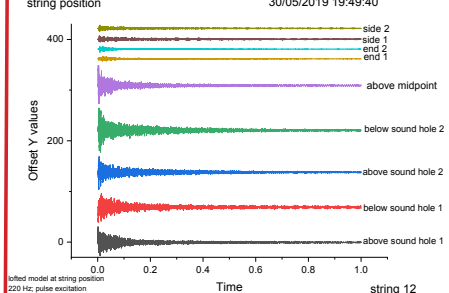

24/05/2019 16:18:12

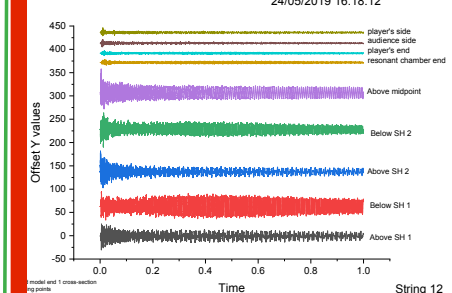

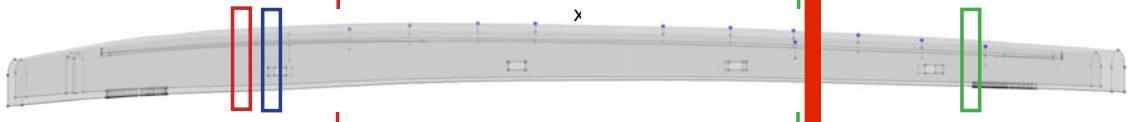

27/05/2019 17:55:43

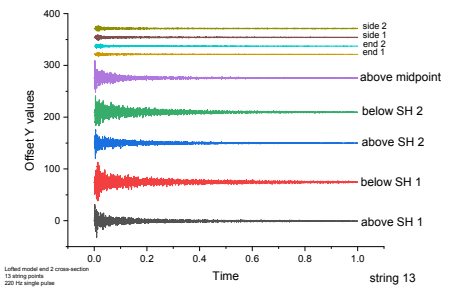

string position 30/05/2019 19:49:40

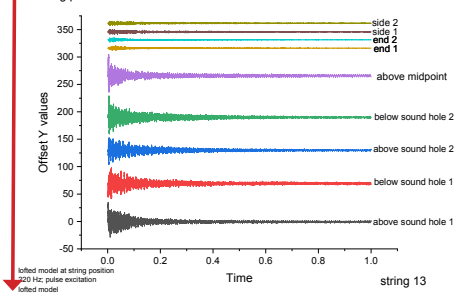

24/05/2019 16:18:12

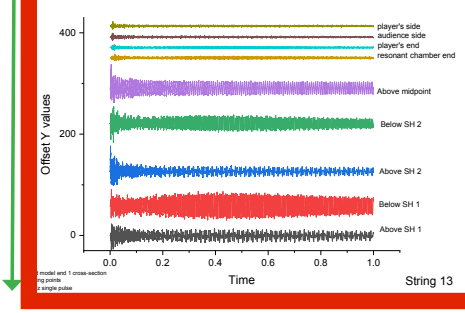

Dataset 6

Waveforms in the internal air cavities

in the transient responses of the lofted model

All probes outside body stacked

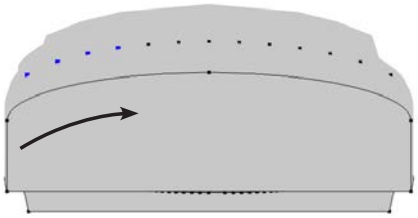

Cross-section 2 - maximum arching

String position - changing arching and tapering

Cross-section 1: minimum arching

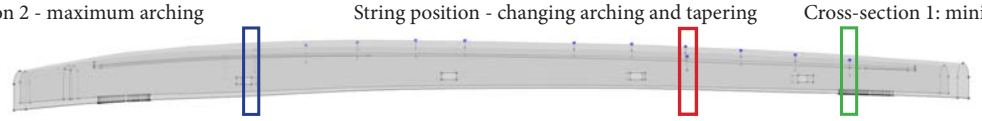

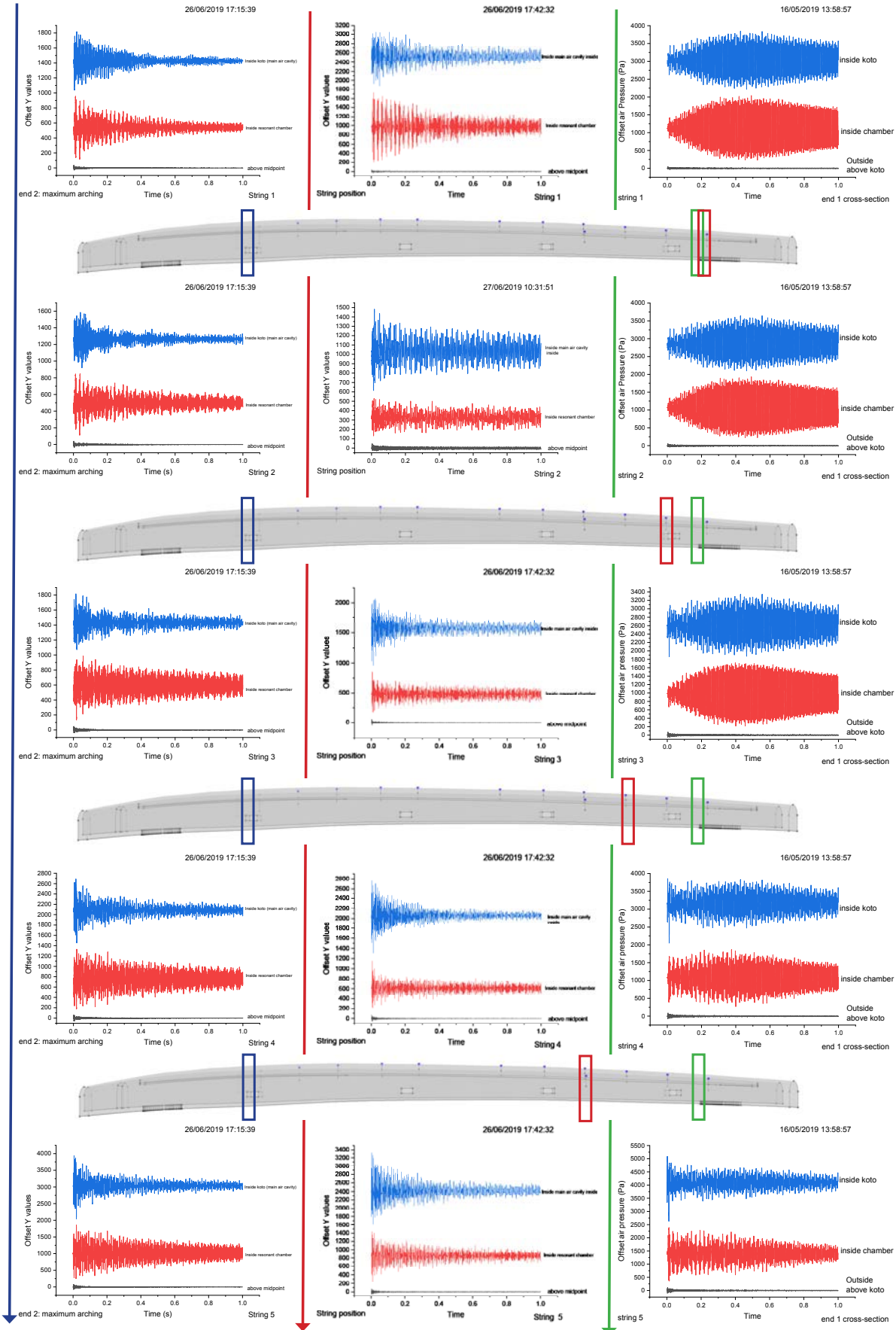

All probes outside body stacked

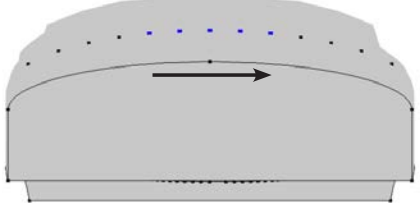

Cross-section 2 - maximum arching

String position - changing arching and tapering

Cross-section 1: minimum arching

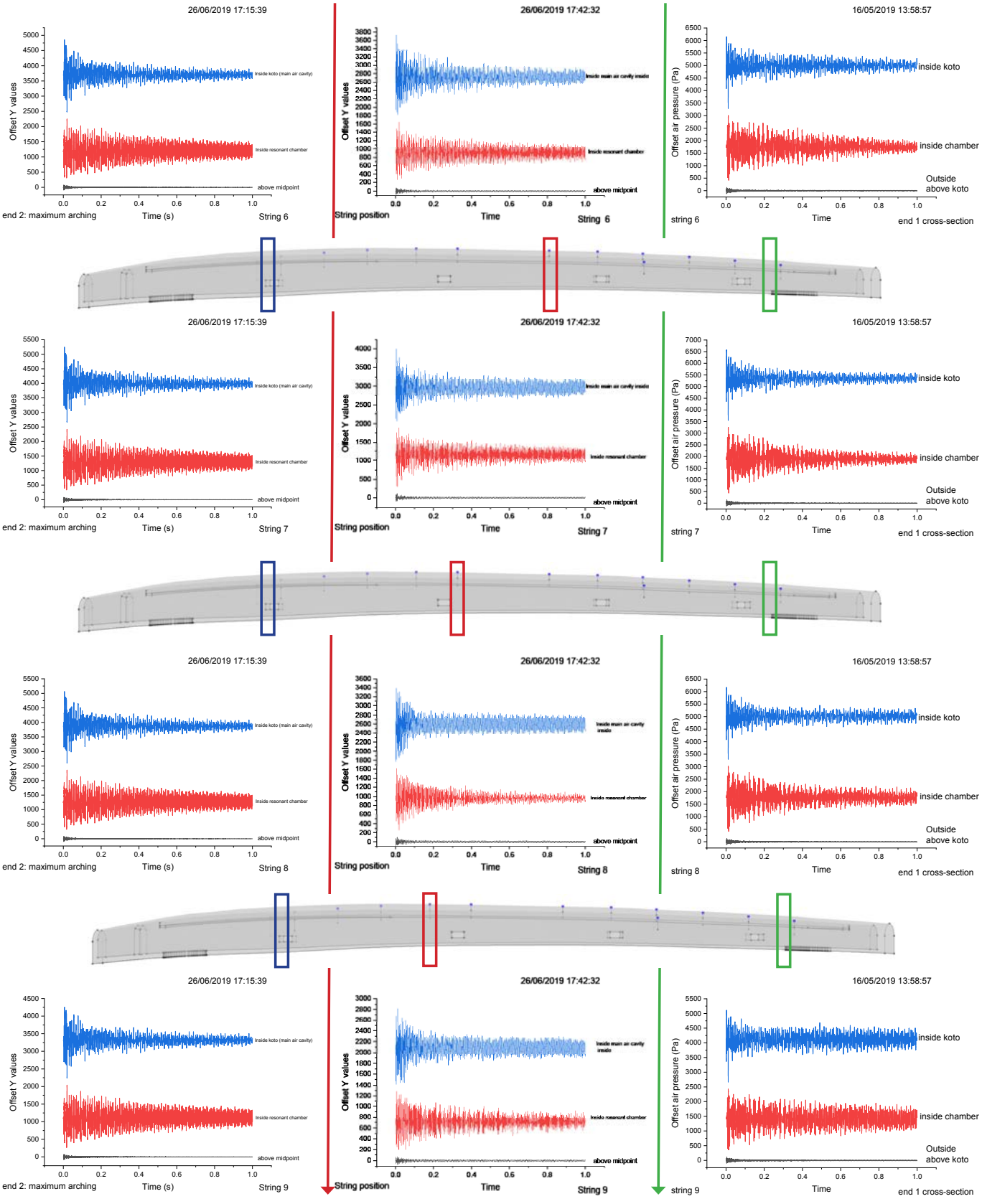

All probes outside body stacked

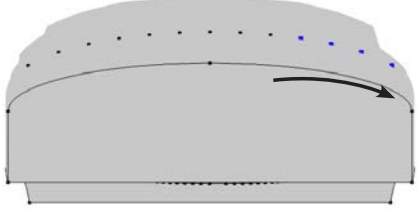

Cross-section 2 - maximum arching

String position - changing arching and tapering

Cross-section 1: minimum arching

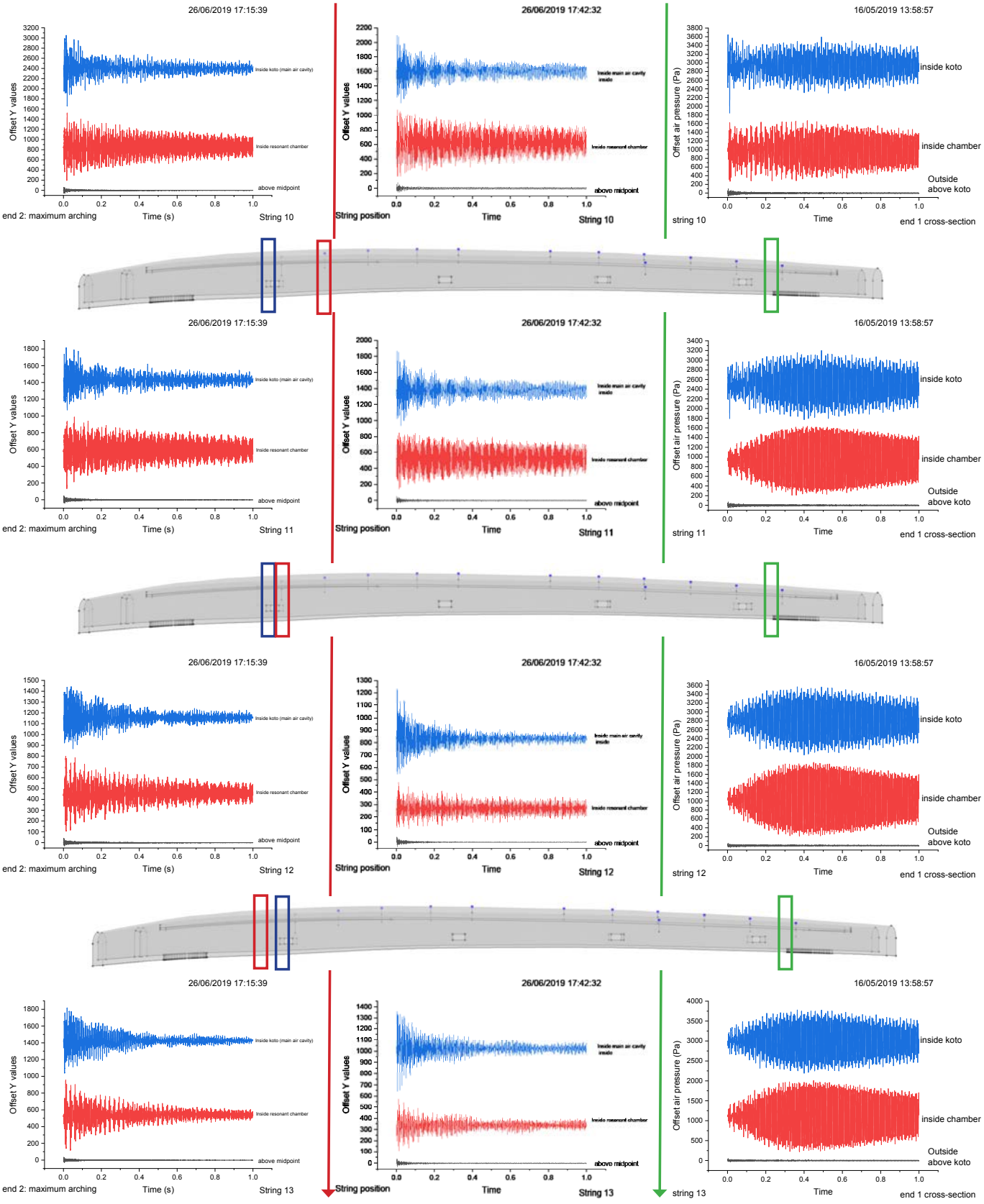

All probes outside body stacked

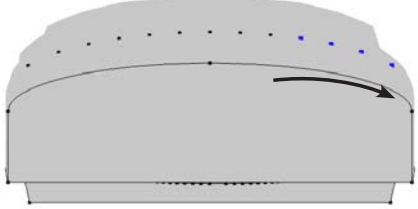

Cross-section 2 - maximum arching

String position - changing arching and tapering

Cross-section 1: minimum arching

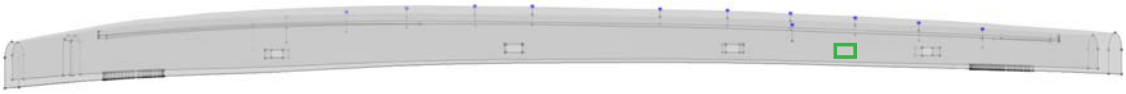

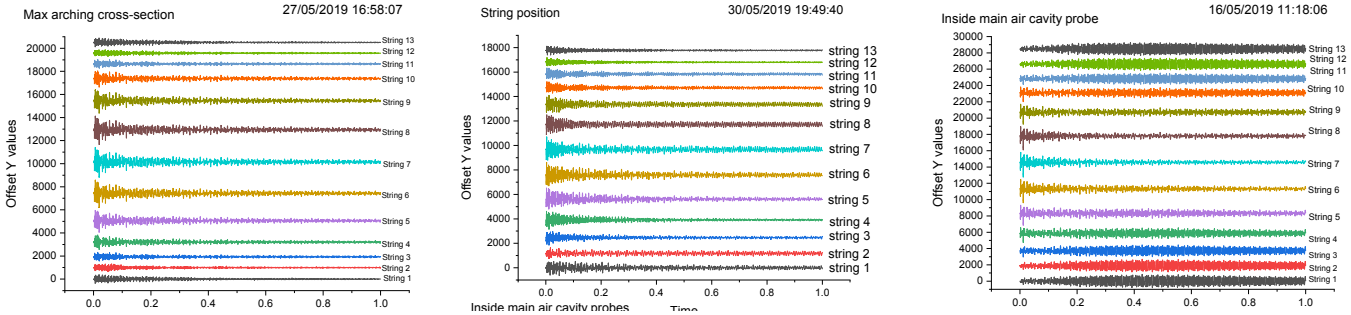

Compilation across all strings - inside main air cavity

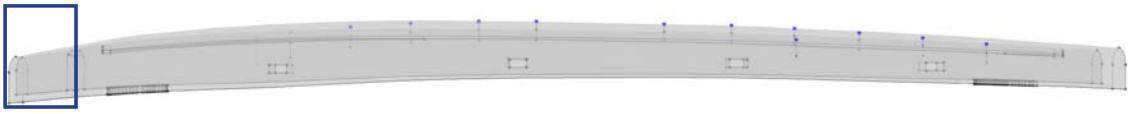

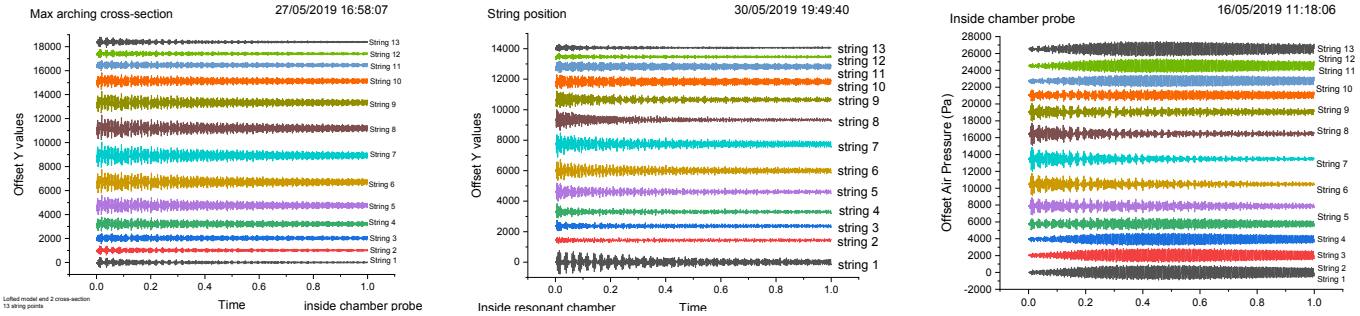

Compilation across all strings - inside resonant chamber

Dataset 7

FFTs inside the small chamber in all excitations

FFT inside resonant chamber across 3 positions for each string

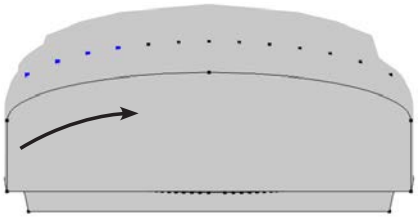

String 1-5

Cross-section 2 - maximum arching

Bridge position

Cross-section 1: minimum arching

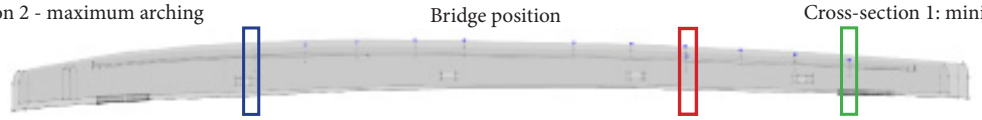

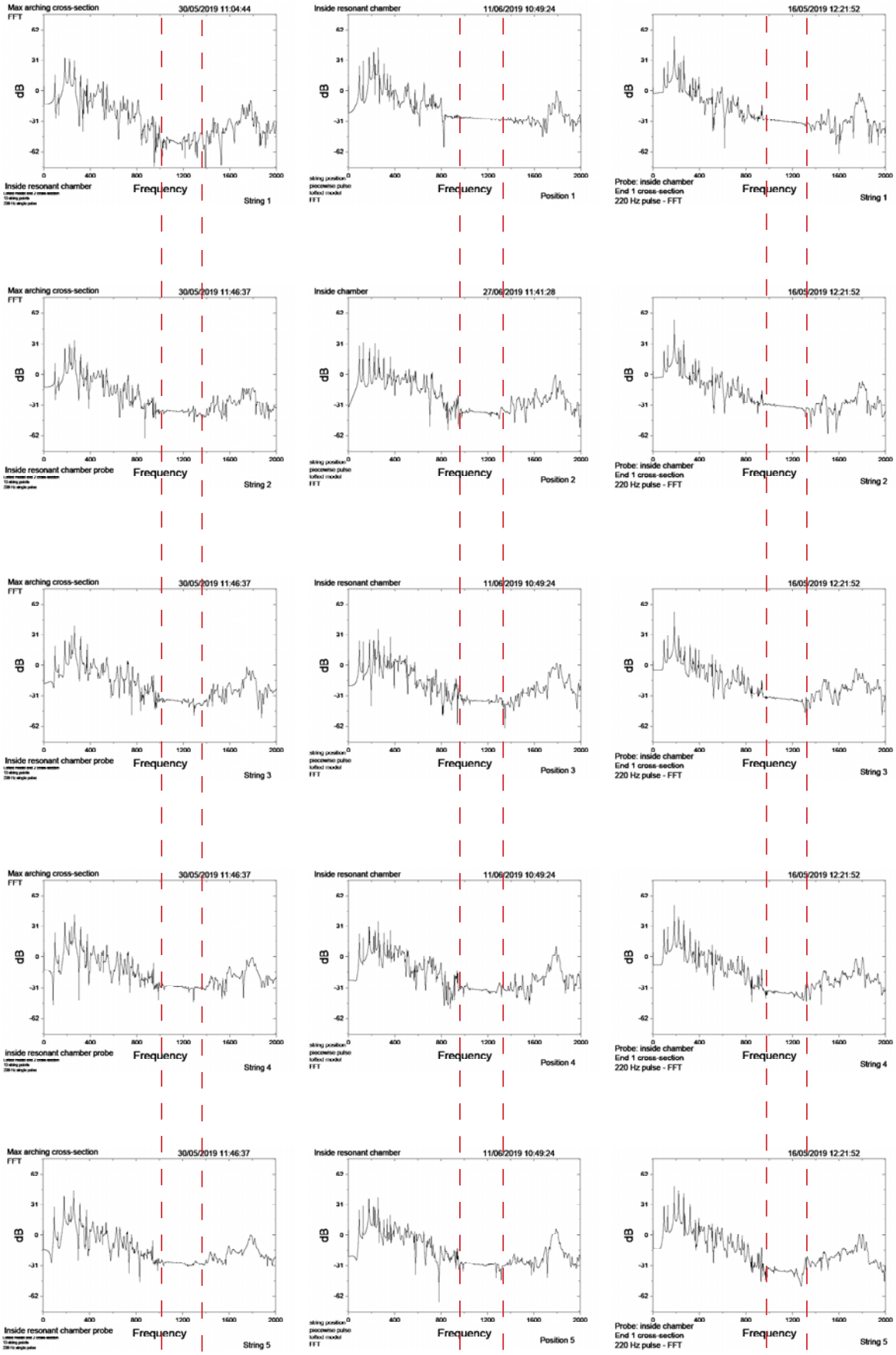

FFT inside resonant chamber across 3 positions for each string

Strings 6-9

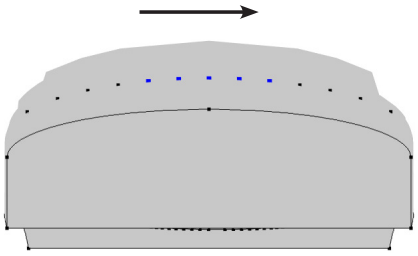

Cross-section 2 - maximum arching

Bridge position

Cross-section 1: minimum arching

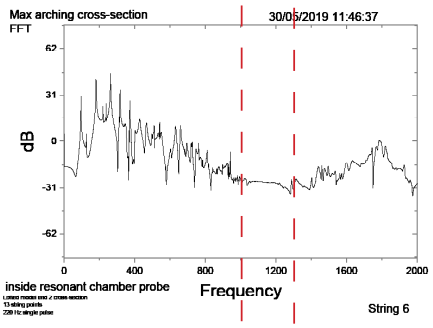

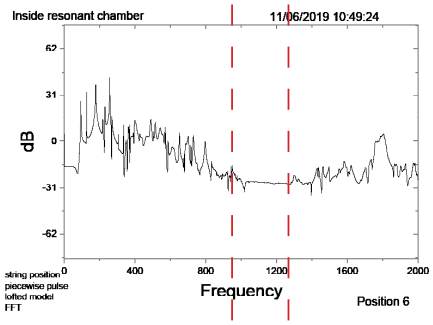

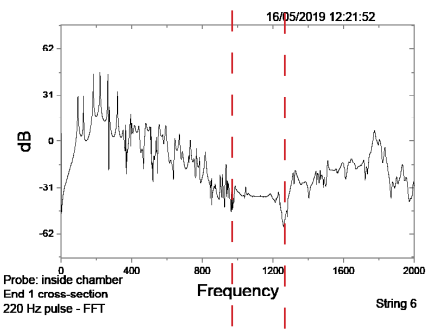

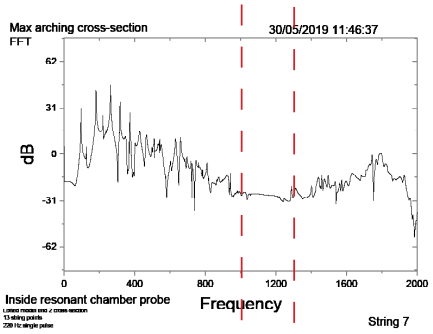

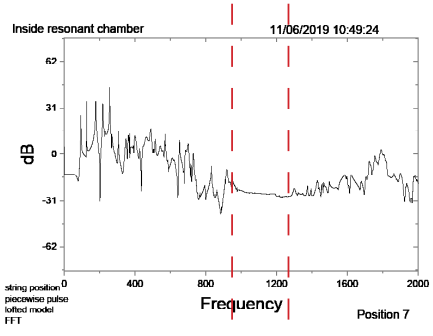

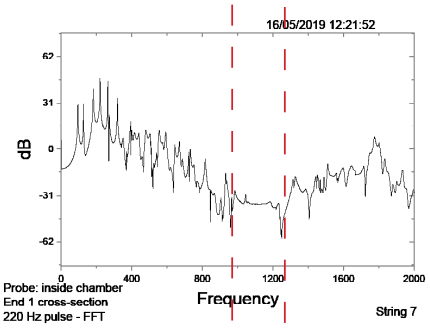

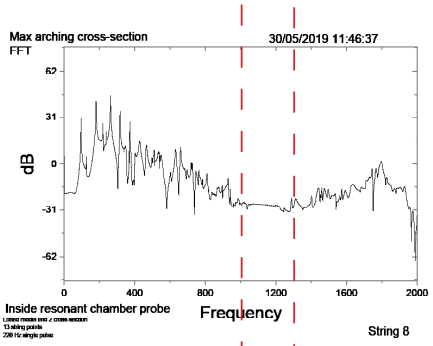

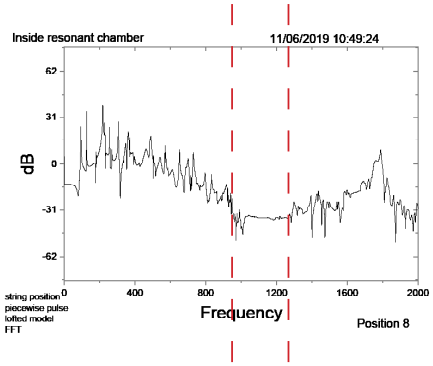

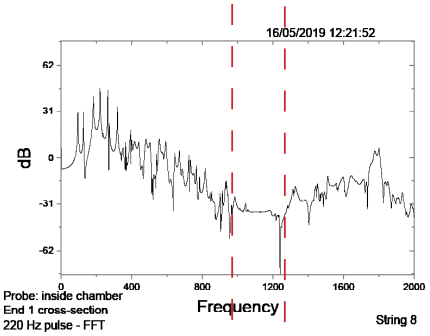

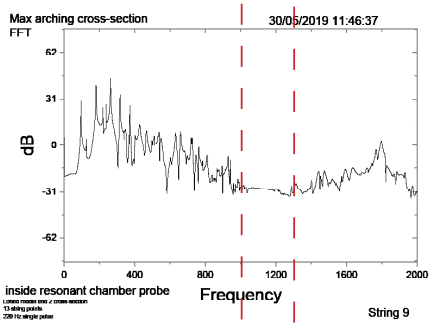

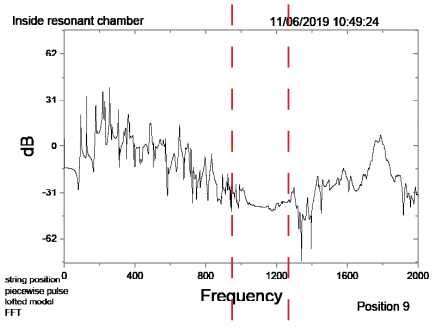

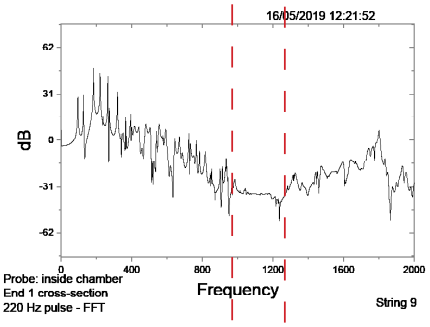

FFT inside resonant chamber across 3 positions for each string

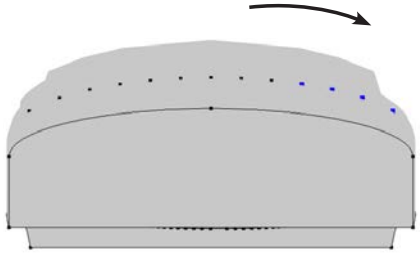

Strings 10-13

Cross-section 2 - maximum arching

Bridge position

Cross-section 1: minimum arching

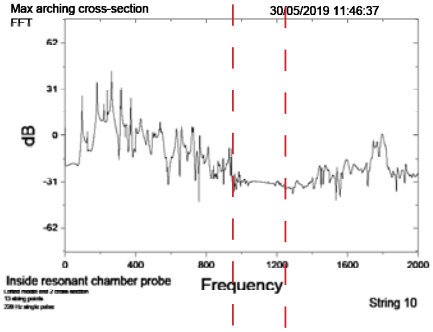

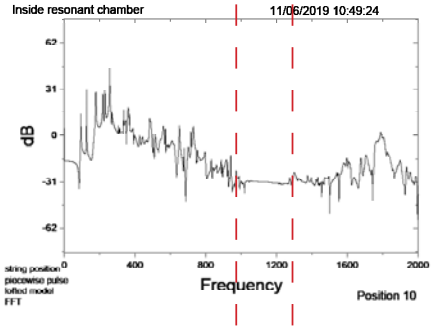

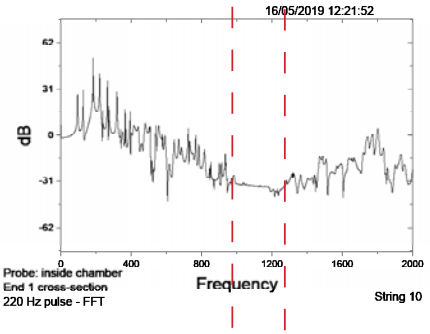

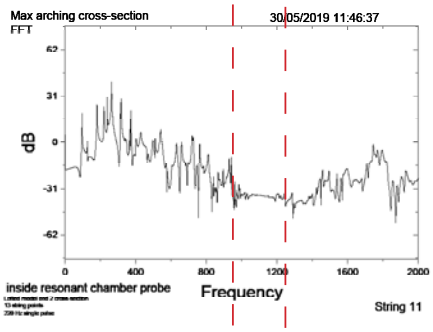

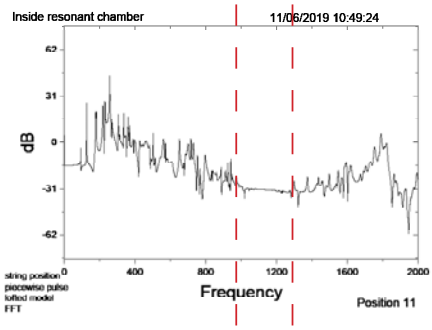

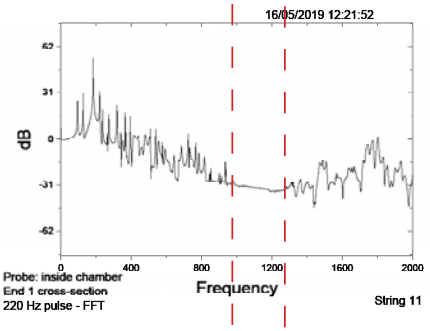

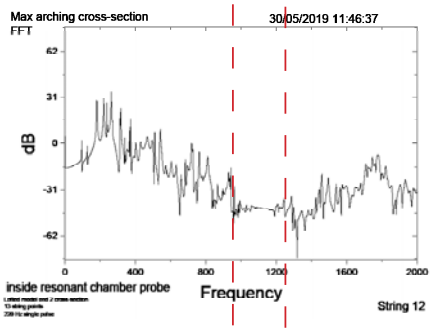

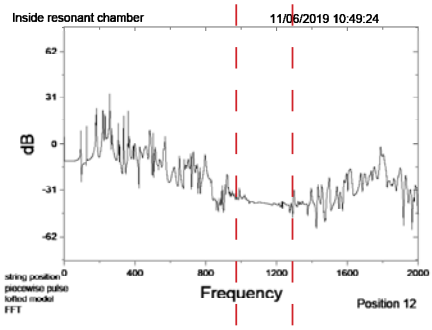

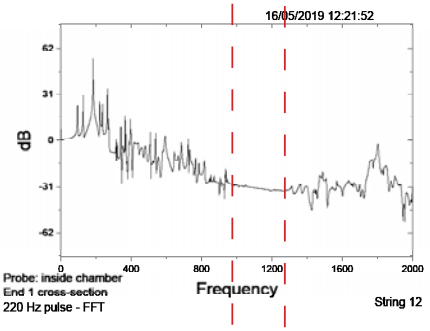

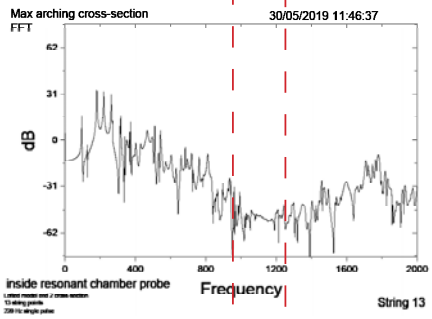

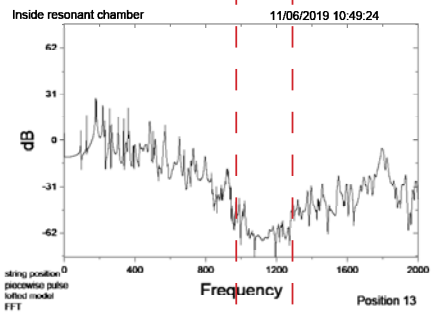

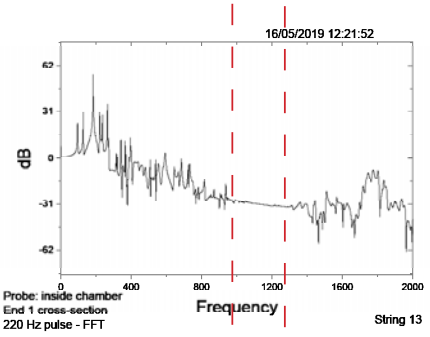

Dataset 8

The summary of the decay analyses

and

comparison with the parameters of excitation

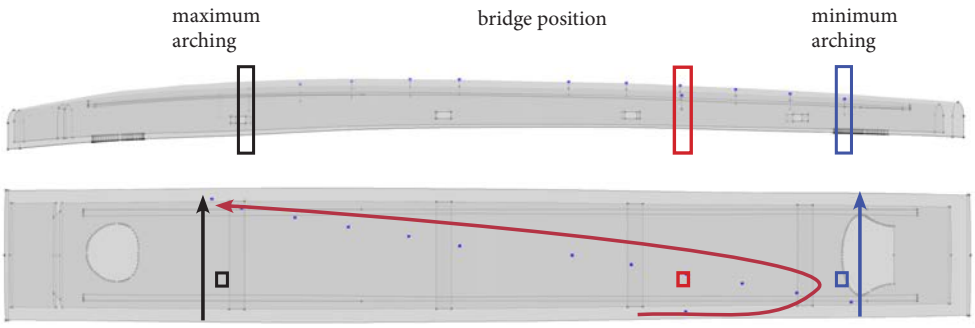

Sample waveform abstraction

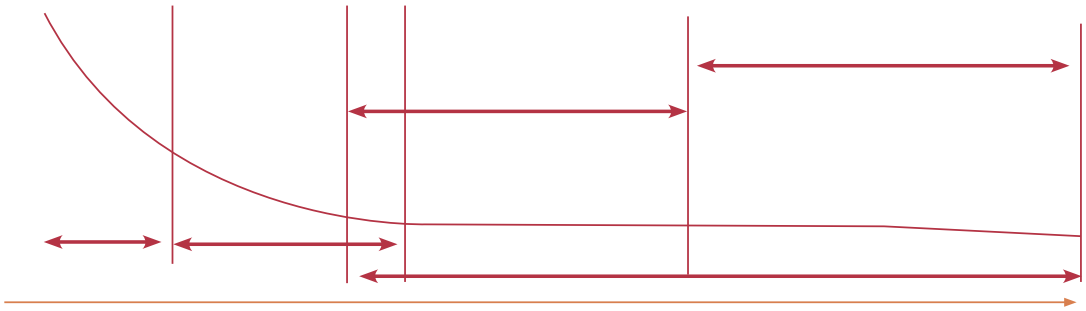

Initial decay t=(0,0.05)s

second decay t=(0.05,0.3)s

Third decay t=(0.25,0.5)s

fourth decay t=(0.5,1)s

size of unresponsive region of frequencies inside chamber (Hz)

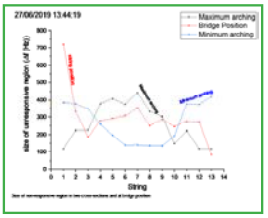

average tail amplitude (|Ā|)

above midpoint

(final decay (0.25,1) s)

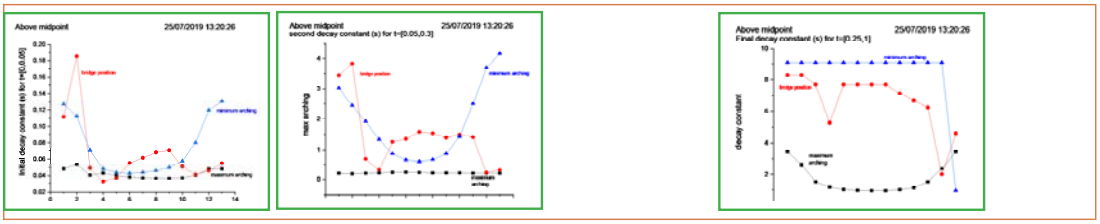

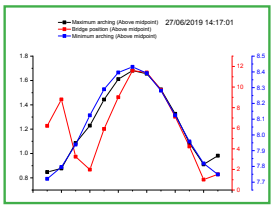

Below SH 1

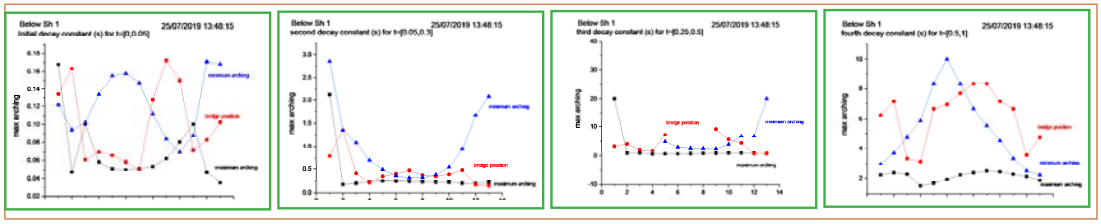

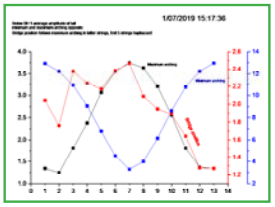

Inside main air cavity

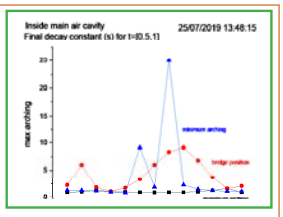

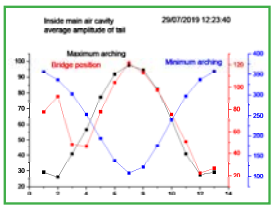

Inside small chamber

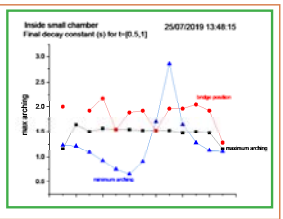

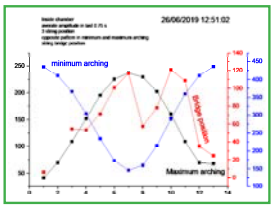

Changes of parameters with excitation point

Δx

thickness of base plate

thickness of top plate

height of air cavity